

1-1-1990

Spectroscopic investigation of crystal morphology in semi-crystalline polymers; Spectroscopic investigation of restricted geometries in monolayers of adsorbed polymers

David Allen Waldman
University of Massachusetts Amherst

Follow this and additional works at: https://scholarworks.umass.edu/dissertations_1

Recommended Citation

Waldman, David Allen, "Spectroscopic investigation of crystal morphology in semi-crystalline polymers; Spectroscopic investigation of restricted geometries in monolayers of adsorbed polymers" (1990). *Doctoral Dissertations 1896 - February 2014*. 776.
https://scholarworks.umass.edu/dissertations_1/776

This Open Access Dissertation is brought to you for free and open access by ScholarWorks@UMass Amherst. It has been accepted for inclusion in Doctoral Dissertations 1896 - February 2014 by an authorized administrator of ScholarWorks@UMass Amherst. For more information, please contact scholarworks@library.umass.edu.



312066007716670

1. SPECTROSCOPIC INVESTIGATION OF CRYSTAL MORPHOLOGY
IN SEMI-CRYSTALLINE POLYMERS
2. SPECTROSCOPIC INVESTIGATION OF RESTRICTED GEOMETRIES
IN MONOLAYERS OF ADSORBED POLYMERS

A Dissertation Presented

By

DAVID ALLEN WALDMAN

Submitted to the Graduate School of the
University of Massachusetts in partial fulfillment
of the requirements for the degree of

DOCTOR OF PHILOSOPHY

May 1990

Department of Polymer Science and Engineering

© Copyright by David Allen Waldman 1990

All Rights Reserved

1. SPECTROSCOPIC INVESTIGATION OF CRYSTAL MORPHOLOGY
IN SEMI-CRYSTALLINE POLYMERS

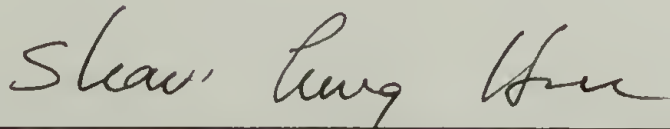
2. SPECTROSCOPIC INVESTIGATION OF RESTRICTED GEOMETRIES
IN MONOLAYERS OF ADSORBED POLYMERS

A Dissertation Presented


by

DAVID ALLEN WALDMAN

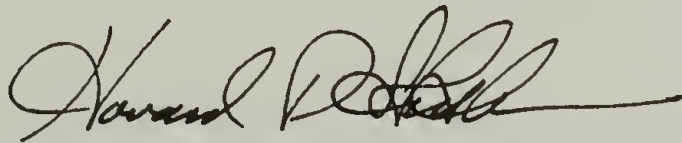
Approved as to style and content by:



Shaw L. Hsu, Chairman of Committee



Thomas J. McCarthy, Member



Howard D. Stidham, Member



William J. MacKnight, Department Head
Polymer Science and Engineering

To my mother, Henny
October 23, 1925 - May 1, 1987

" Choose Life "

ACKNOWLEDGEMENTS

I wish to acknowledge the guidance, support and encouragement given to me by my advisor, Professor Shaw Ling Hsu, through the course of my graduate studies. It has been a privilege to have as an advisor an individual so dedicated to the development of graduate students. I would also like to thank the other members of my committee, Professor Thomas J. McCarthy, and Professor Howard D. Stidham for their keen insight, helpful suggestions and genuine interest.

I want to give special thanks to the numerous other individuals who made this endeavor more enjoyable and stimulating. In particular I would like to express my sincere appreciation to Dr. Chih Chang, James Lasch, Peter Kim, Han Sup Lee, Nick Reynolds, Cun Feng Fan, Brant Kolb, Damo Iyengar and Joan Brennan for their assistance, friendship and numerous animated discussions. The diligent synthetic assistance of Brant Kolb is recognized, as are the relations with Professors Fei Jei Lu and Ying Kang Wang.

The continual support, encouragement and love of my mother, father, and brothers are acknowledged with much love and appreciation. The persistent pursuit of education by my parents is recognized with admiration. Finally the love, patience, support, sacrifice and understanding from my wife, Eileen, will never be fully appreciated.

ABSTRACT

1. SPECTROSCOPIC INVESTIGATION OF CRYSTAL MORPHOLOGY
IN SEMI-CRYSTALLINE POLYMERS
2. SPECTROSCOPIC INVESTIGATION OF RESTRICTED GEOMETRIES
IN MONOLAYERS OF ADSORBED POLYMERS

MAY 1990

DAVID ALLEN WALDMAN, B.S., UNIVERSITY OF MASSACHUSETTS

Ph.D., UNIVERSITY OF MASSACHUSETTS

Directed by: Professor Shaw Ling Hsu

The highly ordered long range structure associated with the crystalline core of semi-crystalline linear aliphatic polyesters, is evaluated using Raman spectroscopy. Polarization modulation reflection infrared spectroscopy, and x-ray photoelectron spectroscopy, are utilized to determine the degree of structural and chemical anisotropy in ultra thin glassy polymer films formed by monolayer chemisorption of functionalized polystyrene onto external surfaces. In both cases the morphological characterization is restricted to the determination of polymer structure in regions that are on the order of 100 angstroms or less in thickness.

The frequency of the longitudinal acoustic mode (LAM-1) normal mode vibration is inversely related to the crystal stem length. It is found in the very low frequency region of

the Raman spectrum for these linear aliphatic polyesters. It is utilized to directly determine the crystal thickness, the distribution of crystal stem lengths, and the longitudinal Youngs modulus. The existence of multiple low frequency components is studied as a function of degree of supercooling, monomer chemical structure, crystal packing, and crystal thickening.

Polarization modulation reflection infrared measurements, and a segmental orientation model based solely upon relative intensities, are used to determine the average chain axis orientation relative to the surface normal for sulfur functionalized polystyrenes adsorbed to Au surfaces. The orientation of the polystyrene chain is higher for the PS₉₅-PPS₅ adsorbed film (0.29) than for the thiol endcapped polystyrene (0.22). The higher copolymer orientation can be attributed to the slightly longer strongly interacting part of the structure. The block is sufficiently long to enable a higher grafting density.

Results for other copolymers indicate that a structural transition occurs in the adsorbed copolymer films between 95:5 and 90:10 molar ratios, for a degree of polymerization around 600. The transition from anisotropic to an isotropic polystyrene conformation is related to the XPS film thickness, and thus the grafting density. Segregation in the chemical composition exists as shown by XPS. The degree of segregation is related to the propylene sulfide block length relative to the overall degree of polymerization. If the

interaction strength is sufficiently large then a critical block length will exist which will determine whether the buoy structure can form an oriented brush in solution and a collapsed oriented ultra thin film.

TABLE OF CONTENTS

	<u>Page</u>
ACKNOWLEDGMENTS.....	v
ABSTRACT.....	vi
LIST OF TABLES.....	xiii
LIST OF FIGURES.....	xv
Chapter	
1. THESIS OBJECTIVES.....	1
Background and Goals.....	1
Overview of Dissertation.....	5
References.....	9
2. THE LONGITUDINAL ACOUSTIC MODE AS A MORPHOLOGICAL TOOL FOR SEMI-CRYSTALLINE POLYMERS.....	13
Origin of This Unusual Vibrational Mode.....	13
The Exact Relationship between LAM Measurements and Chain Length Distribution.....	23
Perturbing Effects on the LAM Measurements.....	30
Linear Aliphatic Polyesters as a Model to Define Influence of Intermolecular Effects	33
Transplanar Structure.....	26
Regularly Spaced Asymmetric Masses.....	27
Single Crystal Morphology.....	27
References.....	39

3.	CHARACTERIZATION OF LINEAR ALIPHATIC POLYESTER SINGLE CRYSTALS	43
	Background.....	43
	Preparation and Characterization of Crystalline Mats..	43
	Dilute Solution Crystallization.....	43
	Annealing of Crystal Mats.....	49
	Characterization Experimental.....	50
	Results and Discussion.....	52
	Previous Studies.....	52
	SAXS Analysis of Polyester Single Crystal Mats ..	55
	Raman Analysis of As Grown Linear Aliphatic Polyester Single Crystal Mats.....	66
	Low Temperature Raman Analysis.....	78
	Raman Analysis of Annealed Polyester Single Crystal Mats.....	94
	Low Frequency Region.....	94
	Mid Frequency Region.....	108
	References.....	118
4.	NORMAL COORDINATE ANALYSIS OF THE LONGITUDINAL ACOUSTIC MODE IN LINEAR ALIPHATIC POLYESTERS.....	122
	Introduction.....	122
	Background.....	123
	Normal Coordinate Analysis.....	126
	Results and Discussion.....	136
	References.....	168
5.	SYNTHESIS OF MODEL POLYMERS FOR ADSORPTION STUDIES...170	
	Introduction.....	170
	Synthesis of Styrene-Propylene Sulfide Block Copolymers.....	175
	Background.....	175
	Methods.....	177
	Purification.....	179
	Styrene.....	179
	Propylene Sulfide(PS).....	180

	THF.....	181
	Procedure for Synthesis.....	184
	Results and Discussion.....	185
	Oxidative Instability.....	185
	Coupling of Copolymers via Disulfide Formation..	192
	Procedure for Cleavage of Disulfide Linkages....	193
	Final Copolymer Samples.....	194
	References.....	200
6.	DOUBLE MODULATION EXTERNAL REFLECTION SPECTROSCOPY...	204
	Introduction.....	204
	Description and Advantages of Differential Method....	206
	Optimization of Polarization Modulation Spectroscopy.....	217
	Optical Components.....	217
	Alignment Procedure.....	227
	Removal of DC Offset From s-Polarization.....	231
	Lock-in Detection.....	233
	Mathematical Treatment For Polarization Modulation External Reflection Infrared Spectroscopy.....	241
	References.....	251
7.	SPECTROSCOPIC ANALYSIS OF FUNCTIONALIZED POLYSTYRENE ADSORBED ON METAL SURFACES.....	253
	Introduction.....	253
	Experimental.....	258
	Materials.....	258
	Methods.....	259
	Thiol-Terminated Polystyrene (PS _x -SH).....	260
	Styrene-Propylene Sulfide Block Copolymers (PS _A -PPS _B).....	260
	Adsorption of Polymers.....	261
	Coextruded Films.....	262
	Polarization Modulation External Reflection Spectroscopy (PMGRS) ⁴⁴	262

Results And Discussion.....	262
Characterization With XPS And Contact Angle.....	264
Surface Grafting Density.....	297
Characterization by Polarization Modulation	
External Reflection Infrared Spectroscopy.....	306
Orientation Model And Results.....	320
Transition From Anisotropic to Isotropic.....	345
References.....	352
8. SUMMARY AND SUGGESTIONS FOR FUTURE STUDY.....	356
BIBLIOGRAPHY.....	372

LIST OF TABLES

Table	Page
1.	Crystallization conditions for growth of linear aliphatic polyester single crystals.....46
2.	Low angle x-ray diffraction of polyester single crystals.....65
3.	Low frequency data obtained in Raman spectra for as grown (10-8) and (9-8) polyester single crystals.....72
4.	Weighting of low frequency Raman intensity from temperature and frequency factors.....82
5.	Structural parameters of the proposed geometries of linear aliphatic polyester oligomers.....133
6.	Force constants used to define intrachain potential functions for normal coordinate analysis of model oligomers of linear aliphatic polyesters.....136
7.	Frequencies of two LAM-1-like vibrations calculated for model oligomers of linear aliphatic polyesters.....141
8.	Table showing frequencies of LAM-1-like modes calculated for a series of even-even, and odd-even linear aliphatic ester oligomers with different end group structures.....159
9.	Molecular weight distribution and polydispersity of Polystyrene-Propylene Sulfide diblock copolymers synthesized by anionic methods.....199
10.	Table showing calculated attenuation in the XPS photoemission signal, I^S , as a function of takeoff angles, $\theta = 15, 30, 50, \text{ and } 75^\circ$, for overlayer thicknesses of $Z = 1.0 \text{ to } 50 \text{ \AA}$, for a substrate mean free path, λ_S , of 22 \AA273

11. Table showing the calculated number of adsorbed chains, N_{ad} , and collapsed adsorbed film thicknesses, t_{ad} , as a function of both the degree of polymerization for polystyrene and the solvent conditions.....302
12. Table showing the calculated number of polymer chains, N_{re} , that would be necessary to exist inside of each sphere at the C^* grafting condition(factor by which C^* must be exceeded), and the number of chains grafted per nm^2 , N_G , in order to effect a continuous film of amorphous density for a certain molecular weight and film thickness.....304
13. Table showing the average angles from the symmetric, θ_s , and asymmetric, θ_{as} , transition moments, and the chain axis, θ_c , to the surface normal (Z), and the corresponding average transition moment and segmental orientation for ultra thin films prepared by adsorption of thiol endcapped polystyrene and copolymer PS₉₅-PPS₅...350

LIST OF FIGURES

Figure	Page
1.	Schematic of the longitudinal acoustic mode of vibration LAM-1 for an all trans planar segment..16
2.	Schematic representation of the contributions of CC stretching and CCC bending coordinates to the normal coordinates $V_1 - V_6$18
3.	Representation of a polyethylene crystal lamellae depicting the tilted crystal stem and fold surface region.....21
4.	Small-angle X-ray diffraction(a), (c) and low frequency Raman(b), (d) for polyethylene.....25
5.	Structural parameters for the planar zig-zag conformation in the crystalline region of linear aliphatic polyesters(right) and lateral packing of planar chains (top) and (bottom).....36
6.	Small angle x-ray scattering of the (9-8) polyester single crystals (a) as-grown sample, (b) $T_A = 50\text{ }^\circ\text{C}$, (c) $T_A = 58\text{ }^\circ\text{C}$, (d) $T_A = 60\text{ }^\circ\text{C}$57
7.	Low-frequency Raman spectra obtained for the as-grown and annealed (9-8) polyester single crystals.....60
8.	Low-frequency Raman spectra obtained for the as-grown and annealed (10-16) polyester single crystals.....62
9.	C-H bending region(left) and low-frequency region (right) in Raman spectra obtained for as grown top) (9-8) polyester, and (bottom) polyethylene single crystals.....68
10.	Low-frequency region in Raman spectra obtained for as grown (10-8) polyester single crystals, (top) $T_{CRY} = 39\text{ }^\circ\text{C}$, and (bottom) $T_{CRY} = 33\text{ }^\circ\text{C}$70
11.	Low-frequency region in Raman spectra obtained for as grown (top) (9-8), and (bottom) (10-8) polyester single crystals with same degree of undercooling ($\Delta T = 13\text{ }^\circ\text{C}$).....77

12.	Low-frequency region in Raman spectra obtained for as grown (9-8) polyester single crystals ($T_{CRY} = 33\text{ }^{\circ}\text{C}$) at (a) room temperature (top) and (b) $-110\text{ }^{\circ}\text{C}$ (bottom).....	80
13.	Low-frequency region in Raman spectrum, obtained for as grown (9-8) polyester single crystals ($T_{CRY} = 33\text{ }^{\circ}\text{C}$) at room temperature, with a function fit to remove the background contribution.....	85
14.	Low-frequency region in Raman spectrum, obtained for as grown (9-8) polyester single crystals ($T_{CRY} = 33\text{ }^{\circ}\text{C}$) at room temperature, after subtraction of background contribution.....	87
15.	Temperature and frequency weighted low-frequency region of background subtracted Raman spectrum for as grown (9-8) polyester single crystals ($T_{CRY} = 33\text{ }^{\circ}\text{C}$) at room temperature.....	89
16.	Low-frequency region in Raman spectra obtained for as grown (9-8) polyester single crystals ($T_{CRY} = 27\text{ }^{\circ}\text{C}$) at (a) room temperature (top) and (b) $-125\text{ }^{\circ}\text{C}$ (bottom).....	92
17.	Low-frequency region in Raman spectra obtained at room temperature for annealed (9-8) polyester single crystals ($T_{CRY} = 33\text{ }^{\circ}\text{C}$).....	96
18.	Low-frequency region in Raman spectra obtained at room temperature for annealed (10-8) polyester single crystals ($T_{CRY} = 39\text{ }^{\circ}\text{C}$).....	98
19.	Low-frequency region in Raman spectra obtained at room temperature for annealed (9-8) polyester single crystals ($T_{CRY} = 27\text{ }^{\circ}\text{C}$).....	100
20.	Low-frequency region in Raman spectra obtained at $-125\text{ }^{\circ}\text{C}$ for as-grown and annealed (9-8) polyester single crystals ($T_{CRY} = 33\text{ }^{\circ}\text{C}$).....	102
21.	Crystal stem length in (\AA) as a function of annealing temperature in ($^{\circ}\text{C}$) for polyester single crystals (9-8) grown at $T_{CRY} = 33\text{ }^{\circ}\text{C}$ and (10-8) grown at $39\text{ }^{\circ}\text{C}$	105
22.	CH_2 twisting and bending regions in Raman spectra obtained at room temperature for annealed (9-8) polyester single crystals grown at $T_{CRY} = 27\text{ }^{\circ}\text{C}$	111

23.	CH ₂ twisting and bending regions in Raman spectra obtained at (a) low temperature(- 125 °C) and (b) room temperature for annealed (9-8) polyester single crystals.....	114
24.	CH ₂ twisting and bending regions in Raman spectra obtained at room temperature for as grown (9-8) polyester single crystals as a function of crystallization temperature.....	117
25.	Chemical structure of various model linear aliphatic polyester oligomers evaluated by normal coordinate analysis.....	129
26.	Structural parameters used in normal coordinate calculations for oligomers of linear aliphatic polyesters.....	130
27.	Atomic displacements for the two LAM-1-like modes calculated for two model oligomers of linear aliphatic polyesters.....	142
28.	Atomic displacements for one LAM-1-like mode calculated for model oligomer (10-8) ₄	148
29.	Atomic displacements for one LAM-1-like mode calculated for model oligomer (9-8) ₄	150
30.	Atomic displacements for one LAM-1-like mode calculated for model oligomer (9-8) ₄ with ester terminal groups.....	154
31.	Atomic displacements for one LAM-1-like mode calculated for model oligomer (9-8) ₄ with methylene sequence terminal groups.....	156
32.	Atomic displacements for three LAM-1-like modes calculated for model oligomer (6-10) ₃ with methylene sequence terminal groups.....	161
33.	Atomic displacements for two LAM-1-like modes calculated for model oligomer (10-8) ₃ with methylene sequence terminal groups.....	163
34.	Atomic displacements for three LAM-1-like modes calculated for model oligomer (6-8) ₅ (shortened by one ester group) with methylene sequence terminal groups.....	165
35.	Schematic for anionic synthesis of (a) thiol endcapped Polystyrene by addition of 1 to 2 equivalents of propylene sulfide to the living polymer (top), and (b) living diblock copolymers of	

	Styrene-Propylene Sulfide (middle) and (c) reaction for termination of (b) by addition of either acidic methanol or ethyl bromide in the presence of dithiothreitol (bottom)	174
36.	Gel permeation chromatography(GPC) of THF solutions of thiol endcapped Polystyrene-Propylene Sulfide diblock copolymers(conc. = 1 mg/ml), as a function of time under nitrogen atmosphere, and solvent purification.....	187
37.	Schematic depicting reaction pathways of unstable thiol endcapped Polystyrene-Propylene Sulfide diblock copolymers to form degradation products consisting of unzipped propylene sulfide blocks and (a) dithianes, (b) trithiapane and propylene, and (c) cyclic oligomers of propylene sulfide (x = 3, 4, 5).....	189
38.	Schematic for (a) oxidative coupling of thiol and or thiolate terminated Polystyrene-Propylene Sulfide AB diblock copolymers, to form triblock ABBA copolymers via linking of diblocks through disulfide formation, and (b) termination with oxidatively stable ethyl endcap.....	190
39.	Gel permeation chromatography(GPC) of 1 mg/ml THF solutions of Polystyrene-Propylene Sulfide diblock copolymers (PS ₉₅ -PPS ₅) (top), and (PS ₇₅ -PPS ₂₅) (bottom), with oxidatively coupled component(left), and after reduction with DTT and stable ethyl endcapping(right).....	196
40.	Gel permeation chromatography(GPC) of 1 mg/ml THF solution of Polystyrene-Propylene Sulfide diblock copolymer (PS ₉₀ -PPS ₁₀), with (a) oxidatively coupled component, and (b) after reduction with DTT and stable ethyl endcapping.....	197
41.	FT-IR ERS spectra of thin films, 90 Å, 260 Å, and 2680 Å, (top) to (bottom), of poly(acrylonitrile-co-styrene) adsorbed on aluminum.....	206
42.	Calculated dependence of the absorption factors for a 10 Å film of acetone on gold, for the parallel (A _p) and perpendicular (A _s) polarizations at the wavenumber of maximum adlayer absorption, (1720 cm ⁻¹), as a function of angle of incidence, (top), and the calculated variation in the parallel absorption factor (A _p) as a function of wavenumber and angle of incidence for the same film.....	209

43. Schematic for polarization modulation experimental method coupled with FT-IR grazing incidence external reflection spectroscopy.....211
44. Schematic for the electric field components of the resultant electromagnetic wave at the boundary of a conducting surface.....212
45. Schematic for the grazing incidence reflection cell and polarizer components mounted inside the Nicolet 60SX sampling compartment.....219
46. Schematic for a half-wave retardation plate, (top), and the resulting 90° rotation of the incident electric field plane of polarization, as depicted by the electric field vectors at the incident and exit planes of the crystal.....222
47. Calculated reflectivity as a function of wavenumber for transverse electric and magnetic components reflected from gold layers 10, 20, 50, 75, 100, 150, and 200 nm in thickness, at the optimum incident angle of 88°.....226
48. Single beam polarization modulation grazing incidence external reflection infrared spectra for reflectivity from a vapor deposited Au surface, 2000 Å in thickness, immediately after deposition, (top), and for same surface after slide was heated to 350 °C under nitrogen purge for two 30 minute intervals, (bottom).....229
49. Single beam polarization modulation grazing incidence external reflection infrared spectra for reflectivity from a vapor deposited Au surface, 2000 Å in thickness, immediately after deposition, (bottom), and for same surface after adsorption of copolymer PS₉₅-PPS₅ from dilute solution(1 mg/ml), (top).....238
50. Single beam grazing incidence external reflection infrared spectra for reflectivity from a vapor deposited Au surface, 2000 Å in thickness, immediately after deposition, (bottom), and for same surface after adsorption of copolymer PS₉₅-PPS₅ from dilute solution(1 mg/ml), (top).....240
51. Schematic for the structure of copolymers with a strongly interacting block, after adsorption to a metal substrate.....265
52. Schematic depicting the change in the effective XPS sampling depth, $D = \lambda \sin\theta$, due to rotation of the

	sample stage so that the takeoff angle, θ , relative to the detector (analyzer) corresponds to 90° (top), and 10° (bottom).....	268
53.	Plot of substrate intensity attenuation for XPS photoemission signal, I^S , showing calculated decreasing exponential relations as a function of takeoff angle, θ , and overlayer thickness, Z , for a mean free path value, λ_S , of 22 Å for Au_{4f} photoelectrons of KE 1170 eV ejected through an adsorbed polymer layer.....	270
54.	XPS survey spectra, at 75° (a) and 15° (b) takeoff angles, of a freshly vapor deposited 1500 Å Au surface on a glass microscope slide, for Mg $K\alpha$ excitation(300 W, 15 KeV).....	275
55.	XPS survey spectra for PS ₇₅ -PPS ₂₅ adsorbed to Au from 1mg/ml cyclohexane solution at 35.5 °C, for 75° , (a), and 15° , (b), takeoff angles, and for similarly adsorbed PS ₉₀ -PPS ₁₀ for 75° , (c), and 15° , (d), takeoff angles respectively.....	278
56.	XPS multiplex spectra for the C_{1s} region, at a resolution of 0.5 eV, for PS ₇₅ -PPS ₂₅ adsorbed to Au from 1mg/ml cyclohexane solution at 35.5 °C, for 75° , (a), and 15° , (b), takeoff angles, and for similarly adsorbed PS ₉₀ -PPS ₁₀ for 75° , (c), and 15° , (d), takeoff angles respectively.....	280
57.	Sulfur composition as a function of the sine of the takeoff angle, from XPS multiplex spectra for the S_{2p} core level at a resolution of 0.5 eV, for copolymers PS ₇₅ -PPS ₂₅ , (top), and PS ₉₀ -PPS ₁₀ , (bottom), adsorbed to Au.....	282
58.	C/S atomic composition ratios as a function of the sine of the takeoff angle, from XPS multiplex spectra for the C_{1s} , and S_{2p} core levels, at a resolution of 0.5 eV, for copolymers PS ₇₅ -PPS ₂₅ , (top), and PS ₉₀ -PPS ₁₀ , (bottom), adsorbed to Au..	284
59.	Atomic composition for carbon and gold, as a function of the sine of the takeoff angle, from XPS multiplex spectra for the C_{1s} , and Au_{4f} core levels, at a resolution of 0.5 eV, for copolymers PS ₇₅ -PPS ₂₅ , (top), and PS ₉₀ -PPS ₁₀ , (bottom), adsorbed to Au.....	287

60. XPS survey spectra, at takeoff angles of 75° , (a), and 15° , (b), of PS₉₅-PPS₅ adsorbed to Au.....290
61. Sulfur composition, (top), and C/S atomic composition ratio, (bottom), as a function of the sine of the takeoff angle, from XPS multiplex spectra for the C_{1s}, and S_{2p} core levels, at a resolution of 0.5 eV, for copolymer PS₉₅-PPS₅ adsorbed to Au.....293
62. XPS survey spectra for thiol endcapped polystyrene adsorbed to Au from 1mg/ml cyclohexane solution at 35.5°C , at takeoff angles of 75° , (a), and 15° , (b).....296
63. Polarization modulation external reflection infrared energy spectra, obtained at grazing incidence, for an adsorbed layer of 80K thiol endcapped polystyrene, (top), and for the same Au surface before it was exposed to the polymer solution, (bottom).....308
64. Polarization modulation external reflection infrared energy spectra, obtained 1.5° below grazing incidence, for an adsorbed layer of 80K thiol endcapped polystyrene, (top), and for the same Au surface before it was exposed to the polymer solution, (bottom).....310
65. Single beam spectra, $I_{dc}(\bar{\nu})$, (top), and the reference throughput, $I_{odc}(\bar{\nu})$, (bottom), representing the instrument throughputs (dc spectra) for the same Au surfaces as Figures 63 and 64...314
66. The differential polarization modulation grazing incidence reflection spectra, directly proportional to $[A_p(\bar{\nu})]$, for an adsorbed layer of 80K thiol endcapped polystyrene.....316
67. The CH stretching region of the PMGRS spectrum, (solid), and transmission spectrum, (dotted), for the adsorbed thiol endcapped polystyrene in Figures 63-66, and an isotropic dispersion of the same polymer (2% in KBr) respectively.....319
68. Schematic for orientation model based solely upon relative intensities for one polarization, where the angle between the symmetric (M_s) and asymmetric (M_{as}) transition moments is 90° , and for any specific average angle θ that defines a cone which

	one transition moment (M_s) sweeps out between itself and a reference axis, which is assigned to be the surface normal (Z direction), the other transition moment (M_{as}) exists in a plane normal to (M_s) with an average angle ψ to z.....	325
69.	Schematic for spherical triangle relationships utilized to determine the average angle between the local chain axis and the surface normal, θ_c , once the average angles from Z to M_s and M_{as} , θ_s , and θ_{as} respectively, are obtained.....	330
70.	Isotropic spectrum for the copolymer PS ₇₅ -PPS ₂₅ , for a 2% dispersion in KBr.....	336
71.	Isotropic spectrum for poly(propylene-sulfide), for a 2% dispersion in KBr.....	338
72.	The [$A_p(\tilde{\nu})$] PMGRS CH stretching region for the copolymer PS ₇₅ -PPS ₂₅ , adsorbed onto a vapor deposited gold substrate from cyclohexane at 34.5°C.....	341
73.	The [$A_p(\tilde{\nu})$] PMGRS CH stretching region for the copolymer PS ₉₀ -PPS ₁₀ , adsorbed onto a vapor deposited gold substrate from cyclohexane at 34.5°C.....	343
74.	The [$A_p(\tilde{\nu})$] PMGRS CH stretching region for the copolymer PS ₉₅ -PPS ₅ , adsorbed onto a vapor deposited gold substrate from cyclohexane at 34.5°C.....	347

CHAPTER 1

THESIS OBJECTIVES

Background and Goals

The main objectives of this thesis research concern the characterization of polymer structure by vibrational spectroscopy. The principal reason for using vibrational spectroscopy as a morphological tool is because it is an extremely selective technique. High frequency vibrations are localized modes involving only a few nuclei. In this case the vibrations can be assigned unambiguously, and the direction of transition moments can also be well defined. Juxtaposed to these are the low frequency vibrations, which are highly coupled and therefore involve a number of atoms. In general, these vibrations can be utilized to characterize chain conformation or packing at a much more specific or localized level than other methods such as diffraction.

If the transition moment directions associated with an absorption band are well defined, then the relative orientation of individual structural units of a polymer can also be specified.¹⁻³ The overall chain segmental orientation, with respect to a director axis which is typically parallel to the stretch direction, can then be determined from polarization (dichroic ratio) measurements.⁴ Similarly, the degree of chain elongation, in a stretched network of chains, can be established from both dichroism

and/or birefringence.^{1,5-7} As a result of Fourier transform infrared and Raman instrumentation, the dichroism method enables a distinct advantage in both accuracy and precision. Such measurements have been extremely useful in determining microstructure in amorphous, semi-crystalline, and liquid crystal polymers, and enabling it to be related to a number of important macroscopic properties.

The results of two structural studies; 1) A Spectroscopic Investigation of Crystal Morphology in Semi-crystalline Polymers and 2) A Spectroscopic Investigation of Restricted Geometries in Monolayers of Adsorbed Polymers, are reported in this thesis. These were carried out utilizing the selectivity and specificity of vibrational spectroscopy. In the former, the highly ordered long range structure associated with the crystalline core of semi-crystalline linear aliphatic polyesters, is evaluated using Raman spectroscopy. The objective of the second study is the application of infrared spectroscopy to determine the degree of structural anisotropy in ultra thin glassy polymer films. These are formed by monolayer chemisorption of functionalized polystyrene onto external surfaces. In both cases the morphological characterization is restricted to the determination of polymer structure in regions that are on the order of 100 angstroms or less in thickness.

The longitudinal acoustic mode (LAM), found in the very low frequency region of the Raman spectrum, provides a unique

and sensitive morphological tool for the study of microstructural features of semi-crystalline polymers, in the spatial range of 10 to 600 angstroms.⁸⁻¹¹ The frequency of this normal mode vibration, which involves the simultaneous motion of all atoms of the entire straight chain segment, is inversely related to the crystal stem length. It can therefore be utilized to directly determine both the crystal thickness, and the distribution of crystal stem lengths contained within lamellae.¹²⁻²¹ For polymers with trans planar crystal structures, the vibration extends over the entire length of the all trans segment. It is therefore sensitive to conformation and the existence and/or incorporation of defects contained within the crystalline core.²²⁻²⁷ The attainable lamellae thickness, and the effect of such defects, both constitute critical parameters for the structural and mechanical properties of semi-crystalline polymers. Although the characteristics and origins of the LAM are well understood for polyethylene, they are not nearly as well understood for other semi-crystalline polymers. The first study addresses these considerations and establishes that LAM can be used to characterize the long range crystal structure of another class of semi-crystalline polymers.

Thin polymer films, and the adsorption of polymers and copolymers to external surfaces, are extremely important in a diverse number of technological areas such as adhesion, corrosion, biological interfaces, microelectronics,

filtration, diffusion and lubrication. Studies on adsorption and desorption by ellipsometry, viscosity, chromatography, ESR, and infrared spectroscopy have been useful in determining the kinetics of adsorption, the adsorbance and thickness of the adsorbed polymer layer, and the degree of surface coverage.²⁸⁻⁴³ All of these properties are important parameters in the above applications. The structure of block copolymers at or near a surface, when one block is preferentially attracted to the substrate surface, is of particular significance. One reason is that copolymers provide a simple and versatile method for steric stabilization of colloidal particles suspended in a solution.

Although a considerable amount of work has been carried out regarding the determination of adsorbed layer properties in solution for a number of polymers, little work regarding the structure of the collapsed solid film exists. Specific structural information pertaining to the orientation of polymers in the collapsed solid film state, after having been adsorbed from solution onto substrates, is lacking. The selectivity of infrared spectroscopy enables specific orientations to be measured, provided the sensitivity is sufficient. Segregation in the chemical composition of block copolymer adsorbed layers may be due to the tendency of copolymer chains to self-associate by micro-phase separation, and thus form organized structures.^{44,45} When the strength of interaction, of the sub-units in the attracted block to the

surface, is of sufficient magnitude then self-association occurs regardless.⁴⁶⁻⁴⁸ The length of the attracted block will affect the grafting density and thus the adsorbed layer thickness. The second study focuses on the structural effects induced in collapsed ultra thin polymer films by strongly interacting sub units in block copolymers. External reflection infrared spectroscopy is utilized to determine the degree of structural anisotropy, while segregation in chemical composition is ascertained by x-ray photoelectron spectroscopy.

Overview of Dissertation

Chapter 2 provides a background discussion of the longitudinal acoustic mode and establishes its usefulness as a morphological tool for the study of long range crystal structure in linear aliphatic polyesters. It outlines the physical basis of the LAM vibration, and the structural information it can provide as compared to electron microscopy and x-ray scattering methods. The exact relationship between LAM measurements and the chain length distribution is discussed. The role of perturbing effects on LAM measurements due to intermolecular interactions, end effects, and conformational defects is considered. The reasons for choosing linear aliphatic polyesters for a study of the effects on the LAM vibration of asymmetric mass placements, internal to the crystal chain structure, are established.

Chapter 3 presents a study of long range crystal structure in single crystals of linear aliphatic polyesters. The conditions and results for the preparation of single crystal mats by crystallization from dilute solution are outlined. The results from measurements using Raman spectroscopy, x-ray scattering and differential scanning calorimetry are presented and discussed. The relationship between the model for a long elastic rod and the LAM vibration in linear aliphatic polyesters, is established by the frequency of the lowest frequency most intense band observed in the Raman spectrum. The usefulness of Raman spectroscopy in determining long range crystal structure and packing in linear aliphatic polyesters is established by annealing experiments.

Chapter 4 presents a normal coordinate analysis of the longitudinal mode for a series of model oligomers of linear aliphatic polyesters. The origin of the LAM vibration in linear aliphatic polyesters is investigated. The effect of inclusion of off-axis masses on the LAM vibration of a single chain, is reported and analyzed as a function of chain length, for both even-even and odd-even structures. An evaluation is made for the coupling of transverse to longitudinal acoustic modes, as a possible explanation for the observed low frequency experimental results presented in Chapter III. This is done by examination of the calculated

Cartesian displacement projection along the chain axis, for normal modes which satisfy the criteria of a LAM vibration.

Chapter 5 contains the pertinent conditions pertaining to the synthesis of thiol terminated polystyrene, and block copolymers of styrene-propylene sulfide. The methods used for the anionic synthesis, including the purification of monomers and solvents, and the synthesis procedure itself, are discussed. Special attention was placed upon the oxidative stability of these copolymers, and details are given for the steps necessary to accomplish this.

Chapter 6 presents the double modulation external reflection spectroscopic method. The advantages of this technique over conventional grazing incidence infrared reflection spectroscopy are discussed. Details of the experimental optimization necessary when the double modulation method is used in conjunction with external reflection, are outlined. Limitations of this measurement technique are presented along with a mathematical treatment.

Chapter 7 contains results from reflectance infrared spectroscopy of adsorbed functionalized polystyrene surfaces. The double modulation technique was utilized to determine that the chain conformation, in ultra thin films of adsorbed polystyrene, differs from that of the bulk state. A model is presented which enabled orientations, relative to the metal substrate within the adsorbed polymer films, to be determined

without dichroic ratios. It is shown that the strength of interaction of the polymer sub units, and the relative number of strongly interacting units, can alter such orientations and affect the conformation of the polymer chains. X-ray photoelectron spectroscopy results are also presented. These show that a segregation in chemical composition occurs in adsorbed monolayer films of block copolymers, when one block is strongly interacting with the surface.

In chapter 8 a summary of conclusions is presented based upon the experimental and theoretical results of the two studies. Future considerations for continued research in both areas are outlined with the emphasis placed upon the later study.

References

1. Stein R. S. *J. Polymer Sci.*, **1958**, 28, 83.
2. Fraser, R. D. B. *J. Chem. Phys.*, **1953**, 21, 1511.
3. Fraser, R. D. B. *J. Chem. Phys.*, **1956**, 24, 89.
4. Fraser, R. D. B. *J. Chem. Phys.*, **1958**, 28, 1113.
5. Marrinan, H. J. *J. Polymer Sci.*, **1959**, 39, 461.
6. Treloar, L. R. G., *The Physics of Rubber Elasticity*, Oxford, 1949.
7. Roe, R. J., Krigbaum, W. R. *J. Appl. Phys.*, **1964**, 35, 2215.
8. Mizushima, S. I.; Shimanouchi T. *J. Am. Chem. Soc.*, **1949**, 71, 1320.
9. Schaufele, R. F.; Shimanouchi, T. *J. Chem. Phys.*, **1967**, 47, 3605.
10. Tasumi, M.; Krimm, S. *J. Chem. Phys.*, **1967**, 46, 755.
11. Shimanouchi, T.; Tasumi, M. *Indian J. Pure Appl. Phys.*, **1971**, 9, 958.
12. Peticolas, W. L.; Hibler, G. W.; Lippert, J. L.; Peterlin, A.; Olf, H. *Appl. Phys. Lett.*, **1971**, 18, 87.
13. Folkes, M. J.; Keller, A.; Stejny, J.; Goggin, P. L.; Fraser, G. V.; Hendra, P. J. *Colloid Polym. Sci.*, **1975**, 253, 354.
14. Olf, H. G.; Peterlin, A.; Peticolas, W. L. *J. Polym. Sci.: Polym. Phys. Ed.*, **1974**, 12, 359.
15. Hsu, S. L.; Krimm, S.; Krause, S.; Yeh, G. S. Y. *J. Polym. Sci.: Polym. Lett. Ed.*, **1976**, 14, 195.

16. Hartley, A.; Leung, Y. K.; Booth, C.; Shepherd, I. W. *Polymer*, **1976**, *17*, 354.
17. Rabolt, J. F.; Fanconi, B. J. *Polym. Sci.: Polym. Lett. Ed.*, **1977**, *15*, 121.
18. Woodward, L. A.; Long, D. A. *Trans. Faraday Soc.*, **1949**, *45*, 1131.
19. Snyder, R. G.; Krause, S. J.; Scherer, J. R. *J. Polym. Sci.: Polym. Phys. Ed.*, **1978**, *16*, 1593.
20. Snyder, R. G.; Scherer, J. R. *J. Polym. Sci.: Polym. Phys. Ed.*, **1980**, *18*, 421.
21. Koenig, J. L.; Tabb, D. L. *J. Macromol. Sci. Phys.*, **1974**, *B9*, 141.
22. Dlugosz, J.; Fraser, G. V.; Grubb, D.; Keller, A.; Odell, J. A.; Goggin, P. L. *Polymer*, **1976**, *17*, 471.
23. Fraser, G. V.; Hendra, P. J.; Cudby, M. E. A.; Willis, H. A. *J. Mater. Sci.*, **1974**, *9*, 1270.
24. Reneker, D. H. *J. Polym. Sci.*, **1962**, *59*, S39.
25. Reneker, D. H.; Fanconi, B. J. *Appl. Phys.*, **1975**, *46*, 4144.
26. Wang, Y. K.; Waldman, D. A.; Stein, R. S.; Hsu, S. L. *J. Appl. Phys.*, **1982**, *53*, 10, 6591.
27. Wang, Y. K.; Waldman, D. A.; Lasch, J. E.; Stein, R. S.; Hsu, S. L., *Macromolecules*, **1982**, *15*, 1452.
28. Kolthoff, I. M.; Gutmacher, R. G. *J. Phys. Chem.*, **1952**, *56*, 740-745.
29. Frisch, H. L.; Hellman, M. L.; Lundberg, J. L. *J. Polym. Sci.*, **1959**, *38*, 441.

30. Felter, R. E.; Moyer, E. S.; Ray Jr., L. N. *J. Polym. Sci.*, **1969**, B7, 529-533.
31. Felter, R. E.; Ray Jr., L. N. *J. Colloid Interface Sci.*, **1970**, 32, 349.
32. Koopal, L. K.; Lyklema, J. *J. Chem. Soc., Faraday Discuss.*, **1975**, 59, 230.
33. Howard, G.J.; Woods, S.J. *J. Polym. Sci., A-2*, **1972**, 10, 1023-1028.
34. Sadakne G. S.; White, J. L. *J. Appl. Polym. Sci.*, **1973**, 17, 453.
35. Linden, C. V.; Leemput, R. V. *J. Colloid Interface Sci.*, **1978**, 67, 48-62.
36. Linden, C. V.; Leemput, R. V. *J. Colloid Interface Sci.*, **1978**, 67, 63-69.
37. Cohen Stuart, M. A.; Scheutjens, J. M. H. M.; Fleer, G. *J. J. Polym. Sci: Polym. Phys. Ed.*, **1980**, 18, 559-573.
38. Stromberg, R. R.; Tutas, D. J.; Passaglia, E. *J. Phys. Chem.*, **1965**, 69, 11, 3955-3963.
39. Peyser, P.; Stromberg, R. R. *J. Phys. Chem.*, **1967**, 71, 2066.
40. Takahashi, A.; Kawaguchi, M.; Hirota, H.; Kato, T. *Macromolecules*, **1980**, 13, 4, 884-889.
41. Kawaguchi, M.; Takahashi, A. *J. Polym. Sci: Polym. Phys. Ed.*, **1980**, 18, 2069-2076.
42. Kawaguchi, M.; Maeda, K.; Kato, T.; Takahashi, A. *Macromolecules*, **1984**, 17, 1666-1671.

43. Kawaguchi, M.; Hattori, S.; Takahashi, A.
Macromolecules, **1987**, *20*, 178-180.
44. Marques, C.; Joanny, J. F.; Leibler, L. *Macromolecules*,
1988, *21*, 4, 1051-1059.
45. Leibler, L.; Orland, H.; Wheeler, J. J. *Chem. Phys.*,
1983, *79*, 3550.
46. de Gennes, P. G. *Adv. Colloid and Interface Sci.* **1987**,
27, 189-209.
47. Rossi, G.; Cates, M. E. *Macromolecules*, **1988**, *21*, 5,
1372-1377.
48. Milner, S. T.; Witten, T. A.; Cates, M. E.
Macromolecules, **1988**, *21*, 8, 2610-2619.

CHAPTER 2

THE LONGITUDINAL ACOUSTIC MODE AS A MORPHOLOGICAL TOOL FOR SEMI-CRYSTALLINE POLYMERS

Origin of This Unusual Vibrational Mode

The Longitudinal Acoustic Mode (LAM), which can be found in the low frequency region of Raman spectra, provides a unique and sensitive morphological tool for the study of microstructural features of semi-crystalline polymers, in the spatial range of 10 to 600 Å. The ability to utilize vibrational spectroscopy to investigate long range crystalline structure, is based on the fact that the fundamental frequency (ν_1) of this vibrational mode is inversely proportional to chain length (L) as shown in Equation 1.

$$\nu_m = (m/2cL)(E_c/\rho_c)^{1/2} \quad (1)$$

This relationship was first established for a series of intense vibrations observed for a homologous series of crystalline n -paraffins C_nH_{2n+2} .^{1,2} Low frequency Raman spectra of these short-chain polymethylenes exhibited a band progression whose frequencies varied inversely and continuously as a function of chain length. The crystalline paraffin chain was approximated as a continuous thin elastic rod of length L . The frequencies, in wavenumbers (cm^{-1}), of the vibrations of the rod can then be directly related to the

single chain modulus E_c and density ρ_c . The mode order is m , and C is the speed of light.

Normal vibrational analysis subsequently established the molecular origin of this particular vibration as the symmetric, accordion-like longitudinal vibration with antinodes at the chain ends (Figure 1).³⁻⁴ Good agreement was established between the frequencies observed for the finite chains, and the calculated vibrational branch frequencies for an infinite polymethylene chain in a crystal unit cell.²⁻⁵ The observed frequencies fall on the ν_9 and ν_5 branches of the dispersion curves, calculated for the normal modes of vibration of polyethylene chains as a function of the phase difference, δ_m , between neighboring CH_2 groups. Further studies revealed that for small m ($m < n/3$) the LAM could be described essentially as C-C stretching modes, as shown in Figure 2, which have phase differences of

$$\delta_m = m \pi / n \quad (2)$$

between each of the chemical repeat units along the chain.⁵ In Equation (2) n is the number of methylene groups. The large intensity associated with this vibration for $m = 1$, can also be attributed to the exceedingly large change in polarizability. Polarized Raman measurements on oriented polyethylene confirmed that the maximum LAM intensity is obtained for the scattering component associated with the

FIG. 1 Schematic of the longitudinal acoustic mode of vibration LAM-1 for an all trans planar segment. Length of solid arrows represent the relative atomic displacements of backbone carbon atoms in an *n*-alkane.

LONGITUDINAL ACOUSTIC MODE

$$\Delta v = (m / 2 c L) (E / \rho)^{1/2}$$

$$\Phi = m \pi / N_c$$

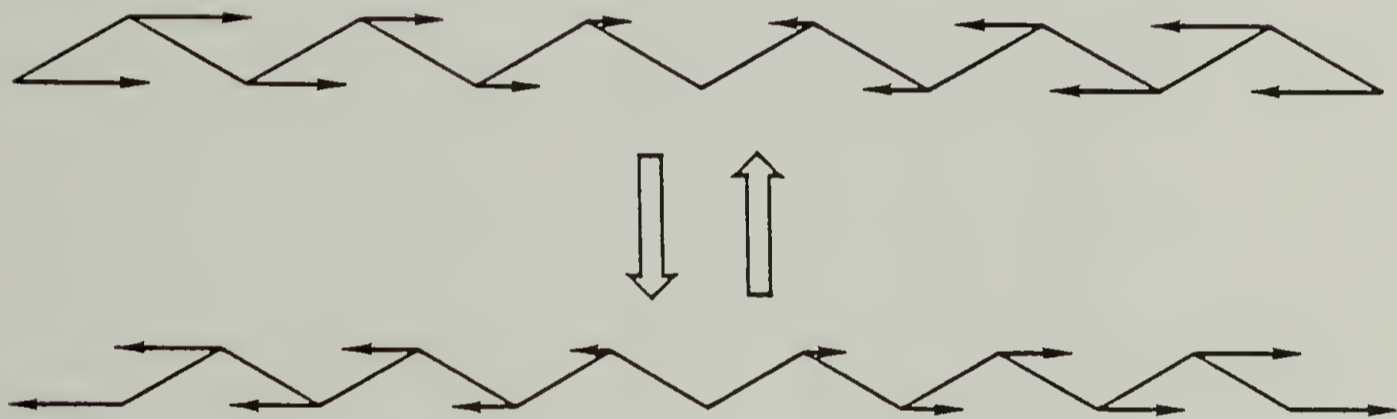


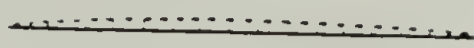
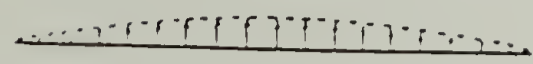
FIG. 2 Schematic representation of the contributions of CC stretching and CCC bending coordinates to the normal coordinates $v_1 - v_6$. The length of arrow is proportional to the value of the eigenvector matrix element with the CCC bending elements being scaled up by a factor of 10. This figure is adapted from reference 5.

S

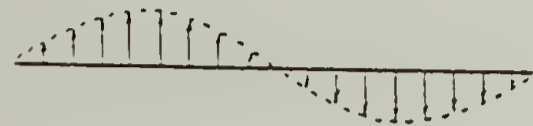
CC stretching

CCC bending

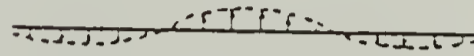
1



2



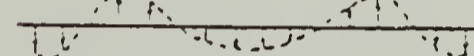
3



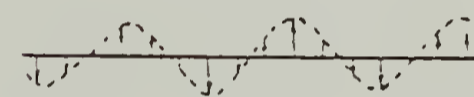
4



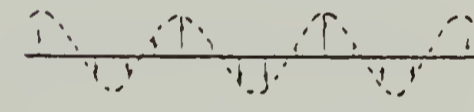
5



6



7



chain backbone. Since L is proportional to n , Equation (1) could be rewritten as

$$v_m = a (m/n) \quad (3)$$

where

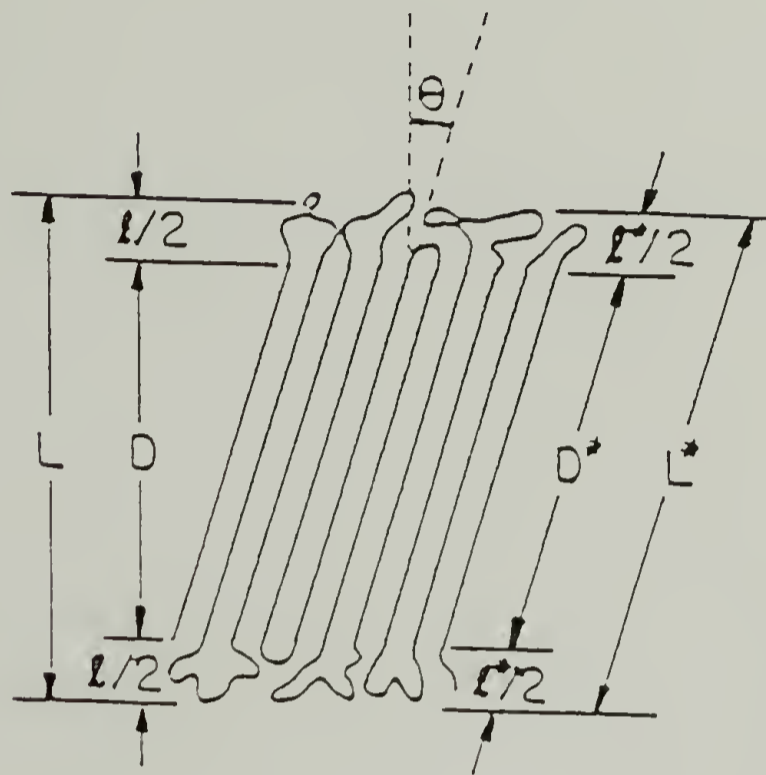
$$a = [1/\{2 c (1.275 \times 10^{-8} \text{ cm})\}] (E_c/\rho_c)^{1/2} \quad (4)$$

Additional observations indicated that this fundamental mode exists in the low frequency Raman spectra of a large number of semicrystalline polymers. These included polyethylene (PE) (single crystals^{6,7} and bulk⁸), linear aliphatic polyesters,⁷ and the helical structures of isotactic polypropylene (IPP),⁹ poly(ethylene oxides) (PEO),¹⁰ and poly(oxymethylene) (POM)¹¹. The frequency of the longitudinal acoustic mode with $m = 1$, LAM-1, is a direct measure of the length of the straight chain segment (crystal stem length) in the lamellae. This is shown schematically in Figure 3 as the crystal stem length (D^*), for a polyethylene crystal lamellae. The frequency varies inversely with the x-ray long period. This indicates that the actual straight crystal stem length is the critical parameter, and that the low frequency Raman peak could be correlated with the lamellar thickness if the tilt angle is known.

The frequency and the shape of LAM measurements can then be interpreted to represent the most probable chain length and the straight chain length distribution. Similar

FIG. 3 Representation of a polyethylene crystal lamellae depicting the tilted crystal stem and fold surface region.

SCHEMATIC DRAWING OF POLYETHYLENE CRYSTAL LAMALLAE



- $l^* / 2$ disordered fold surface
- D^* crystal stem length
- L^* long period
- θ chain tilt angle
- L apparent long period
- D apparent crystal stem length

structural information can be obtained by using wide angle or small angle scattering in conjunction with thermal analysis. The advantage of using LAM is clear, since diffraction techniques depend on long term order of the polymer system. Conversely, vibrational spectroscopy only depends on short term order or disorder. Typically, the distribution in chain lengths is sufficiently broad so that it can be obtained from the LAM bandshape without consideration of instrumental broadening, or the natural line width of the vibration. The LAM-1 will have a frequency that is sufficiently high to be resolved from the Rayleigh scattered incident light, provided that Youngs modulus (E) is large enough, and the value of the polymer density (ρ) is low enough. The exact frequency-chain length relationship can be altered by variation in temperature, end effects, and strong intermolecular interactions. In addition, the effect caused by convolution of the band with the sloping wing of the Rayleigh line must be considered.¹²⁻¹⁵

Electron microscopy and small-angle X-ray scattering (SAXS) are complementary methods for determination of long range crystal structure. These provide information on the thickness of the lamallae layer including the disordered material of the fold surface. Electron microscopy is insensitive to the presence of conformational defects in the crystal stems. For the latter, a periodic fluctuation in electron density, which requires regularity in the lamellar

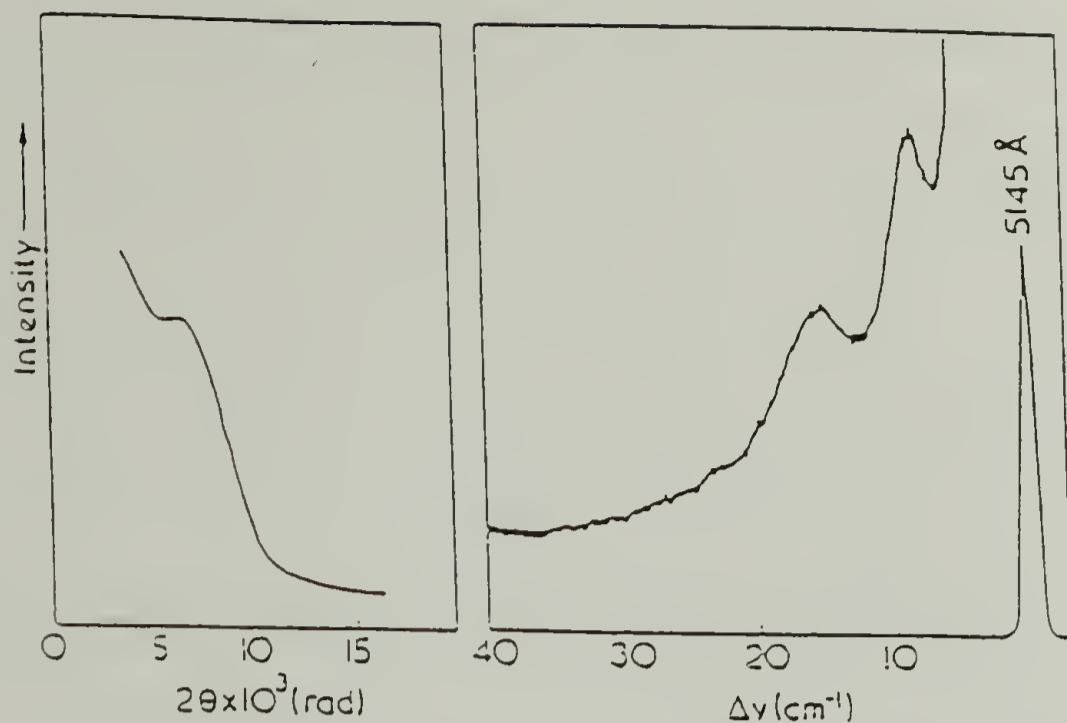
stacking, is required for the observation of a discrete maximum. An example is shown in Figure 4. This maximum is related by Bragg's law to the apparent lamellar long period(L), which is shown in Figure 3. If the chain tilt angle is established then the actual lamellar long period(L*) can be determined.

The particular sensitivity of LAM-1 to crystallization kinetics and crystal morphology is shown in Figure 4.¹⁶ The Raman spectrum exhibits a bimodal distribution of lamellar thickness which was not apparent from small angle X-ray scattering.¹⁶ The single X-ray spacing was due to a lamellae thickness representative of an average periodicity. This spacing changed, and the higher frequency LAM⁻¹ disappeared, when the sample was subjected to hot solvent treatment that dissolved the thinner lamellae.

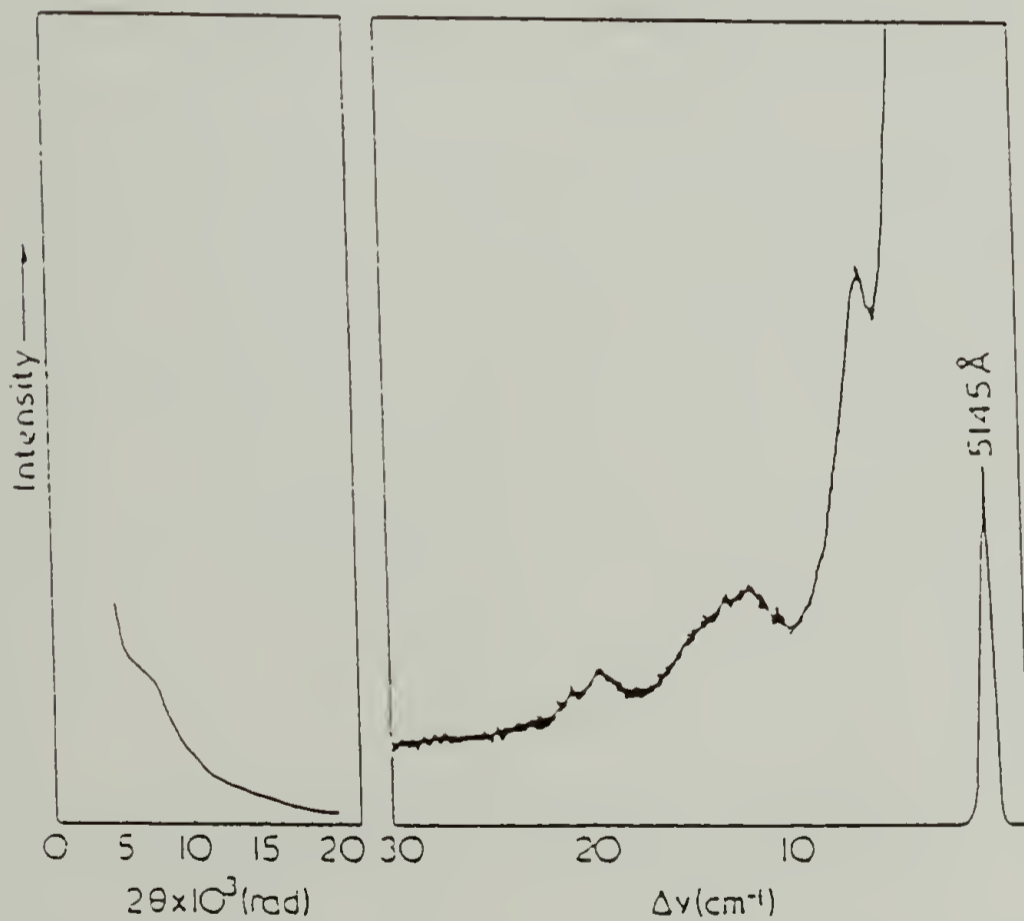
The Exact Relationship between LAM Measurements and Chain Length Distribution

Although the frequency-chain length inverse relationship for polymethylene is well characterized, quantitative analysis is still somewhat obscure, especially for helical polymers. The relation between the measured Raman intensity, after elimination of Rayleigh scattering contributions, and the true crystal stem length distribution, is shown below according to the treatment of Snyder.^{13,14} The Raman

FIG. 4 Small-angle X-ray diffraction(a), (c) and low frequency Raman(b), (d) for polyethylene.



(a) SAXD pattern and (b) Raman spectrum of isothermally crystallized bulk PE ($T_c=126^\circ\text{C}$) with one maximum in the SAXD pattern and with two LAM-1 in the Raman spectrum.



(c) SAXD pattern and (d) Raman spectrum of isothermally crystallized bulk PE ($T_c=127.9^\circ\text{C}$) with one maximum in the SAXD pattern and with two LAM-1 and a weak LAM-3 in the Raman spectrum.

intensity for a particular scattering geometry G from a molecule M , can be expressed as

$$I(M,k,G) \propto [(v_0 - v_{M,k})^4 / v_{M,k} B(v_{M,k},T)] S(M,k,G) \quad (5)$$

where $S(M,k,G)$ is the Raman scattering activity, v_0 is the excitation frequency, which is much greater than $v_{M,k}$ which is the k th mode frequency and

$$B(v_{M,k},T) = 1 - \exp(-h c v_{M,k} / k_B T) \quad (6)$$

is the Boltzmann factor resulting from considering the relative population of the low lying vibrational states. Here k_B is the Boltzmann constant, T the sample temperature and h is Planck's constant.

The Raman scattering activity, $S(M,k,G)$, is proportional to the square of the polarizability derivative, $[\alpha'(n,k,cc)]^2$, for a molecule M with scattering geometry cc . In this geometry the polarization of the incident light is parallel to that of the scattered light, and both are parallel to the chain axis. If $n \gg k$ and k is odd then $[\alpha'(n,k,cc)]^2$ is proportional to $1/n^2$. Therefore, the Raman intensity is inversely proportional to both the Boltzmann factor and the mode frequency or

$$I(n,k) \propto C_1 / [v_{M,k} B(v_{M,k},T) n] \quad (7)$$

If the chain is unperturbed by intermolecular effects and has a length much greater than the chemical repeat unit, as is the case for polyethylene, then

$$v (LAM-k) = (k/2cL) (E/\rho)^{1/2} \quad (8)$$

and, since v is proportional to $1/n$, where $L \cong 1.27(n)$, then

$$I(n,k) \propto C'_1 / k B(v_{M,k}, T) \quad (9)$$

For N_n molecules, where N_n is defined as the number of molecules with n chemical repeat units, the total intensity can then be expressed as

$$I^T(n) \propto C'_1 N_n / B(v_n, T) \quad (10)$$

Thus the total intensity is directly proportional to the number of molecules in the scattering volume and is inversely proportional to the Boltzmann factor.

Let $f(n) = N_n / \sum_i N_i$ be the mole fraction of chains with n segments. This distribution function can be related to the theoretical Raman intensity of LAM-1 through

$$f(n) \propto B(v_{M,k}, T) I^T(n) \quad (11)$$

without including the normalization factor $\sum_i N_i$. The mole fraction can then be expressed in terms of the observed intensity (I_V) of the LAM-1 band, through the equation for a long elastic rod. Since $L \cong 1.27(n)$, and Equation (8) suggests that v and n are reciprocally related, then

$$(\partial n / \partial v) \propto v^{-2} \quad (12)$$

The total intensity in terms of the observed intensity I_v at frequency v , is

$$I^T(n) = \int I_v dv \quad (13)$$

and therefore

$$I^T(n) \propto \int I_v v^2 dn \quad (14)$$

Finally, the distribution function in terms of the observed Raman intensity is

$$f(n) \propto B(v,T) v^2 I_v \propto v [\alpha' (n,k,cc)]^2 \quad (15)$$

For a continuous distribution of straight chain segments this function is therefore the observed LAM intensity weighted by the Boltzmann factor and the square of the frequency (v^2). Furthermore, the distribution function in terms of the number of chains of n segments, can be expressed in terms of the scattering activity, which itself can be expressed in terms of the observed intensity (I_v) as

$$[\alpha' (n,k,cc)]^2 \propto (I_v)(v) B(v,T) \quad (16)$$

The LAM bands of polymers are therefore composite bands made up of a continuum of overlapping components associated with different crystal stem lengths. This derivation shows that the band maximum cannot be directly correlated to the most probable chain length in the chain length distribution.¹³

The two distribution functions, one in the frequency space and the other in chain length, will have a net offset with an apparent shift toward higher frequency. This offset will also be exaggerated by a broad band shape.¹⁴

Transformation of the LAM band to the chain length distribution function is not perturbed by the inherent bandwidth of LAM. The LAM-1 halfwidth decreases linearly with the reciprocal of the chain length to a value of about 1.5 cm^{-1} .³⁶ For polyethylene the following relationship is applicable, based upon the known values for the elastic constant and density.

$$\nu = 3093 / L \quad (17)$$

where the length L is in Angstrom units.

The intensity of LAM-1 from a unit volume of polymer is then

$$I^T = K \sum_n (\nu_0 - \nu_n)^4 N_n S_n / \nu_n B(\nu_n, T) \quad (18)$$

where N_n is the number of straight chains having n repeat units and I^T is the $\sum I^T(n)$ from individual chains of n chemical repeats. Then the total intensity is

$$I^T = K' \sum_n N_n (b/L_n) / \nu_n B(\nu_n, T) \quad (19)$$

$$= K' \sum_n N_n (b/L_n) / (a/L_n) B(\nu_n, T) \quad (20)$$

$$= K'' \sum_n N_n B(\nu_n, T)^{-1} \quad (21)$$

At room temperature, for a typical lamellar thickness (100Å), the Boltzmann factor can be approximated as

$$B(\nu_n, T) \cong h c \nu_n / k_B T \quad (22)$$

and thus the total intensity is related to frequency by

$$I^T = K''' \sum_n N_n \nu_n^{-1} \quad (23)$$

If L_T is the total length of straight chains in the scattering volume then

$$L_T = \sum_n N_n L_n \quad (24)$$

where L_n is proportional to ν_n^{-1} . The observed integrated intensity is then

$$I^T \cong K''' L_T \quad (25)$$

It is therefore proportional to the total length of straight chain segments, and thus is sensitive to the crystallinity of the sample.

Perturbing Effects on the LAM Measurements

The LAM-1 mode is a normal mode of vibration which involves the simultaneous motion of all atoms of the entire straight chain segment. Its intensity, frequency, and in fact, shape, are greatly influenced by the existence of conformational defects.^{15,17-22} The origins of the LAM-1 vibration, and the associated atomic motions, have been well

established for n-alkanes and polyethylene.^{2-5,19,23-29} The characteristics of the LAM vibrations observed for other types of semi-crystalline polymers, however, are not nearly as well understood, and thus necessitate further study. In particular, the limits for applying the inverse frequency vs. chain length relationship, fit to the longitudinal acoustic vibration of a long elastic rod, are not known for semi-crystalline polymers.

An important perturbing factor may be the effect of interchain interactions. These are present as a result of the occurrence of functional groups, both as an integral part of the backbone structure and as regularly spaced pendant side groups. Such lateral interchain interactions may result in significant perturbing forces which could have a profound effect on the LAM vibration. The concept of an isolated crystalline chain undergoing bond stretching and valence angle bending, in a cooperative manner over the entire crystal stem length, while being decoupled from the next chain by folds at the crystalline-amorphous interface, may also be invalid. In fact, decoupled chains are not even strictly valid for n-paraffins, since the observed LAM-1 are consistently higher than the corresponding calculated frequencies because of the existence of interlamellar couplings.^{5,28} Although intermolecular interactions and packing effects have been shown in the past to have a small effect upon the LAM vibration for polyethylene, nevertheless,

end effects can clearly be observed.³⁰⁻³⁹ Differences in methyl end group packing in *n*-paraffins, which especially for shorter homologs results in differing interlamellar (longitudinal) forces, can increase the unperturbed (decoupled chain) frequency by several cm^{-1} .³³⁻³⁶

The influence of unrestricted mass and force perturbations at the ends of an isolated composite rod were shown to satisfactorily account for the observed frequencies for *n*-paraffins, perfluoro *n*-alkanes and monodisperse methylene-oxyethylene-methylene triblock oligomers.^{30-32,39} The former study resolved the discrepancy between the values of E_c obtained from LAM-1 and X-ray diffraction. In polyethylene, both longitudinal forces acting at the crystalline chain ends and fold surface mass perturbations, arise from the existence of an interfacial boundary region contiguous with the crystalline zone. These result in corrections to the classical theory for an unperturbed rod.^{30-32,35-37}

The role of intermolecular interactions may play an even larger role for helical polymers. For these structures, the observed LAM-1 frequency is significantly higher (about 60% for isotactic polypropylene)⁹ than that expected from observed or calculated values of E_c and measured SAXS spacings.⁹⁻¹¹ The atomic motions in the LAM are not required to be strictly parallel to the chain axis, as is the case for transplanar structures. Torsional modes will contribute to

the LAM-1, and as a result the atomic motions will contain radial components. The modulus of the single helical chain is dominated by torsional motions, so perturbing forces arising from a composite rod will be significant.³⁰ The influence of transverse forces arising from lateral interactions and geometric effects may produce additional perturbations on the LAM motion.^{33,40} It seems reasonable now that the model using an unperturbed elastic rod, may have to be considered as an exception to the rule when evaluating LAM observed for other semi-crystalline polymers.

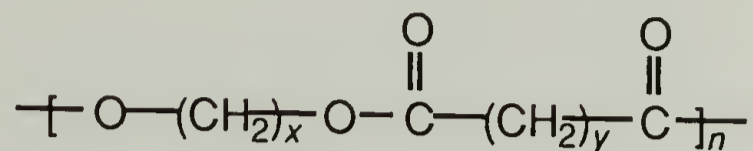
For most cases, contributions from physical effects such as packing and asymmetric mass placement^{27-29,34,41,42} and chemical differences which affect intermolecular interactions, could greatly perturb the LAM vibration.^{38,43} Substantially longer repeat lengths which dictate greater inertial effects from fold structures may also be a factor. In the later studies, hydrogen bonding interactions at chain ends of stearyl alcohol ($n\text{-C}_{18}\text{H}_{37}\text{OH}$)³⁸ and α,ω -dicarboxylic acids,⁴³ resulted in observed shifts in the LAM-1 frequency to values higher and lower respectively, than anticipated when expected mass effects were considered.

Linear Aliphatic Polyesters as a Model to Define Influence of Intermolecular Effects

An investigation of the low frequency Raman region for a series of linear aliphatic polyesters has been undertaken in

order to attempt to determine the exact nature of the LAM vibrations for this class of semi-crystalline polymers.

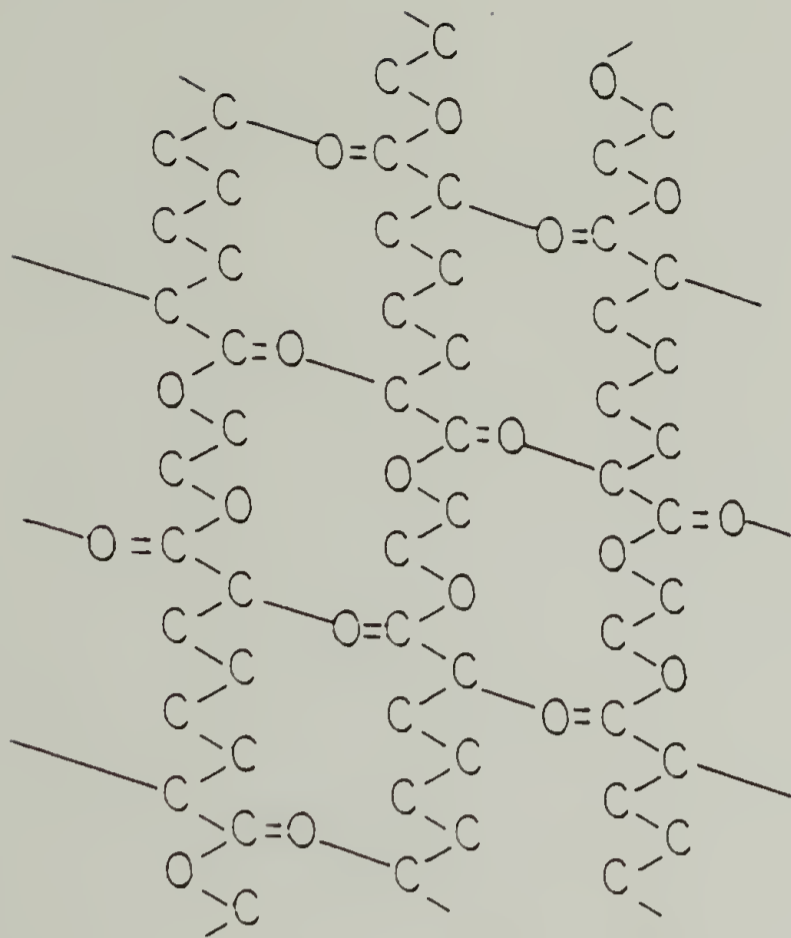
These polyesters have a chemical structure represented as



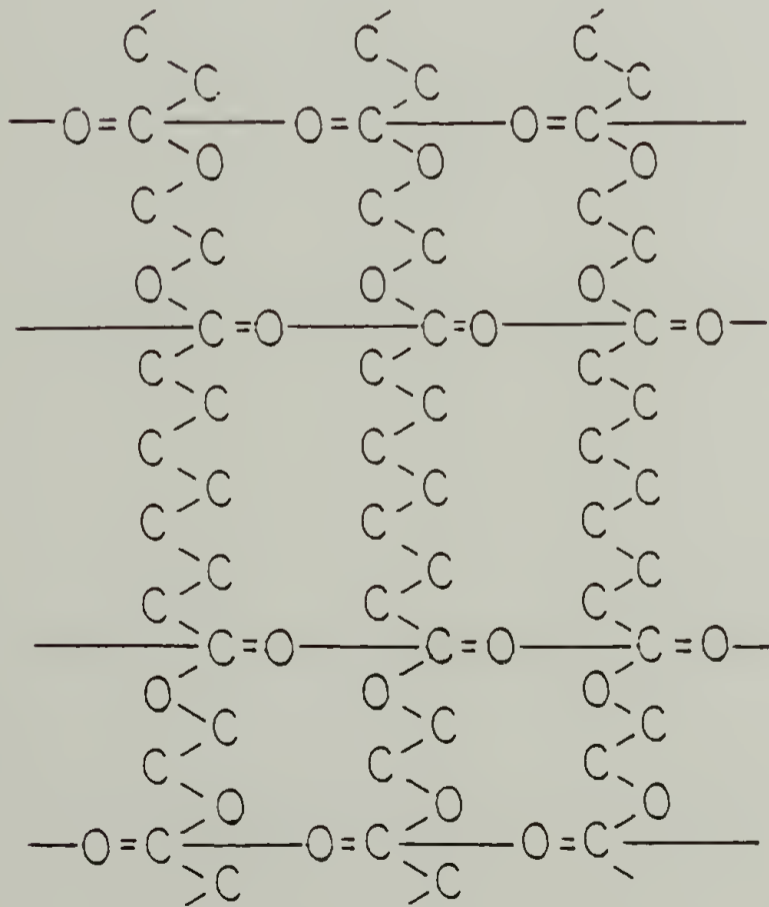
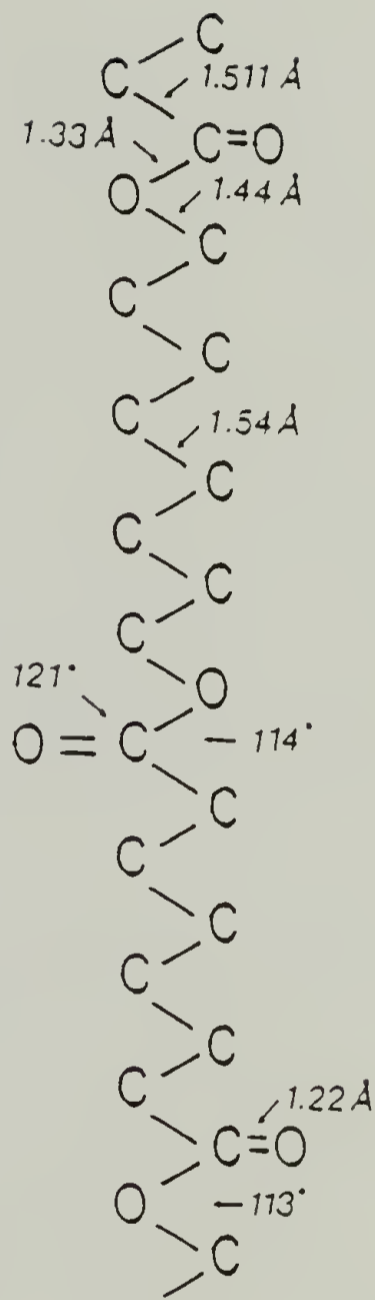
where the diol group is comprised of (x) methylene linkages and the acid group with (y) methylene linkages. Polyester chains of sufficiently high (x) and (y) have been shown by fiber x-ray studies to have essentially a planar zig-zag conformation in the crystalline regions, as found for polyethylene.⁴⁴⁻⁴⁶ The ester group is only slightly out of the plane defined by the methylene backbone. The structural parameters for the planar zig-zag conformation, with the condition that the number of methylene sequences in the diol group is greater than or equal to (2), and in the acid group is greater than (4), are very similar to polyethylene. The parameters which differ, as shown in Figure 5, are the bond lengths of the C-C bond connected to the C=O and the C-O bonds, and the bond angles which involve the carbon of the carbonyl group. Based on their structures it would be expected that the LAM modes, if they can be found, would be similar to those observed for polyethylene.

These polyesters, however, have one significant structural difference as compared to polyethylene. This is due to the presence of a large off axis mass relative to the

FIG. 5 Structural parameters for the planar zig-zag conformation in the crystalline region of linear aliphatic polyesters(right) and lateral packing of planar chains (top) and (bottom). Polyesters can crystallize in two crystallographic forms, orthorhombic(bottom) and monoclinic(top). The staggering of chains in the even-even polyester occurs in the $\{0\ k\ 0\}$ planes.



STRUCTURE OF EVEN-EVEN POLYESTER



STRUCTURE OF EVEN-ODD POLYESTER

backbone, which arises from the regularly spaced carbonyl groups in the chemical structure. In addition there is an odd-even effect on the placement of these groups with respect to the chain axis. As shown in Figure 5, aliphatic polyesters with an even number of methylene units in both functional groups will have neighboring carbonyls alternating sides of the backbone. Those with an odd number in either the acid or diol group will have carbonyls alternating sides of the backbone in pairs, while those with an odd number of methylene units in both functional groups will have carbonyls on only one side of the backbone structure. In all these cases the ester linkages are regularly spaced along the chain backbone. Polyesters therefore allow examination of the perturbing effects due to "asymmetric" chain structures, and of well defined intermolecular effects.

A series of linear aliphatic polyesters from (x=5, y=8) to (x=10, y=16) were available. These polyesters were synthesized⁴⁷ from appropriate glycols and dibasic acid dimethyl (or diethyl) esters by ester exchange. The number-average molecular weights (M_n) of the polyesters used for single crystal formation were in the range of 12,000 to 13,000. The samples were purified by repeated precipitation and M_n values were estimated by vapor-pressure osmometry. Details of the preparations and characterization are given elsewhere.⁴⁴ Single crystals with a range of lamellae thicknesses, can be prepared by crystallization in dilute

solution at various undercoolings, from solvents such as 2-butyl alcohol, 2-hexyl alcohol and iso-pentyl acetate.^{44,47} Sections of crystal mats grown from dilute solution were utilized for investigations in the very low frequency region of the Raman spectrum, and for both small and wide angle X-ray scattering (SAXS, WAXS) studies.

A series of experiments in which the supercooling conditions were varied, but in a manner such that the growth, isolation and collection for each temperature could be assured of being accomplished under isothermal conditions was effected. Annealing of the single crystal mats was carried out at various temperatures and durations of time. This was necessary in order to establish which of the multiple bands, exhibited in the low frequency region of the Raman spectra, were sensitive to crystal core thickness or straight chain stem length. The manner in which the crystal thickness increases (stepwise or continuous) and the overall magnitude, enabled determination of the macroscopic crystal structure.

References

1. Mizushima, S. I.; Shimanouchi T. *J. Am. Chem. Soc.*, **1949**, 71, 1320.
2. Schaufele, R. F.; Shimanouchi, T. *J. Chem. Phys.*, **1967**, 47, 3605.
3. Tasumi, M.; Shimanouchi, T. *J. Chem. Phys.*, **1965**, 43, 1245.
4. Tasumi, M.; Krimm, S. *J. Chem. Phys.*, **1967**, 46, 755.
5. Shimanouchi, T.; Tasumi, M. *Indian J. Pure Appl. Phys.*, **1971**, 9, 958.
6. Peticolas, W. L.; Hibler, G. W.; Lippert, J. L.; Peterlin, A.; Olf, H. *Appl. Phys. Lett.*, **1971**, 18, 87.
7. Folkes, M. J.; Keller, A.; Stejny, J.; Goggin, P. L.; Fraser, G. V.; Hendra, P. J. *Colloid Polym. Sci.*, **1975**, 253, 354.
8. Olf, H. G.; Peterlin, A.; Peticolas, W. L. *J. Polym. Sci.: Polym. Phys. Ed.*, **1974**, 12, 359.
9. Hsu, S. L.; Krimm, S.; Krause, S.; Yeh, G. S. Y. *J. Polym. Sci.: Polym. Lett. Ed.*, **1976**, 14, 195.
10. Hartley, A.; Leung, Y. K.; Booth, C.; Shepherd, I. W. *Polymer*, **1976**, 17, 354.
11. Rabolt, J. F.; Fanconi, B. *J. Polym. Sci.: Polym. Lett. Ed.*, **1977**, 15, 121.
12. Woodward, L. A.; Long, D. A. *Trans. Faraday Soc.*, **1949**, 45, 1131.

13. Snyder, R. G.; Krause, S. J.; Scherer, J. R. *J. Polym. Sci.: Polym. Phys. Ed.*, **1978**, *16*, 1593.
14. Snyder, R. G.; Scherer, J. R. *J. Polym. Sci.: Polym. Phys. Ed.*, **1980**, *18*, 421.
15. Koenig, J. L.; Tabb, D. L. *J. Macromol. Sci. Phys.*, **1974**, *B9*, 141.
16. Dlugosz, J.; Fraser, G. V.; Grubb, D.; Keller, A.; Odell, J. A.; Goggin, P. L. *Polymer*, **1976**, *17*, 471.
17. Fraser, G. V.; Hendra, P. J.; Cudby, M. E. A.; Willis, H. A. *J. Mater. Sci.*, **1974**, *9*, 1270.
18. Reneker, D. H. *J. Polym. Sci.*, **1962**, *59*, S39.
19. Reneker, D. H.; Fanconi, B. *J. Appl. Phys.*, **1975**, *46*, 4144.
20. Wang, Y. K.; Waldman, D. A.; Stein, R. S.; Hsu, S. L. *J. Appl. Phys.*, **1982**, *53*, 10, 6591.
21. Wang, Y. K.; Waldman, D. A.; Lasch, J. E.; Stein, R. S.; Hsu, S. L. *Macromolecules*, **1982**, *15*, 1452.
22. Strobl, G. R.; Eckel, R. *Colloid & Polym. Sci.*, **1980**, *258*, 570.
23. Takeuchi, H.; Shimanouchi, T.; Tasumi, M.; Vergoten, G.; Fleury, G. *Chem. Phys. Lett.*, **1974**, *28*, 449.
24. Wu C.; Nicol, M. J. *Chem. Phys.*, **1973**, *58*, 11, 5150.
25. Scherer J. R.; Snyder, R. J. *J. Chem. Phys.*, **1980**, *72*, 11, 5798.
26. Fanconi, B.; Crissman, J. *J. Polym. Sci.: Polym. Lett. Ed.*, **1975**, *13*, 421.

27. Mazur J.; Fanconi, B. *J. Chem. Phys.*, **1979**, 71, 5069.
28. Jakes, J.; Krimm, S. *Macromolecules*, **1971**, 4, 605.
29. Chang, C.; Krimm, S. *J. Appl. Phys.*, **1983**, 54, 10, 5526.
30. Hsu, S. L.; Krimm, S. *J. Appl. Phys.*, **1976**, 47, 4265.
31. Hsu, S. L.; Krimm, S. *J. Appl. Phys.*, **1977**, 48, 4013.
32. Hsu, S. L.; Ford, G. W.; Krimm, S. *J. Polym. Sci.: Polym. Phys. Ed.*, **1977**, 15, 1769.
33. Chang, C.; Krimm, S. *J. Polym. Sci.: Polym. Phys. Ed.*, **1979**, 17, 2163.
34. Khoury, F.; Fanconi, B.; Barnes, J. D.; Bolz, L. H. *J. Chem. Phys.*, **1973**, 59, 5849.
35. Strobl, G. R.; Eckel, R. *J. Polym. Sci.: Polym. Phys. Ed.*, **1976**, 14, 913.
36. Glotin, M.; Mandelkern, L. *J. Polym. Sci.: Polym. Phys. Ed.*, **1983**, 21, 29.
37. Fraser, G. V. *Ind. Journ. Pure & Appl. Phys.*, **1978**, 16, 344.
38. Rabolt, J. F.; *J. Polym. Sci.: Polym. Phys. Ed.*, **1979**, 17, 1457.
39. Swales, T. G. E.; Teo, H. H.; Domszy, R. C.; Viras, K.; King, T. A.; Booth, C. *J. Polym. Sci.: Polym. Phys. Ed.*, **1983**, 21, 1501.
40. Chang, C.; Krimm, S. *J. Polym. Sci.: Polym. Phys. Ed.*, **1984**, 22, 1871.
41. Olf, H. G.; Fanconi, B. *J. Chem. Phys.*, **1973**, 59, 1, 534.

42. Barnes, J. D.; Fanconi, B. M. *J. Chem. Phys.*, **1972**, *56*, 5190.
43. Minoni, G.; Zerbi, G. **1982**, *22*, 3654.
44. T. Kanamoto, T. Tanaka, and H. Nagai, *J. Polym. Sci.*, **1971**, *A2*, **9**, 2043.
45. C.S. Fuller and C.J. Frosch, *J. Am. Chem. Soc.*, **1939**, *61*, 2575.
46. Y. Chatani, Y. Okita, H. Tadakoro, and Y. Yamashita, *Polym. J.*, **1970**, *1*, 555.
47. T. Kanamoto, *J. Polym. Sci.: Polym. Phys. Ed.*, **1974**, *12*, 2535.

CHAPTER 3

CHARACTERIZATION OF LINEAR ALIPHATIC POLYESTER SINGLE CRYSTALS

Background

All of the studies reported here were carried out on polyesters prepared directly from dilute solution grown single crystals [0.05% in iso amyl acetate ($\text{CH}_3\text{COOC}_5\text{H}_{11}$)]. The crystals were grown by the self seeding method at well defined temperatures (± 1.0 °C). Sections of crystal mats were annealed. The Raman spectroscopic method was used in conjunction with both small-angle and wide-angle x-ray diffraction methods, in addition to thermal analysis. The LAM technique is a unique morphological method utilized to obtain microstructural information which cannot be obtained by other means. Conversely, the LAM observed for polyesters has clarified the molecular motions giving rise to this unusual vibration.

Preparation and Characterization of Crystalline Mats

Dilute Solution Crystallization

The dissolution temperatures of various polyesters in several solvents were established by a light scattering technique. This was accomplished by passing an Argon ion laser (514.5 nm), at an output level of 100 mW, through a 25

ml aliquot of the solution. The throughput, determined by the amount of scattering, was monitored with a Coherent model 210 power meter accurate to ± 2.5 mW. For accurate and stable temperature control the solution had been placed in an ethylene glycol/water bath, which was maintained in a Haake model A81 proportionally controlled heater/cooler circulator. The bath temperature was monitored with a built in Platinum thermocouple and digital readout accurate to ± 0.1 °C. Typically the laser throughput was on the order of only 10 % until the temperature was within 2.0 °C of the dissolution temperature (T_{dis}), at which point it had risen to 50 %. At this point the temperature was increased more slowly (1.0 °C/20 min), and the throughput rose quickly over the less than 2.0 °C interval until it reached over 95 % at T_{dis} . The dissolution temperatures (T_{dis}) and bulk melting points (T_m) determined for the linear aliphatic polyesters in this study are listed in Table 1. These polyester samples were available, courtesy of Kanomato's group.

For each polyester, the temperature of the solution to be used for crystallization would then be increased an additional 10 °C above T_{dis} . It was held at that temperature for a minimum of 30 minutes, in order to insure that the largest nuclei were dissolved. This solution, homogeneous by the above detection means, was subsequently placed in the temperature controlled bath at the preset and equilibrated value. This temperature was that chosen for the particular

TABLE 1 Crystallization conditions for growth of linear aliphatic polyester single crystals. T_M is the bulk melting temperature, T_D the dissolution temperature, T_{CRY} the crystallization temperature, ΔT the degrees of undercooling, and the solvent is iso amyl acetate($CH_3COOC_5H_{11}$). These represent typical growth conditions for the single crystals studied.

TABLE 1

Crystallization Conditions For Growth Of
Polyester Single Crystals

Polyester	T _M (°C)	BULK	SOLVENT	T _{DIS} (°C)	T _{CRY} (°C)	ΔT (°C)
10-8	76.6	(0.6)	i-AA	52.0	39.0	13.0
10-8			i-AA	52.0	33.0	19.0
10-16	89.0	(0.5)	i-AA	62.0	39.0	23.0
9-8	69.3	(0.3)	i-AA	46.0	33.0	13.0
9-8			i-AA	46.0	27.0	19.0
6-8	61.8	(0.4)	i-AA	40.5		

isothermal crystallization conditions required to achieve the desired degree of supercooling. The length of a critically sized nucleus is inversely proportional to the degree of supercooling.¹ The respective crystallization temperatures, T_{cry} , and values for degrees of undercooling, ΔT , are listed in Table 1 for the linear aliphatic polyesters studied.

Typically the solution was maintained at the respective crystallization temperature ($T_{\text{cry}} \pm 0.1$ °C) for a period of 5 days. Isothermally grown crystals usually appeared over a period of 12 to 48 hours. After 5 days of isothermal conditions solvent was carefully removed from the solution by pipette, without disturbance of the crystals precipitated at the flask bottom. The crystallization solution could then be separated into 50 ml testtubes, which were still maintained at T_{cry} . The single crystals in these were allowed to settle so that they would be isolated at the bottom. Additional solution was removed from each testtube, until there remained less than 10 ml of solution in each. This process was carried out in order to insure that collection of the crystals, by suction filtration, could be accomplished quickly so that the collection temperature would be close to T_{cry} . The number of uncrystallizable elements able to participate in the crystallization process decreases with time.² The solution being filtered was about 10 times more concentrated than during crystallization, making diffusion to the actively growing crystal sites more difficult. The free

energy of activation, ΔG_{η} , which governs short distance diffusion of the crystallizing element across the phase boundary, increases with decreasing temperature.² Thus any crystallization that may have occurred during the filtration process at potentially higher supercoolings, would have been negligible relative to the fraction crystallized at the well controlled T_{cry} . Collection was carried out by filtration with a millipore filter vacuum suction setup, using teflon (pore size 0.5μ) filters. The typical time for filtering was about 2 minutes per tube. Rinsing of the crystal mat was done with fresh solvent, which had first been heated to the crystallization temperature. Drying of the crystal mats was done in a vacuum oven at room temperature for a period of 60 hours. The crystal mats were left on the filter paper during the drying. Dimensions of the crystal mats were typically 15 mm in diameter, and less than 0.5 mm in thickness. Sections of these mats, as well as those grown at higher temperatures, were used for structural characterization by DSC, SAXS, and Raman spectroscopy.

Crystallizations at the higher temperatures or smaller degree of supercoolings, listed in Table 1 for Polyesters 10,8 and 9,8, could not be accomplished without using the self-seeding technique of Blundell.³⁻⁵ This was done by pre-crystallization at a lower crystallization temperature for 36 hours, and then using these crystals as nuclei templates. Thus the single crystal solution, obtained at the lower T_{cry} ,

was heated slowly (1.0 °C/20 min) to the predetermined T_{dis} , and then heated an additional 10 °C and maintained at that temperature for 1 hour. The degree of heating above the determined T_{dis} is known to affect the kinetics of crystallization since the number of surviving nuclei will vary. Isothermal crystallization, through self-nucleated crystal growth, was then carried out by quenching this solution to the higher desired T_{cry} and maintaining this temperature with the above temperature controlled bath for a period of at least 5 days. For polyester 10-8 the higher T_{cry} was 39.0 °C ($\Delta T = 13.0$ °C), and for polyester 9-8, which had a T_{dis} of 46.0 °C, the higher T_{cry} was 33.0 °C ($\Delta T = 13.0$ °C).

Annealing of Crystal Mats

Annealing of sections of prepared single crystal mats was accomplished by first sealing sections in disposable pipettes, and then placing the pipettes in water filled test tubes suspended in the above temperature controlled bath. In this manner annealing conditions could be easily and accurately varied and/or maintained for specific time intervals. Quenching from the annealed state was done either in cold air or ice water. Unless otherwise noted, a section of a single crystal mat was annealed for 2 hour intervals at increasingly higher temperatures. After annealing at each of these temperatures, starting at the lowest, the sample was quenched and the Raman spectrum was obtained. Under these

annealing conditions, the uncertainty normally associated with sample history is not a factor.

Characterization Experimental

Small-angle X-ray scattering(SAXS) data was obtained at room temperature, on a Statton camera(unless otherwise noted), using nickel filtered Cu K α radiation, with wavelength of 1.5418 Å. The sample to detector distance(L) was 313.2 mm. Film, in stacks of three, was used for detection, with exposure times of about 8 hours for each sample. Sections of crystal mats were positioned so that the mat plane was perpendicular to the radiation. Braggs's law was used to obtain the long spacings, according to

$$m \lambda = 2 d \sin \theta \quad (27)$$

where

$$\theta = 1/2 [\tan^{-1} (X/L)] \quad (28)$$

for X being the measured reflection spacing. Thus d may be defined as

$$d = m \lambda / [\sin (\tan^{-1} (X/L))] \quad (29)$$

Additional SAXS data were obtained with a Rigaku Denki instrument with a recording diffractometer. Four thousand counts were taken at each angle with an increment step of 1 minute. The data was Lorentz corrected.

Raman spectra were obtained with a Jobin Yvon HG.2S Ramanor double monochrometer, equipped with a Jobin Yvon controller, concave holographic gratings, and a Spectra Physics 165 argon ion laser operated at 514.5 nm at an output level so that 100 mW impinged upon the sample. Slit settings of 4 by 120 μm were typically used, corresponding to about 1.5 cm^{-1} bandpass. This setting was chosen to maximize stray light rejection while still maintaining sufficient throughput to obtain spectra with good signal to noise(S/N) ratios. Spectra were generally obtained at room temperature, but certain samples were also studied at lower temperatures by using a Harney-Miller cell cooled by chilled nitrogen gas.

A Cromenco System Three microcomputer with an added Cromenco Tuart board was used to control wavenumber scanning and to record digital intensity values. The spectral signal was detected by a RCA C31034 photomultiplier in a cooled housing(Products for Research model TE 104 TS-RF). The PMT signal was processed by a PAR 1120 amplifier-discriminator, before passing to a PAR 1105 analog ratemeter and then to an analog strip chart recorder. Simultaneously the PAR 1105 provided a digital pulse for each photon, enabling photon counting by a Canberra model 1773 digital scaler. The spectra were run at slow scan speeds(0.05 $\text{cm}^{-1}/\text{sec}$) with a step resolution of 0.2 cm^{-1} in order to achieve good S/N. Raman data were then transferred via a RS-232 serial port to either a Nicolet 7199 FT-IR system or to an IBM System 9000

microcomputer for further analysis. All the necessary software were developed.

A Perkin-Elmer DSC-7 differential scanning calorimeter was used to study melting behavior. The temperature scale was calibrated using Indium. Sections of the same crystal mats used for Raman spectroscopy were used for DSC. The reported thermograms were recorded at a heating rate of either 2.5 or 10.0 °C/minute.

Results and Discussion

Previous Studies

Comprehensive X-ray diffraction studies on highly oriented cold drawn fibers, of moderate molecular weight (10K to 18K) linear aliphatic polyesters, were first carried out by Fuller, Erickson and Frosch in the late thirties.⁶⁻⁸ It was noted that the crystal structures for polyesters of ethylene glycols differed depending upon the number of methylene units in the acid group. In all cases the chain molecules were arranged parallel to the fiber axis and had essentially a planar zig-zag type backbone structure. The measured densities showed that each unit cell contained 2 chains. The interplanar spacings parallel to the fiber axis were very close to those deduced for the paraffin C₂₉H₆₀ so the cell dimensions are determined by the hydrocarbon part of the chain. The difference between the observed period and that calculated from the chemical repeat (C-C = 1.54 Å, C-O =

1.43Å), however, was such that the backbone could not be fully planar. For the odd esters, the chains were arranged so that repeating units line up with terminating and median carbonyl groups in planes perpendicular to the fiber axis(orthorhombic). In even esters, although ester groups are in horizontal planes they are packed inclined to the fiber axis(monoclinic).

A further study⁸ on the decamethylene glycol series, also of moderate molecular weight, up through poly(decamethylene sebacate), or polyester 10-8, showed that the observed and calculated(based on planar zig-zag) fiber periods agreed within 0.3 Å. In this case, however, it was determined that the odd esters(10-3 and 10-7) had reflections of large spacings that arose from planes inclined to the fiber axis. Thus in some chains the carbonyl groups are located in planes inclined to the fiber axis(40° for 10-3 and 49° for 10-7). This was the first evidence of polymorphism (orthorhombic and monoclinic) in the same transplanar linear aliphatic polyester. Evidence of more than one crystal phase was also present for the even esters(10-4 and 10-6) and in a study by Girolamo et al.⁹ for polyester (6,10). The differences in these crystal arrangements were attributed to a relative shift along the chain axis in either the bc or ac plane. Polymorphism was particularly evident for the decamethylene glycol series due to a dilution of the polar

ester groups, thereby resulting in a lowering of the energy between different crystal forms.¹⁰

Wide and small angle X-ray studies of sedimented crystal mats for aliphatic polyesters (4,10), (6,10), and (10,10) by Girolamo et al.⁹, and (6,8) and (10-16) by Kanamoto et al.¹¹ demonstrated that the chains are perpendicular to the lamellar surface. It was concluded, however, that two different structures of polyester lamellae existed for the former series depending upon the chemical composition (length of glycol). Based upon both fiber and single crystal mat studies it is generally accepted that the chain axis is perpendicular to the lamellar surface regardless of the crystal packing. Morphological studies by Kanamoto et al.¹¹ showed that with increasing methylene sequence length in the chemical repeat units these polyesters crystallized with more regular morphology. The crystals generally were true or truncated lozenges, with the hollow pyramidal structure characteristic of polyethylene single crystals.

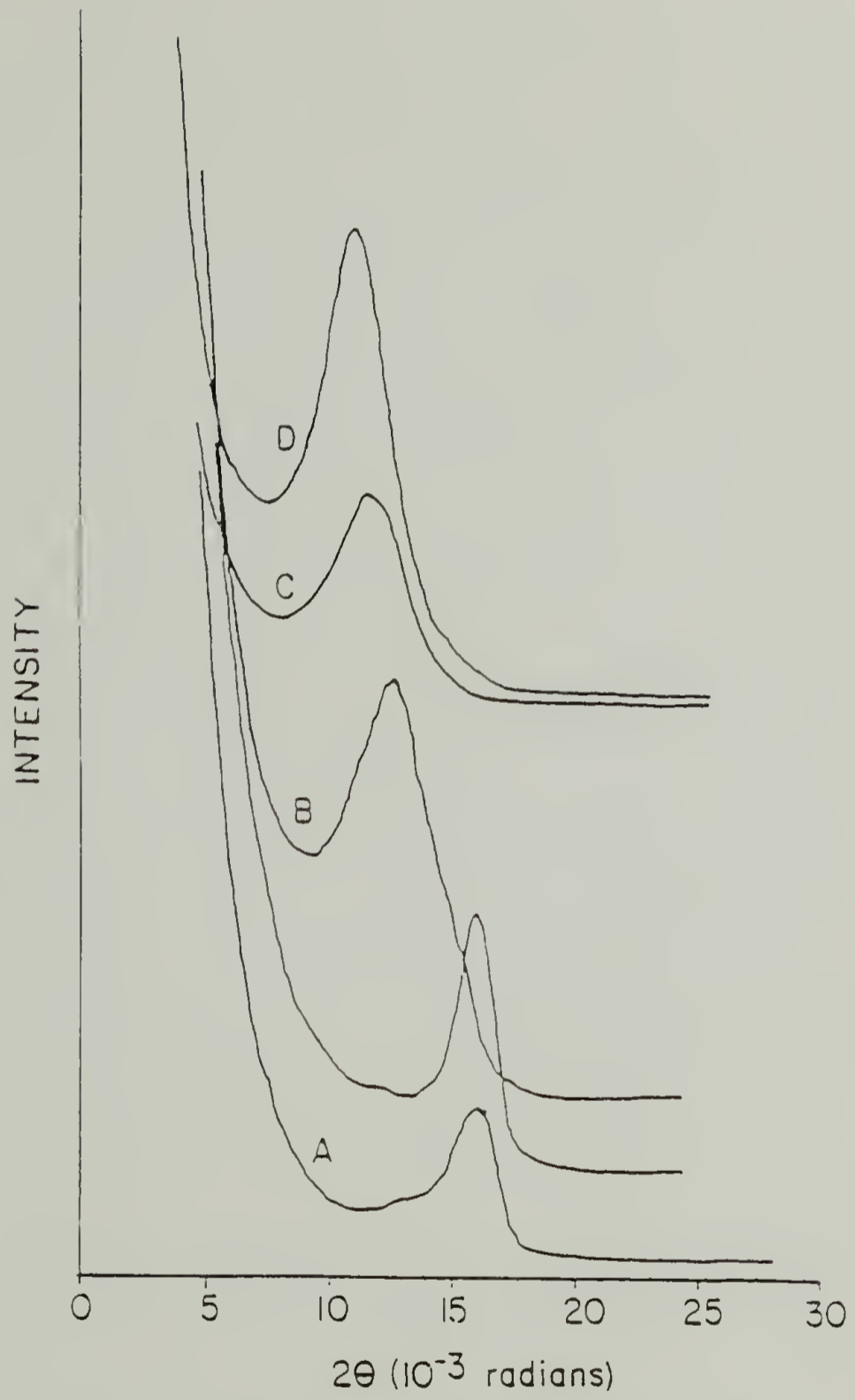
The long period increased continually with an increase in the temperature of crystallization and annealing. This was only expected for polyester (10-16) which has a crystal morphology exhibiting the energetically preferred (hkl) fold surface combined with specific disorder in ester group protrusion along the chain.¹² These results were consistent with the model proposed earlier which considered a mixture of different fold lengths.⁹

SAXS Analysis of Polyester Single Crystal Mats

Small-angle X-ray scattering data was obtained for the (9-8) and (10-8) polyesters. Based on previous studies, it was assumed that chains are perpendicular to the lamella surface. Therefore no adjustment for chain tilt angle is taken to calculate the straight chain stem length. For the as grown and annealed 9-8 crystals, only one one peak was observed in each case (Figure 6). Although the data suggests one discrete lamellar thickness, this observation is insufficient to rule out the existence of a second population due to long range periodicity requirements as shown in Figure 4 in Chapter 2.

The as grown long period is about 95 Å, which corresponds to about 3.8 chemical repeats for a straight repeat length of 25.09 Å. Assuming the molecular weight is 12K, for a calculated repeat weight of 326.5 g/mole the total number of straight chain stems of this length possible is 9.7, assuming tight folds. This figure would be high for polyesters, for each fold must be an integer number of half monomer units in order for the carbonyl groups to come into register in the crystalline regions.^{9,12} The long period observed for the annealed crystals is ~133 Å, or 5.3 repeats. This increase in long period is only 40 %, which is much smaller than the 300 % obtainable for polyethylene.

FIG. 6 Small angle x-ray scattering of the (9-8) polyester single crystals (a) as-grown sample, (b) $T_A = 50\text{ }^\circ\text{C}$, (c) $T_A = 58\text{ }^\circ\text{C}$, (d) $T_A = 60\text{ }^\circ\text{C}$. T_A is temperature at which single crystal mats were annealed. Low frequency Raman in Figure 7 is for the same samples.



The very low frequency Raman spectra obtained for the polyester (9-8), crystallized in 2-butanol, is shown in Figure 7. This is the same sample for which the SAXS is shown in Figure 6. The spectrum of the as grown sample exhibits an unusually broad band, assigned to the LAM based upon its intensity, and frequency.^{13,14} The half-width is about 15 cm^{-1} , which is quite large when compared to that of polyethylene (5 cm^{-1}) prepared under similar conditions. When the polyester was annealed above the crystallization temperature, the original single peak could be resolved into two separate components, as is shown in Figure 7c, and 7d. The peak center shifted to lower frequency representative of thickened lamellae which was consistent with the SAXS data. In Figure 8 is shown the low frequency Raman spectra for the as grown and annealed polyester 10-16 single crystals. The spectra exhibit characteristics similar to those in Figure 7.

Usually the existence of such multiple components can be attributed to different lamellar thicknesses, since the LAM measurement represents a direct method for determination of the distribution of crystal stem lengths contained within lamellae.^{15,16} This interpretation, however, was not supported by the data obtained from either SAXS measurements or thermal measurements. Furthermore, the higher frequency component, at about 33 cm^{-1} for (9-8), did not appear to shift upon annealing as did the lower frequency component. This

FIG. 7 Low-frequency Raman spectra obtained for the as-grown and annealed (9-8) polyester single crystals. Band resolution is 1 cm^{-1} ; argon ion laser (5145 \AA) power is 120 mW. Top to bottom: samples annealed for 30 min ($T_A = 60 \text{ }^\circ\text{C}$), 300 min ($T_A = 58 \text{ }^\circ\text{C}$), 2880 min ($T_A = 50 \text{ }^\circ\text{C}$), and the as grown sample [isothermally crystallized from 0.05 % solution (by weight) in 2-butanol]. The narrow band at about 68 cm^{-1} originates from an argon plasma line.

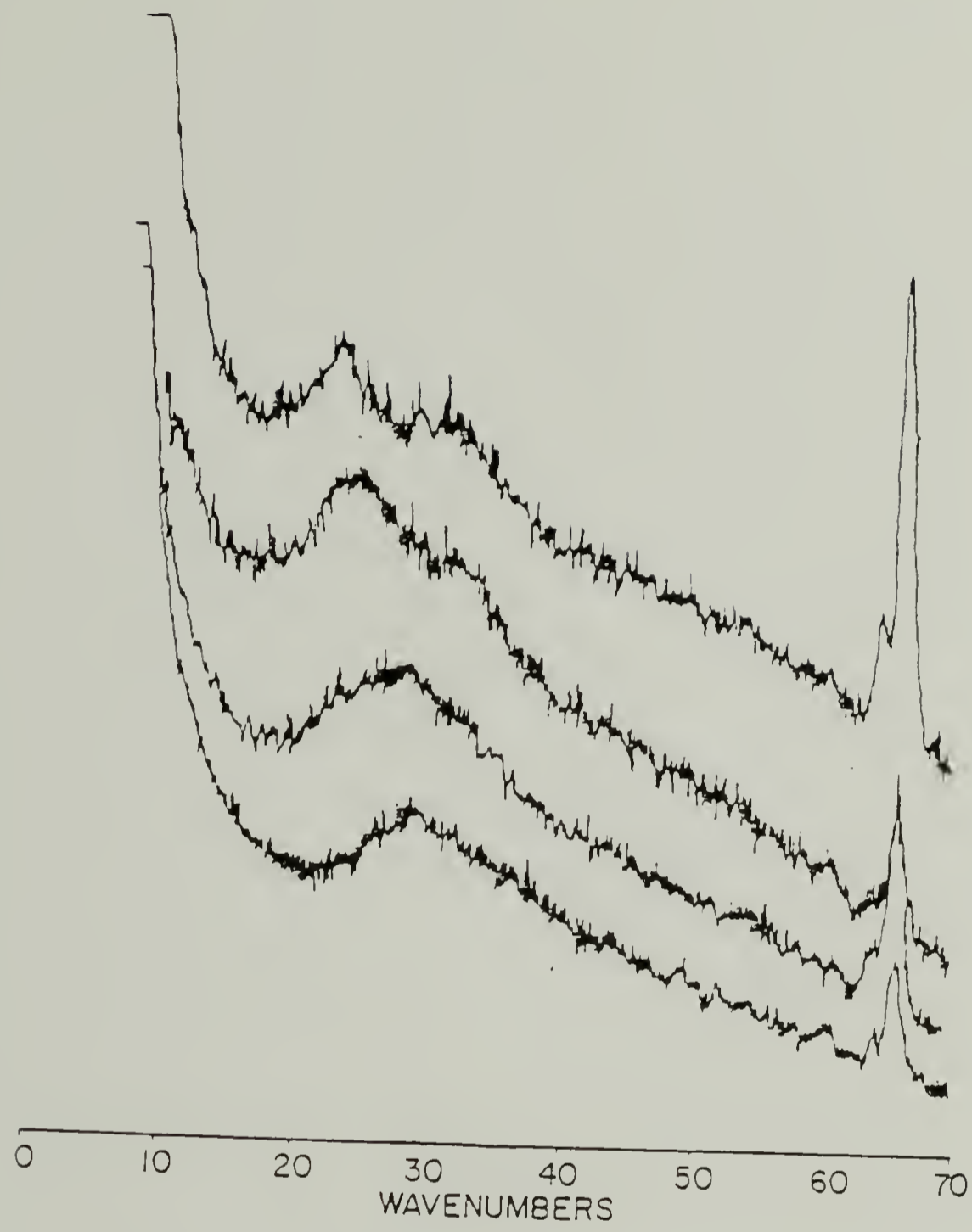
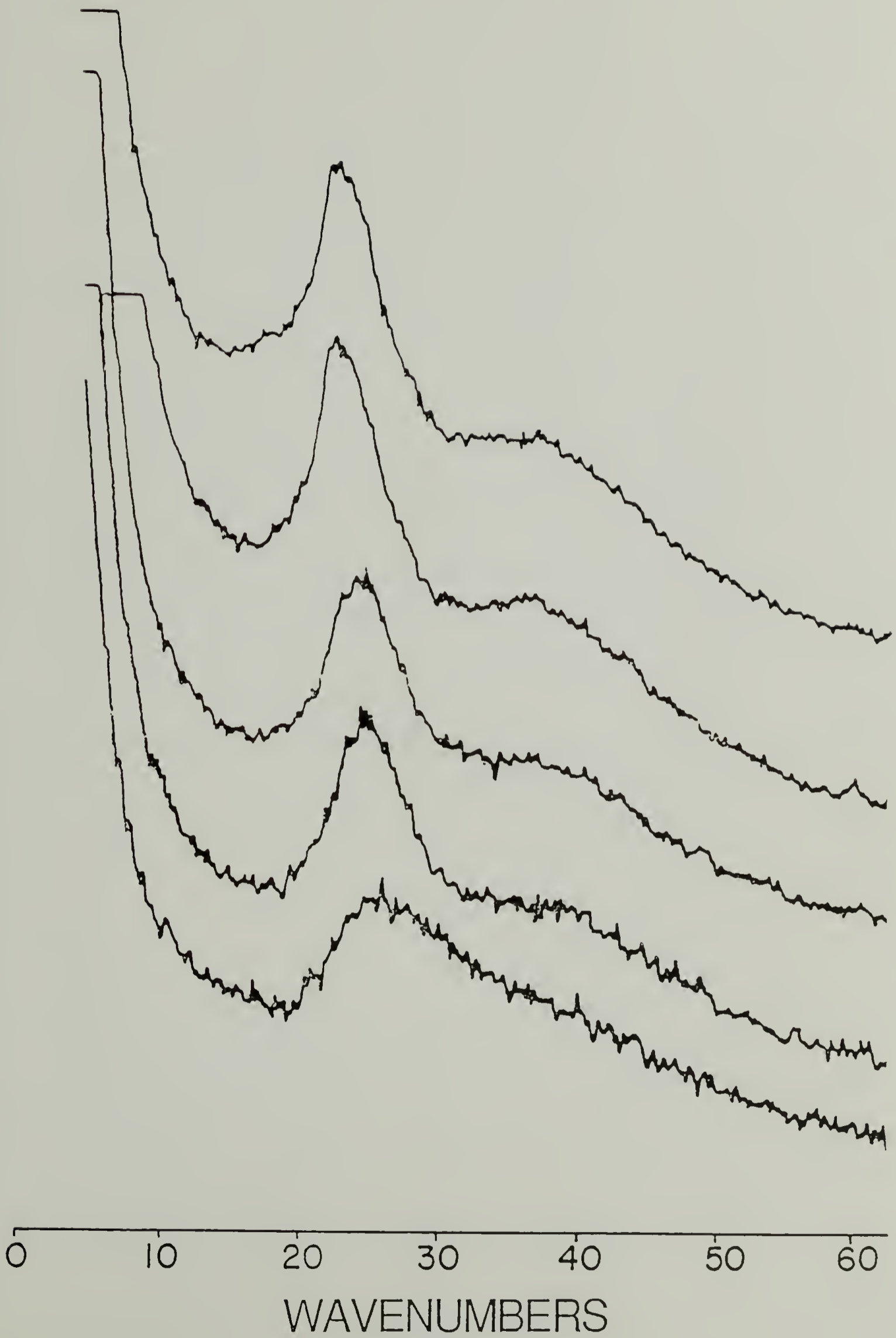


FIG. 8 Low-frequency Raman spectra obtained for the as-grown and annealed (10-16) polyester single crystals. Band resolution is 1 cm^{-1} ; argon ion laser (5145 \AA) power is 120 mW; $T_A = 70 \text{ }^\circ\text{C}$. Top to bottom: samples annealed for 1600, 480, 120, 30 and 0 min. The narrow band at about 68 cm^{-1} originates from an argon plasma line.



was true for the (6-8), (9,8), (10-8) and (10-16) polyester samples prepared in this part of the study.

The room temperature SAXS long periods for polyesters (9,8) and (10,8) as a function of supercooling are shown in Table 2. The principal objective was to further investigate these two in particular, since the odd-even, even-even effect would result in different crystal packing, yet their monomer lengths are similar. For the same degree of supercooling, the determined long periods for the odd-even and even-even polyesters were remarkably similar. This is expected based upon the similar c-axis monomer lengths. The data exhibited at least 3rd order reflections for each case, and there was no evidence for any preferred orientation in the plane parallel to the crystal mat surface. Based upon the WAXS calculated crystal structure for polyester 10-8 (c axis = 27.10 Å), the SAXS periods of 99 and 117 Å correspond to crystal stems of 3.7 and 4.3 repeats, for mats crystallized at T_{cry} of 33.0° and 39.0 °C respectively. For polyester 9-8 the periods of 101 and 115 Å correspond to stems of 4.0 and 4.6 repeats for mats crystallized at 27.0° and 33.0 °C respectively. The estimated error in these determinations is ± 1 Å, based upon ± 0.5 mm for the values of X in Equation 29. In both cases a decrease in undercooling of 6.0 °C resulted in about a half monomer repeat increase in crystal stem length. For these undercoolings, the change in long period is in good agreement

TABLE 2 Low angle x-ray diffraction of polyester single crystals. Growth conditions for these as-grown samples are listed in Table 1. Statton camera used with film detection and nickel filtered Cu K_{α} radiation.

TABLE 2

Low Angle X-ray Diffraction Of
Polyester Single Crystals

Polyester	T _{CRY} (°C)	X (cm) *	d spacing (Å) †	Temp.
10-8	33.0	0.490	99	R.T.
10-8	39.0	0.413	117	R.T.
9-8	27.0	0.480	101	R.T.
9-8	33.0	0.420	115	R.T.
10-16	39.0	0.483	100	R.T.

* $X = L \tan 2\theta$; $L = 313.2$ mm

† $2d \sin\theta = \lambda = 1.5418$ Å

$d = n \lambda / 2 \sin[(\tan^{-1} X/L)/2]$

with earlier data obtained for (2-8), (10-16) and (10,10) polyesters.^{9,12}

Raman Analysis of As Grown Linear Aliphatic Polyester
Single Crystal Mats

Crystallization conditions are important. It was previously determined that regular crystals can only be grown in dilute solution within a confined supercooling range.¹² Such crystals exhibit smooth faces with distinct fold sectors and sharp corners well defined by (110) and (100) planes.¹² Too large a supercooling results in crystals characterized by irregular growth faces. In addition, since the low frequency region in the Raman spectra was to be thoroughly investigated, the effect of temperature, frequency, and chain length distribution corrections could not be ignored.^{15,16} For LAM-1 frequencies above 25 cm^{-1} these corrections are small if the half-widths are less than 10 cm^{-1} .¹⁶

Low frequency Raman data containing one or more intense peaks obtained for 9-8 and 10-8 polyesters are shown in Figures 9 and 10. The band positions, and the half-widths for the lowest frequency most intense band in this region, are listed in Table 3. The existence of only one peak in the SAXS does not rule out the possibility of a bimodal distribution of lamellae thickness,^{17,18} as discussed previously. Using the 1443 cm^{-1} band peak intensity in Figure 9 as a reference, it is apparent that the LAM-1 for this

FIG. 9 C-H bending region (left) and low-frequency region (right) in Raman spectra obtained for as grown (top) (9-8) polyester, and (bottom) polyethylene single crystals. Band resolution is 1 cm^{-1} ; argon ion laser (5145 Å) power is 100 mW. Growth conditions for (9-8) polyester listed in Table 1. Low frequency modes in polyethylene spectrum between about 35 and 85 cm^{-1} result from atmosphere gas lines.

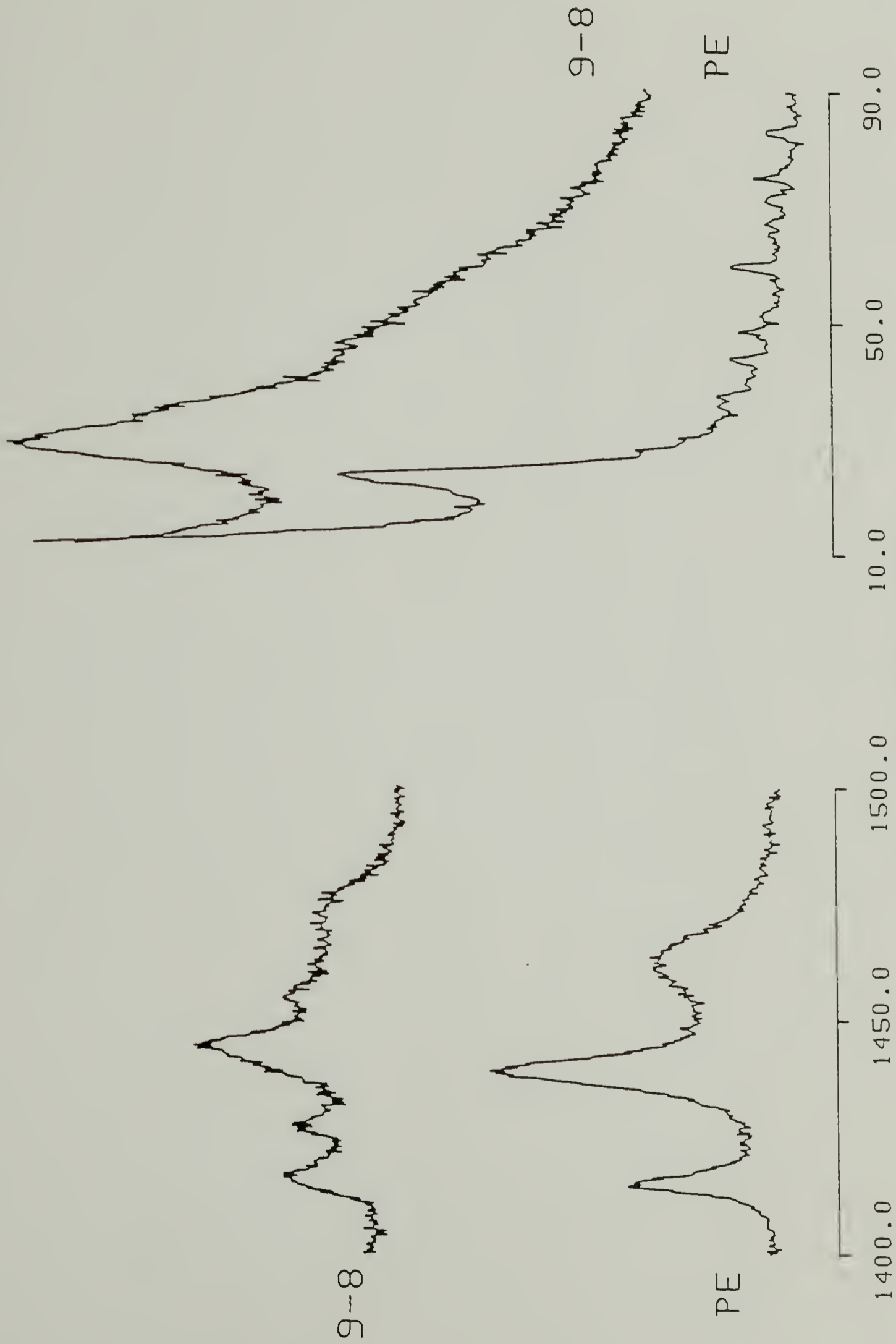


FIG. 10 Low-frequency region in Raman spectra obtained for as grown (10-8) polyester single crystals, (top) $T_{CRY} = 39\text{ }^{\circ}\text{C}$, and (bottom) $T_{CRY} = 33\text{ }^{\circ}\text{C}$. Band resolution is 1 cm^{-1} ; argon ion laser (5145 \AA) power is 100 mW. Growth conditions for (10-8) polyester listed in Table 1.

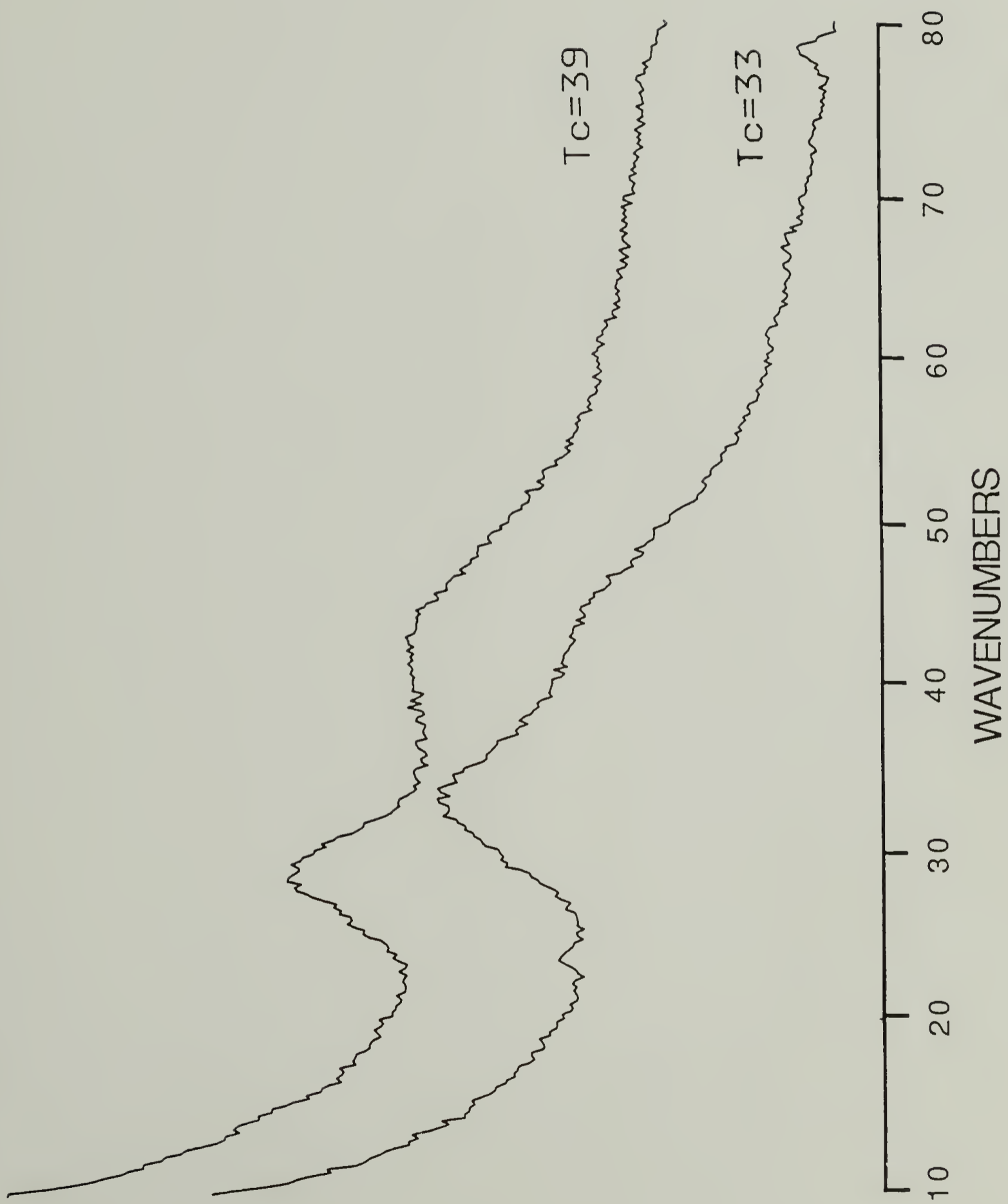


TABLE 3 Low frequency data obtained in Raman spectra for as grown (10-8) and (9-8) polyester single crystals. Growth conditions are listed in Table 1. T_{CRY} is crystallization temperature, $\Delta\nu$ frequency of observed modes, $\Delta\nu_{1/2}$ bandwidth at half height, $T(\text{Raman})$ temperature at which data obtained, and $\Delta\nu \times L$ is Raman frequency SAXS period factor.

TABLE 3

Low Frequency Raman Spectroscopy Of
Polyester Single Crystal Mats

Polyester	T _{CRY} (°C)	$\Delta\nu$ (cm ⁻¹)	$\Delta\nu_{1/2}^*$	T (Raman)	$\Delta\nu \times L^\dagger$
10-8	33.0	33.3, 44.3	9.2	R.T.	3297
10-8	39.0	29.0, 43.3	7.0	R.T.	3393
9-8	27.0	29.6, 40.2, 55.3	8.0	R.T.	2944
9-8	33.0	25.6, 32.0, 43.9	12.8	R.T.	2970

* Bandwidth at half height

† L is experimental SAXS period

polyester crystal, assigned to lowest frequency component, is an intense one. Since the peak frequency is 25.6 cm^{-1} and the complementary SAXS length is 115 \AA , the $[v(\text{cm}^{-1}) \times L(\text{\AA})]$ value is 2944. This compares favorably with the 3093 value obtained for polyethylene.¹⁵ The difference can easily be attributed to differences in c-axis repeat and unit cell density. From these measurements the experimentally calculated c-axis elastic modulus is 358 GPa.

The low frequency region Raman spectra for as grown polyester 10-8, crystallized in iso amyl acetate, are shown in Figure 10. In these room temperature spectra the multiple components are resolved considerably better than in the samples used for Figures 7a and 8a. The lower frequency peak, at 33.3 cm^{-1} for polyester 10-8 crystallized at $T_{\text{cry}} = 33^\circ \text{ C}$, is shifted to a lower frequency (29.0 cm^{-1}) when the crystallization temperature was raised from 33° to 39° C . This is expected if this component is due to the LAM-1, since it would be representative of thicker lamellae due to growth at smaller undercooling. The half-width of the various components observed differ. The higher frequency band in the $T_{\text{cry}} = 33^\circ \text{ C}$ spectrum, at about 44 cm^{-1} , has a half-width of 18.2 cm^{-1} . This is approximately double (1.96) that of the lower frequency component which has a half-width of 9.2 cm^{-1} . For the $T_{\text{cry}} = 39^\circ \text{ C}$ crystal mat, the higher frequency component is also at $\sim 44 \text{ cm}^{-1}$, and its half-width of 14.2 cm^{-1} is double (2.03) that of the 7.0 cm^{-1} value for the lower

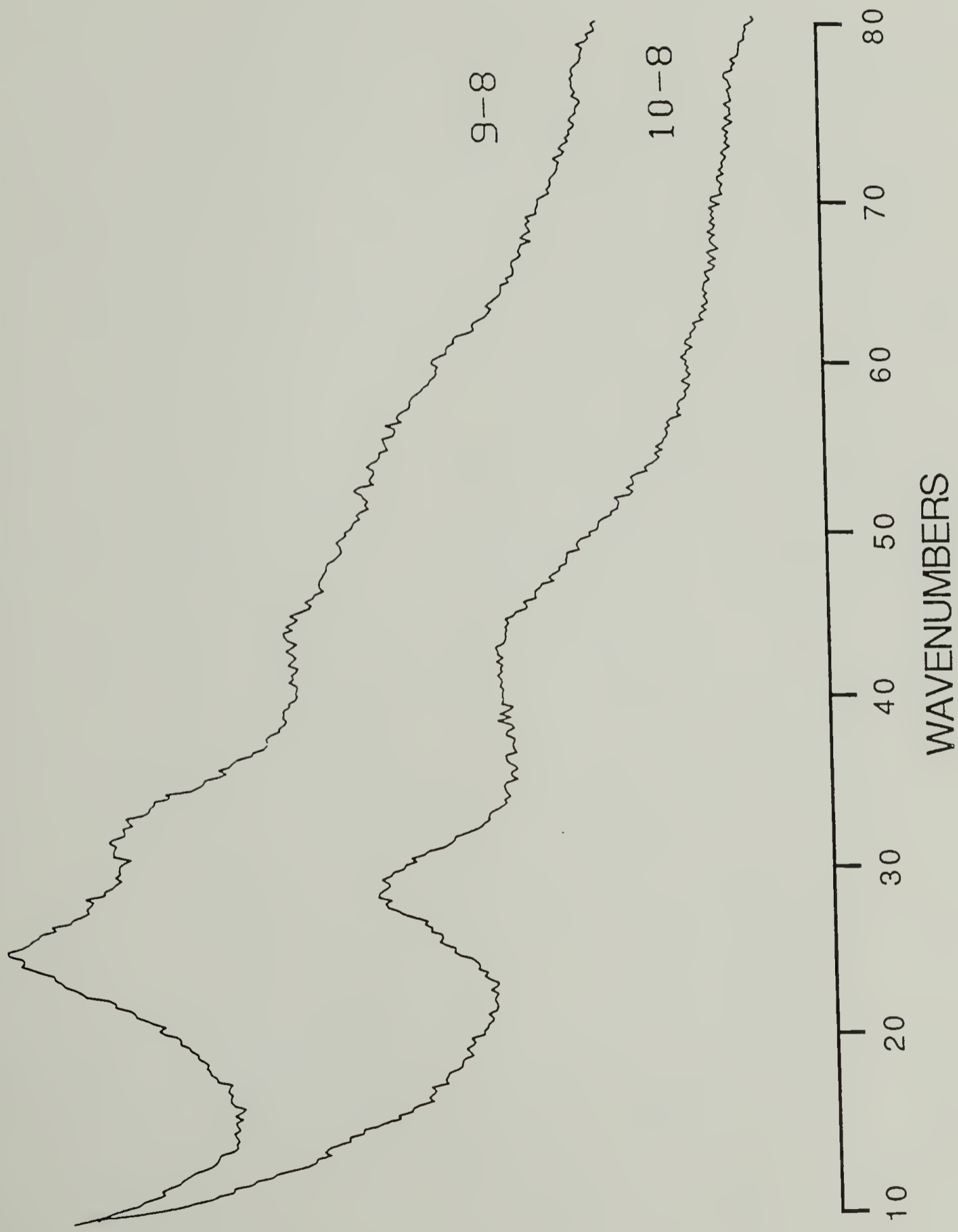
frequency component. The unit cell parameters of Fuller⁸ ($a \sin \beta = 5.0 \text{ \AA}$, $b = 7.4 \text{ \AA}$, and $c = 27.1 \text{ \AA}$) can be used to calculate a crystal density of 1.128 g/cc. Based on single chain modulus and the above density, a LAM frequency of 25.7 cm^{-1} is expected for a c axis length of 109 \AA .

The difference between the measured LAM frequency for polyester 10-8, and that expected based on SAXS measurement, may be due to several reasons: (1) Interlamellar coupling may be significant for aliphatic polyesters, due to dipolar interactions, which would increase the unperturbed frequency.¹⁹⁻²² Such coupling is expected to be greater for monoclinic crystalline forms such as exhibited by 10-8; (2) The fold structures in these polyesters may be significantly longer due to the constraint of carbonyl group registration in the crystal. Although these would act as terminal defect structures and therefore cause a small decrease in the LAM-1 frequency,²³ they could instead result in a larger SAXS period since it is inclusive of the amorphous layer thickness; (3) Lateral interactions, between folds at the surfaces of the single crystals, are expected to result in a decreased LAM-like frequency.²³ Such an intensity redistribution into a group of strong LAM-like modes may be significant due to the polyester chemical structure. Morphological differences between the crystalline structures of 9-8 and 10-8 polyesters may cause the contribution from this effect to be greater for 9-8 polyester.

Based upon Equation 1, and the theoretical density and modulus, the expected crystal stem lengths for LAM-1 frequencies of 33.3 and 29.0 cm^{-1} , would be 84 and 96 Å respectively ($L = 2798/\nu_{\text{LAM-1}}$). These lengths are 0.85 and 0.82 of their experimental SAXS long periods. This indicates that the lamellae thickening that occurred upon decreasing the degree of supercooling, was accompanied by a concurrent thickening of the amorphous layer. The corresponding amorphous region thickness of 15 and 21 Å respectively, are both reasonable considering the repeat lengths and the constraint of carbonyl registration.

Low frequency Raman spectra for 9-8 and 10-8 polyesters are shown in Figure 11. The single crystals are grown at the same degree of undercooling. Although the exact frequencies and band shapes differ, it is apparent that the multicomponent features exhibited are not a function of odd-even or even-even packing effects. The spectrum for 9-8 has contributions from at least 3 bands, while for 10-8 there appears to be only 2 bands. The highest frequency band is at about 44 cm^{-1} in both cases, but its intensity relative to the lowest frequency LAM-1 band differs significantly. For both polyesters the highest frequency band is too low in frequency, too narrow in half-width, and has a larger observed relative intensity than would be expected, in order to be assigned to the LAM-3.

FIG. 11 Low-frequency region in Raman spectra obtained for as grown (top) (9-8), and (bottom) (10-8) polyester single crystals with same degree of undercooling ($\Delta T = 13$ °C). Band resolution is 1 cm^{-1} ; argon ion laser (5145 Å) power is 100 mW. Growth conditions are listed in Table 1.



Low Temperature Raman Analysis

It is known that external modes of the unit cell are sensitive to temperature variation. It is also known that LAM vibrations in polyesters should not be. Raman spectra obtained for 9-8 Polyester at two temperatures are shown in Figure 12. The low temperature spectrum exhibits at least 5 components at 28.3, 34.6, 47.2, 60, and 93 cm^{-1} . The change in frequency of the 3 lowest frequency bands from that at room temperature is 2.6, 2.8, and 3.3 cm^{-1} respectively. The band at about 90 cm^{-1} has a large enough half-width and high enough frequency to be considered a likely candidate for the LAM-3. Its relative intensity is reasonable when compared to that observed for a high density polyethylene extrudate.¹⁶

The exact position and intensity of various vibrations can be considered only if sample temperature is taken into account as described in Chapter 2.²⁴ The Boltzmann and frequency correction factors for observed intensities are shown in Table 4. Ratios of these factors indicate that the shifts to higher frequencies, for the low frequency bands at low temperature, are not the result of an intensity redistribution. Thermal contraction of the unit cell, with decreasing temperature, causes an increase in the intermolecular forces which may increase the LAM-1 frequency slightly.^{19-21,25,26} This has been observed for a number of oligomers and polymers.²⁵⁻³¹ It is not entirely clear whether

FIG. 12 Low-frequency region in Raman spectra obtained for as grown (9-8) polyester single crystals ($T_{CRY} = 33\text{ }^{\circ}\text{C}$) at (a) room temperature (top) and (b) $-110\text{ }^{\circ}\text{C}$ (bottom). Band resolution is 1 cm^{-1} ; argon ion laser (5145 \AA) power is 100 mW .

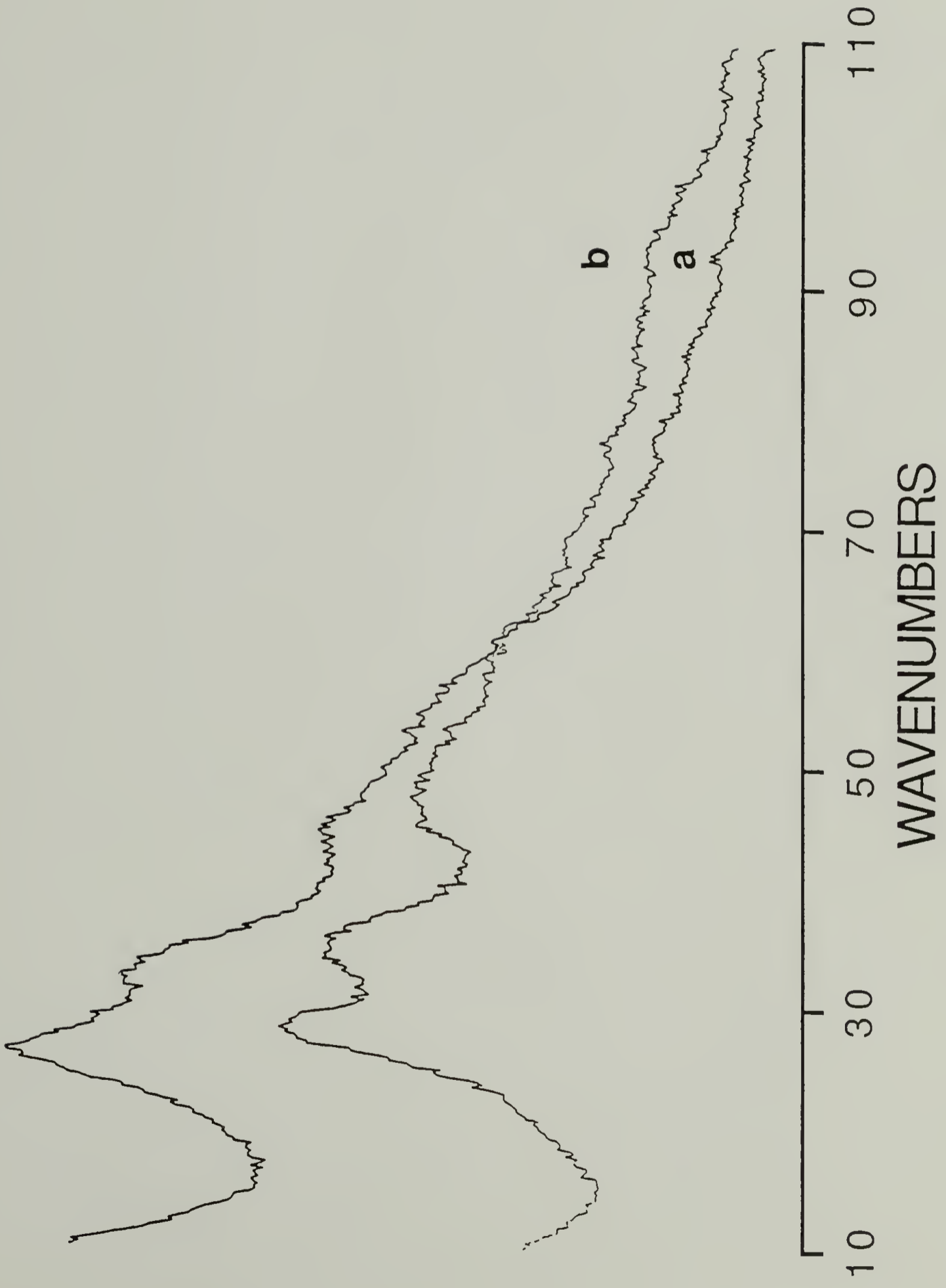


TABLE 4. Weighting of low frequency Raman intensity from temperature and frequency factors. T is temperature at which data obtained, $\Delta\nu$ the frequency of the observed LAM-1, h is Planck's constant, k_B is Boltzmann constant, B is the Boltzmann weighting factor resulting from relative population of low lying vibrational states, and $(B \times \Delta\nu)$ is the frequency/temperature correction factor for intensity.

TABLE 4

Weighting of Low Frequency Raman Intensity From
Temperature And Frequency Factors

T (°K)	ΔV (cm ⁻¹)	$hcV/k_B T$	$B(V, T)^*$	$[B(V, T) \Delta V]$
298	25.6	0.124	0.116	2.97
163	25.6	0.227	0.203	5.19
298	28.3	0.137	0.128	3.62
163	28.3	0.250	0.222	6.28
298	31.8	0.154	0.142	4.51
163	31.8	0.281	0.245	7.79
298	34.6	0.167	0.154	5.33
163	34.6	0.306	0.264	9.13
298	43.9	0.212	0.191	8.38
163	43.9	0.388	0.322	14.14
298	47.2	0.228	0.204	9.63
163	47.2	0.418	0.341	16.10

$$* B = 1 - \exp(h c \Delta V / k_B T)$$

$$h = 6.626 \times 10^{-34} \text{ J sec}, c = 3.0 \times 10^{10} \text{ cm/sec}$$

$$k_B = 1.381 \times 10^{-23} \text{ J/°K}$$

any of the vibrations can be definitively assigned based on the temperature induced variations, since the magnitude of the shifts are similar.

More quantitative analysis requires that background scattering, which can be significant at low frequencies, be subtracted. Background intensity is attributed to stray light at the incident laser frequency which reaches the detector, as well as sample geometry and temperature.^{32,33} Although the shape of the stray light curve is known within a few wavenumbers about the exciting frequency, its contribution can not be extrapolated reliably over the low frequency range plotted.³⁴ A combination of a sloping baseline, and a gaussian and Lorentzian peak centered at 0 cm^{-1} , was utilized to remove the background from the LAM spectra. The background was chosen to fit the low frequency spectra in the 4 to 6 cm^{-1} and 70 to 90 cm^{-1} regions. After the background is subtracted all the low frequency vibrations exhibit an upward shift of 1-3 cm^{-1} . The as obtained data together with temperature and frequency corrected spectra for the 9-8 polyester ($T_{\text{cry}} = 33 \text{ }^\circ\text{C}$) are shown in Figures 13, 14, and 15. It is evident that the corrected spectra exhibit large intensity changes due to frequency weighting. The upward shifts in frequency are reasonable considering the frequency and half-widths of the bands in question.¹⁶

Subtraction of a background from the spectra in Figure 12 enabled an experimental comparison to the intensity ratios

FIG. 13 Low-frequency region in Raman spectrum, obtained for as grown (9-8) polyester single crystals ($T_{CRY} = 33 \text{ }^{\circ}\text{C}$) at room temperature, with a function fit to remove the background contribution. Function is a combination of a sloping baseline, and a gaussian and Lorentzian peak centered at 0 cm^{-1} . The curve was chosen to fit the low frequency spectrum in the $4 \text{ to } 6 \text{ cm}^{-1}$ and $70 \text{ to } 90 \text{ cm}^{-1}$ regions.

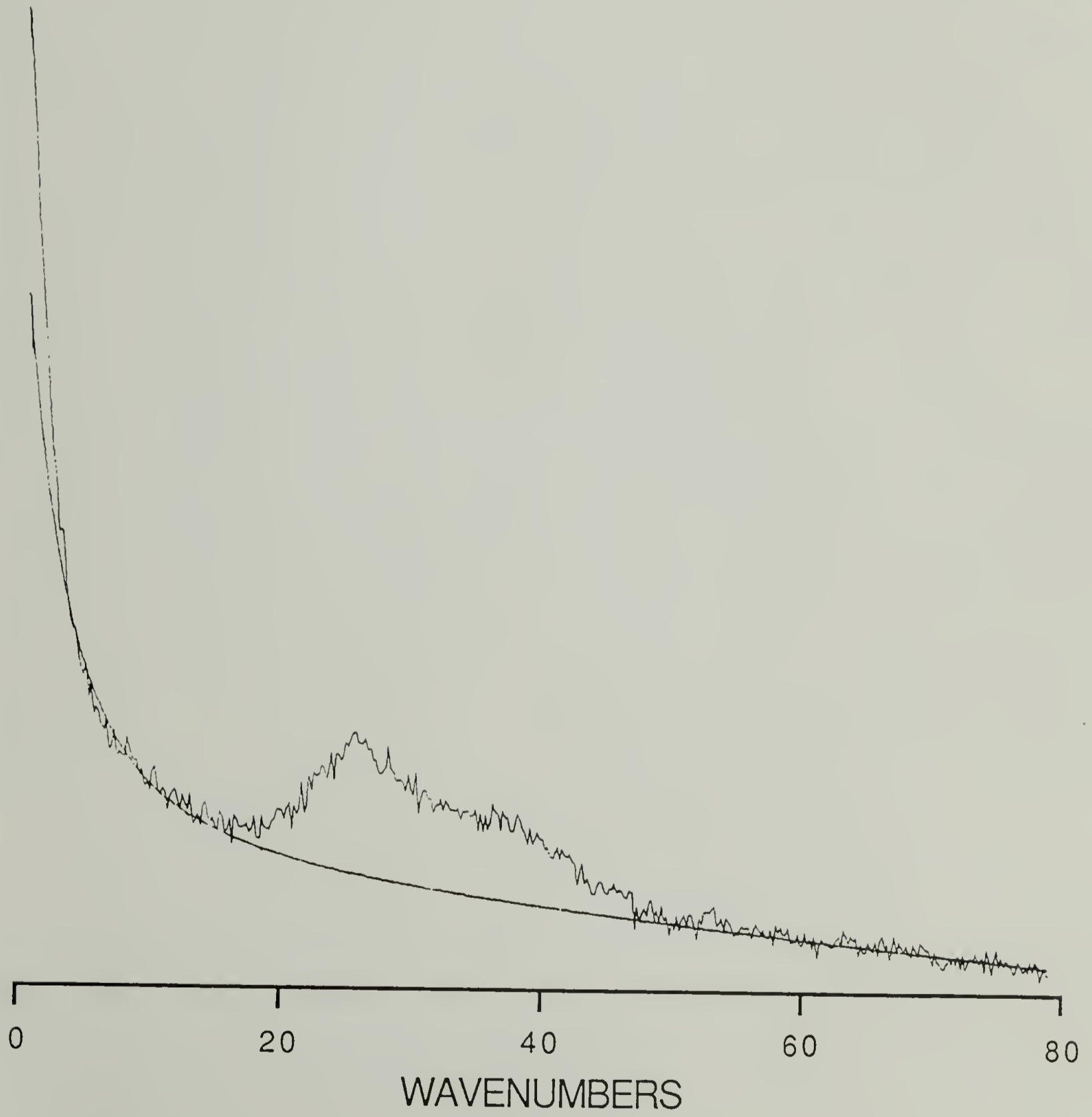


FIG. 14 Low-frequency region in Raman spectrum, obtained for as grown (9-8) polyester single crystals ($T_{CRY} = 33\text{ }^{\circ}\text{C}$) at room temperature, after subtraction of background contribution.

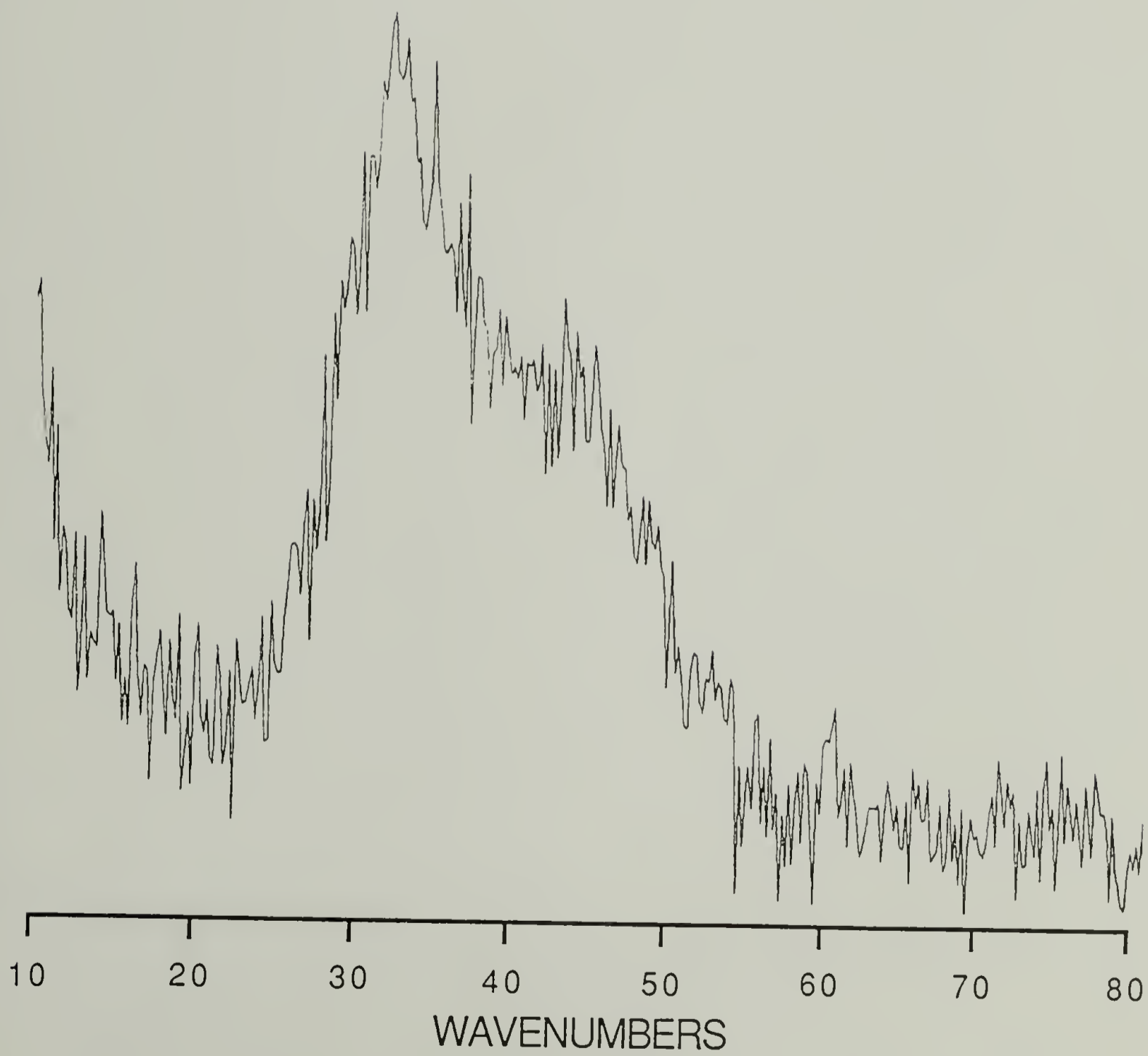
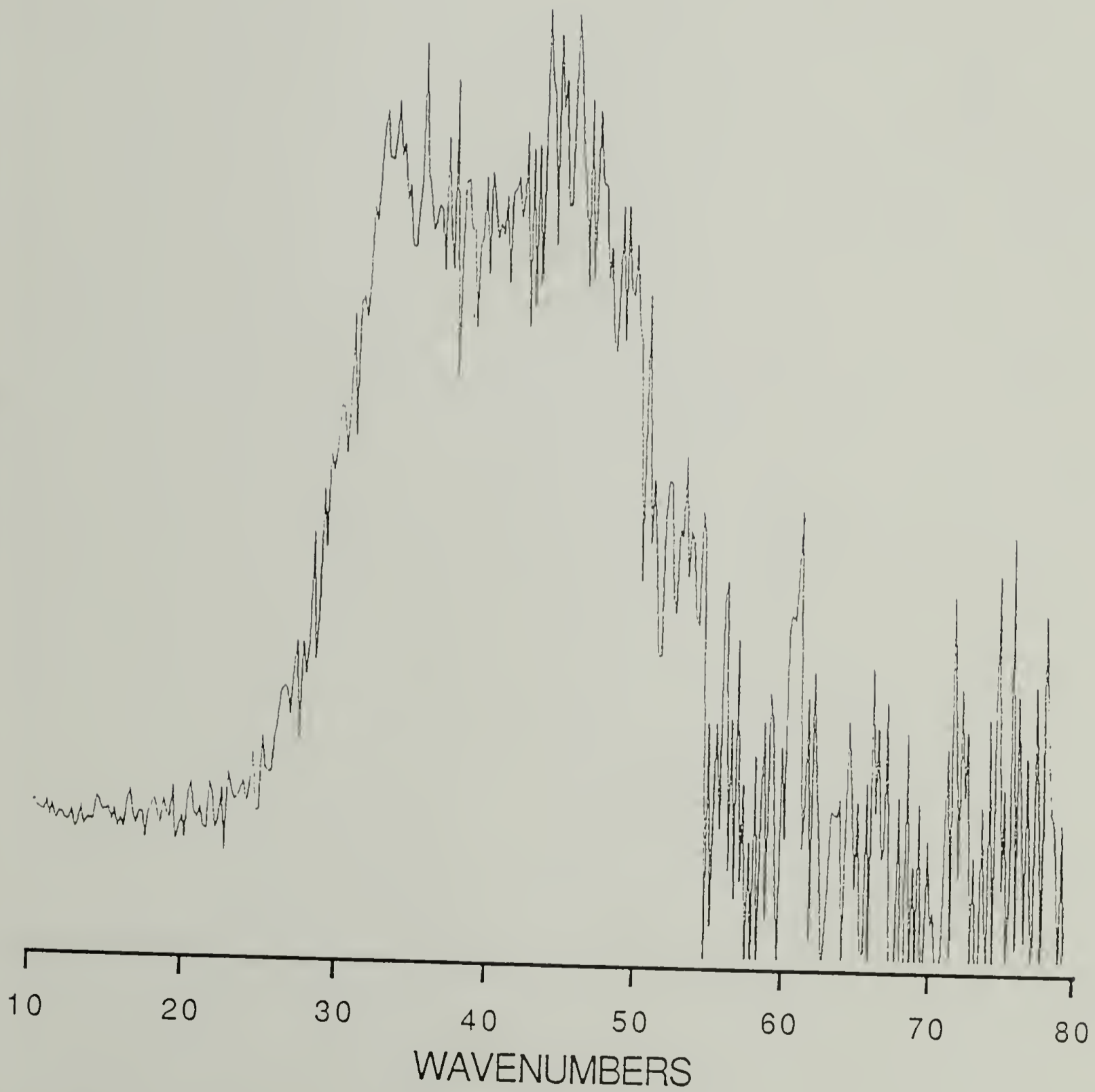


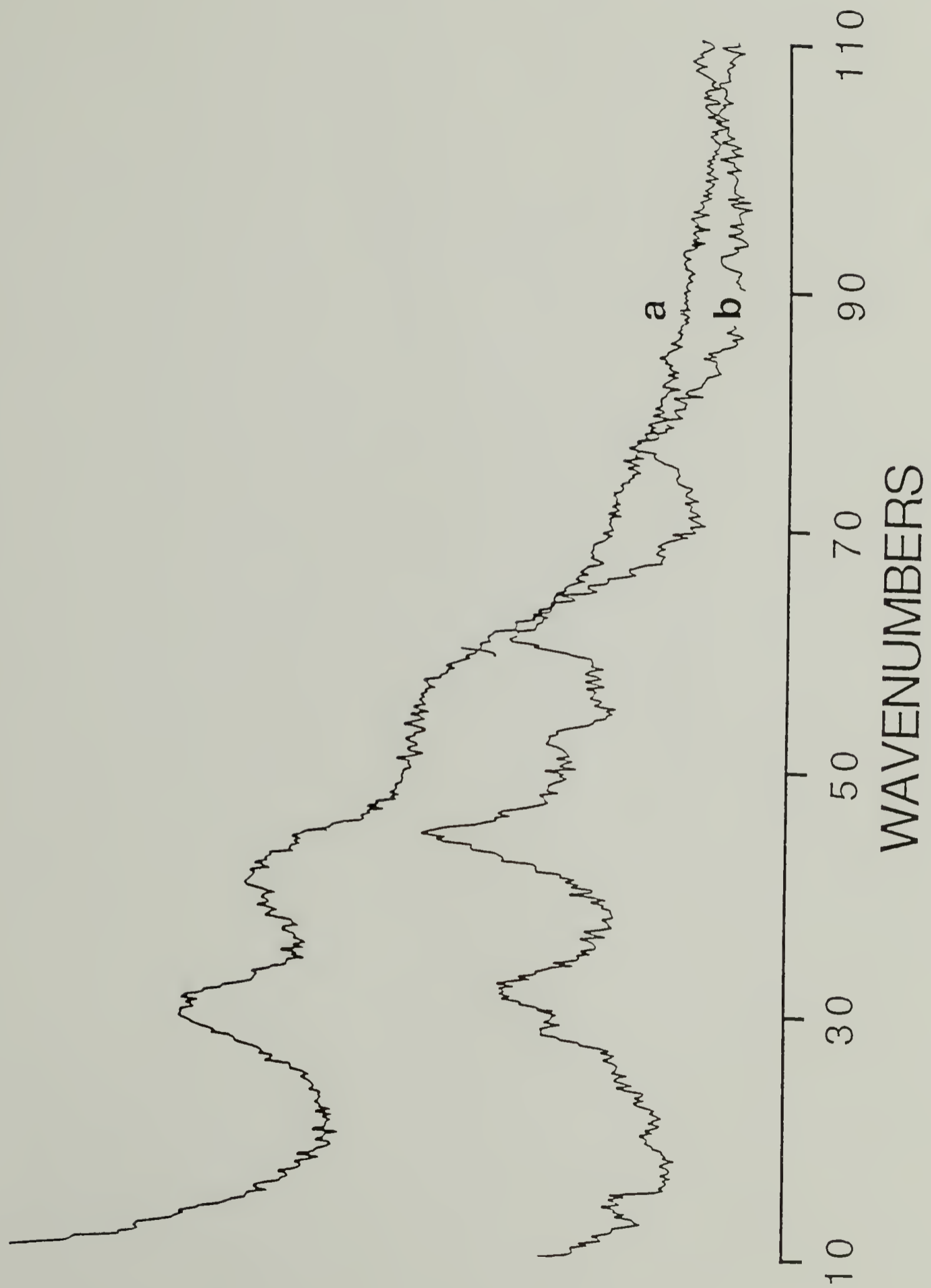
FIG. 15 Temperature and frequency weighted low-frequency region of background subtracted Raman spectrum for as grown (9-8) polyester single crystals ($T_{CRY} = 33 \text{ }^{\circ}\text{C}$) at room temperature.



expected from Table 4. The ratio of the intensity weighting factors for the two lowest frequency bands, (1.52) at room temperature, and (1.45) at $-110\text{ }^{\circ}\text{C}$, indicates that the low temperature spectrum should exhibit a decrease in the relative intensity of the LAM-1 band to the next higher frequency band. The experimental values are 1.25 and 1.09, at 25 and $-110\text{ }^{\circ}\text{C}$ respectively. The weighted ratio of these values represents a relative intensity change that is 10% greater than predicted. Thus there must be other contributing factors which affect the LAM-1 intensity of the linear aliphatic polyesters at low temperatures. Non regular terminal structures (folds and cilia) and lateral interactions between the crystal stems are expected to cause an increase in the force perturbations on LAM-like modes at lower temperatures.^{23,26} The physical origin of such an effect can be attributed to the presence of lateral components in the atomic displacements of the LAM-1, for oligomers of linear aliphatic polyesters.³⁵

Figure 16 shows the low frequency room(16a) and low(16b) temperature spectra ($-125\text{ }^{\circ}\text{C}$) for a polyester 9-8 single crystal mat, crystallized at $27.0\text{ }^{\circ}\text{C}$. The 3 most intense bands are observed at 29.6 (half-width = 8.0 cm^{-1}), 40.2 , and about 55 cm^{-1} at room temperature, and at 31.8 (half-width = 7.5 cm^{-1}), 44.4 , and 60.4 cm^{-1} at $-110\text{ }^{\circ}\text{C}$. An additional three lower intensity bands, in the low temperature spectrum, are at 28.4 , 52.2 , and 76.1 cm^{-1} . The increase in frequency

FIG. 16 Low-frequency region in Raman spectra obtained for as grown (9-8) polyester single crystals ($T_{CRY} = 27\text{ }^{\circ}\text{C}$) at (a) room temperature (top) and (b) $-125\text{ }^{\circ}\text{C}$ (bottom). Band resolution is 1 cm^{-1} ; argon ion laser (5145 \AA) power is 100 mW .



at low temperature for the three higher intensity bands is 2.2, 4.2, and 5.4 cm^{-1} respectively. It is quite evident that only the lowest frequency band shifts by the amount expected for a LAM vibration. The upward shifts of the other two bands are greater by 150 and 164 % respectively. It is possible then to conclude that higher frequency components can be assigned to lattice modes. The existence of polymorphism for the odd-even polyesters is not unusual and should be considered.⁸

Only the lowest frequency component can be assigned to a LAM vibration. There are several differences between the room temperature spectra of the two samples grown with different degree of supercoolings (Figures 12a and 16a). In the former case ($T_{\text{cry}} = 33\text{ }^{\circ}\text{C}$, $\Delta T = 13\text{ }^{\circ}\text{C}$) there are 4 bands in the low frequency region, while in the latter ($T_{\text{cry}} = 27\text{ }^{\circ}\text{C}$, $\Delta T = 19\text{ }^{\circ}\text{C}$) there are only 3. The upward shift of 4 cm^{-1} , for the lowest frequency band (assigned to LAM-1) in the $T_{\text{cry}} = 27\text{ }^{\circ}\text{C}$ spectrum as compared to that at $T_{\text{cry}} = 33\text{ }^{\circ}\text{C}$, is reasonable considering the decrease in SAXS long period of 14 Å. The expected value is 14.8 Å, based upon the calculated frequency/length relationship from Equation 1 and the unit cell parameters of (10-8). The calculated relationship, $L = 2798/v_{\text{LAM-1}}$, is quite close to the experimental values of 2944, and 2990 for the LAM-1 bands of the higher and lower T_{cry} samples respectively. The band at 40.2 cm^{-1} in the $T_{\text{cry}} = 27\text{ }^{\circ}\text{C}$ spectrum (16a) is intermediate in frequency between that

at 31.8 and 43.9 cm^{-1} in the $T_{\text{cry}} = 33\text{ }^{\circ}\text{C}$ spectrum(12a). The next higher frequency band is broad and is at about 55 cm^{-1} for both cases.

Raman Analysis of Annealed Polyester Single Crystal Mats

Low Frequency Region. Assignment of the low frequency vibrations can also be supported by annealing studies. The increase in the lamellar thickness is expected to correspond to the decrease in LAM frequency.^{9,36,37,38} In Figures 17, 18, and 19 are shown the low frequency regions of the Raman spectra for polyester 9-8 ($T_{\text{cry}} = 33\text{ }^{\circ}\text{C}$), polyester 10-8 ($T_{\text{cry}} = 39\text{ }^{\circ}\text{C}$), and polyester 9-8 ($T_{\text{cry}} = 27\text{ }^{\circ}\text{C}$) respectively, as a function of annealing temperature. It is evident that as the annealing temperature was increased, the intense low frequency band changes its position as expected. The frequencies of other bands in Figures 17 and 18 appear to be insensitive to the annealing. This is further confirmed by comparison of low temperature spectra for polyester 9-8. In Figure 20 is shown the low frequency Raman region measured at $-125\text{ }^{\circ}\text{C}$, for the as grown crystal mat(20a) and for the mat annealed at the highest temperature(20b). It is evident that only the lowest frequency band has shifted to an even lower value, while the other bands remained at essentially the same positions. The lowest frequency band, assigned to LAM-1, is better resolved as the annealing temperature was increased. The overall decrease in frequency is similar to but greater than that observed from a lowering of the supercooling

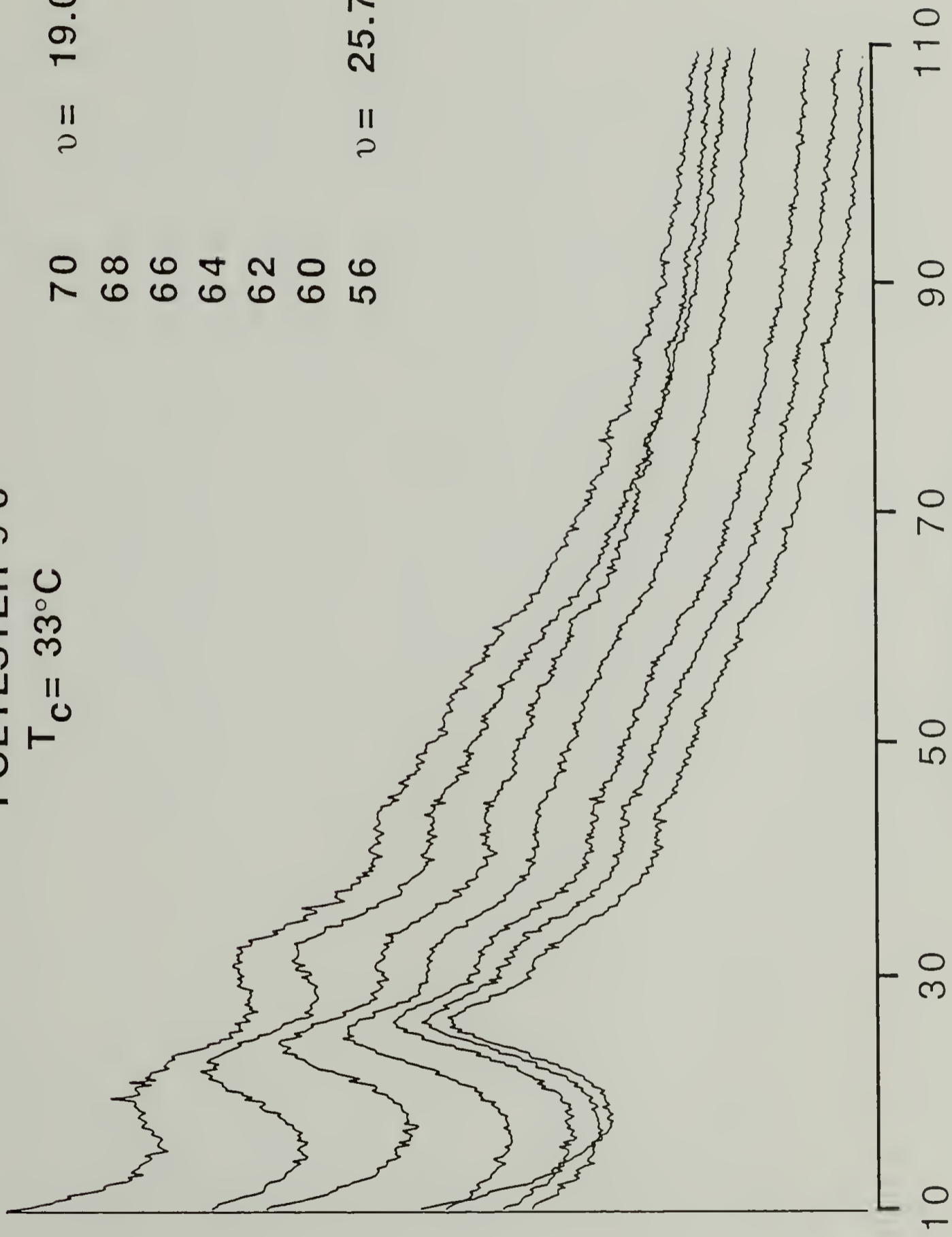
FIG. 17 Low-frequency region in Raman spectra obtained at room temperature for annealed (9-8) polyester single crystals ($T_{CRY} = 33\text{ }^{\circ}\text{C}$). Band resolution is 1 cm^{-1} ; argon ion laser (5145 \AA) power is 100 mW . Top to bottom: sample annealed for 2 hours at ($T_A = 70\text{ }^{\circ}\text{C}$), ($T_A = 68\text{ }^{\circ}\text{C}$), ($T_A = 66\text{ }^{\circ}\text{C}$), ($T_A = 64\text{ }^{\circ}\text{C}$), ($T_A = 62\text{ }^{\circ}\text{C}$), ($T_A = 60\text{ }^{\circ}\text{C}$), and ($T_A = 56\text{ }^{\circ}\text{C}$).

POLYESTER 9-8

$T_c = 33^\circ\text{C}$

T_a in $^\circ\text{C}$

70	$\nu = 19.0 \text{ cm}^{-1}$
68	
66	
64	
62	
60	
56	$\nu = 25.7 \text{ cm}^{-1}$



WAVENUMBERS

FIG. 18 Low-frequency region in Raman spectra obtained at room temperature for annealed (10-8) polyester single crystals ($T_{CRY} = 39\text{ }^{\circ}\text{C}$). Band resolution is 1 cm^{-1} ; argon ion laser (5145 \AA) power is 100 mW. Top to bottom: sample annealed 2 hours at ($T_A = 74\text{ }^{\circ}\text{C}$), ($T_A = 72\text{ }^{\circ}\text{C}$), ($T_A = 70\text{ }^{\circ}\text{C}$), ($T_A = 68\text{ }^{\circ}\text{C}$), ($T_A = 66\text{ }^{\circ}\text{C}$), ($T_A = 64\text{ }^{\circ}\text{C}$), ($T_A = 62\text{ }^{\circ}\text{C}$), ($T_A = 60\text{ }^{\circ}\text{C}$), and ($T_A = 56\text{ }^{\circ}\text{C}$).

T_a in °C

POLYESTER 10-8

$T_c = 39^\circ\text{C}$

74
72
70
68
66
64
62
60
56

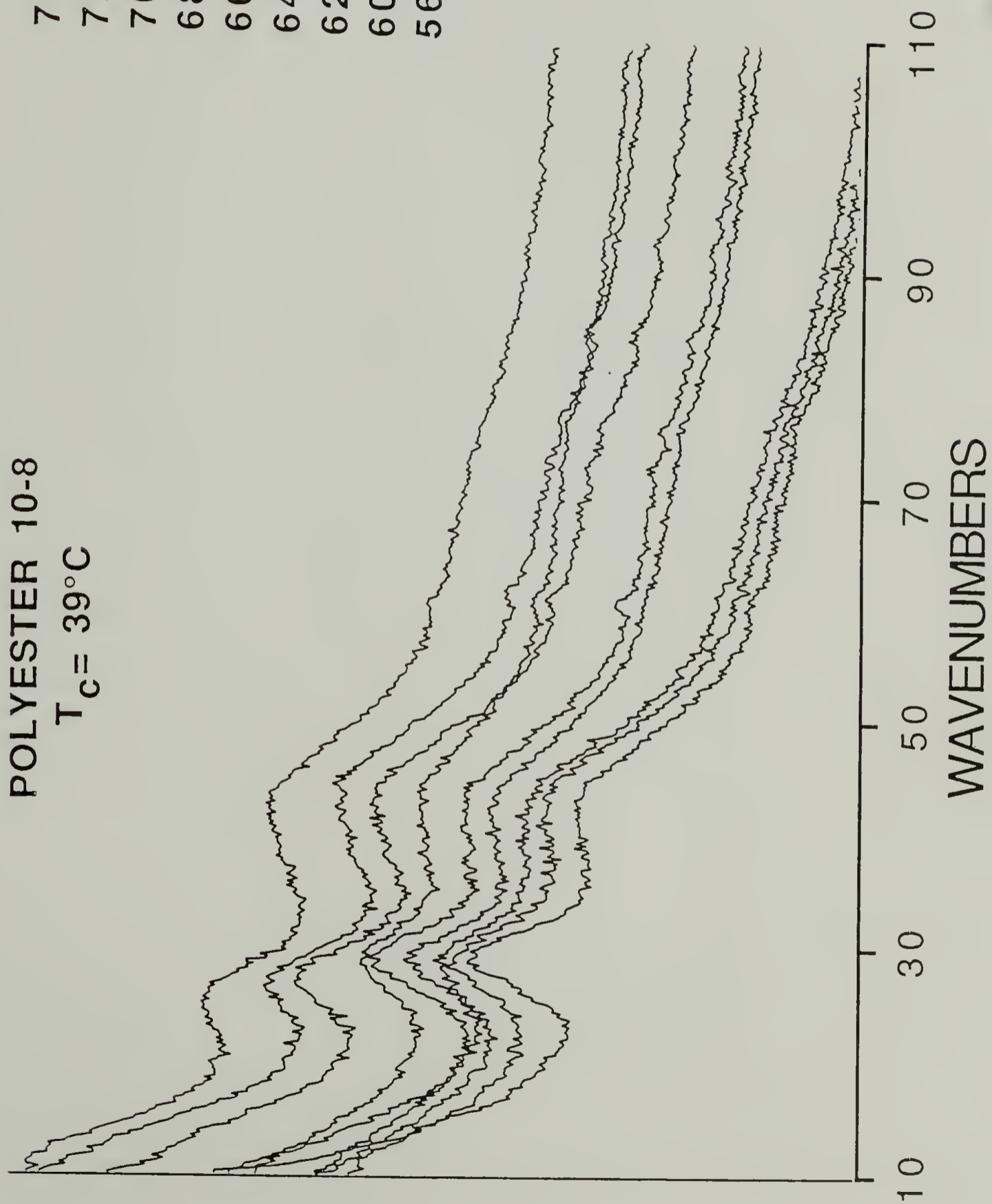


FIG. 19 Low-frequency region in Raman spectra obtained at room temperature for annealed (9-8) polyester single crystals ($T_{CRY} = 27\text{ }^{\circ}\text{C}$). Band resolution is 1 cm^{-1} ; argon ion laser (5145 \AA) power is 100 mW . Top to bottom: sample annealed 2 hours at ($T_A = 68\text{ }^{\circ}\text{C}$), ($T_A = 66\text{ }^{\circ}\text{C}$), ($T_A = 64\text{ }^{\circ}\text{C}$), ($T_A = 62\text{ }^{\circ}\text{C}$), ($T_A = 59\text{ }^{\circ}\text{C}$), and ($T_A = 56\text{ }^{\circ}\text{C}$).

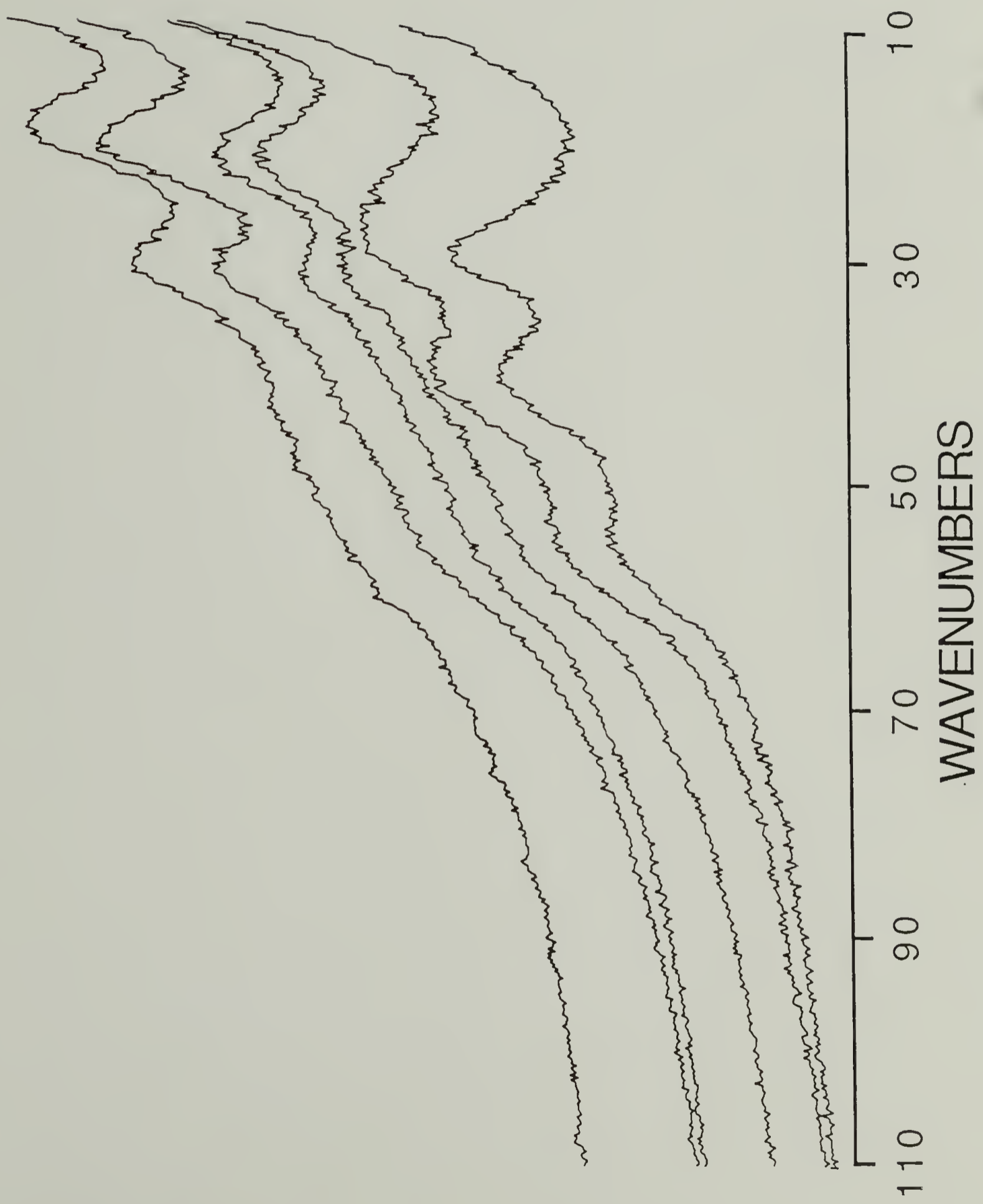
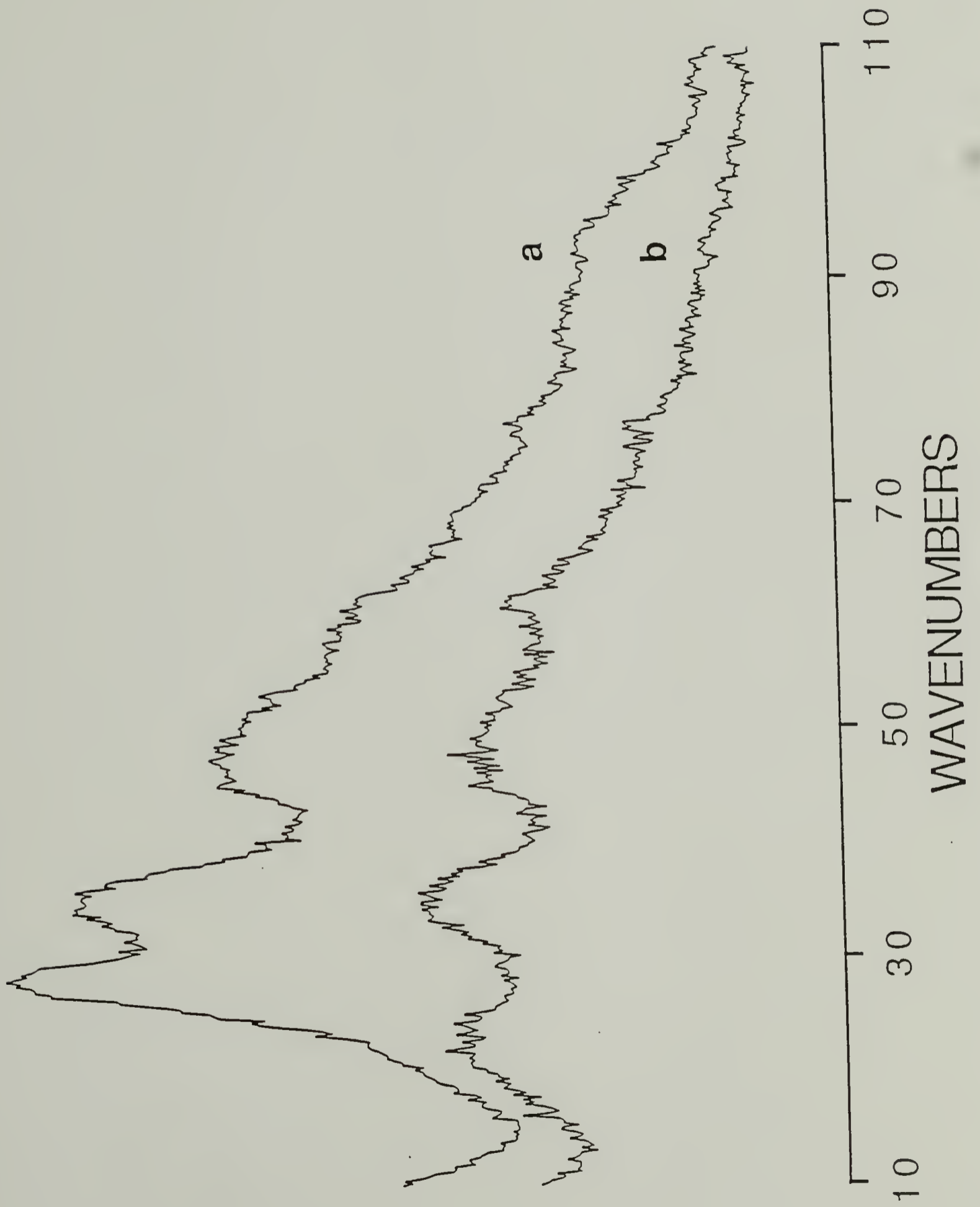


FIG. 20 Low-frequency region in Raman spectra obtained at $-125\text{ }^{\circ}\text{C}$ for as-grown and annealed (9-8) polyester single crystals ($T_{\text{CRY}} = 33\text{ }^{\circ}\text{C}$). Band resolution is 1 cm^{-1} ; argon ion laser (5145 \AA) power is 100 mW . Low temperature spectra for (a) as-grown crystal mat and (b) sample annealed 2 hours at $T_{\text{A}} = 70\text{ }^{\circ}\text{C}$.

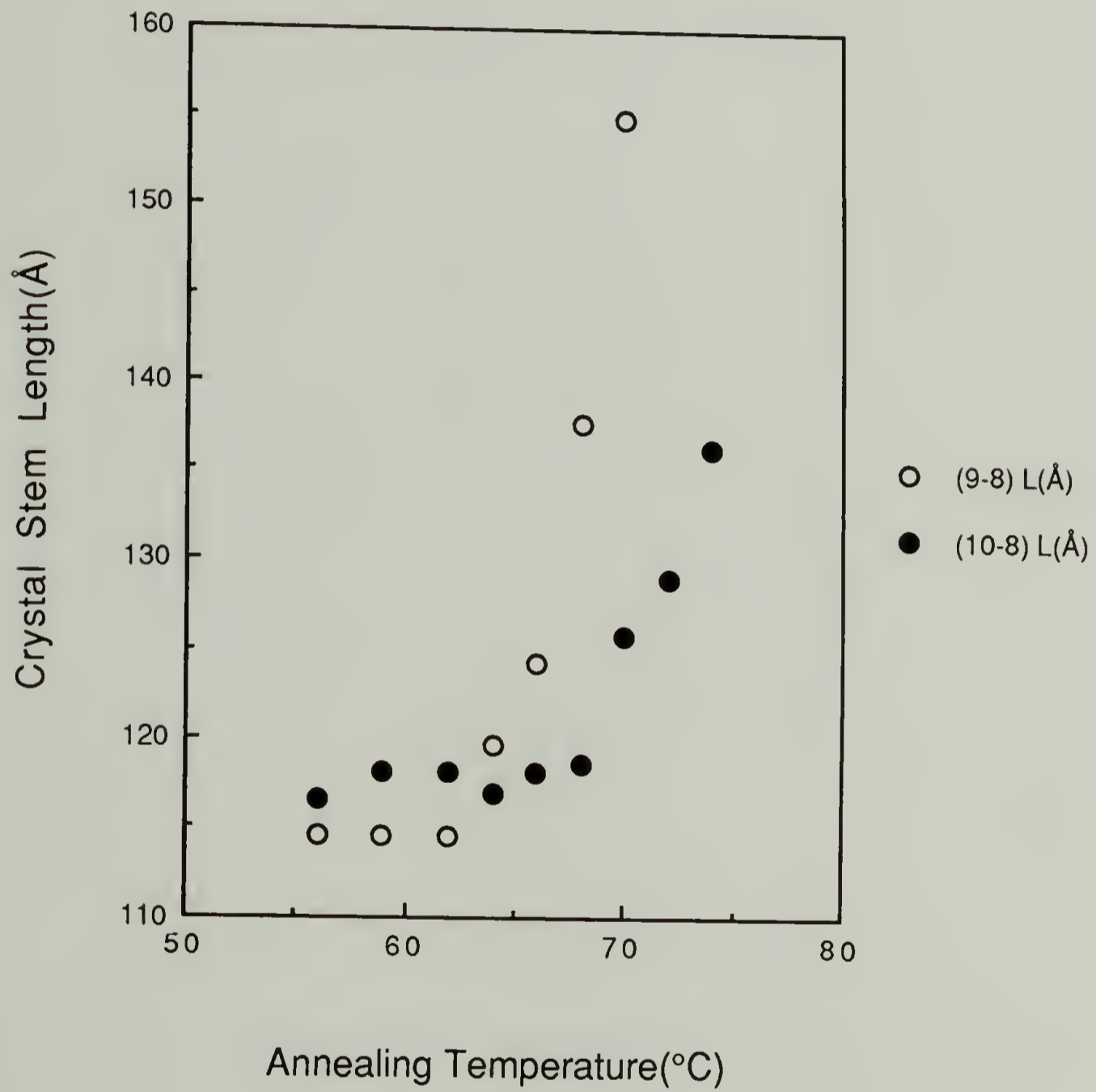


conditions during crystallization. The lowest frequency component can only arise from an increase in crystal stem length in a thickened lamallae.

The spectra obtained for the (9-8) sample annealed at temperatures of 56, 60, 62, 64, 66, 68, and 70 °C are shown in Figure 17. Spectra remain unchanged for annealing temperatures below 62 °C. Based upon the experimental value of $[v(\text{cm}^{-1}) \times L(\text{\AA})] = 2944$ for (9-8) grown at $T_{\text{cry}} = 33$ °C, the exhibited decrease in frequency, from 25.7 to 19.0 cm^{-1} , is representative of a 40 Å increase in crystal stem length (from 115 to 155 Å). This corresponds to an increase of 1.6 monomer repeats per crystal stem, and an average total of 6.2 repeats/stem. These values impose an upward limit of 5.9 folds/chain, if it is assumed that the SAXS period(L) included amorphous layers with tight folds equal to 0.5 monomer units. The decrements in frequency were from 25.7 cm^{-1} at 56, 59, 62 °C, to 24.6 cm^{-1} at 64 °C, to 23.7 cm^{-1} at 66 °C, to 21.4 cm^{-1} at 68 °C, to 19.0 cm^{-1} at 70 °C. These correspond to monotonically incremented changes in stem length of 5.1, 4.5, 13.4, and 17.3 Å respectively, and are plotted versus temperature in Figure 21. Since carbonyl registration is required the two smaller increases confirm the model of Girolamo et al.⁹ for a mixture of folds of different lengths. The two larger increases, at the higher temperatures, are equal to about 1/2 monomer repeat increases in stem length. These later increases could arise from step

FIG. 21 Crystal stem length in (\AA) as a function of annealing temperature in ($^{\circ}\text{C}$) for polyester single crystals (9-8) grown at $T_{\text{CRY}} = 33^{\circ}\text{C}$ and (10-8) grown at 39°C . Lengths based upon the experimental value of $[\nu(\text{cm}^{-1}) \times L(\text{\AA})] = 2944$ and 3393 for (9-8) and (10-8) respectively.

Crystal Stem Lengths After Annealing



type growth, but this can not be determined unequivocally from the data.

Spectra for the 10-8 polyester annealed at 56, 60, 62, 64, 66, 68, 70, 72, and 74 °C are shown in Figure 18. No change in frequency was noted below 68 °C. The decreases in frequency were from 29.1 cm^{-1} at 56 °C, to 28.6 cm^{-1} at 68 °C, to 27.0 cm^{-1} at 70 °C, to 26.3 cm^{-1} at 72 °C, to 24.9 cm^{-1} at 74 °C. Based upon the experimental value of $[v(\text{cm}^{-1}) \times L(\text{\AA})] = 3393$ for (10-8) grown at $T_{\text{cry}} = 39$ °C, the exhibited decrease in frequency is representative of an increase of only 20 Å in crystal stem length to a value 136.3 Å. The increase in stem lengths as a function of annealing temperature is shown in Figure 21. The monotonically increasing length further supports the mixed fold length model, and is in agreement with a SAXS study for polyester 10,10 over a similar temperature range.⁹ The overall magnitude of length change, however, is considerably less than the 70 Å increase to 170 Å determined for polyester 10,10 from SAXS data.⁹ In the above model the crystal structure scheme is such that the shorter stems increase in length to that of the longer stems, thereby resulting in an averaging of lengths until parity is achieved. It is expected then that the band half-width would decrease as the crystalline structure becomes more ordered and uniform during annealing. This was not observed.

An increase of 20 Å, or 0.74 monomer repeats per crystal stem, represents an average total of 5.0 repeats/stem. This value is about 1 less repeat/stem than for (9-8) crystallized with the same degree of undercooling. Such a result may be due to the existence of a longer more disordered fold region in the amorphous layer. In order for carbonyl registration with carbonyl groups alternating sides of the chain the fold length should be greater. This would agree with the disparity noted by Folkes et al. for the SAXS long period and Raman stem length upon annealing of (10,10).³⁹ For a low molecular weight (12K), a longer fold would impose an upward limit for the achievable stem length. If the calculated value for $[v(\text{cm}^{-1}) \times L(\text{Å})] = 2798$ is used, then the absolute crystal lengths decrease, but the increase in length with annealing of 16.2 Å (0.6 monomer repeats) is still small.

Annealing behavior of 9-8 polyester grown at 27.0 °C but annealed at 56, 59, 62, 64, 66, and 68 °C is shown in Figure 19. No change in frequency was noted below 56 °C. The decrease in frequency for the lowest frequency band is from 30.1 cm^{-1} at 56 °C, to 27.7 cm^{-1} at 59 °C, to 22.0 cm^{-1} at 62 °C, to 21.7 cm^{-1} at 64 °C, to 20.8 cm^{-1} at 66, to 19.3 cm^{-1} at 68 °C. Although this band does shift to lower values as a function of annealing temperature, there are also changes evident in both the frequency and intensity of other bands. This differs from other samples shown earlier. At 59 °C the lowest frequency band doubles in half-width. At 62 °C this

band is shifted to 22.0 cm^{-1} which represents an incremented increase in stem length of 30 \AA ($[v(\text{cm}^{-1}) \times L(\text{\AA})] = 2990$). This increase, as well as the total change in length by $62 \text{ }^\circ\text{C}$, is considerably larger than that observed for the (9-8) $T_{\text{cry}} = 33 \text{ }^\circ\text{C}$ case, for the same annealing temperature. For the highest annealed temperature, however, the frequencies of the LAM-1 observed for both cases (9-8 samples grown at the two degree of supercooling) are identical. This indicates that a similar crystal structure has been achieved. In fact the final spectra (top) in Figures 17 and 19 are practically superimposable in terms of both frequency and relative intensity.

The large increase in halfwidth at $59 \text{ }^\circ\text{C}$, for the lowest frequency band, may be attributed to the appearance of a new band at $\sim 32 \text{ cm}^{-1}$. At $62 \text{ }^\circ\text{C}$ the LAM-1 has shifted to a low enough frequency to be cleanly resolved, while other higher frequency bands in this region have disappeared. This new band remains at the same position even though the LAM-1 continues to shift downward for samples annealed at higher temperatures. The behavior of this new band, both in frequency and relative intensity, is quite similar to the band that exists at 32.0 cm^{-1} in all the annealed spectra for (9-8) $T_{\text{cry}} = 33 \text{ }^\circ\text{C}$.

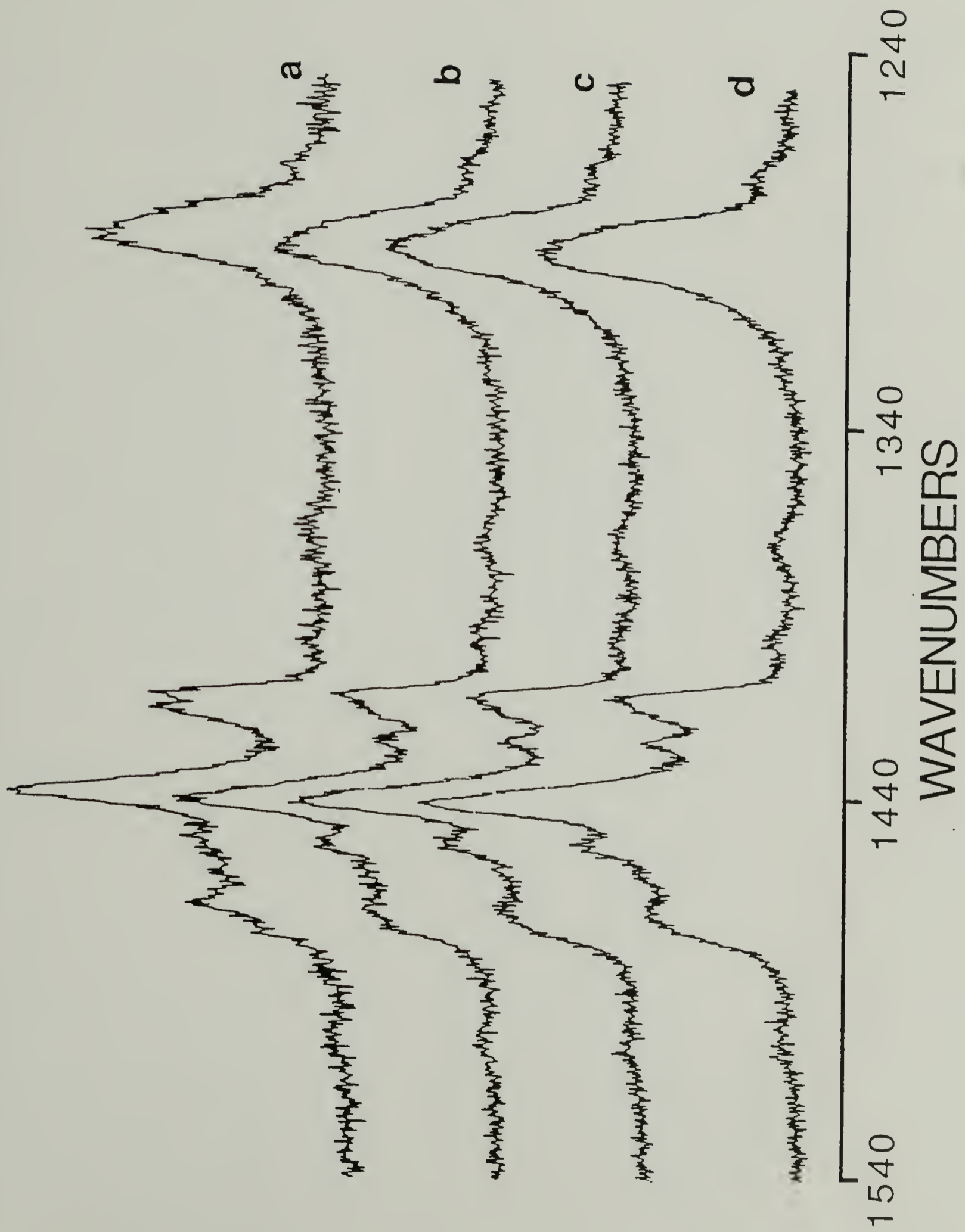
Mid Frequency Region. The Raman spectra obtained suggest that the crystalline structure of polyesters are changing when annealed. In order to shed further light on

the crystalline structural changes accompanying the annealing process, and the behavior of the low frequency bands in Figure 19, the CH bending region of the Raman spectra was also analyzed. Figure 22 shows the CH₂ twisting and bending regions for 9-8 polyester grown at 27 °C, and then annealed at 56(a), 62(b), 64(c), and 66 °C(d). The spectrum in Figure 22(a) is identical to that measured at room temperature before any annealing.

The CH₂ twist mode observed is unusually broad for all the polyester single crystal mats prepared. The large half-width (~14 cm⁻¹) can not be attributed solely to amorphous content, since its contribution would only be expected on the high frequency side of this band (> 1300 cm⁻¹).⁴⁰ In addition WAXS measurements lacked any evidence of an amorphous background, indicating that the crystal mats are highly crystalline. Normal coordinate analysis of fatty acids has shown that coupling occurs between the C_α-C-O stretching and CH₂ wagging vibrations, and C_α-C, C_α-C_β stretching modes.⁴¹ This results in a mixed mode expected to occur in the CH₂ twist region.⁴² Partially resolved components do occur on both the high and low frequency side of the main band, and factor group splitting is observed at low temperatures at the peak center (1296 and 1299 cm⁻¹). The large band width observed may be attributed to the overlapping components.

Generally 5 bands appear in the bending region in the Raman spectra obtained for linear aliphatic polyesters.

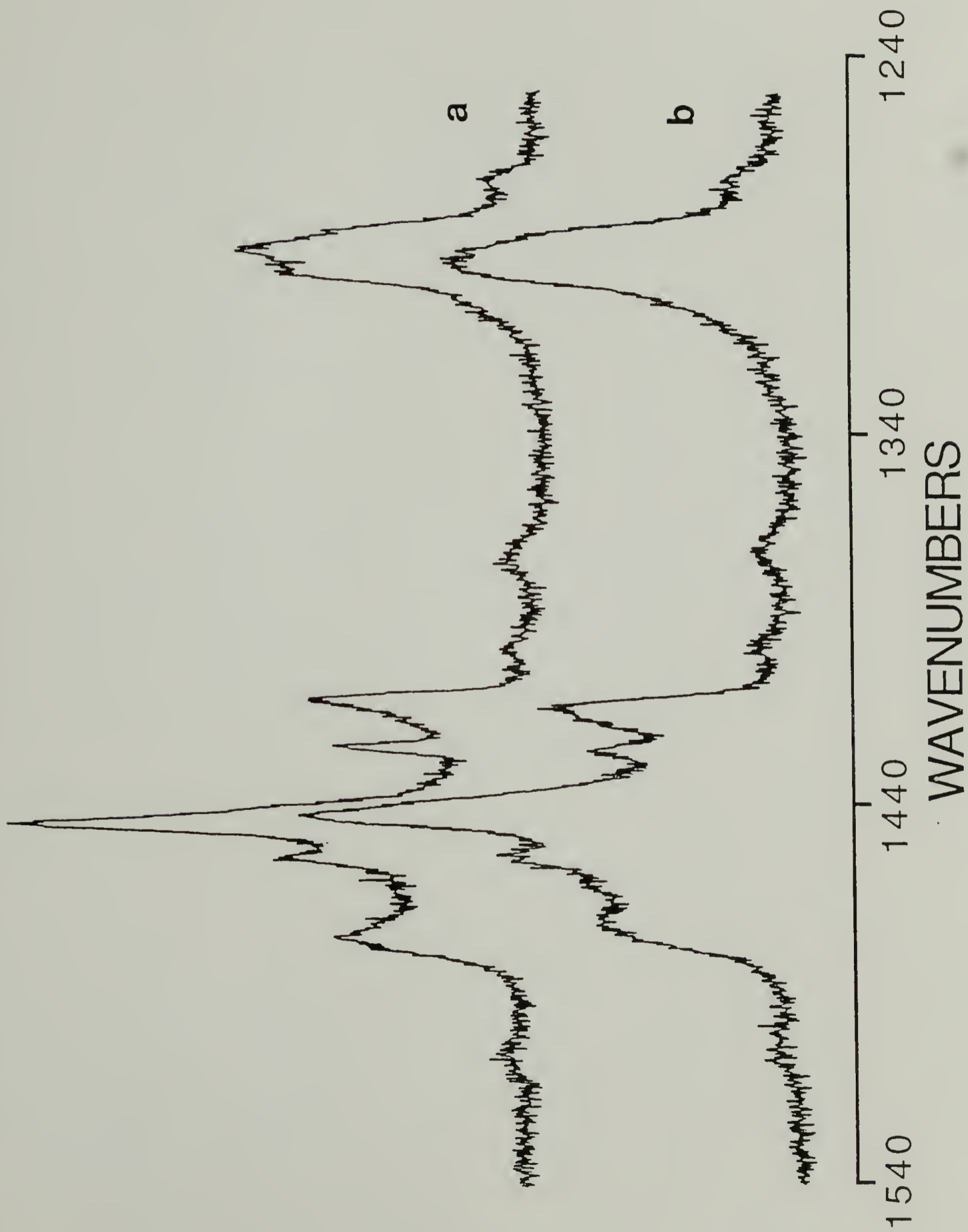
FIG. 22 CH₂ twisting and bending regions in Raman spectra obtained at room temperature for annealed (9-8) polyester single crystals grown at T_{CRY} = 27 °C. Band resolution is 1 cm⁻¹; argon ion laser (5145 Å) power is 100 mW. Samples annealed 2 hours at (a) T_A = 56, (b) T_A = 62, (c) T_A = 64, and (d) T_A = 66 °C.



Bands typically are found at about 1414, 1428, 1443, 1458, and 1476 cm^{-1} .⁴³ The dominant band in this region is at about 1441 cm^{-1} for both Polyester 10-8 and 9-8, regardless of the conditions. This band is attributed to the A_g CH_2 bending of methylene groups with neighboring methylene groups. The band at about 1414 cm^{-1} is also present for both Polyester 10-8 and 9-8, for all the samples prepared. It is assigned to the bending vibrations of methylene groups adjacent to the carbonyl groups (αCH_2). For polyethylene, a band in the Raman spectrum at 1416 cm^{-1} has been utilized to monitor the fraction of crystallinity and the volume fraction of orthorhombic packing.⁴⁰

For 9-8 polyester grown at 27 °C and annealed at increasing higher temperatures, a band at about 1418 cm^{-1} disappears. The band at 1452 cm^{-1} increases in intensity and a new band at about 1425 cm^{-1} appears. These changes occur at the same annealing temperatures as the appearance and disappearance of the low frequency bands in Figure 19, and the corresponding large increase in stem length. The spectra obtained for sample annealed at 66 and 68 °C are shown in Figure 23. The changes in this region for the low temperature spectrum are quite dramatic, with the CH_2 twist band being split, 1441 and 1453 cm^{-1} bands narrowed, and an increase in the intensity of the 1425 and 1471 cm^{-1} bands. The intensity of the 1471 cm^{-1} band has been utilized by Zerbi et al. to monitor the concentration of trans structures.⁴⁴

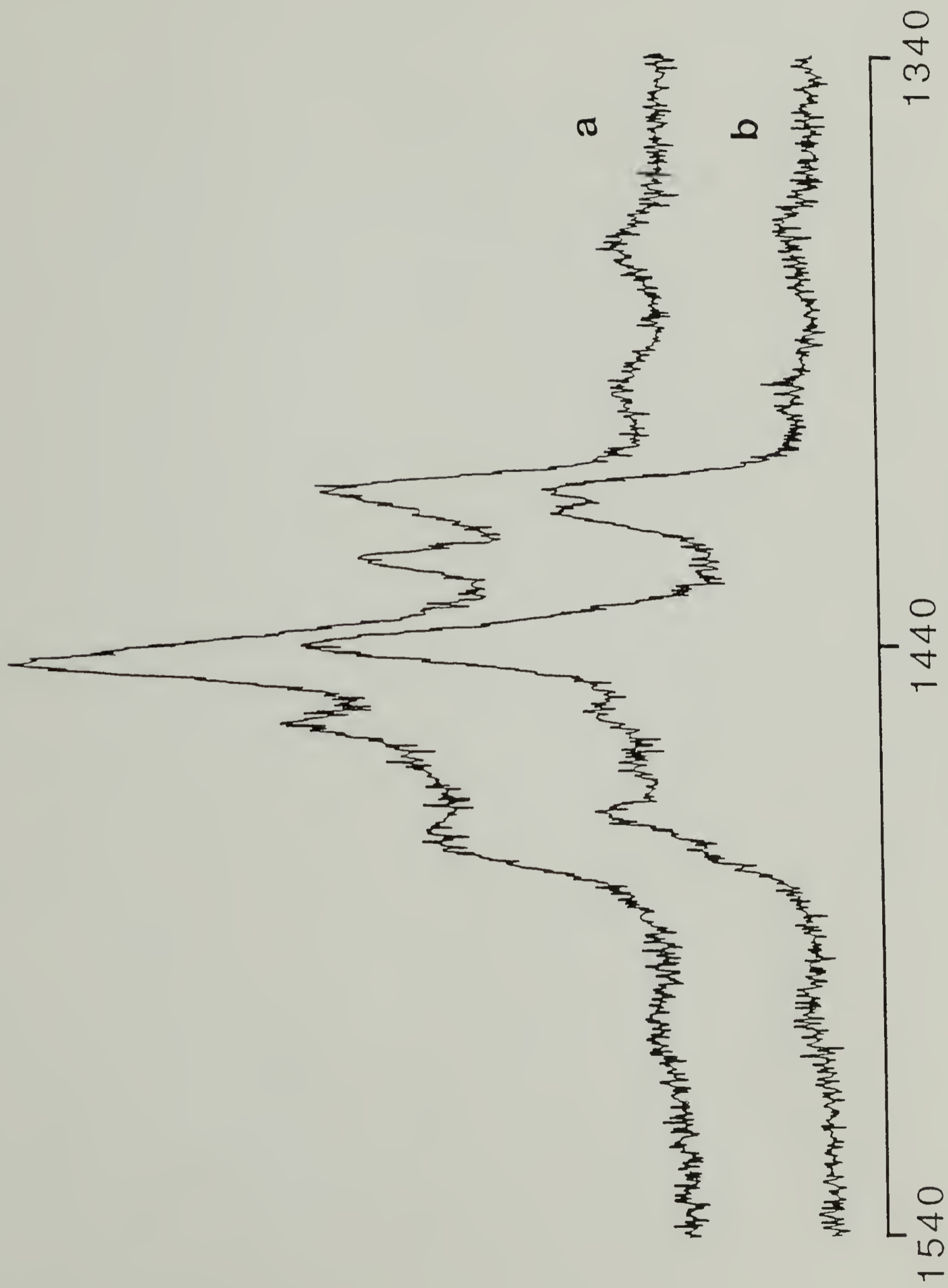
FIG. 23 CH₂ twisting and bending regions in Raman spectra obtained at (a) low temperature (- 125 °C) and (b) room temperature for annealed (9-8) polyester single crystals. Band resolution is 1 cm⁻¹; argon ion laser (5145 Å) power is 100 mW. Crystals grown at T_{CRY} = 27 °C, and annealed 2 hours at (a) T_A = 68 °C, and (b) T_A = 66 °C.



The Raman spectrum (Figure 24) for 9-8 polyester as grown at 33 °C contains the 1425 cm⁻¹ component. The sample grown at lower temperature (27 °C) contains the 1418 cm⁻¹ component. There is no question that the presence or absence of different bands depends on the crystallization conditions. For the 10-8 polyester two bands are present at 1414 and 1422 cm⁻¹ regardless of the crystallization or annealing conditions. Thus upon annealing of the (9-8) T_{cry} = 27 °C crystal mat, a transformation of crystal structure occurs which results in a thickened crystal with a different crystalline packing.

DSC results have indicated that a melting and recrystallization occurs at 62 °C, for the T_{cry} = 27 °C crystal, but not for the T_{cry} = 33 °C sample. WAXS results have indicated that polymorphism occurs for both even-even and odd-even structures, but Polyester 10-8 is expected to have a monoclinic crystalline structure, while (9-8) is expected to be orthorhombic. Based upon the results for the CH₂ bending region in conjunction with the large changes in the low frequency region, and the fact that low frequency bands observed for the T_{cry} = 27 °C sample change much more dramatically, it is reasonable to assign the unusual spectroscopic features in both low and high frequency regions to be associated with different crystalline forms.

FIG. 24 CH₂ twisting and bending regions in Raman spectra obtained at room temperature for as grown (9-8) polyester single crystals as a function of crystallization temperature. Band resolution is 1 cm⁻¹; argon ion laser (5145 Å) power is 100 mW. Growth conditions are listed in Table 1 for (a) T_{CRY} = 33 °C and (b) T_{CRY} = 27 °C.



References

1. Gornick, F.; Hoffman, J. D. *Ind. Eng. Chem.*, **1966**, 58, 2, 41.
2. Turnbull, D.; Fisher, J. C. *J. Chem. Phys.*, **1949**, 17, 71.
3. Blundell, D. J.; Keller, A.; Kovacs, A. J. *J. Polym. Sci.: Part B*, **1966**, 4, 481.
4. Blundell, D. J.; Keller, A.; *J. Macromol. Sci.*, **1968**, B2, 301.
5. Blundell, D. J.; Keller, A.; *J. Macromol. Sci.*, **1968**, B2, 337.
6. Fuller, C. S.; Erickson, C. L. *J. Am. Chem. Soc.*, **1937**, 59, 344.
7. Fuller, C. S.; Frosch, C. J. *J. Phys. Chem.*, **1939**, 43, 323.
8. Fuller, C. S.; Frosch, C. J. *J. Am. Chem. Soc.*, **1939**, 61, 2575.
9. Girolamo, M.; Keller, A.; Stejny, J. *Die Makromolekulare. Chemie*, **1975**, 176, 1489.
10. Fuller, C. S.; Frosch, C. J.; Pape, N. R. *J. Am. Chem. Soc.*, **1942**, 64, 154.
11. Kanamoto, T.; Tanaka, K.; Nagai, H. *J. Polym. Sci.: Part A2*, **1971**, 9, 2043.
12. Kanamoto, T. *J. Polym. Sci.: Polym. Phys. Ed.*, **1974**, 12, 2535.

13. Wang, Y. K.; Shu, P. H. C.; Stein, R. S.; Hsu, S. L. J. *Polym. Sci.: Polym. Phys. Ed.*, **1980**, 18, 2287.
14. Chang, C.; Wang, Y. K.; Waldman, D. A.; Hsu, S. L. J. *Polym. Sci.: Polym. Phys. Ed.*, **1984**, 22, 2185.
15. Snyder, R. G.; Krause, S. J.; Scherer, J. R. J. *Polym. Sci.: Polym. Phys. Ed.*, **1978**, 16, 1593.
16. Snyder, R. G.; Scherer, J. R. J. *Polym. Sci.: Polym. Phys. Ed.*, **1980**, 18, 421.
17. Dlugosz, J.; Fraser, G. V.; Grubb, D.; Keller, A.; Odell, J. A.; Goggin, P. L. *Polymer*, **1976**, 17, 471.
18. Fraser, G. V. *Ind. Journ. Pure & Appl. Phys.*, **1978**, 16, 344.
19. Hsu, S. L.; Krimm, S. J. *Appl. Phys.*, **1976**, 47, 4265.
20. Hsu, S. L.; Krimm, S. J. *Appl. Phys.*, **1977**, 48, 4013.
21. Hsu, S. L.; Ford, G. W.; Krimm, S. J. *Polym. Sci.: Polym. Phys. Ed.*, **1977**, 15, 1769.
22. Minoni, G.; Zerbi, G. J. *Phys. Chem.*, **1982**, 86, 4791.
23. Chang, C.; Krimm, S. J. *Appl. Phys.*, **1983**, 54, 10, 5526.
24. Woodward, L. A.; Long, D. A. *Trans. Faraday Soc.*, **1949**, 45, 1131.
25. Khoury, F.; Fanconi, B.; Barnes, J. D.; Bolz, L. H. J. *Chem. Phys.*, **1973**, 59, 5849.
26. Chang, C.; Krimm, S. J. *Polym. Sci.: Polym. Phys. Ed.*, **1984**, 22, 1871.
27. Fraser, G. V.; Keller, A.; George, E. J.; Dreyfuss, D. *J. Macromol. Sci. Phys.*, **1979**, B16, 295.

28. Rabolt, J. F.; *J. Polym. Sci.: Polym. Phys. Ed.*, **1979**, 17, 1457.
29. Strobl, G. R.; Eckel, R. J. *Polym. Sci.: Polym. Phys. Ed.*, **1976**, 14, 913.
30. Takeuchi, H.; Shimanouchi, T.; Tasumi, M.; Vergoten, G.; Fleury, G. *Chem. Phys. Lett.*, **1974**, 28, 449.
31. Chang, C.; Krimm, S. *J. Polym. Sci.: Polym. Phys. Ed.*, **1979**, 17, 2163.
32. Fraser, G. V.; *Polymer*, **1978**, 19, 857.
33. Harley, R. T.; Hayes, W.; Twisleton, J. F. *J. Phys. (C) Solid State*, **1973**, 6, L167.
34. Scott, J. F. *The Spex Speaker*, **1972**, 17, 2, Spex Industries, Metuchen, NJ, 1972.
35. Chang, C.; Wang, Y. K.; Waldman, D. A.; Hsu, S. L. *J. Polym. Sci.: Polym. Phys. Ed.*, **1984**, 22, 2185.
36. Rabolt, J. F.; Fanconi, B. *J. Polym. Sci.: Polym. Lett. Ed.*, **1977**, 15, 121.
37. Hendra, P. J.; Majid, H. A. *Polymer*, **1977**, 18, 573.
38. Strobl, G. R.; Eckel, R. *Colloid & Polym. Sci.*, **1980**, 258, 570.
39. Folkes, M. J.; Keller, A.; Stejny, J.; Goggin, P. L.; Fraser, G. V.; Hendra, P. J. *Colloid Polym. Sci.*, **1975**, 253, 354.
40. Strobl, G. R.; Hagedorn, W. *J. Polym. Sci.: Polym. Phys. Ed.*, **1978**, 16, 1181.

41. Hayashi, S.; Umemura, J. *J. Chem. Phys.*, **1975**, *63*, *5*, 1732.
42. Conti, G.; Minoni, G.; Zerbi, G. *J. Molec. Struc.*, **1984**, *118*, 237.
43. Holland-Moritz, K.; Hummel, D. O. *J. Molec. Struc.*, **1973**, *19*, 289.

CHAPTER 4

NORMAL COORDINATE ANALYSIS OF THE LONGITUDINAL ACOUSTIC MODE IN LINEAR ALIPHATIC POLYESTERS

Introduction

The principal objective of this study is to clarify the origin of the longitudinal acoustic mode (LAM-1) in linear aliphatic polyesters. In the previous chapter, analysis of low frequency Raman data indicated that not all of the observed bands could be assigned to the LAM. No correlation could be established between the frequency of certain modes exhibited in the low frequency Raman spectra of polyesters and chain length. Even though the structure (chain conformation, density of the unit cell) of aliphatic polyesters is quite similar to *n*-alkanes or polyethylene, the low frequency region of the polyesters differs significantly. Based on previous studies, one of the explanations for the existence of the multiple bands observed is that these may be assigned to the lattice modes of the unit cell or in fact to chain defects. Other studies have suggested that conformational defects can cause a coupling between longitudinal modes and transverse ones, thus activating previously silent vibrations and spreading the intensity from LAM to other vibrations in the low frequency region. The effects of conformational defects are hard to predict and may depend very much on the type of defect. "Sharp" deviations

have proven to be the type of structural defects affecting the intensity and frequency of LAM. In contrast, a slow or gradual twist introduced in a planar zigzag chain hardly affects the LAM at all.

As a result of the C=O and O's along the polyester chain, one can speculate that the presence of an asymmetric mass distribution, within a transplanar structure, can cause coupling of longitudinal and transverse vibrations, in order to account for the unusual observations in the low frequency Raman spectra. Normal coordinate analysis on model oligomers of linear aliphatic polyesters is carried out in this chapter in order to investigate the effect of inclusion of off-axis masses on the LAM vibration. These structures provided an unique opportunity to determine whether regularly spaced off-axis masses can cause coupling resulting in a redistribution of intensities. In light of the experimental results reported in Chapter 3, it is possible that such coupling occurs in the LAM-1, since a distribution of chain lengths and geometrical relationships of the carbonyl location with respect to the crystal stem center is certain to exist.

Background

Normal coordinate analysis has been quite successful in the past in characterizing the the molecular basis of the LAM. Early studies by Schaufele, Shimanouchi and Tasumi clearly established the origins of the LAM vibration for n -

alkanes and the associated atomic motions.^{1,2} They determined that for transplanar structures the LAM-1 mode was centrosymmetric, and could be described essentially as superposed CC stretching modes which have phase differences of $\delta_m = m\pi/n$ for $m=1$ in LAM-1, $m=3$ in LAM-3 etc. The atomic motions were shown to be almost exclusively in the chain direction. No displacements occurred perpendicular to the backbone plane and lateral in-plane displacements were nearly zero. The utility of such calculations was extended by Reneker and Fanconi³ when they examined the effect of local defect structures on the LAM intensity and frequency for n -alkane chains. In the region of the defect skeletal twisting and bending motion contributed to the LAM vibration. Decreases in the LAM intensity were predicted when the localized defects were anywhere but on the chain ends. It is known that such conformational defects within the crystal will effectively decouple the LAM vibration, so that the remaining trans segments on each side of it will vibrate with a frequency characteristic of their shortened length.^{4,5} Further calculations by Scherer and Snyder⁶ determined that the center of the intensity distribution moved to higher frequencies as the all trans segment length decreased. These calculated results were later experimentally verified for highly extruded polyethylene.⁶⁻⁸ If two crystals are of the same thickness, as measured by SAXS or electron microscopy, and one contains more defects, then the stem length

distribution measured by LAM-1 will be broadened towards shorter lengths for the crystal with more defects.

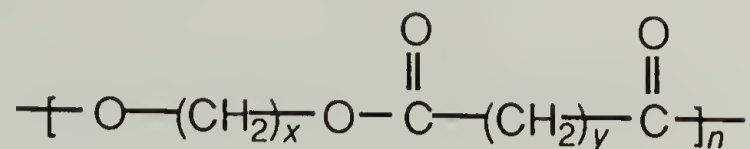
The existence of transverse acoustical modes of the *n*-paraffins was expected in the very low frequency region based upon the calculations of polyethylene.^{9,10} The calculated frequencies were critically dependent upon the lattice interactions. Olf and Fanconi experimentally assigned certain low frequency bands exhibited by *n*-alkanes to the in-plane and out-of-plane transverse acoustical branches.¹¹ In a later normal mode calculation Mazur and Fanconi¹² showed that sizeable distortions in the longitudinal motions occurred for C₁₁H₂₄ and C₁₃H₂₈. Transverse motions of LAM-1 exhibited an atomic displacement phase relationship characteristic of the transverse acoustic mode (TAM-*m*) for *m*=4. This was attributed to coupling between LAM-1 and TAM-4 for a particular length *n*-alkane only. An extensive normal coordinate calculation by Chang and Krimm on the effect of terminal and connecting fold structures, masses, and perturbing forces showed that a number of LAM like modes can occur in the place of the unperturbed LAM-1.¹³ These could be distributed among a range of frequencies, each of lower intensity than for the unperturbed case, and with contributions from transverse displacements. The LAM-1 frequency was determined to be most sensitive to the structure of the first 6 methylene groups in the defect structure connected to the all trans segment, and hardly sensitive to the structure beyond that.

The placement of the off axis masses within the structure of oligomers of aliphatic polyesters can be easily varied by; (1) Altering the number of methylene groups within the monomer repeat, and (2) Changing the location of the beginning and end of the chain with respect to the first and last carbonyl groups. This type of asymmetric mass arrangement within the crystalline core had not been considered in the previous studies. Effects due to the overall length of the chain, chain segments of ether or ester linkages, and odd-even versus even-even structures, can also be investigated. This study considers these effects upon LAM-1.¹⁴ Results are based upon calculated intensities and atomic motions for the LAM-1 and other modes of similar frequency. In all cases a LAM-1 characterized by centrosymmetric in plane longitudinal atomic motions can be identified. In some instances additional LAM-1 like modes were calculated at nearby frequencies. These exhibited more complex atomic motions with significant transverse in-plane contributions in the atom displacements.

Normal Coordinate Analysis

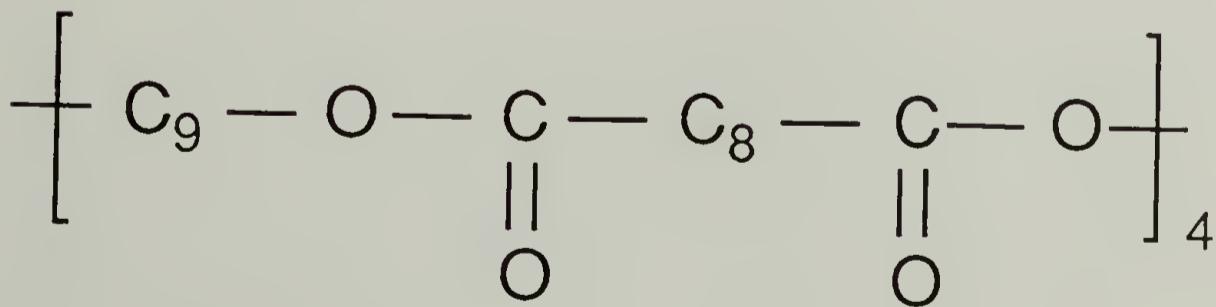
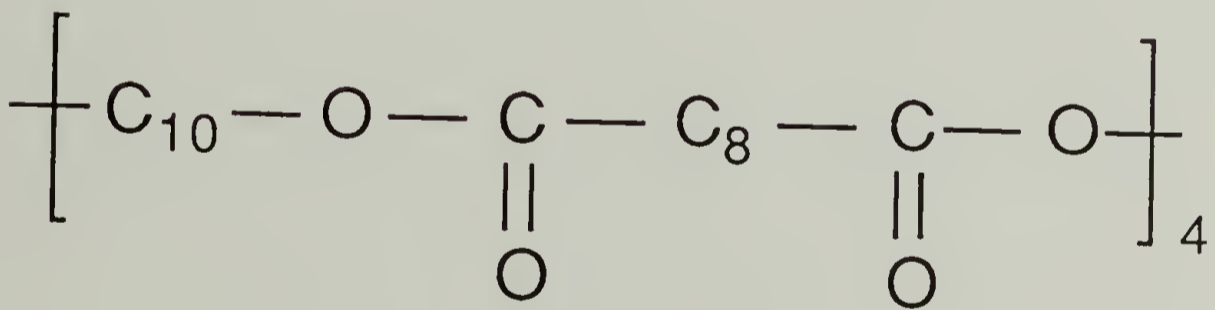
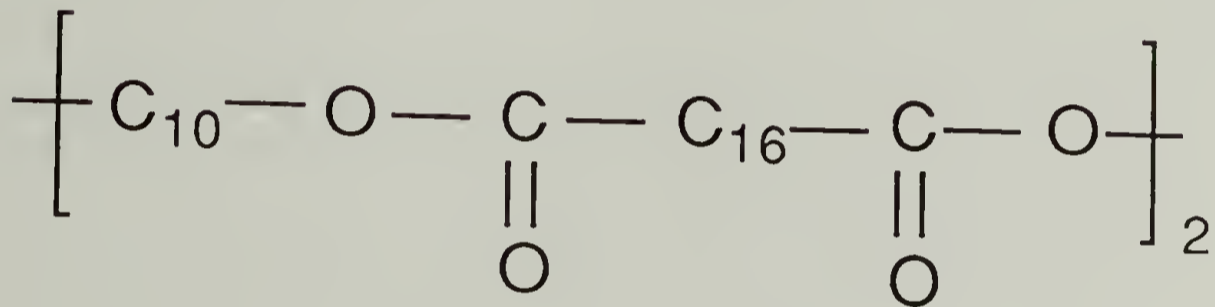
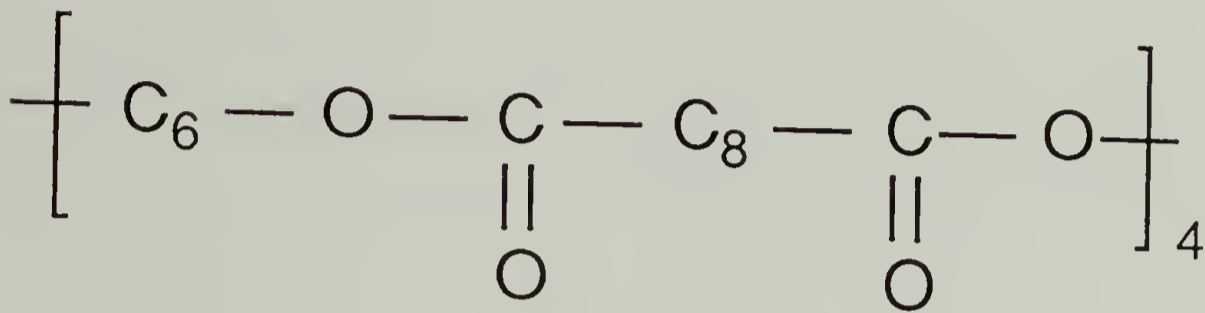
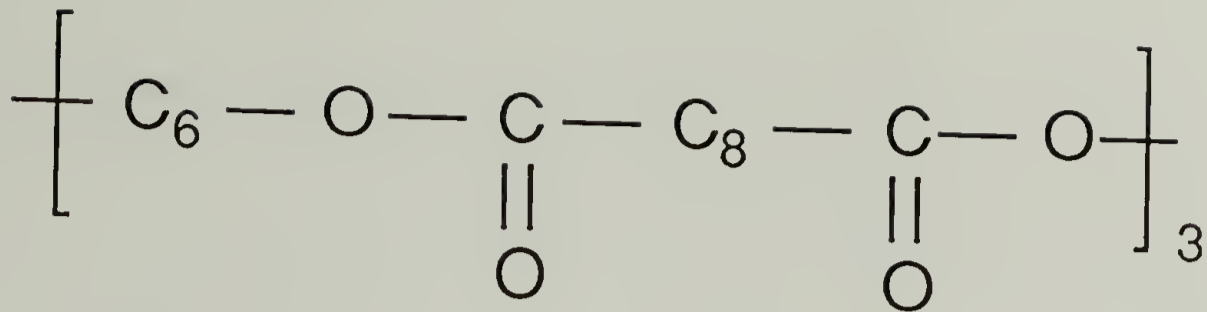
Polyester chains of sufficiently high x and y have essentially a planar zigzag conformation in the crystal with the ester-group plane only slightly out of the plane defined by the zigzag of the methylene sequences. For initial

analysis three model oligomers were selected. These are shown in Figure 25 as



for $x = 6$, $y = 8$ and $n = 3$ and 4 , and for $x = 10$, $y = 16$, $n = 2$, respectively. These molecules have a total chain length ranging from 66 to 88Å. Such molecules are somewhat shorter than the measured SAXS spacings, but are sufficiently long and contain enough repeat units to show the effects of the methylene sequence length variations and the overall chain length. In order to reduce the complexity of the computation single chain structure with the point-mass approximation was used, with CH₂ and CH₃ groups taken as atoms of 14 and 15 a.m.u., respectively. This approximation is not expected to alter the validity of the calculations. Only the skeletal modes are of interest, and the force field was developed in a point-mass approximation specifically to analyze these. Furthermore, the consequences of the general trends are more important than exact numerical results. The structures of 6-8 and 10-16 polyesters used in these calculations were taken from previous x-ray studies.¹⁵⁻¹⁷ The structural parameters for both polyesters are defined in Figure 26 and listed in Table 5. For the 6-8 polyester, oligomers were chosen with the same methylene sequence length but different overall chain length. The 10-16 oligomer represents a molecule

FIG. 25 Chemical structure of various model linear aliphatic polyester oligomers evaluated by normal coordinate analysis. Oligomers $(6-8)_3$, $(6-8)_4$, and $(10-16)_2$ were evaluated first, while longer oligomers such as $(10-8)_4$, and $(9-8)_4$ were later considered for length, odd-even, and even-even effects. No hydrogens are included in chemical structures since point-mass approximations were utilized.



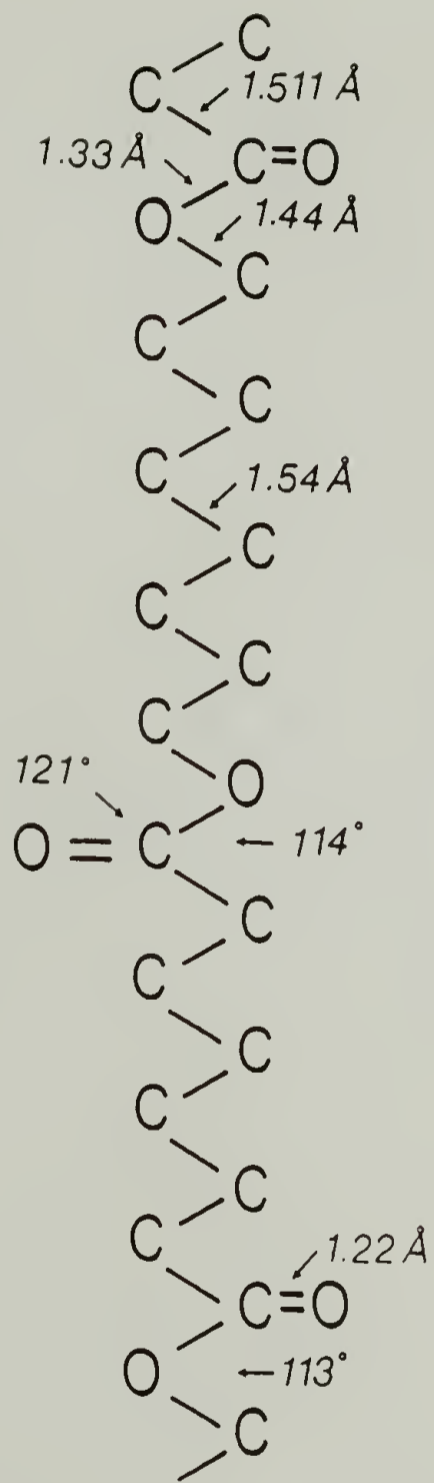


FIG. 26 Structural parameters used in normal coordinate calculations for oligomers of linear aliphatic polyesters.

TABLE 5. Structural parameters of the proposed geometries of linear aliphatic polyester oligomers. Values for bond lengths and angles for polyesters (6-8) and (10-16) are taken from previous x-ray studies.

TABLE 5

Structural Parameters of the Proposed Geometries of Polyester Oligomers

Bond/angle	Length (Å) / angle (deg)		
C=O	1.22		
O—CO	1.33		
CC—O	1.44		
OC—C	1.511		
CC—CC	1.54		
< COC	113		
< COC	114		
< COC	121		
	<u>Molecule I</u>	<u>Molecule II</u>	<u>Molecule II</u>
	$\begin{array}{c} \text{O} \quad \text{O} \\ \parallel \quad \parallel \\ (\text{C}_6\text{OCC}_8\text{CO})_3 \end{array}$	$\begin{array}{c} \text{O} \quad \text{O} \\ \parallel \quad \parallel \\ (\text{C}_6\text{OCC}_8\text{CO})_4 \end{array}$	$\begin{array}{c} \text{O} \quad \text{O} \\ \parallel \quad \parallel \\ (\text{C}_{10}\text{OCC}_{16}\text{CO})_2 \end{array}$
Number of atoms	60	80	64
Number of internal coordinates	180	242	190
Chain length(Å)	66.2	88.4	74.4

intermediate in length between the two 6-8 oligomers, but with different internal structures.

The intrachain potential functions for the model compounds were directly transferred from those used for poly(ethylene terephthalate)¹⁸ and skeletal approximation of *n*-alkanes.³ The 29 force constants used are listed in Table 6. Although this type of approximation has proved to be useful in structural characterization of polyesters,¹⁹ it should be emphasized that the purpose of the calculation is to try to understand how perturbations of the ester groups modify LAM, rather than to obtain exact calculated frequencies. For such large molecules it is impractical and time consuming to carry out normal coordinate calculations using localized symmetry coordinates constructed from internal coordinates. Therefore all calculations were carried out in Cartesian coordinate space. The Wilson GF matrix method was used. The G matrix elements (inverse kinetic energy coefficients) were computed in terms of atomic masses and the specified geometrical parameters. The F matrix (containing the potential energy elements) was composed of blocks of external coordinates corresponding to Cartesian displacement coordinates of bond stretches, angle bends, torsions, and interactions between stretches and bends.

In the calculated spectra there are many skeletal-deformation vibrations in the low-frequency region. The criterion for a vibration to be LAM or LAM-like is that it

TABLE 6. Force constants used to define intrachain potential functions for normal coordinate analysis of model oligomers of linear aliphatic polyesters. Values directly transferred from those used for poly(ethylene terephthalate) and skeletal approximations of *n*-alkanes.

TABLE 6

 Force Constants Used in the Normal Coordinate Calculation

CC ν	4.622	CO'—C*O'	0.288
CCC δ	1.000	O'C—CO	0.8086
CCCC τ	0.045	CO—CC''	1.2197
CC—CC'	0.132	O'C—CC''	0.8446
CCC—CCC'	0.300	O''CO—CC''	0.0648
CC—CCC'	0.170	O'CO—CO''	0.0648
C=O ν	11.476	C''CO—CO'	0.45
C—O' γ	6.7147	OCO'—CO	0.45
C*—O' γ	4.2902	C''CO'—CC''	0.6932
C=O op	0.587	C''CO'—CO'	1.1975
CO'C*	1.5792	C*O'C—CO'	0.6252
OCO'	1.3484	C*O'C—C*O'	0.45
C''CO	1.246	CC*O'—C*O'C	-0.001
C''CO'	1.967	C*O'C—O'CC''	0.0924
CC*—C*O'	0.8286		

should be mainly an in-plane motion with a node at the center of the chain and antinodes with maximum longitudinal displacement of opposite phase at chain ends. The identification of such a mode can be accomplished by examining the calculated Cartesian eigenvectors of each normal vibration. The absolute Raman intensity of the LAM-like vibrations can be estimated by using the bond polarizability theory described previously.¹² In the simplest approximation, the intensities of various LAM-like modes can be approximated by the squared sum of the associated eigenvectors of the internal coordinates of the backbone. The validity of this intensity calculation, however, depends on an accurate assessment of the polarizability change of each bond and angle. For methylene sequences, this information is available from previous analyses of *n*-alkanes.¹² The value, however, for any bond or angle coordinate involving oxygen is not known. Therefore, exact intensity calculations for these polyester segments are not possible. In this study, since the ester groups only comprise a very small portion of the chain segments, the polarizabilities of the coordinates of the ester groups were set to those of *n*-alkanes.

Results and Discussion

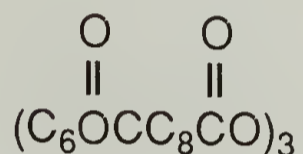
The assignment of very intense bands in the low-frequency Raman spectra of polyesters to LAM rests principally on the inverse frequency versus chain length

dependence.²⁰ This relationship is qualitatively expected and is observed for the polyester system, as described in the previous chapter. It is unusual, however, to see multiplet structures associated with the LAM of dilute-solution-grown polymeric single crystals. Since the LAM frequency is sensitive to the length of straight chain segments, changes in bandwidth or multiple components are attributed to changes in the distribution of straight chain segments. The LAM doublet of linear aliphatic polyesters, shown in Chapter 3, Figure 7, cannot be attributed to two distinguishable chain-length distributions. Wide-angle x-ray scattering showed that the chain stems are perpendicular to the single-crystal mat.¹⁵ The small-angle scattering, shown in Chapter 3, Figure 6, exhibits a single peak for all cases, thus suggesting one discrete lamellar thickness.

It can be argued that the SAXS is sensitive to long-range periodicity, the sum of the crystalline layer and the amorphous interface. In contrast, the LAM is only sensitive to the regularity of chain conformation (straight chain length) or local order. The information obtained from the two techniques is thus complementary, not identical. Considering the relative intensity of the two components, it would be rather unlikely for a second population of lamellae to be completely absent in SAXS. In addition, when samples are annealed, only one component (that at the lowest frequency) moves to a lower frequency corresponding to

longer straight stem length in a thickened lamella. The second component remains essentially at the original position. This is true for all 6-8, 9-8, 10-8, and 10-16 polyester samples.

From normal vibrational calculations for these large molecules a number of skeletal motions are found. From consideration of the eigenvectors as described previously, two LAM-like vibrations have been found for each of the three structures considered. The frequencies of these vibrations are listed in Table 7. The two LAM-1 like vibrations of molecule I



are calculated to be 37.7 and 41.5 cm^{-1} , with the higher-frequency component the more intense. Judging from the Cartesian displacement projection along the chain axis, it can be concluded that the 41.5 cm^{-1} component has more LAM character than the 37.7 cm^{-1} component. Both vibrations, however, contain large contributions from transverse motions. The atomic displacements associated with these two modes are shown in Figure 27a. The reason for having two strong LAM-like vibrations is the coupling between the longitudinal and transverse acoustic motions. As demonstrated in the mono- or disubstituted bromoalkanes^{13,21} any off-axis unbalanced masses will tend to introduce lateral motions, thus causing significant coupling between pure longitudinal and transverse

TABLE 7. Frequencies of two LAM-1-like vibrations calculated for model oligomers of linear aliphatic polyesters. Intensity ratios of (6-8)₃, (6-8)₄, and (10-16)₂ are based upon the squared sum of the associated eigenvectors of the internal coordinates of the backbone.

TABLE 7

LAM-like Modes Calculated for Polyester Oligomers

Structure	LAM-like 1	LAM-like 2	Intensity Ratio
$\begin{array}{c} \text{O} \quad \text{O} \\ \parallel \quad \parallel \\ (\text{C}_6\text{OCC}_8\text{CO})_3 \end{array}$	41.5	37.7	4.6:1
$\begin{array}{c} \text{O} \quad \text{O} \\ \parallel \quad \parallel \\ (\text{C}_6\text{OCC}_8\text{CO})_4 \end{array}$	30.7	35.0	5:1
$\begin{array}{c} \text{O} \quad \text{O} \\ \parallel \quad \parallel \\ (\text{C}_{10}\text{OCC}_{16}\text{CO})_2 \end{array}$	37.8	36.9	4.4:1

FIG. 27 Atomic displacements for the two LAM-1-like modes calculated for two model oligomers of linear aliphatic polyesters. (a) Molecule I, (6-8)₃, top: 41.5 cm⁻¹ mode, bottom: 37.7 cm⁻¹ mode. (b) Molecule III, (10-16)₂, top: 37.8 cm⁻¹ mode, bottom: 36.9 cm⁻¹ mode.



a



b



displacements.^{3,12} Consequently, the resulting mixed modes contain characteristics of both. The intensities of these modes depend on the nature and extent of departure from the uniform linear chain. This type of mixing is prohibited in a linear-chain model based on symmetry considerations.

The two LAM-s calculated for the molecule with longer chain length, molecule II, are at 35.0 and 30.7 cm^{-1} . In this case the 30.7 cm^{-1} component is the more LAM-like vibration. When compared to molecule I, molecule II has a chain length increased by one additional repeat unit. As a result a corresponding decrease in the LAM frequency is expected. The frequency of the less intense component remained essentially unchanged. This is consistent with the experimental observations showing that the frequency of one component is sensitive to changes in the straight stem length, while that of the other is not.

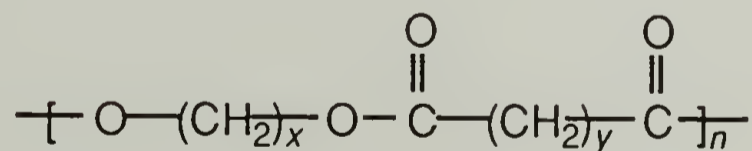
For molecule III, two LAMs are also found. The calculated frequencies are close together at 37.8 and 36.9 cm^{-1} , with the 37.8 cm^{-1} band being the more LAM-like. Since its chain length at 74.4 Å is intermediate between those of molecules I and II, the frequency calculated for molecule III is also found between the LAM of the two molecules. The atomic displacements associated with these two modes are shown in Figure 27b. From Equation (1) the product of the frequency and the chain length is expected to be proportional to $(E/\rho)^{1/2}$. The calculated values are 2747, 2714, and 2812

\AA cm^{-1} for molecules I, II, and III, respectively. All of these values depart somewhat from the experimental ones calculated by using the SAXS periodicity and the observed LAM frequencies. Some of this difference can be attributed to the impossibility of estimating the amorphous contribution to the SAXS periodicity. Polyester chains of sufficiently high x and y have essentially a planar zigzag conformation in the crystal with the ester-group plane only slightly out of the plane defined by the zigzag of the methylene sequences. Since the chain conformation is similar, the c -axis elastic modulus for these polyesters should not be significantly different from that of polyethylene. As a result of the ester groups, single-chain densities should all be greater than that of polyethylene. Thus the calculated values should all be smaller than the nearly 3000\AA cm^{-1} found for polyethylene.^{1,22-24} As compared to the 10-16 polyester, the somewhat smaller values for the 6-8 polyesters may then be due to the larger percentage of the ester group relative to the number of methylene sequences.

Ideally it is also necessary to compare the intensities of the two calculated modes to the observed ones. Furthermore, the relative intensity calculation for the two components should incorporate the effects of occupation probabilities of various vibrational levels in the very low-frequency region.²⁵ The difficulty with the intensity analysis can be seen in Figure 7 of Chapter 3. The LAMs

found for polyesters are often superimposed on the wings of the Rayleigh line. It is difficult, if not impossible, to remove the Rayleigh contribution reliably to obtain the true LAM band shape and intensity. Several computer fitting techniques were attempted which led to contradictory results. When the factor $f = \nu[1 - \exp(-h\nu/RT)]$ is taken into account, the observed intensity ratio should be closer to 6:1 for the bands calculated at 36 and 41 cm^{-1} . When the bands are well separated, as in the annealed samples, the intensity expected will be further modified. The most simplistic approach is to define the base line by connecting the minima of each peak. In this case the integrated intensities of the two peaks are roughly 5:1, fairly close to the calculated values.

Further calculations were then carried out on model oligomers which had an additional monomer repeat, so that the transplanar chain length was in the range experimentally determined (over 100Å). The molecules are shown in Figure 25 as



for $x = 10$, $y = 8$, $n = 4$ and for $x = 9$, $y = 8$, $n = 4$. These two molecules have a total chain length of 109 Å and 104 Å respectively. From examination of the eigenvectors there is only one LAM-1 like mode identified for both cases. This is at 25.7 and 26.5 cm^{-1} respectively. The atomic displacements,

shown in Figures 28 and 29, indicate that for $(9-8)_4$ the motion of the LAM is almost purely longitudinal, while for $(10-8)_4$ there are significant contributions from in-plane motions perpendicular to the chain axis. The motions in the latter case are similar to those of the three shorter molecules. The circles represent the carbonyl oxygen positions relative to those of the backbone. The atomic displacements of the calculated modes close in frequency to the LAM-1 exhibit in-plane motions that are almost entirely perpendicular to the backbone axis. In addition the correct phase relationship along the backbone for a LAM-1 is not satisfied.

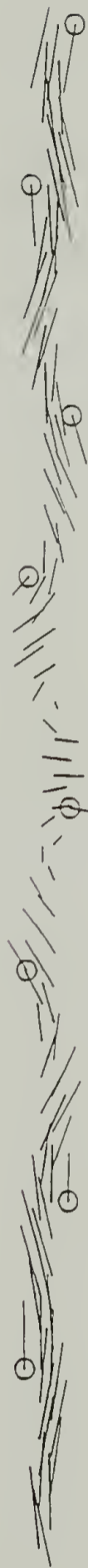
Relative intensity calculations of the modes close in frequency to the LAM-1, are based upon the squared sum of the associated eigenvectors of the internal coordinates of the backbone (stretching and bending). These indicate that in the case of $(9-8)_4$ no other mode has a LAM-like intensity contribution greater than 0.1% of the identified LAM-1 at 26.5 cm^{-1} . For $(10-8)_4$ the mode at 21.6 cm^{-1} has the greatest relative intensity, but it is only 5% of the value determined for the perturbed LAM-1 at 25.7 cm^{-1} . These results are for oligomers with lengths similar to that of the measured lamellar thickness, assuming the relationship between frequency and length for an unperturbed rod. The $(10-8)_4$ result (one mode dominant in relative intensity and one minor) is quite similar to that reported for A-C₇₄-A, where A

FIG. 28 Atomic displacements for one LAM-1-like mode calculated for model oligomer (10-8)₄. LAM-1 vibration is at 25.7 cm⁻¹. and other calculated TAM-like modes are at 21.6 cm⁻¹, 26.8 cm⁻¹ and 32.3 cm⁻¹. Open circles represent the carbonyl oxygen positions relative to those of the backbone.

IO-8, 96 ATOMS



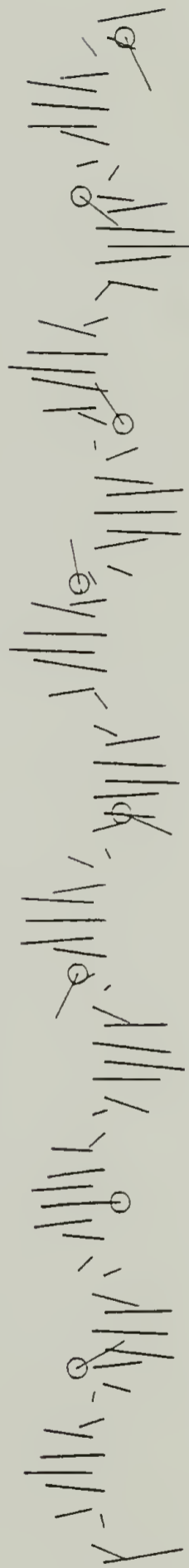
D18DISP1
v, 21.56



D18DISP
v, 25.74

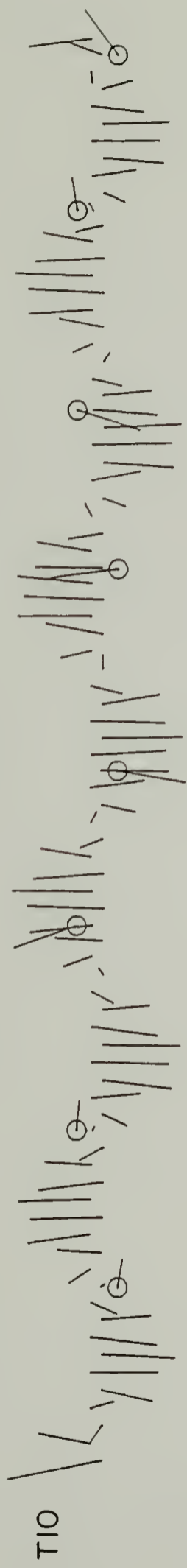


D18DISP2
v, 26.78



D18DISP3
v, 32.26

FIG. 29 Atomic displacements for one LAM-1-like mode calculated for model oligomer (9-8)₄. LAM-1 vibration is at 26.5 cm⁻¹. and other calculated TAM-like modes are at 24.1 cm⁻¹, 29.7 cm⁻¹ and 35.8 cm⁻¹. Open circles represent the carbonyl oxygen positions relative to those of the backbone.

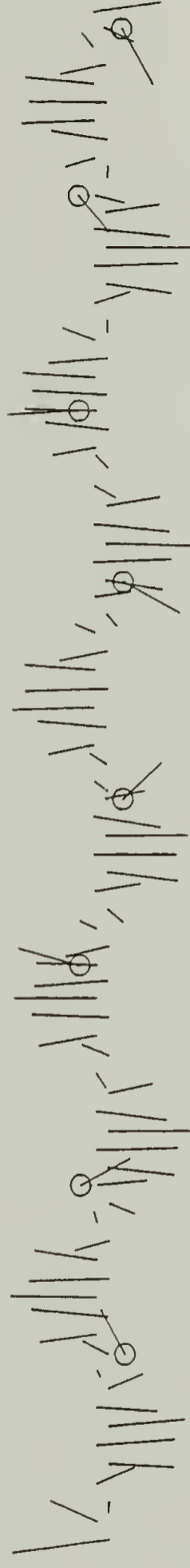


T10

D98DISP1
24.14

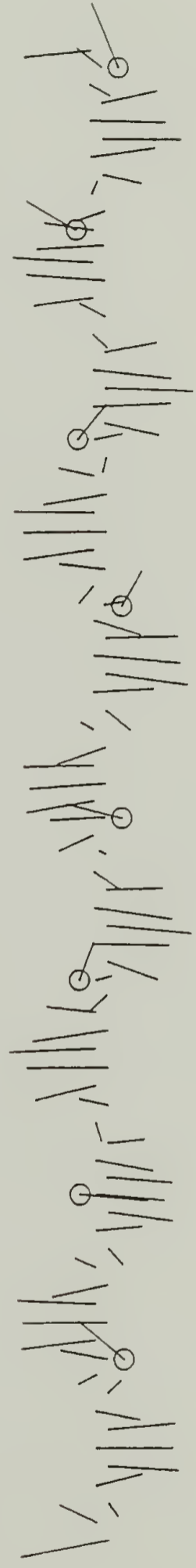


D98DISP
26.46



T12

D98DISP2
29.72



T13

D98DISP3
35.83

represents an end structure of 6 CH₂ groups in a nonregular conformation.¹³ The existence of a few LAM-like modes over a narrow frequency range each with reduced intensity from the unperturbed case is not indicated. The computed results do not agree with the experimentally observed relative intensities, since neither an asymmetric band envelope nor multiple components with significant intensity are predicted.

It was suspected that the length of internal methylene sequences could be responsible for the coupling, since the atomic motions indicated that nodes were located at or near the ester locations. In order to determine whether this was the case the boundary conditions of the calculation were altered, so that the chain length was maintained but the beginning and ending positions of the molecule differed. This was carried out for the (9-8)₄ molecule. The three cases evaluated had 92, 95, and 95 atoms but the endgroup structures were methylene sequence and ester, ester and ester, and methylene sequences respectively. In the third case the off-axis carbonyl groups alternate in pairs from one side of the backbone to the other and are therefore symmetrical with respect to the molecule center. In the first and second cases, the carbonyl positions are not arranged symmetrically relative to the molecule center.

The calculated LAM-1 frequencies are 26.5, 25.6 and 25.6 cm⁻¹ respectively. In all three cases only one LAM-1-like mode can be identified from the phase relationship of the

eigenvector components. No other mode has a relative intensity that is greater than 0.1 % of that calculated for the respective LAM-1. The atomic displacements for the three molecules are shown in Figures 29, 30, and 31. For the methylene sequence endgroups case the motion is almost purely longitudinal for the outer thirds of the molecule, and in the middle there is evidence of in-plane contributions. This is different from the other two cases which exhibit small contributions of in-plane motion along the entire backbone of the molecules. This demonstrates the importance of the geometrical relationship of the off-axis masses relative to the chain center. The methylene sequence end group structure has the most symmetric arrangement and also the smallest contribution of in-plane motions to the LAM-1 vibration.

The effect on the positions of the nodes of the transverse motions for the three different end group structures can be determined from the atomic displacements. The nodes do not necessarily occur at or near the ester groups, but rather at the same positions along the backbone in terms of distance from the chain ends. This suggests the phase relationship of the transverse motions is not the result of specific internal methylene sequence lengths, but is a function of the overall chain length and is independent of the carbonyl positions along the chain.

None of the 4 repeat oligomer structures display any significant LAM-like contribution in modes close in frequency

FIG. 30 Atomic displacements for one LAM-1-like mode calculated for model oligomer (9-8)₄ with ester terminal groups. LAM-1 vibration is at 25.6 cm⁻¹, and other calculated TAM-like modes are at 23.0 cm⁻¹, 28.3 cm⁻¹ and 34.1 cm⁻¹. Open circles represent the carbonyl oxygen positions relative to those of the backbone.

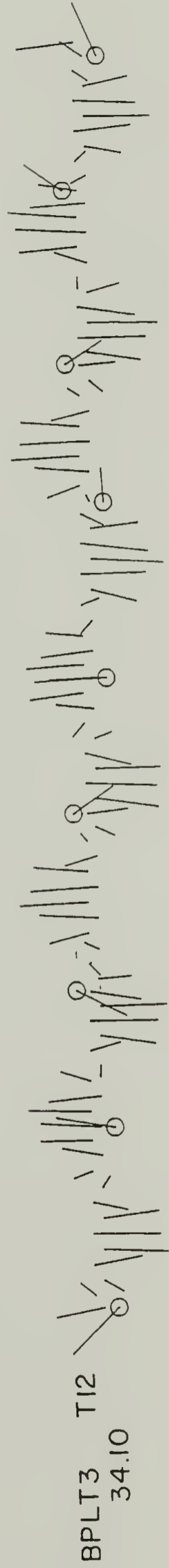
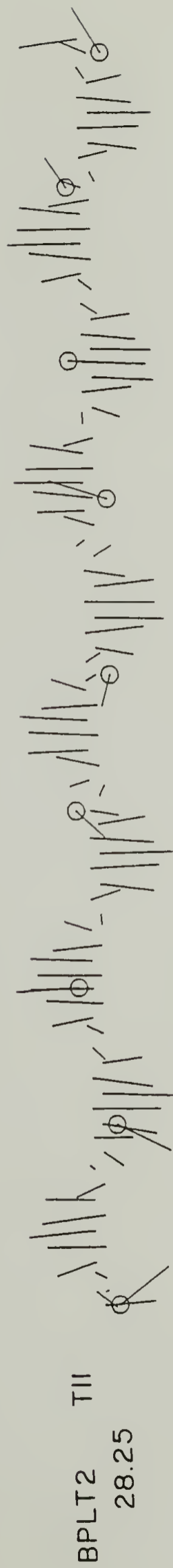


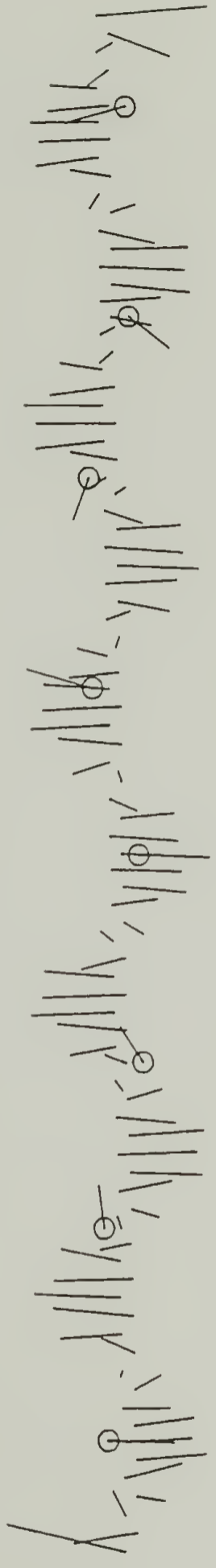
FIG. 31 Atomic displacements for one LAM-1-like mode calculated for model oligomer (9-8)₄ with methylene sequence terminal groups. LAM-1 vibration is at 25.7 cm⁻¹. and other calculated TAM-like modes are at 23.7 cm⁻¹, 28.7 cm⁻¹ and 34.3 cm⁻¹. Open circles represent the carbonyl oxygen positions relative to those of the backbone.



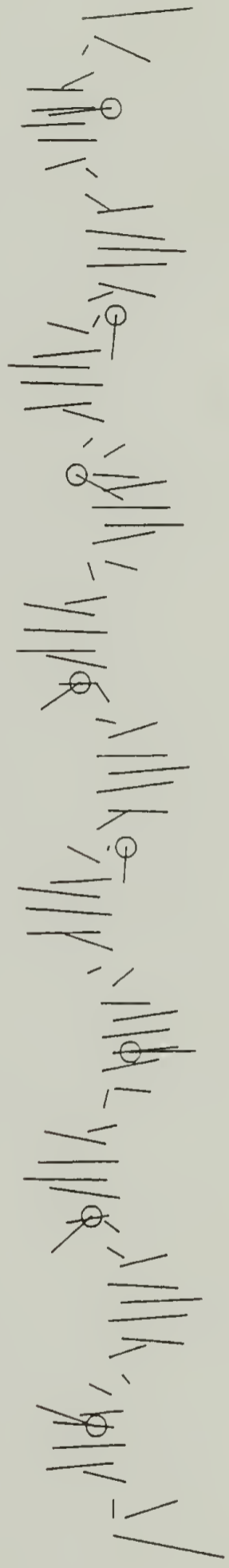
FPLTI
v,23.70



FPLT
v,25.65



FPLT2
v,28.73



FPLT3
v,34.33

to the LAM-1. Naturally the effect of chain length dependence was considered as a possible explanation, since this had been observed for *n*-alkanes. Results for *n*-alkanes indicated that chain length was important.¹¹⁻¹³ Results from additional calculations on shorter molecules, such as (6-10)₃ and (10-8)₃, together with those of the longer ones are tabulated in Table 8. The even-even oligomer molecules with 80 atoms have at least one other LAM-1 like mode with relative intensities that are significantly greater than for the corresponding 4 repeat oligomer case. The structures for (6-10)₃ and (10-8)₃ both have endgroups of methylene sequences, so that the carbonyl groups alternating sides of the chain axis are arranged symmetrically about the chain center. The relative intensities for these two cases approached that of the (6-8) molecules, and may have been larger for structures with nonsymmetrical off-axis mass arrangements.

The atomic displacements, shown in Figures 32 and 33 for (6-10)₃ and (10-8)₃ respectively, exhibit much larger contributions of transverse motions in the LAM-1 than for the 4 repeat length cases. In addition, the motions for the other LAM-1-like modes have much larger in-plane longitudinal contributions resulting in larger relative intensities. For comparison, the atomic displacements for the (6-8)₅ molecule are shown in Figure 34. The calculated more LAM-1-like vibration at 25.6 cm⁻¹ has atomic displacements with more in-

TABLE 8. Table showing frequencies of LAM-1-like modes calculated for a series of even-even, and odd-even linear aliphatic ester oligomers with different end group structures. Intensity ratios relative to the LAM-1 mode, based upon the eigenvector method, are listed for other normal modes in phase with LAM-1.

TABLE 8

LAM-1-like Modes Calculated for Even-Even and Odd-Odd

Linear Aliphatic Polyester Oligomers

Chemical Structure	Number of Atoms	End Group Structure	$\nu_{\text{LAM-1}}$	Other Frequencies in Phase w/LAM-1	Intensity Ratio with Respect to LAM-1: Eigenvector Method
(9-8)4	92	CH ₂ , C(=O)O, C(=O)O, CH ₂	26.5	None	$\leq .001$
(9-8)4	95	C(=O)O, C(=O)O, CH ₂ , CH ₂	25.6	None	$\leq .002$
(9-8)4	95	CH ₂ , CH ₂	25.6	None	$\leq .007$
(9-6)4	95	CH ₂ , O-C(=O)O	25.9	None	
(6-9)4	93	CH ₂ , O-C(=O)O	26.7	None	$I_{42.4}/I_{26.7} = 0.1$ ($\frac{I_{30.0}}{I_{26.7}}, \frac{I_{24.4}}{I_{26.7}} \leq .005$)
(6-9)3	80	H ₂ C-O-C(=O)O	30.9	None	$I_{42.2}/I_{30.9} = .04$ ($\frac{I_{32.2}}{I_{30.9}}, \frac{I_{27.4}}{I_{30.9}} \leq .001$)
(6-8)4	80	CH ₂ , C(=O)O	30.5	34.9, 26.8	$\frac{I_{34.92}}{I_{30.53}} = .36$, $\frac{I_{26.78}}{I_{30.53}} = .09$
(6-10)3	80	CH ₂ , CH ₂	31.0	33.6, 26.6	$\frac{I_{33.64}}{I_{30.98}} = .14$, $\frac{I_{26.60}}{I_{30.98}} = .04$
(10-8)3	80	CH ₂ , CH ₂	30.7	31.1	$\frac{I_{31.09}}{I_{30.08}} = .12$
(10-8)4	96	CH ₂ , C(=O)O	25.7	21.6	$\frac{I_{21.56}}{I_{25.74}} = .05$

FIG. 32 Atomic displacements for three LAM-1-like modes calculated for model oligomer $(6-10)_3$ with methylene sequence terminal groups. LAM-1 vibrations are at 31.0 cm^{-1} , 33.6 cm^{-1} and 26.6 cm^{-1} with the latter two containing mostly transverse atomic displacements from TAM-like modes. A higher frequency TAM mode calculated at 42.6 cm^{-1} is also shown. Open circles represent the carbonyl oxygen positions relative to those of the backbone.

6-10, 80 ATOMS



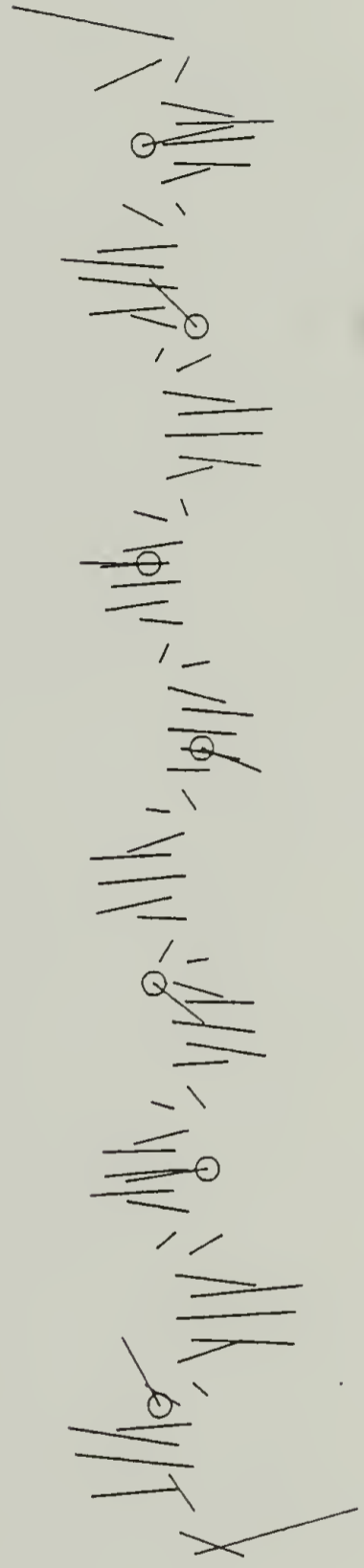
D6ISDISI
v, 26.60



D6IDIS
v, 30.98



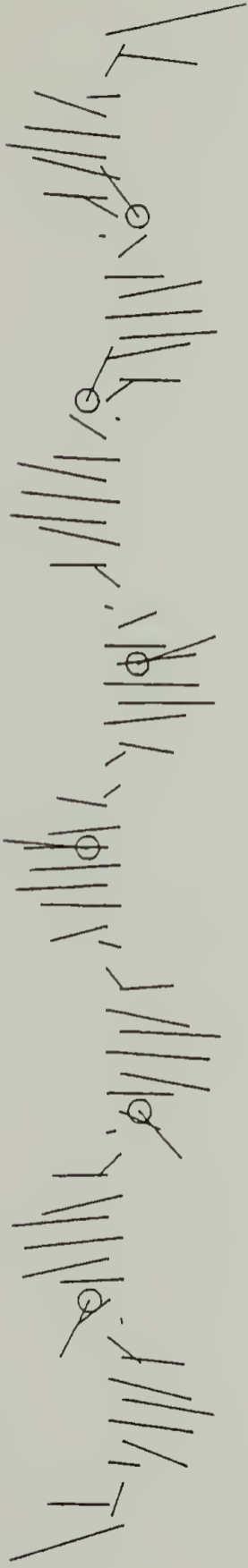
D6ISDIS2
v, 33.64



D6ISDIS3
v, 42.64

FIG. 33 Atomic displacements for two LAM-1-like modes calculated for model oligomer $(10-8)_3$ with methylene sequence terminal groups. LAM-1 vibrations are at 30.7 cm^{-1} and 31.1 cm^{-1} with the latter one containing mostly transverse atomic displacements from TAM-like modes. Higher and lower frequency TAM modes calculated at 38.7 cm^{-1} and 24.8 cm^{-1} are also shown. Open circles represent the carbonyl oxygen positions relative to those of the backbone.

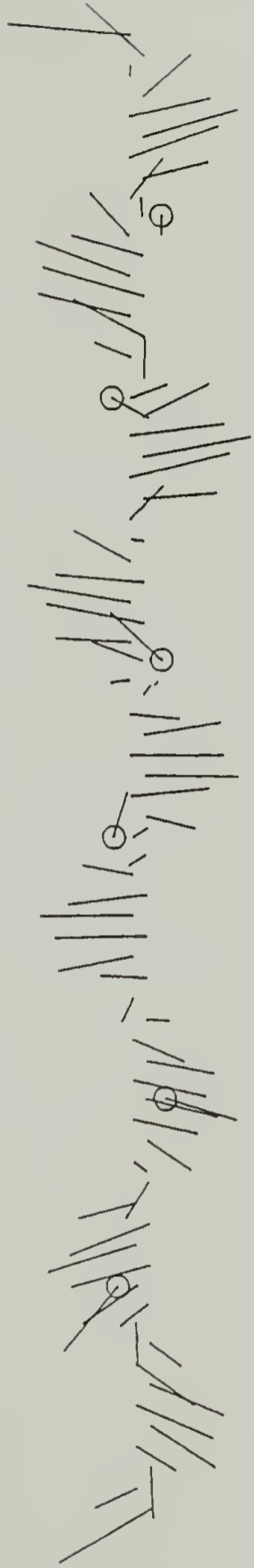
10-8, 80 ATOMS



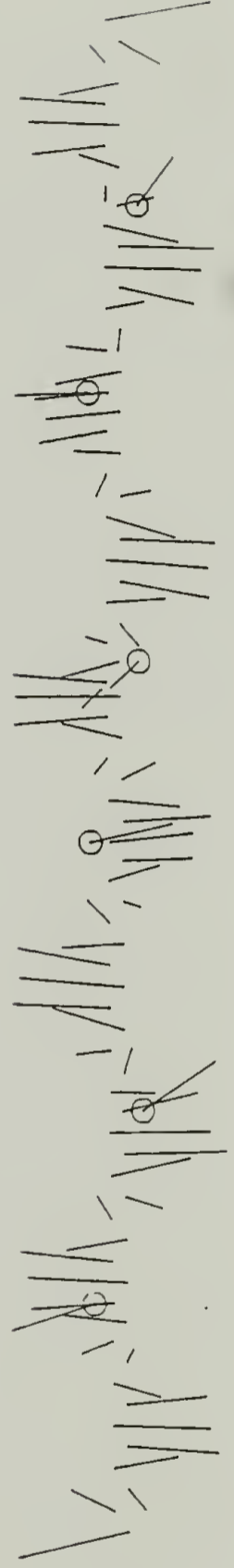
D18SDISI
 ν , 24.74



D18SDIS
 ν , 30.68



D18SDIS
 ν , 31.09



D18SDIS3
 ν , 38.66

FIG. 34 Atomic displacements for three LAM-1-like modes calculated for model oligomer (6-8)₅ (shortened by one ester group) with methylene sequence terminal groups. LAM-1 vibration is at 25.6 cm⁻¹. Two other LAM-like vibrations containing mostly transverse atomic displacements from TAM-like vibrational modes are at 23.4 cm⁻¹ and 27.6 cm⁻¹. A higher frequency TAM vibration calculated at 33.6 cm⁻¹ is also shown. Open circles represent the carbonyl oxygen positions relative to those of the backbone.

POLYESTER 6-8

97 ATOMS



D68BDIS1

; 23.43



D68BDIS2

; 25.62



D68BDIS3

; 27.60



D68BDIS4

; 33.56

plane longitudinal character than for the shorter (6-8) oligomers (such as shown in Figure 27). The transverse contributions to the atomic motions of the LAM-1, however, increase along the length of the oligomer from one end to the other. This is also the case for the most LAM-1-like vibration of the (6-10)₃, (6-8)₃ and (10-8)₃ oligomers, although more so for the former. Such positional dependence, for the magnitude of the transverse contribution to the atomic motions in the calculated LAM-1, is not exhibited by the (10-8)₄, (9-8)₄, (9-6)₄, (9-6)₃, and (6-9)₃ oligomers. Furthermore, in none of the cases did an odd-even oligomer show any evidence of other LAM-1-like modes. This conclusion is based upon examination of the respective calculated Cartesian eigenvectors of each normal vibration.

In summary, the observed LAM-like vibrations in linear aliphatic polyesters have been partially clarified by the normal vibrational analyses. The ester groups with their unbalanced mass units can significantly influence the coupling between the longitudinal and transverse motions. Apparently, when the chains are uniform the long elastic rod is quite appropriate for describing the LAM vibration. Chain length has been shown to be an important factor in the relative importance of the influence of unbalanced masses. Shorter chains with regularly spaced off-axis masses exhibit increased coupling relative to longer chains with the same distances between these masses. This result is similar to

that obtained for calculations on *n*-alkanes with terminal and/or connecting fold structures of nonregular conformations.¹³ For the case of short *n*-alkanes it was shown that several LAM-like modes with reduced intensities existed over a wide frequency range (68 cm⁻¹ for C₂₂). For *n*-alkanes of longer trans length the intensities increased, and the frequency range over which these modes were found decreased significantly (7 cm⁻¹ for C₈₂). Thus the influence of non backbone masses within the trans segment, upon the LAM-1 calculated for oligomers of linear aliphatic polyesters, is similar to that found for masses acting as defect structures terminating or connecting trans segments.

The geometric arrangement of the off-axis masses, relative to the molecule center, has a larger perturbation effect upon LAM-1 when masses are asymmetrically situated (no center of inversion). The location of nodes in the transverse contributions to the skeletal atomic motions of the low frequency normal modes is a function of chain length and normal mode and not carbonyl position. A distinct even-even and odd-even effect, on the degree of coupling, was determined to be the case for the chain lengths and monomer structures investigated. It is possible that the odd-even polyester may exhibit similar coupling for chain lengths longer than those calculated. It is expected, however, that when localized structural defects exist, then deviations from this idealized model will occur.

References

1. Schaufele, R. F.; Shimanouchi, T. *J. Chem. Phys.*, **1967**, *47*, 3605.
2. Shimanouchi, T.; Tasumi, M. *Indian J. Pure Appl. Phys.*, **1971**, *9*, 958.
3. Reneker, D. H.; Fanconi, B. *J. Appl. Phys.*, **1975**, *46*, 4144.
4. Perterlin, A. *Colloid and Polymer Sci.*, **1975**, *253*, 809.
5. Shu, P. H.; Burchell, D.J.; Hsu, S. L. *J. Polym. Sci.: Polym. Phys. Ed.*, **1980**, *18*, 1421.
6. Scherer J. R.; Snyder, R. J. *J. Chem. Phys.*, **1980**, *72*, 11, 5798.
7. Wang, Y. K.; Waldman, D. A.; Stein, R. S.; Hsu, S. L. *J. Appl. Phys.*, **1982**, *53*, 10, 6591.
8. Wang, Y. K.; Waldman, D. A.; Lasch, J. E.; Stein, R. S.; Hsu, S. L. *Macromolecules*, **1982**, *15*, 1452.
9. Tasumi, M.; Shimanouchi, T. *J. Chem. Phys.*, **1967**, *43*, 1255.
10. Tasumi, M.; Krimm, S. *J. Chem. Phys.*, **1967**, *46*, 755.
11. Olf, H. G.; Fanconi, B. *J. Chem. Phys.*, **1973**, *59*, 1, 534.
12. Mazur J.; Fanconi, B. *J. Chem. Phys.*, **1979**, *71*, 5069.
13. Chang, C.; Krimm, S. *J. Appl. Phys.*, **1983**, *54*, 10, 5526.
14. Chang, C.; Wang, Y. K.; Waldman, D. A.; Hsu, S. L. *J. Polym. Sci.: Polym. Phys. Ed.*, **1984**, *22*, 2185.

15. Kanamoto, T.; Tanaka, T.; Nagai, H. *J. Polym. Sci.: Polym. Phys. Ed.*, **1971**, *9*, 2043..
16. Fuller, C. S.; Frosch, C. J. *J. Am. Chem. Soc.*, **1939**, *61*, 2575.
17. Chatani, Y.; Okita, Y.; Tadakoro, H.; Yamashita, Y. *Polym. J.*, **1970**, *1*, 555.
18. Boerio, F. J.; Bahl, S. K.; McGraw, G. E. *J. Polym. Sci.: Polym. Phys. Ed.*, **1976**, *14*, 1029.
19. Tadokoro, H.; Kobayashi, M.; Yoshidome, H.; Tai, K.; Makino, D. *J. Chem. Phys.*, **1968**, *49*, 3359.
20. Wang, Y. K.; Shu, P. H. C.; Stein, R. S.; Hsu, S. L. *J. Polym. Sci.: Polym. Phys. Ed.*, **1980**, *18*, 2287.
21. Hartley, A.; Leung, Y. K.; Booth, C.; Shepherd, I. W. *Polymer*, **1976**, *17*, 354.
22. Strobl, G. R.; Eckel, R. J. *Polym. Sci.: Polym. Phys. Ed.*, **1976**, *14*, 913.
23. Hsu, S. L.; Krimm, S. *J. Appl. Phys.*, **1976**, *47*, 4265.
24. Snyder, R. G.; Krause, S. J.; Scherer, J. R. *J. Polym. Sci.: Polym. Phys. Ed.*, **1978**, *16*, 1593.
25. Woodward, L. A.; Long, D. A. *Trans. Faraday Soc.*, **1949**, *45*, 1131.
26. Chang, C. *Ph.D. thesis*, University of Michigan, **1983**.

CHAPTER 5

SYNTHESIS OF MODEL POLYMERS FOR ADSORPTION STUDIES

Introduction

In order to investigate the structure of ultra-thin polymer films adsorbed from dilute solution onto external metallic substrates, development of a model polymer system is required first. A number of factors have to be considered, as a result of the significant research effort in this area. This has mainly concerned elucidation of the properties of adsorbed polymers in solution. Factors such as polydispersity, molecular weight, quality of solvent, polymer concentration, and the strength of interaction with the substrate, have been shown to affect both the kinetics and degree of adsorption of an adsorbed layer in solution,¹⁻¹⁶ as well as the thickness of the adsorbed layer^{1,6,10-14,16} from which chain dimensions and expansion factors have been determined.

A necessary condition for adsorption of polymers to a surface, is that the cumulative magnitude of the binding energy (surface-segment interactions) be sufficient to overcome both the resulting enthalpic and entropic barriers. These are due to loss of solvent/surface and polymer/solvent interactions, and the decrease in translational and conformational entropy (0.5 and 1.0 kT),¹⁷ respectively,

accompanying adsorption of polymer segments. If polystyrene is functionalized with sulfur containing groups, then the magnitude of the specific interactions, between available surface sites of a gold substrate and the incorporated functional groups, will be increased substantially over the typical nonbonded and/or weak hydrogen bonding surface/segment interaction energies. Studies on small molecule thiols and sulfides have estimated that the binding energies due to coordination of sulfur to 3 Au atoms is on the order of 15 to 30 kcal/mole¹⁸, or about 15 to 50 times greater than the above surface/segment energies.

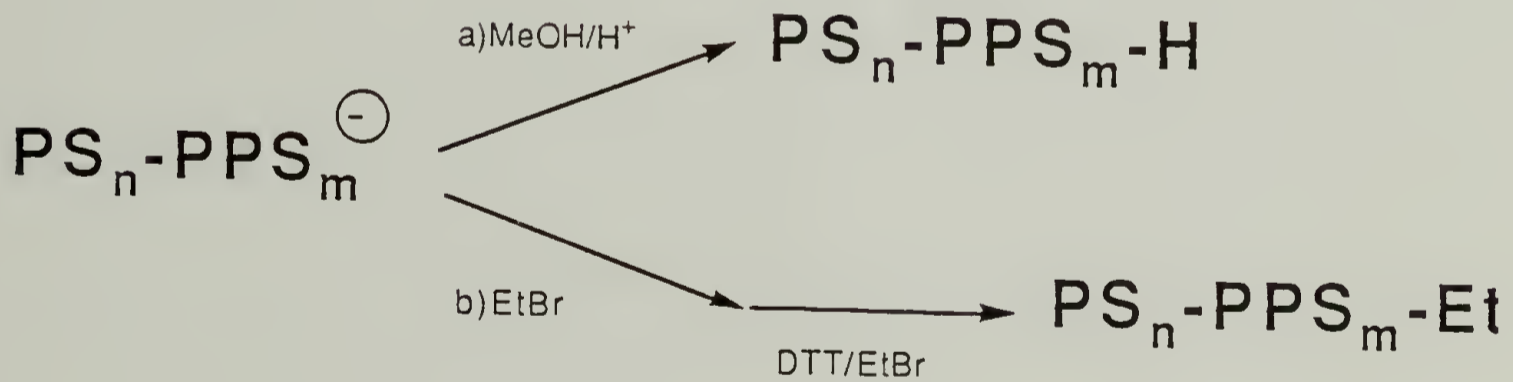
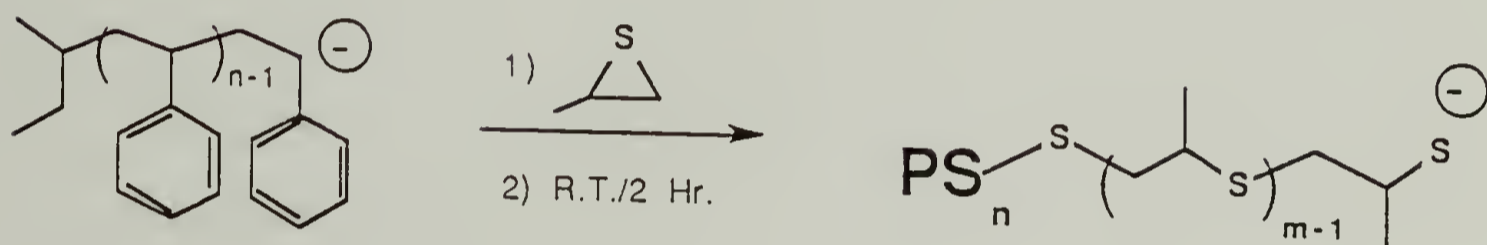
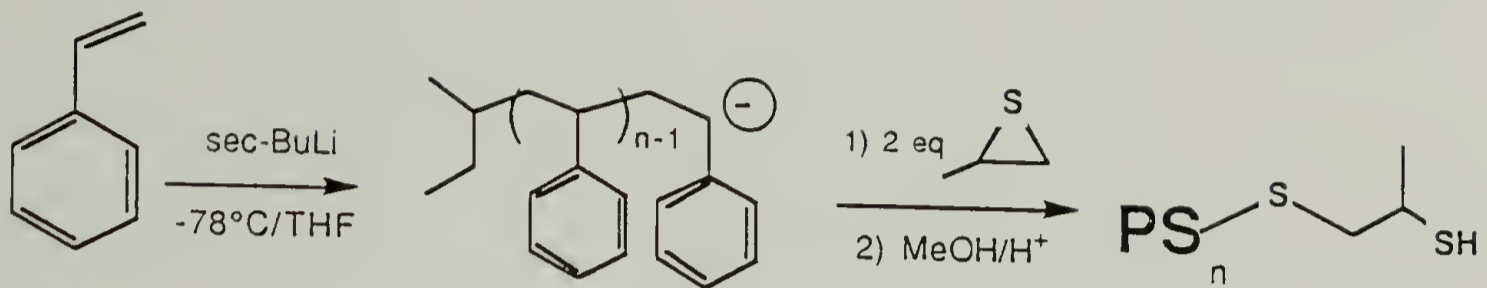
Sulfur functionalized anionically synthesized polystyrenes can be synthesized as either polystyrene endcapped with a thiol, or polystyrenes copolymerized with propylene sulfide such that different length propylene sulfide blocks are incorporated. If the degree of polymerization is on the order of 800 or less, then the molecular weight regime will be low enough for the specific S-Au interactions to dominate the energetics of the typical surface/segment binding energy contribution to the overall ΔG_{ads} . Unfunctionalized polystyrene in this molecular weight range does not adsorb under good solvent conditions (from THF) while the above polymers do.¹⁹ These chemically modified polystyrenes therefore decrease the dependence of adsorbance and thickness on the thermodynamic quality of the solvent. Solvent/solvent, segment/segment, and solvent/segment

interactions will not be a significant factor in ΔG_{ads} . The expected result is that adsorption of these polystyrenes will be influenced by their chemical composition, with the endcap case enabling the highest grafting density and the longest propylene sulfide block copolymer the lowest.^{20,21}

Furthermore, since the substrate surface is Au, factors that must be considered for adsorption of polystyrene onto metal-oxide surfaces, such as hydration effects on the potential polymer-surface interaction sites and adsorbed polymer structure^{22,23} can be ignored.

Modified polystyrenes, consisting of thiol terminated chains of various molecular weights, and diblock copolymers of polystyrene and propylene sulfide with compositions of varying molar block ratios but constant overall degree of polymerization, were synthesized as shown in Figure 35. The molecular dimensions over which interactions with the metal surface exist could be altered because of the sulphur containing structural units.^{18,24,25} If the distorted configuration inferred from previous solution studies exists for these polymers, then it should be further modified by specific interactions with the substrate which could effect distinct orientations. Anionic synthesis enabled a high degree of monodispersity to be achieved. This series of modified polystyrenes were readily soluble in common solvents, so that they could be adsorbed from dilute solution onto glass supported vapor deposited metal substrates.

FIG. 35 Schematic for anionic synthesis of (a) thiol endcapped Polystyrene by addition of 1 to 2 equivalents of propylene sulfide to the living polymer (top), and (b) living diblock copolymers of Styrene-Propylene Sulfide (middle) and (c) reaction for termination of (b) by addition of either acidic methanol or ethyl bromide in the presence of dithiothreitol (bottom). The first method of termination yields an oxidatively unstable thiol endcap. The second method provides a stable ethyl endcap and yields diblock copolymers with no disulfide linkages.



Synthesis of Styrene-Propylene Sulfide Block Copolymers

Background

The object of the synthesis reported here was to prepare thiol endcapped Polystyrene and Styrene-Propylene Sulfide Block Copolymers with 1) A high degree of monodispersity, and 2) In such a manner as to maintain the overall degree of polymerization but alter the molar block ratios of the two polymers. The method of choice was anionic polymerization. The high reactivities of sulfur containing heterocycles for anionic reactions, due to ring strain²⁶ and the high nucleophilicity of the thiolate, make them good candidates.

Anionic polymerization of propylene sulfide to high molecular weight has been previously reported to be living with no evidence of termination or monomer transfers.²⁷ Block copolymers of styrene, α -methylstyrene, isoprene, butadiene and methacrylate with ethylene sulfide (ES) and propylene sulfide (PS) have also been reported.²⁸⁻³⁴ Studies of these copolymers arose from the interest in comparison of mechanical properties of block copolymers having crystalline, glassy, and rubbery domains. Triblock (ABA) copolymers containing crystalline domains from blocks of ES and rubbery domains of polyisoprene, exhibited both improved network stability and tensile strengths with less temperature dependence, compared with ABA block copolymers of polystyrene-polybutadiene-polystyrene.³³ ABC block copolymers

from styrene, isoprene or butadiene, and ES are strong resilient elastomers with improved thermal stability compared with the conventional styrene/butadiene block copolymers.³⁴

The vinyl monomer was polymerized first and then used to initiate the polymerization of the thiirane, or phosgene was used to couple the active lithium thiolate end groups to poly(α -methylstyrene) to form ABA triblocks. The initiation in these cases was found to go by a sulfur extrusion (desulfurization) mechanism, by reaction of the carbanion with the thiirane, to yield the thiolate and the corresponding alkene.²⁹ The crossover reaction between the poly(α -methylstyrene)lithium species and propylene sulfide in THF is thus carried out at -78 °C and the remaining slow propagation at +25 °C. Narrow molecular weight distributions indicated a fast crossover reaction from active poly(α -methylstyrene) to propylene sulfide.

Anionic polymerizations, in general, require extreme cleanliness in all aspects of the experimental work up. This requirement is even more stringent when one is making block copolymers, such as styrene-propylene sulfide, and specifically end capped chains. Whereas in small molecule reactions a 50 % yield may be satisfactory, in polymerizations of this sort such results represent failure. It is necessary to obtain essentially 100% conversion because of the difficulty in purification of polymeric products. In addition, in most cases only small amounts of very reactive

compounds (10-100 mmol; per 30ml) are utilized. The high reactivity of the propagating species requires that special attention be given to reaction vessels, solvents, temperatures and purification procedures. Molecular weight (MW) is important consideration because at higher MW less anions are present, and thus smaller amounts of impurity can be tolerated.

There are essentially two possible sources of water (impurities) in these reactions. 1) Impurities brought in by transfer processes. 2) Those already present in the reagents and solvent. For the first type it is conceivable that their effect can be minimized by scaling up the reaction and improving the overall experimental technique. The second source, however, should not be influenced by scale up but instead requires a judicious choice of drying agents and methods. There are also problems specifically associated with the PPS block. During the synthesis of PS/PPS block copolymers a number of types of problems were encountered for which remedies were established. These will be discussed below.

Methods

All reactions were done in base bath cleaned glassware that was stored in a drying oven at approximately 80-100 °C for at least 12 hours. All glassware was assembled hot, under N₂ purge. Only teflon stopcocks were used. Grease was

used and found preferable to teflon sleeves on ground glass joints. Three different types of reaction vessels were used. A 250 ml Schlenk flask was the vessel of choice in most cases. It enabled much more homogeneous stirring and bigger volumes than the thin Schlenk tubes. Pop bottle glassware was used but small pieces of black rubber would inevitably appear in the solvent due to puncturing of the seal during transfers. In the case of THF, the seal was extensively swelled. These pieces were suspected of causing unwanted termination steps during polymerizations. Thus the use of beverage bottles with THF as the solvent is thus not recommended. All transfers were done via cannula or gas tight luer tip syringe. All needles and cannula were cleaned with hexane, 1M HCl, 1M NaOH, H₂O, and acetone, and then purged dry and kept in oven until right before use. Transfers were also facilitated by a portable ante-chamber³⁵ made from 3" x 9mm glass tubing fitted on both ends with the appropriate septa.

All reactions were done under prepurified N₂ direct from the tank (6-9 psi). During the assembly and transfers latex gloves were worn at all times to minimize contamination by hand sweat and oils. All assembled glassware (reaction vessels, distillation, trap to trap, and storage apparatus) were further dried by purging 10 min with N₂ then a repeated vacuum/heating/N₂ backfill cycle. All solvents and monomers were distilled directly before use. *sec*-BuLi was diluted

with dry hexane (or heptane) and stored in a 15 ml Schlenk tube with desiccant, in a freezer and also at 0 °C on the bench.

Purification

The purification of solvents and monomers evolved during the synthesis project. At first solvents such as THF (Aldrich) and cyclohexane (Aldrich) were used fresh from continuous Na/Bz₂CO (benzophenone) stills. The monomers were distilled from CaH₂ under reduced pressure. These conditions were not sufficient since dead polymer fractions, and low degree of polymerizations resulted. The purifications which effected the best polymerization results were quite different from these, and are described below.

Styrene

Approximately 300 ml of styrene (Fisher) was distilled from CaH₂ (@ 30 mm Hg) and then stored in a storage flask in the freezer. It was then further dried just prior to use following a procedure developed by Morton.³⁶ Approximately 1-4 ml of 0.5 M Bu₂Mg (ALFA) in hexane (Aldrich) was cannulated into a purged Schlenk tube (grease joint), and then the solvent was pumped off leaving a white solid. Styrene (10-20 ml) was added and stirred at room temperature for 1-4 hours, at which time the solution became bright yellow in color. The color indicates living polymerization of styrene and thus absence of H₂O, and other impurities. Since this

polymerization is extremely slow, the dry styrene can be used over a period of a few days. The solution was attached to a (trap to trap) distillation apparatus and degassed 3 times before it was transferred. It was then transferred to a 15 ml Schlenk tube via cannula and used within the hour for polymerization. GC was used to monitor the stored (yellow) styrene for higher MW components (dimers etc.), but none were found even in styrene that had been over Bu_2Mg for a few weeks.

Propylene Sulfide (PS)

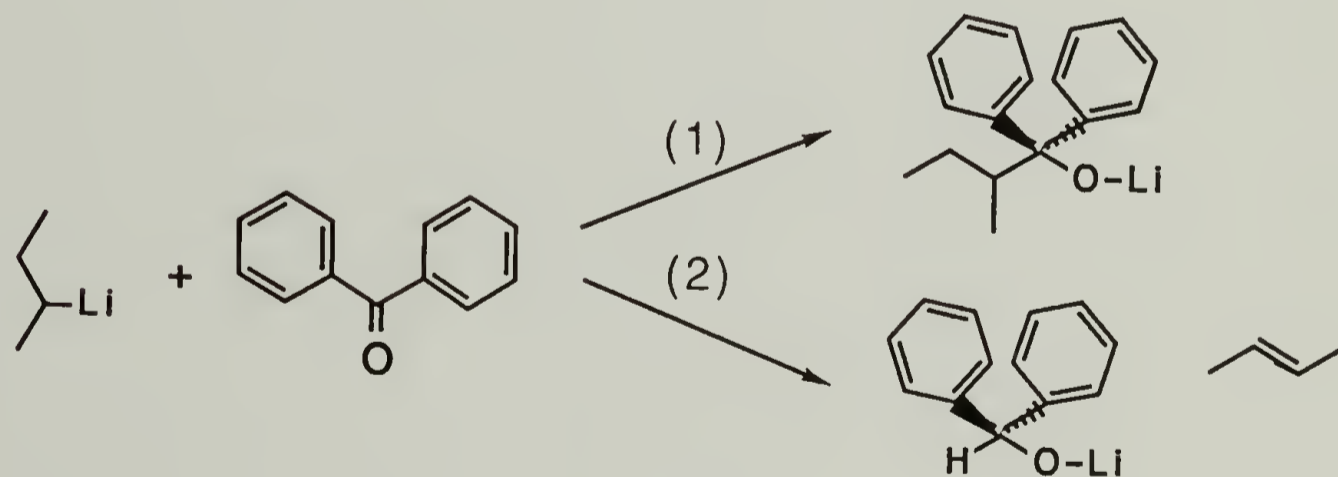
The PS drying procedure reported in the literature for all PPS block copolymer synthesis is distillation from CaH_2 . Even after repeated drying with CaH_2 the addition of PS (Aldrich) to living polystyryl lithium resulted in a substantial fraction of dead polystyrene as shown by GPC elutions. Since the dead homopolymer could not be isolated from the diblock copolymer this was not acceptable. This has probably been a problem in past studies, but of all the studies involving copolymers of PS or ES only two could be found that reported results which included examples of GPC chromatograms.^{30,34} In both of these studies the procedure involved the sequential addition of the thiirane monomer, and the existence of dead blocks is evident. Attempts to find a new drying agent were complicated by the fact that propylene sulfide is polymerized by a number of standard agents including CaH_2 . Sodium and NaH polymerized it too quickly (on

the order of minutes) to be useful. When Bu_2Mg was added to freshly distilled PS (from CaH_2) the solution turned bright orange and polymerized slowly (about 1 hour) at room temperature. When the PS was (trap to trap) distilled from this, the resulting subsequent copolymer exhibited no evidence by GPC of dead polystyrene. It should be noted that, if the PS, (trap to trap) distilled from orange Bu_2Mg solution is then added back to fresh Bu_2Mg no color change occurs. This indicates that the Bu_2Mg removed some impurity from the system. If the PS is not predried with CaH_2 before the Bu_2Mg treatment then the monomer polymerizes much more violently. The subsequent polymerization yields a small amount of dead polystyrene and upon addition of Bu_2Mg to the monomer the orange color reappears. This indicates that what was responsible for the orange color also caused the dead polystyrene.

THF

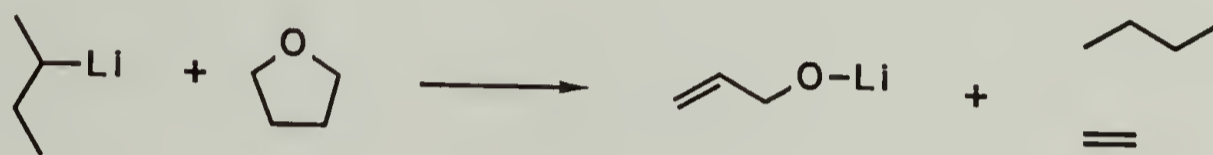
At first THF was used from a continuous Na/ Bz_2CO still where it was refluxed for at least 12hr over purple ketyl before use. It was found that successful polymerizations could be accomplished with this, and narrow symmetrical molecular weight distributions could be obtained. There was, however, disagreement between the calculated molecular weight, based upon volumes, and the experimental value obtained from GPC results. This was important since a particular degree of polymerization was desired. It was

concluded that this problem had something to do with using THF out of a continuous Na/Bz₂CO still, since the gradual accumulation of some sort of impurity could occur in the still reservoir. The magnitude of the above disagreement changed with time, so it seemed reasonable that the contaminant concentration could vary over the time period that occurred after a fresh still was set up. The impurity apparently competed with styrene for *sec*-BuLi, and thus may have been Bz₂CO itself, benzaldehyde or some other products. For the case of Bz₂CO two possibilities could be direct addition or hydride transfer, shown below in routes 1 and 2 respectively. It should be noted that for Na/Bz₂CO in THF, in the presence of PS, S₂Na₂ formation with regeneration of Bz₂CO, has been reported.³⁷



The procedure that was finally utilized with success, in terms of achieving the predicted degree of polymerization, involved the use of *sec*-BuLi (1.3 M in hexane; Aldrich). When *sec*-BuLi is added to THF at -78 °C it first dries the solvent

and then a light green color appears. In this manner the dryness of THF could be monitored after it was already in the reaction flask. If the temperature of the solvent mixture is subsequently allowed to rise to room temperature then the *sec*-BuLi reacts rapidly with the THF and the products are innocuous to the polymerization. The reaction products are butane, ethylene and the lithium enolate of acetaldehyde³⁸ as shown below.



The drying procedure for THF was therefore done as follows. First the THF was pre-dried by refluxing over CaH_2 . The required volume was then cooled to -78°C in a Schlenk tube and the lithium reagent was added until a green color was obtained. This was left for 30 min, then degassed, and distilled (trap to trap) into a new tube. The THF was then transferred to the reaction flask, cooled to -78°C , and a small amount of *sec*-BuLi was added to just give a perceptible pale green coloration. The THF was allowed to warm up for about 30 minutes, at which time its color was clear. It was then ready to cool back down to be used for the reaction.

Procedure for Synthesis

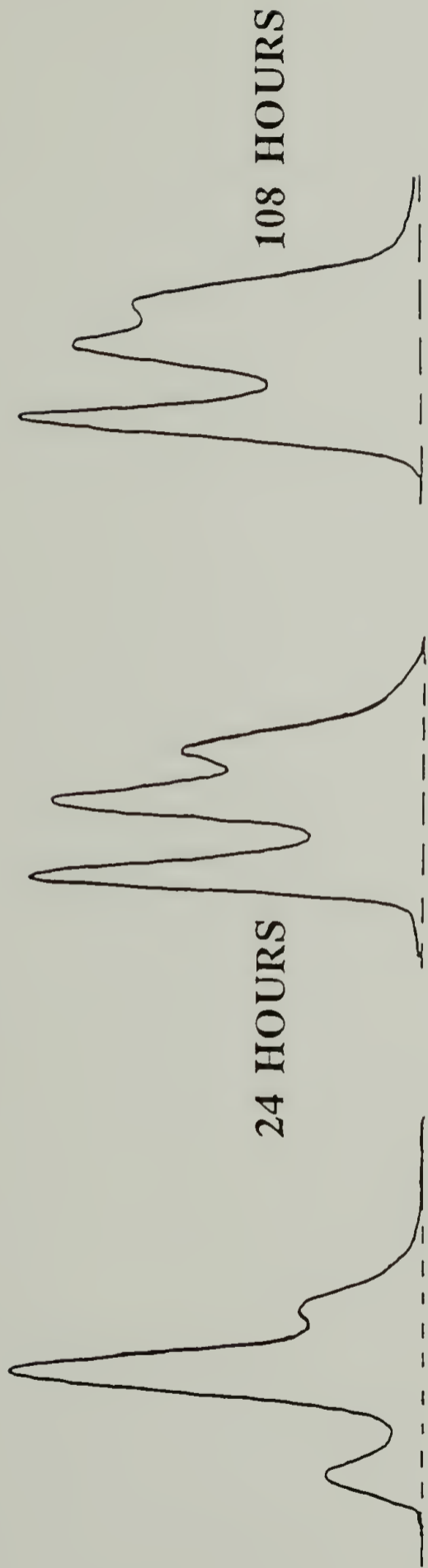
The dried solvent (25 ml THF) in the reaction vessel was cooled to $-78\text{ }^{\circ}\text{C}$ and then stirred. The stoichiometric amount of *sec*-BuLi was added via syringe. The styrene, typically 2 ml was added last via syringe and the characteristic orange/red color was obtained. The reaction was allowed to proceed for 15-30 min, which was more than sufficient time for completion as determined by GC. The appropriate amount of PS was then added via syringe to maintain the overall degree of polymerization constant, at which time the orange color disappeared. Aliquots of the polystyrene polymerization were taken to determine the polydispersity and molecular weight of the polystyrene block. The copolymerization was allowed to warm to room temperature and proceed until complete conversion as determined by GC (usually about 2 hours). Endcapping of the block copolymers was achieved by addition of either 1) Degassed acidic methanol which was allowed to react for about 30 minutes, or 2) Degassed distilled ethyl bromide. The copolymer was then precipitated in degassed cold methanol, purified by dissolution in HPLC grade THF, reprecipitated in methanol, and dried at reduced pressure.

Results and Discussion

Oxidative Instability

The first method yielded a block copolymer which was oxidatively unstable so that the resulting propylene sulfide block depolymerized, and/or coupled at room temperature, and in solution. This was caused by the instability of the thiolate or thiol endgroup which is present during the reaction and after acidic work-up respectively. By monitoring with GPC (Figure 36) it was found that the endgroup was involved in two detrimental reactions; 1) Degradation of the polymer presumably by an unzipping reaction or cyclic oligomer formation (Figure 37), and 2) The coupling of the copolymers by disulfide formation (Figure 38 route (a)). It was established that both the amount of triblock (from coupling) and polystyrene homopolymer increased with respect to the diblock fraction, when the copolymer was dissolved with or without a gold substrate present for adsorption studies. Representative GPC chromatograms showing such increases as a function of time in solution are in Figure 36. The lowest elution time component is the coupled diblock, the middle is the copolymer, and the highest elution time is representative of the polystyrene homopolymer. It was also found that vials of the stored polymers, endcapped by method 1, had a characteristic sulfur odor when opened.³⁹ This suggests depolymerization in the solid state, since the smell

FIG. 36 Gel permeation chromatography (GPC) of THF solutions of thiol endcapped Polystyrene-Propylene Sulfide diblock copolymers (conc. = 1 mg/ml), as a function of time under nitrogen atmosphere, and solvent purification. Increasing elution time is toward the right in each chromatogram. Chromatograms on (top) are for a solution with HPLC sure/seal THF after 30 min. (left), 24 hours (middle), and 108 hours (right). Chromatograms on (bottom) are of 24 hour solutions, which had submerged vapor deposited Au coated (1800 Å) glass microscope slides, where the THF was HPLC sure/seal (left) and was freshly distilled from Na/benzophenone (right).



HPLC SURE/SEAL THF
UNDER N₂

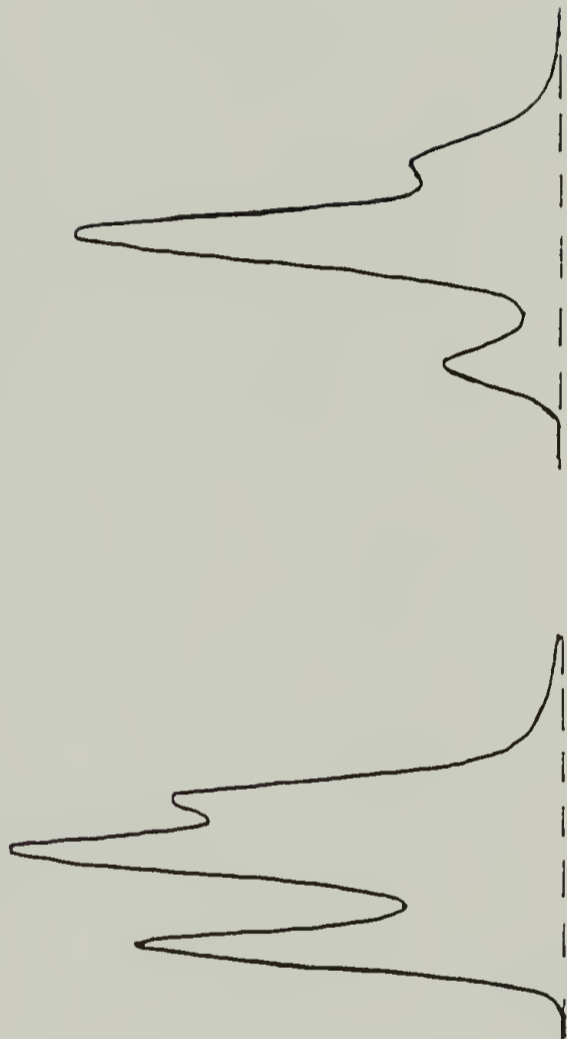
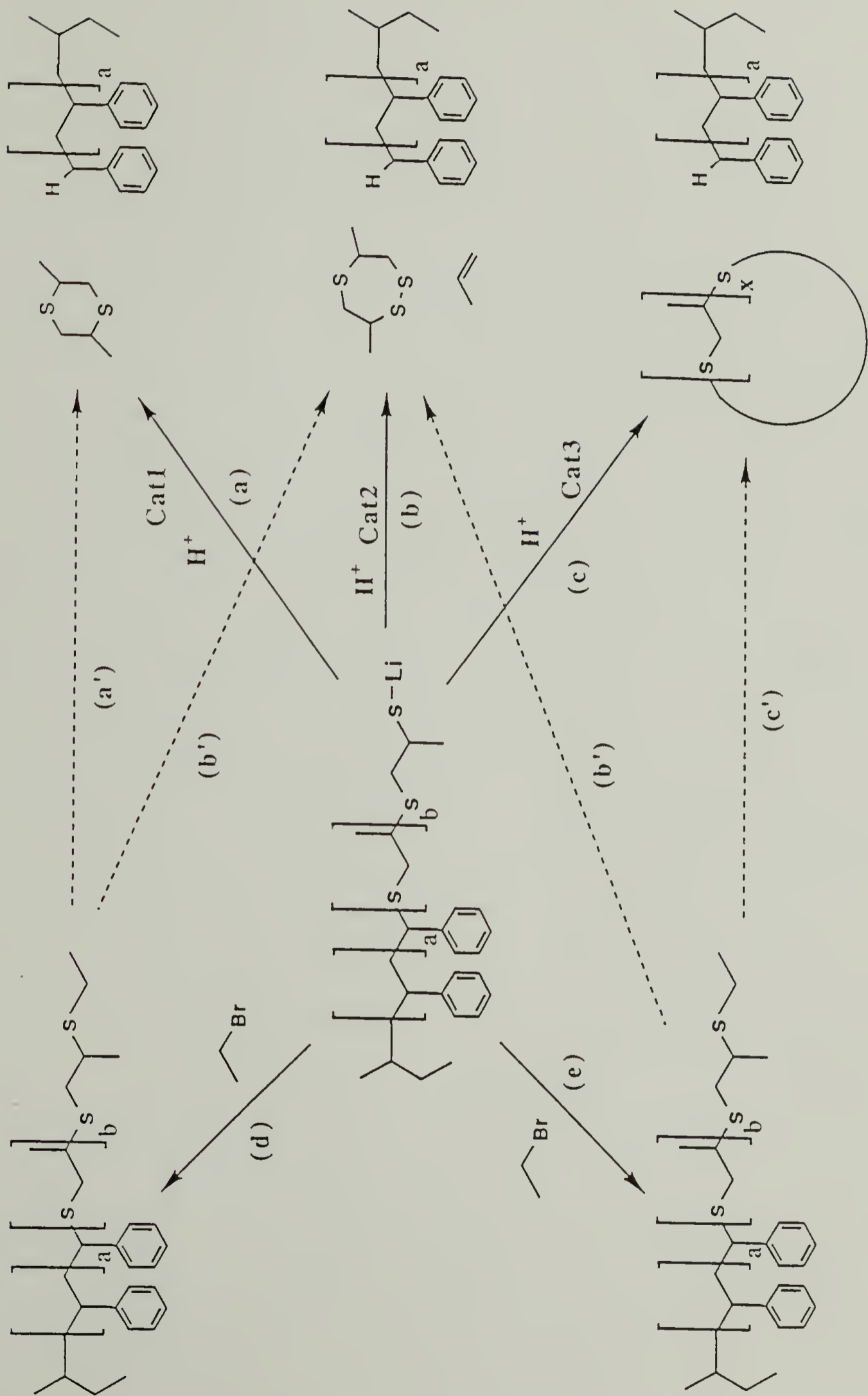


FIG. 37 Schematic depicting reaction pathways of unstable thiol endcapped Polystyrene-Propylene Sulfide diblock copolymers to form degradation products consisting of unzipped propylene sulfide blocks and (a) dithianes, (b) trithiapane and propylene, and (c) cyclic oligomers of propylene sulfide ($x = 3, 4, 5$). Copolymers successfully endcapped with ethyl bromide (e), (f) are chemically stabilized.



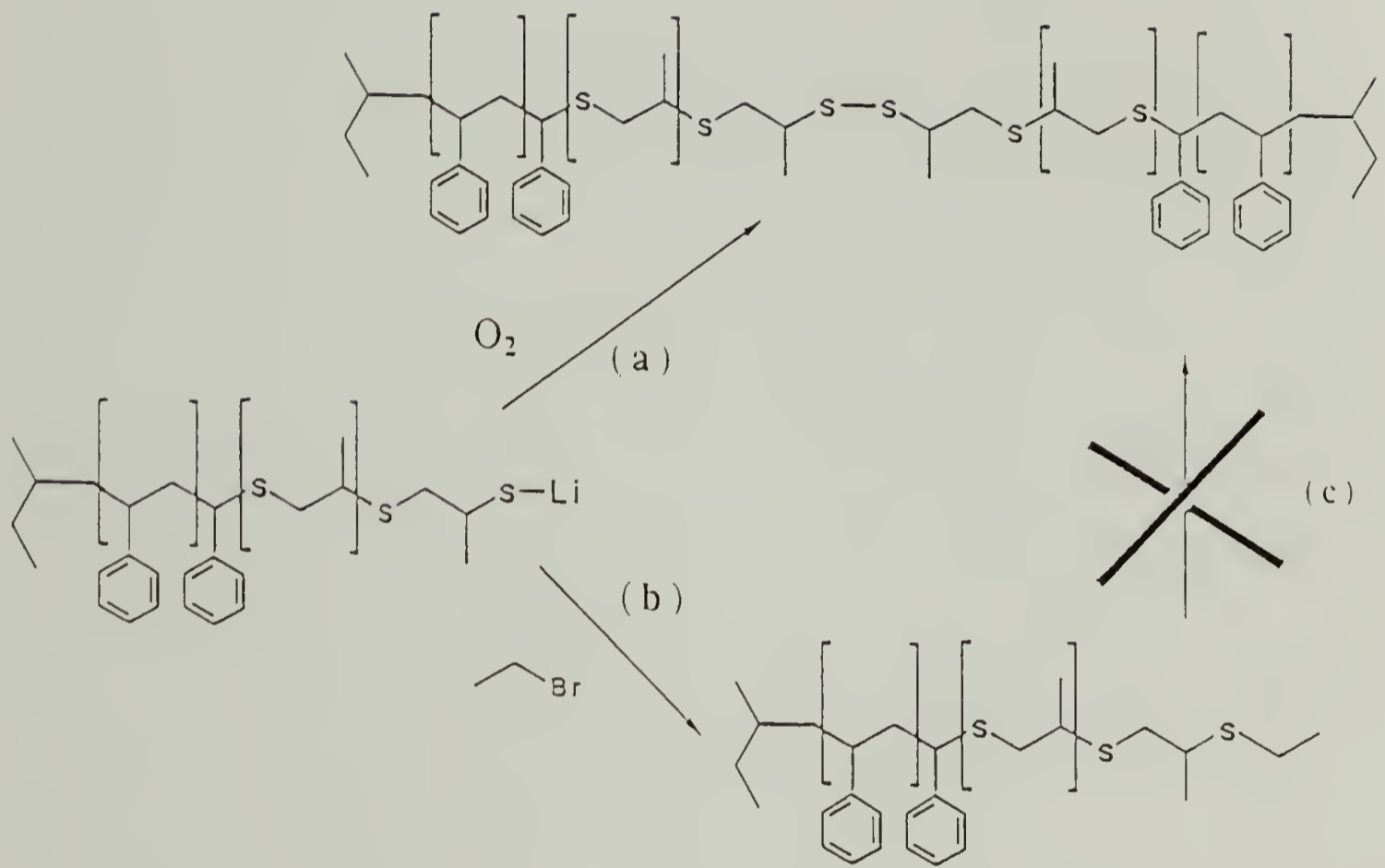


FIG. 38 Schematic for (a) oxidative coupling of thiol and or thiolate terminated Polystyrene-Propylene Sulfide **AB** diblock copolymers, to form triblock **ABBA** copolymers via linking of diblocks through disulfide formation, and (b) termination with oxidatively stable ethyl endcap.

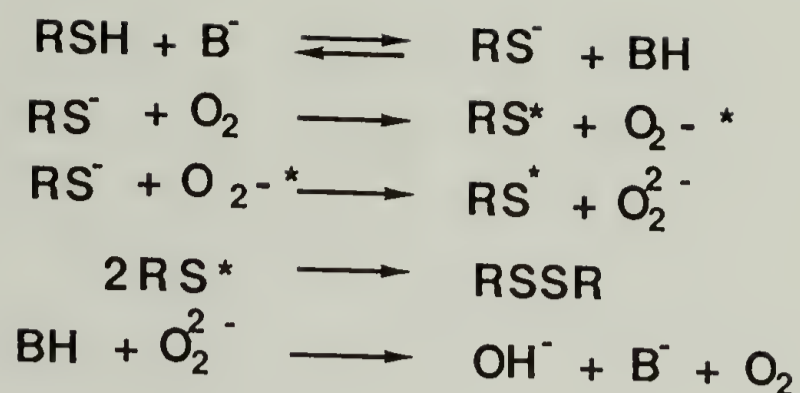
was not present when the polymers were precipitated. This is not unexpected since acid catalyzes the depolymerization and those polymers were precipitated in acidic methanol.⁴⁰

Degradation of ring opened polymers by an unzipping process is not unusual if proper endcapping is not carried out to remove the kinetic pathway for depolymerization. The fact that dithianes do not polymerize suggests that PPS may be particularly susceptible to such reactions. It is expected that PPS will degrade by some combination of (a), (b), and/or (c) pathways shown in Figure 37, depending on the given conditions. Simonds and subsequently Sigwalt^{37,40} reported the degradation of high MW stereospecific monodisperse PPS by Et_3OBF_4 into various ratios of the dithiane, cyclic trimers, tetramers, pentamers and trithiapane and the corresponding olefin. The ratio of each depends on the type of thiirane polymerized and the amount of catalyst. The sulfur atoms of the thiol and the sulfide are nucleophilic enough to form sulfonium ions upon reaction with the catalyst. This in turn causes both the sulfur of the sulfonium ion and the alpha carbons to be subject to nucleophilic displacement reactions by other sulfur atoms in the chain. PPS was found to show a preponderance of trithiapane over the dithiane, and thus attack at the sulfur is more prevalent. For the copolymerizations in this study such a good alkylating agent will not exist. The sulfides themselves may then not be nucleophilic enough to attack and

the thiol groups. This is supported by previous experimental evidence since Nevin²⁸ reported that thiol endcapped polymers were unstable and others^{30,41} used ethyl bromide and allyl bromide to endcap and control this instability. Endcapping with ethyl bromide, as per method 2 above, resulted in copolymers that were stable to depolymerization both in bulk and in solution by GPC.

Coupling of Copolymers via Disulfide Formation

Oxidative coupling of thiol-terminated copolymer chains, however, resulted in disulfide formation (shown in Figure 38), which even with a rigorous synthetic route varied in content from 3 to 15% by GPC area fraction. The disulfide formation is base-catalyzed and occurred to the greatest extent in the reaction vessel and/or during workup. Intermolecular association between free ends of growing chains of PS initiated by alkyl-lithium occurs in THF.⁴² This increases the likelihood that disulfide formation can not be completely prevented during the polymerization/workup. The oxidation of thiols to disulfides is a well known facile reaction that can be accomplished by even mild oxidizing agents.⁴³⁻⁴⁵ This oxidation will occur upon reaction with molecular oxygen and is catalyzed by base, according to the following mechanism.



Since these disulfide linkages interconnect copolymer chains, the presence of these dimers regardless of the endcapping procedure, meant that for the stable ethyl sulfide endcap case this termination step did not proceed to 100% yield. A certain fraction of thiol endcaps would variably form and then couple, so that the dimer formation could not be completely suppressed. From an adsorption standpoint such chemistry is undesirable since ellipsometry, GPC, and viscometric studies have clearly demonstrated that under competitive conditions, high molecular weight species will preferentially adsorb over lower. In addition those copolymers that were coupled would be ABA triblocks with the propylene sulfide block as the internal one.

Procedure for Cleavage of Disulfide Linkages

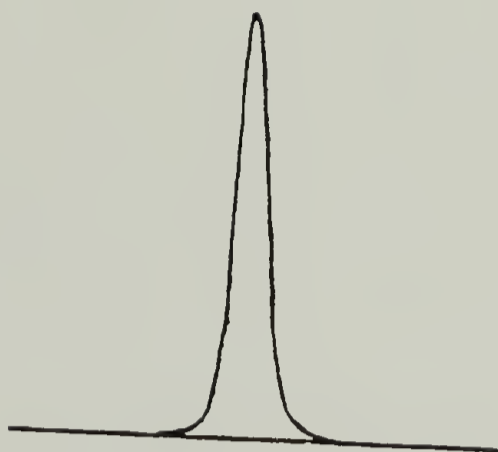
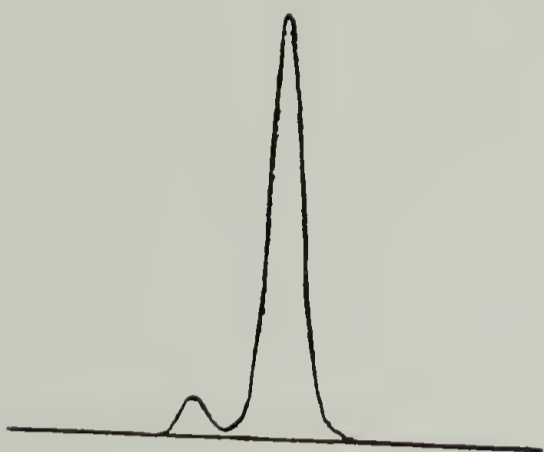
Therefore for the ethyl endcapped copolymers only, an additional step was carried out, which consisted of using excess dithiothreitol (Aldrich) (DTT) in THF or DMF/NaOH to reductively cleave any existing disulfide linkages.⁴⁶ Ethyl bromide was again added for final endcapping in the presence

of DTT. This process was monitored by GPC to insure that all high molecular weight components that arose from disulfide formation were cleaved (Figures 39,40).

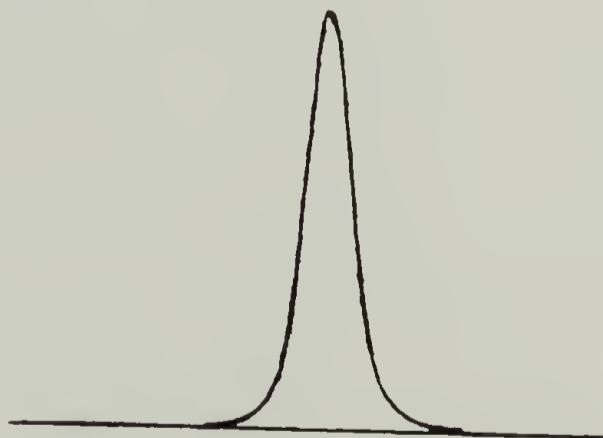
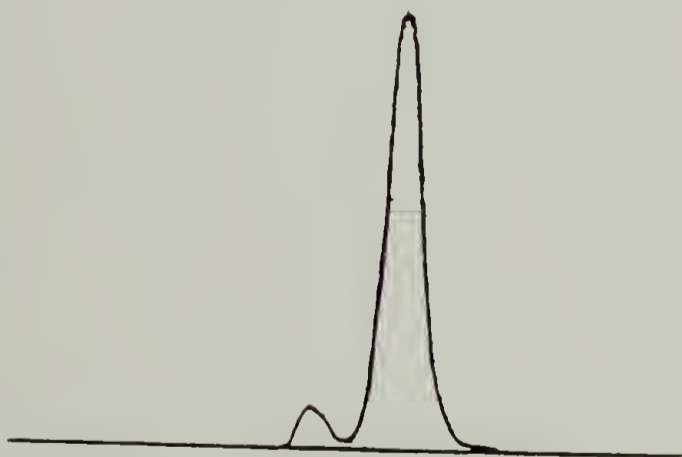
Final Copolymer Samples

The resulting copolymers (PSA-PPSB) were highly monodisperse (< 1.15 PDI), with a constant overall degree of polymerization of approximately 600 monomer units, but varying molar block ratios (Table 9), and were readily soluble in common solvents. Results from microanalysis, listed in Table 9, agreed closely with stoichiometries determined from both measured volumes and relative intensities exhibited by the CH stretching bands in transmission infrared spectra of pressed pellets of 2 % copolymer in KBr.

FIG. 39 Gel permeation chromatography(GPC) of 1 mg/ml THF solutions of Polystyrene-Propylene Sulfide diblock copolymers (PS₉₅-PPS₅) (top), and (PS₇₅-PPS₂₅) (bottom), with oxidatively coupled component(left), and after reduction with DTT and stable ethyl endcapping(right). Area fraction of triblock copolymer in chromatographs on left is ~ 10 %.



Elution Time →



Elution Time →

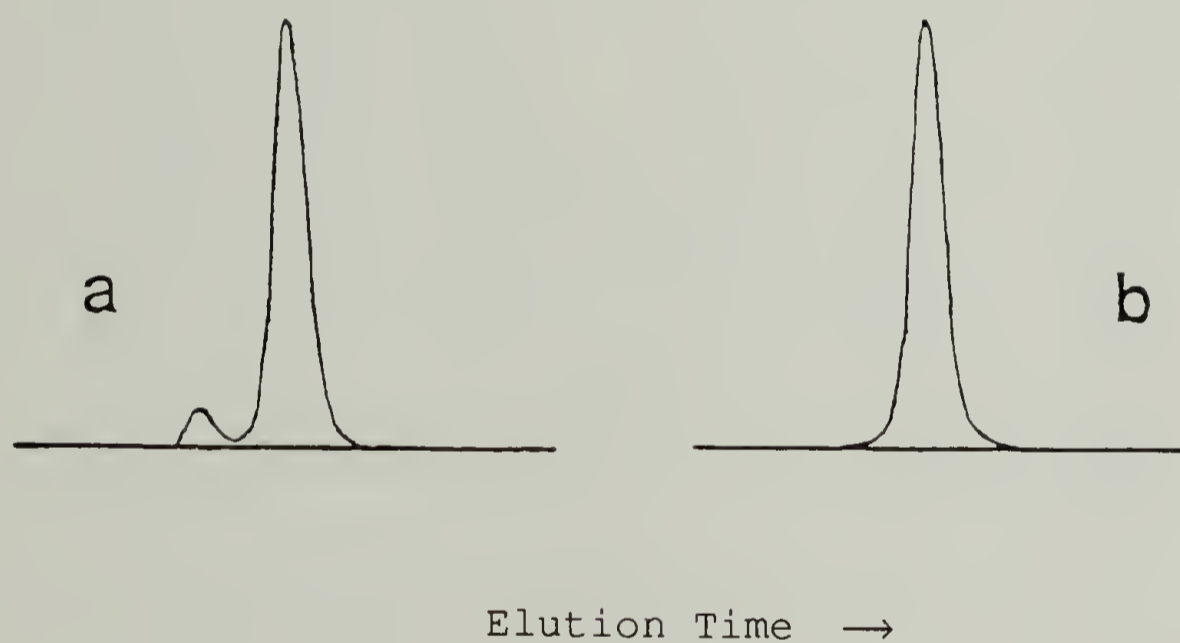


FIG. 40 Gel permeation chromatography (GPC) of 1 mg/ml THF solution of Polystyrene-Propylene Sulfide diblock copolymer (PS₉₀-PPS₁₀), with (a) oxidatively coupled component, and (b) after reduction with DTT and stable ethyl endcapping. Area fraction of triblock copolymer component in chromatograph on left is ~ 10 %.

TABLE 9. Molecular weight distribution and polydispersity of Polystyrene-Propylene Sulfide diblock copolymers synthesized by anionic methods. All copolymers are free of disulfide linkages, and are stably endcapped with ethyl groups. Molar stoichiometries were determined by microanalysis. All listed molecular weights are relative to that of Polystyrene.

TABLE 9

PS_A-PPS_B Characteristics

Samples	M _n	M _w /M _n
PS ₅₀ -PPS ₅₀	58,169	1.07
PS ₇₅ -PPS ₂₅	67,631	1.14
PS ₉₀ -PPS ₁₀	64,312	1.04
PS ₉₅ -PPS ₅	63,180	1.04
PS ₁₀₀	65,398	1.06
PS ₉₀ -PPS ₁₀	81,717	1.06
PS ₁₀₀	80,020	1.07

References

1. Kolthoff, I. M.; Gutmacher, R. G. *J. Phys. Chem.*, **1952**, *56*, 740-745.
2. Frisch, H. L.; Hellman, M. L.; Lundberg, J. L. *J. Polym. Sci.*, **1959**, *38*, 441.
3. Felter, R. E.; Moyer, E. S.; Ray Jr., L. N. *J. Polym. Sci.*, **1969**, *B7*, 529-533.
4. Felter, R. E.; Ray Jr., L. N. *J. Colloid Interface Sci.*, **1970**, *32*, 349.
5. Koopal, L. K.; Lyklema, J. *J. Chem. Soc., Faraday Discuss.*, **1975**, *59*, 230.
6. Howard, G.J.; Woods, S.J. *J. Polym. Sci., A-2*, **1972**, *10*, 1023-1028.
7. Sadakne G. S.; White, J. L. *J. Appl. Polym. Sci.*, **1973**, *17*, 453.
8. Linden, C. V.; Leemput, R. V. *J. Colloid Interface Sci.*, **1978**, *67*, 48-62.
9. Linden, C. V.; Leemput, R. V. *J. Colloid Interface Sci.*, **1978**, *67*, 63-69.
10. Cohen Stuart, M. A.; Scheutjens, J. M. H. M.; Fleer, G. *J. J. Polym. Sci.: Polym. Phys. Ed.*, **1980**, *18*, 559-573.
11. Stromberg, R. R.; Tutas, D. J.; Passaglia, E. *J. Phys. Chem.*, **1965**, *69*, 11, 3955-3963.
12. Peyser, P.; Stromberg, R. R. *J. Phys. Chem.*, **1967**, *71*, 2066.

13. Takahashi, A.; Kawaguchi, M.; Hirota, H.; Kato, T. *Macromolecules*, **1980**, *13*, 4, 884-889.
14. Kawaguchi, M.; Takahashi, A. *J. Polym. Sci.: Polym. Phys. Ed.*, **1980**, *18*, 2069-2076.
15. Kawaguchi, M.; Maeda, K.; Kato, T.; Takahashi, A. *Macromolecules*, **1984**, *17*, 1666-1671.
16. Kawaguchi, M.; Hattori, S.; Takahashi, A. *Macromolecules*, **1987**, *20*, 178-180.
17. Kirshenbaum, I. *J. Polymer Sci.*, **1965**, *3A*, 1869-1875.
18. Nuzzo, R. G.; Fusco, F. A.; Allara, D. L. *J. Am. Chem. Soc.*, **1987**, *109*, 2358-2368.
19. Stouffer, J. M.; McCarthy, T. J. *Macromolecules*, **1988**, *21*, 5, 1204-1208.
20. Hoeve, C. A.; DiMarzio, E. A.; Peyser, P. J. *Chem. Phys.*, **1965**, *42*, 7, 2558-2563.
21. Scheutjens, J. M. H. M.; Fleer, G. J. *J. Phys. Chem.*, **1980**, *84*, 178-190.
22. Griot, O.; Kitchener, J. A. *Trans. Faraday Soc.*, **1965**, *61*, 1026.
23. Joppien, G. R. *Makromol. Chem.*, **1975**, *176*, 1129.
24. Porter, M. D.; Bright, T. B.; Allara, D. L.; Chidsey, C. E. D. *J. Am. Chem. Soc.*, **1987**, *109*, 3559-3568.
25. Nuzzo, R. G.; Zegarski, B. R.; Dubois, L. H. *J. Am. Chem. Soc.*, **1987**, *109*, 733-740.
26. Stille, J. K.; Empen, J. A. *Polym. Prepr.*, **1965**, *6*, 619.
27. Boileau, S.; Sigwalt, P. *Compt. Rend.*, **1961**, *252*, 882.

28. Nevin, R. S.; Pearce, E. M. *Polymer Letters*, **1965**, *3*, 487.
29. Morton, M.; Kammereck, R. F. *J. Am. Chem. Soc.*, **1970**, *92*, 10.
30. Morton, M.; Kammereck, R. F.; Fetters, L. J. *Macromolecules*, **1971**, *4*, 11.
31. Morton, M.; Mikesell, S. L. *J. Macromol. Sci.- Chem.*, **1973**, *A7*, *7*, 1391.
32. Gourdenne, A. *Block Copolymers*, ed. S. Aggarwal, **1970**, Plenum Press, New York.
33. Hale, P. T.; Pope, G. A. *Eur. Polym. J.*, **1975**, *11*, 677.
34. Cooper, W.; Hale, P. T.; Walker, J. S. *Polymer*, **1974**, *15*, 175.
35. This idea for this type of ante chamber was created by Brant. U. Kolb, Polymer Science & Engin. Dept., Univ. of MA/Amherst, MA.
36. Morton, M.; Fetters, L. J. *Rubber Chem. & Tech.*, **1975**, *8*, *3*, 359.
37. Sigwalt, P.; Spassky, N. *Ring Opening Polymerization* Vol. 2, ed. K. J. Ivin and T. Saegusa, **1984**, Elsevier Press, Chapter 10.
38. Bates, R. B.; Kroposki, L. M.; Potter, D. E. *J. Org. Chem.*, **1972**, *37*, 560.
39. This was true for samples used in a previous study reported by Stouffer, J. M., Ph.D. Thesis, **1987**.
40. Simonds, R. P.; Goethals, E. J. *Makromol. Chem.*, **1978**, *179*, 1689.

41. Roggero, A.; Zotteri, L.; Proni, A.; Gandini, A.; Mazzei, A. *Eur. Polym. J.*, **1976**, *12*, 837.
42. Campos-Lopez, E.; Leon-Gross, A; Ponce Velez, M. A. J. *Polym. Sci.*, **1973**, *11*, 3021.
43. March, J. *Advanced Organic Chemistry 2nd ed.*, **1977**, McGraw-Hill.
44. Streitwieser, A.; Heathcock, C. *Introduction to Organic Chemistry 2nd ed.*, **1981**, Macmillan Pub.
45. Ohno, A.; Oae, S. *Organic Chemistry of Sulfur*, ed. Oae, S., **1977**, Plenum Press, New York.
46. Cleland, W .W.; *Biochemistry*, **1964**, *3*, *4*, 480.

CHAPTER 6

DOUBLE MODULATION EXTERNAL REFLECTION SPECTROSCOPY

Introduction

The combination of signal to noise limitations, extreme dynamic range requirements, artifacts caused by non-uniformities in the various experimental conditions, and the prohibitive time necessary to obtain reasonable experimental results, have limited the use of external reflection infrared spectroscopy (ERS)^{1,2} as a sensitive tool for characterization of polymer surfaces and interfaces. In fact, the experimental limit for infrared detection of thin layer polymer surfaces is about 90 Å.³ In that case the most intense peaks could be resolved at the lowest thickness of 90 Å, as shown in Figure 41, but no structural information could be ascertained.

In order to obtain information concerning the molecular packing and orientation of chains in ultra thin polymer films, an approach such as direct differential polarization acquisition⁴⁻⁷ is required. This method enables the greatest spectral contrast to be achieved, so that the selectivity and specificity advantages of infrared spectroscopy can be realized.^{1,2} For a plane-surfaced metal covered by an isotropic homogeneous ultrathin film, the calculated parallel polarization absorption factor is on the order of 10^5 times

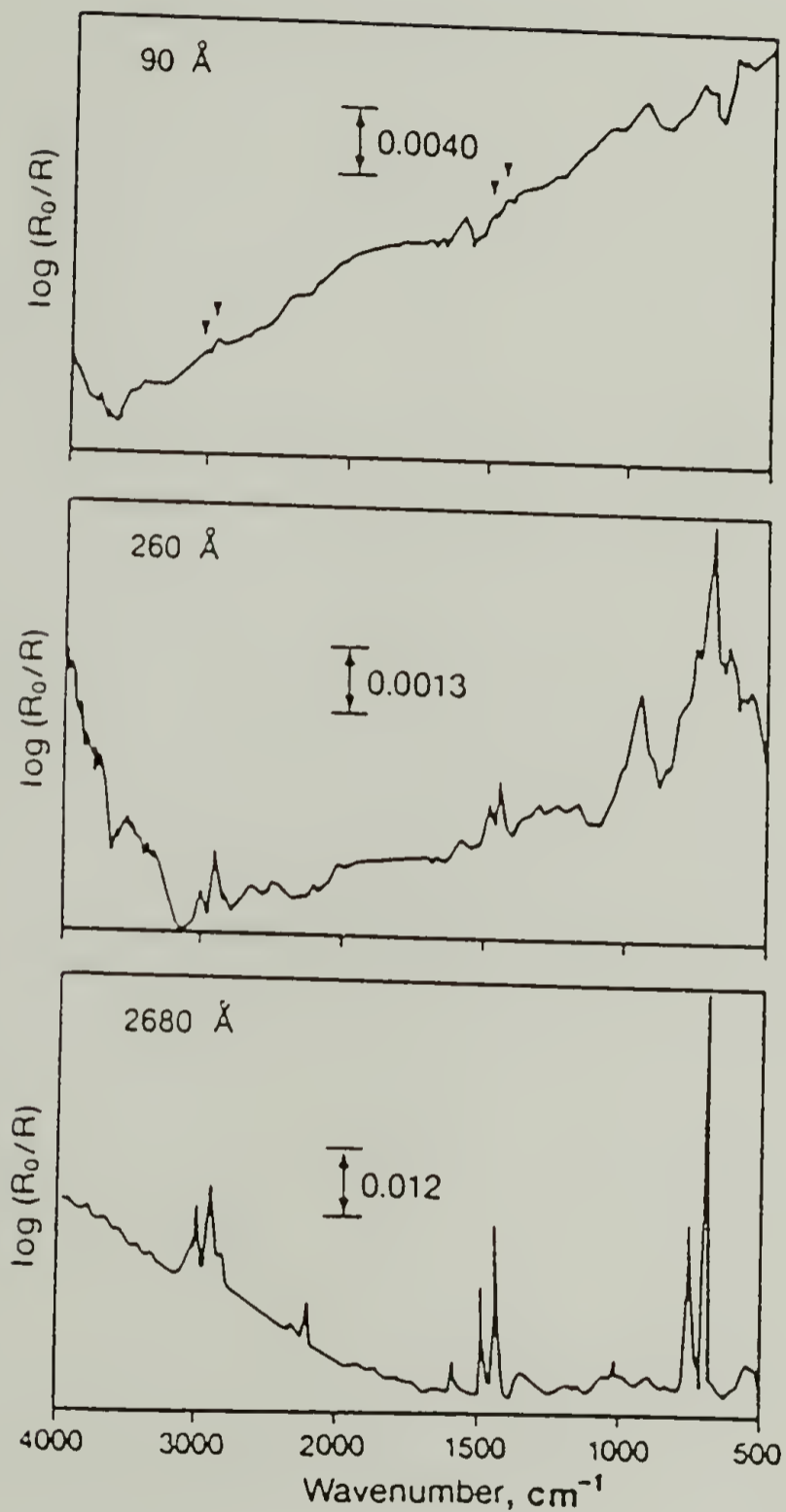


FIG. 41 FT-IR ERS spectra of thin films, 90 Å, 260 Å, and 2680 Å, (top) to (bottom), of poly(acrylonitrile-co-styrene) adsorbed on aluminum. The 90 Å film was the detection limit for this experiment (adapted from Ishitani, *et al.*, 1982).

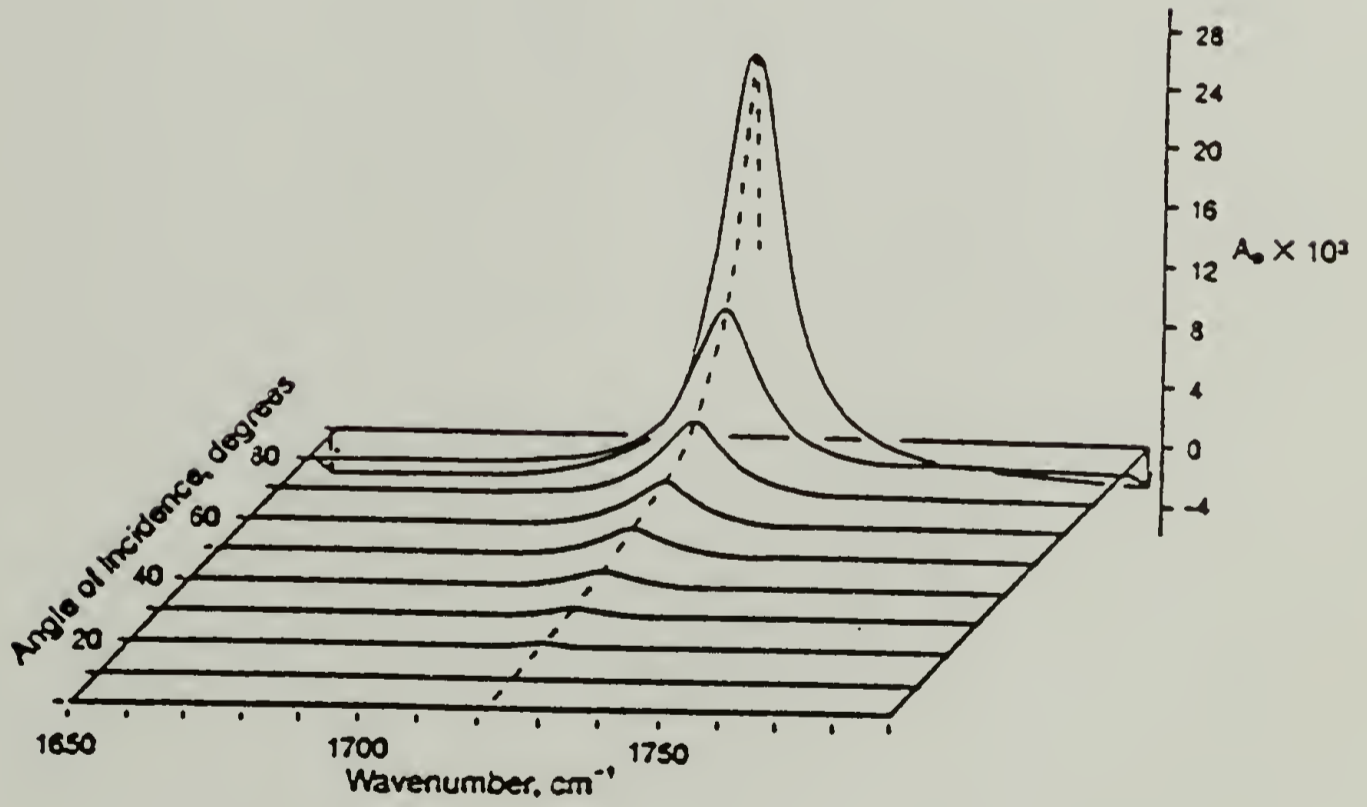
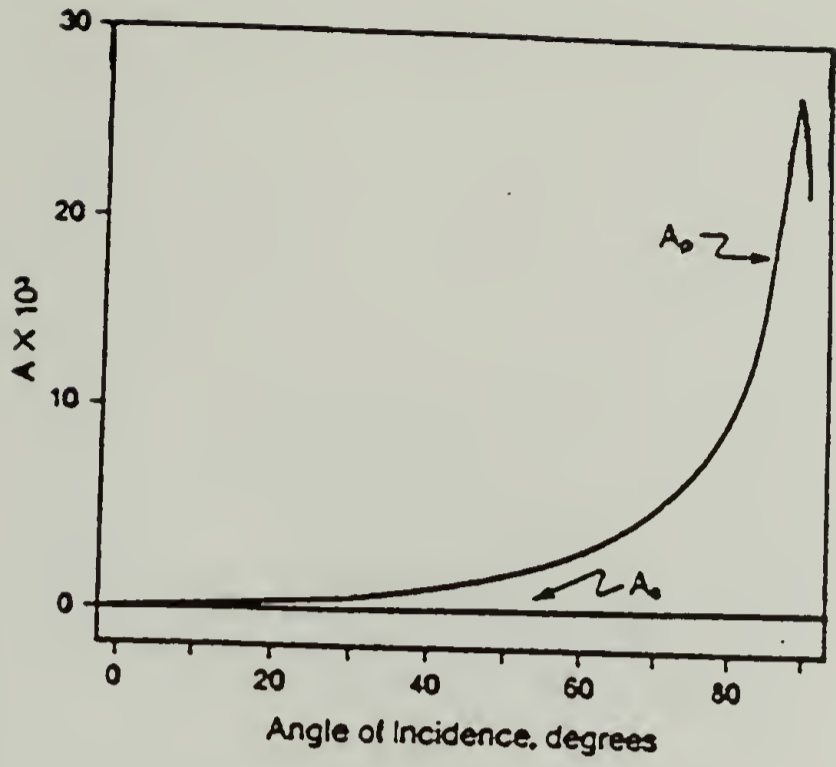
greater than that for perpendicular polarization at the optimum angle of incidence.^{1,2} Absorption factors for a 10 Å film of acetone on a gold substrate are shown in Figure 42. It is this difference in absorption factors that determines the ultimate spectral contrast.

The thickness of polymeric mono and multilayer structures, prepared by spontaneous chemisorption from dilute solution onto polycrystalline metal substrates, is only on the order of 10 to 30 Å. For adsorbed polymer films this thickness is too low to be structurally characterized by ERS orientation measurements. By utilization of the polarization modulation technique vibrational spectra of polymeric surface species can be obtained.⁸ These spectroscopic measurements can elucidate aspects of the chemistry and physics of polymer surfaces and interfaces, since they provide direct information concerning structure and bonding. This information is necessary as part of a comprehensive characterization of interfacial structure.

Description and Advantages of Differential Method

Polarization modulation is a direct differential method by which external reflection infrared spectra can be obtained. In FTIR differential polarization spectroscopy (DM-FT), coupled with (ERS)⁶, two differently polarized incident IR light beams are alternately passed into the external reflection assembly. This enables modulation

FIG. 42 Calculated dependence of the absorption factors for a 10 Å film of acetone on gold, for the parallel (A_p) and perpendicular (A_s) polarizations at the wavenumber of maximum adlayer absorption, (1720 cm^{-1}), as a function of angle of incidence, (top), and the calculated variation in the parallel absorption factor (A_p) as a function of wavenumber and angle of incidence for the same film. [Adapted from Golden, G. G., 1985(Ref 20.)].



between the two reflection polarizations. The polarization modulation is rapid relative to the modulation of the FTIR signal. As a result the differential polarization signal can be detected by a phase sensitive amplifier(lock-in amp.) synchronized with the driving frequency of the alternating polarization. The mathematical treatment for Polarization Modulation Grazing incidence external Reflection infrared Spectroscopy(PMGRS) is developed later in this chapter.

There are inherent advantages for such a measurement technique. The resultant small difference signal is typically on the order of 10^{-4} absorbance units or less. It can therefore be measured more accurately as the amplitude of a periodically varying AC signal which is averaged over many oscillations. In addition, the phase sensitive amplifier can be utilized as a noise filter. Noise which has frequency components below that of the polarization modulation frequency, as well as interfering noise which is at the modulation frequency but is not in phase with the detected signal, is rejected.

Incorporation of polarization modulation in ERS, with Fourier Transform Infrared Spectroscopy(FTIR), enables the differential reflection polarization measurement to be obtained with several additional advantages. The most important of these is Connes's advantage, which results from the continuous calibration of the infrared frequencies by utilization of laser zero-crossing counting.⁹ This enables

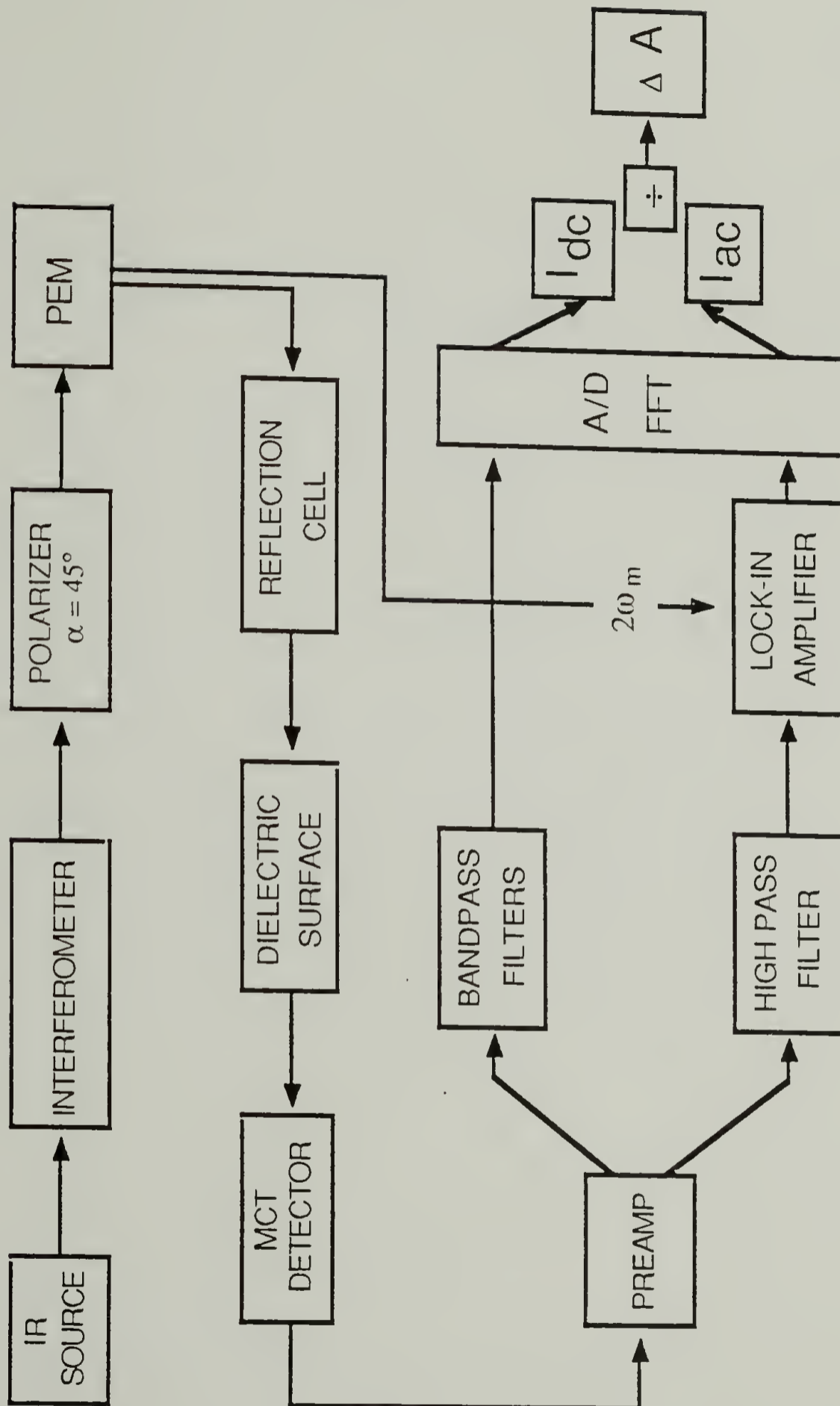
consecutive spectra to be obtained with a high degree of accuracy and precision. Reasonable measurement times for high signal to noise spectra, are usually the result of Jacquinot's advantage of increased throughput, and Fellgett's advantage of multiplexing.⁹

For the case of ERS of thin films at high angles of incidence, the additional throughput detected as reflectance from the metal substrate is actually unnecessary. This results in an extreme dynamic range requirement. Even with the advantage of multiplex detection, the attenuation in energy due to the absorbing species is barely tractable. ERS of polyfunctional organic monolayers, prepared by Langmuir-Blodgett and self-assembly techniques, has been limited by the difficulty of the ERS measurement, and more importantly by the inherent dynamic range necessitated.¹⁰⁻¹⁹ The PMGRS method of measurement allows both the dynamic range and the signal to noise problems to be addressed. The full advantage of the increased throughput and multiplex detection inherent to the FTIR technique can then be realized. A schematic of the polarization modulation experiment when coupled with FTIR/ERS is shown in Figure 43.

Typically, less than 10^3 scans signal averaged will yield an acceptable final spectrum for the reflection polarization difference.⁸ The dynamic range of 10:1 is sufficient to preserve the signal to noise ratio required for FTIR-ERS measurement. For ordinary external reflection from

FIG. 43 Schematic for polarization modulation experimental method coupled with FT-IR grazing incidence external reflection spectroscopy. Interferometer is a Nicolet 60SXB, polarizer is a Cambridge Physical Sciences wire grid, PEM is a Hinds International series II photoelastic modulator, reflection cell is a modified Harrick VRA assembly, dielectric surface is polished KBr on a rotating stage, MCT is an Infrared Associates narrow band detector, preamp is the first amplification stage on the detector hardware, high pass filter is a single stage bandpass filter, lock-in is an EG & G Princeton Applied Research model 124A lock-in amplifier, and bandpass filters, A/D conversion, and fast Fourier transform(FFT) are done using existing Nicolet 60SXB hardware and software.

POLARIZATION MODULATION EXTERNAL REFLECTION

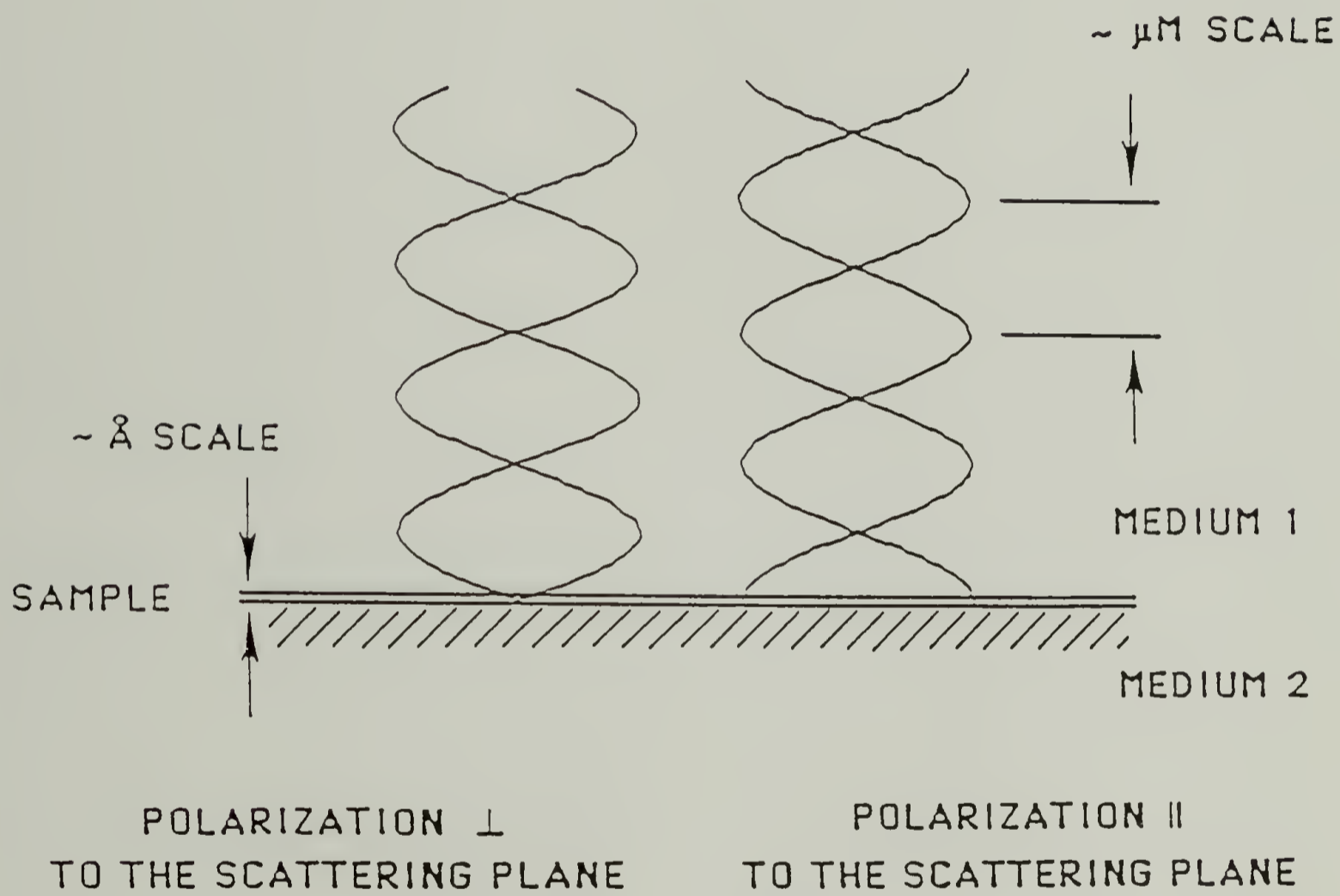


a thin film, a spectrum with a $10^5:1$ dynamic range would be necessary to achieve the same result. In fact, in such a measurement it is prudent to polarize the incident radiation in the direction parallel to the scattering plane. This diminishes the detected reflectivity and thus also the dynamic range, by eliminating the perpendicular reflectivity component, R_{per} . At near grazing angle incidence R_{per} is of comparable magnitude to that of R_{par} , the parallel reflectivity component. Although this condition holds near grazing incidence, only R_{par} contains the useful information. This results from the boundary conditions for the resultant electromagnetic wave, which are imposed by the conducting metal substrate and the thin film geometry of the polymer surface.^{1,2}

The node that exists for the R_{per} component at the surface, due to a 180° phase shift upon reflection, is shown schematically in Figure 44. The amplitude of the standing wave for R_{per} does not reach a maximum until a distance of $\lambda/4$ from the surface. This distance is on the order of 2.5 to 10.0×10^4 Å, or a thousand times that of the polymer film thickness. Elimination of R_{per} via polarization therefore reduces the dynamic range and increases the sensitivity of the ERS measurement. Polarization modulation maximizes this effect and actually increases the sensitivity by several orders of magnitude. It therefore enhances the attainable

FIG. 44 Schematic for the electric field components of the resultant electromagnetic wave at the boundary of a conducting surface. A zero electric field component exists parallel to the surface or perpendicular to the scattering plane. The standing wave varies harmonically as $(\cos \omega t)$ and nodal points exist at $x = 0, \lambda/2, \lambda, 3\lambda/2 \dots$ for x being the distance normal to the surface. A significant electric field component exists at the conducting surface boundary normal to the surface or parallel to the scattering plane. The standing wave has a maximum value at the surface (antinode) and nodal points exist at $x = \lambda/4, 3\lambda/4, 5\lambda/2 \dots$ where x is on the order of 7000 to 25000 Å.

STANDING ELECTROMAGNETIC WAVES
NEAR METALLIC SURFACE



measurable limit that is imposed by the signal to noise ratio for the thin film geometry in ERS measurements.

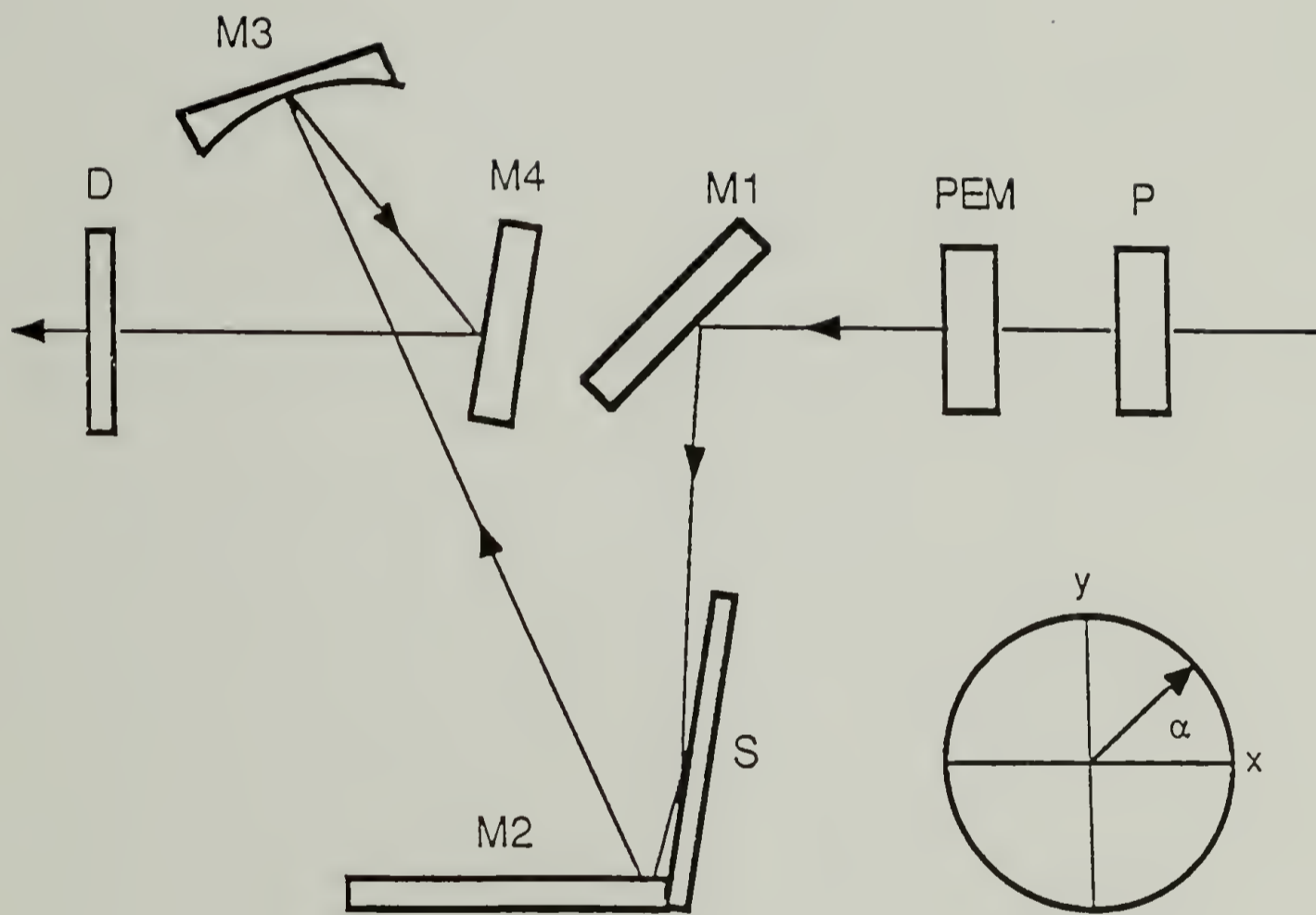
The polarization modulation scheme can also reduce the artifacts which would normally be present in polarization subtraction spectra.⁵ In successive polarization measurements the intensities of the two polarized beams may not be uniform over the area the IR beam impinges upon. This can cause artifacts such as interference fringes to be generated. At the grazing incidence of ERS measurements this becomes an even more critical condition. Artifacts are normally present in both the ratio or difference spectra of two different polarizations. These will be reduced by the modulation scheme. This is accomplished by utilization of the AC advantage. Amplitudes corresponding to the two polarization conditions are produced, detected, filtered and averaged over a large number of oscillations in a short time interval.⁵ This reduces the random noise contributions, and results in high time resolution for the polarization difference determination. In addition, the overall number of scans can be reduced from the more than 10,000 necessary for ERS to a value typically less than 500 when using polarization modulation. Thus baseline nonlinearities and drift can be virtually eliminated. These are prevalent in thin film ERS measurements, as a result of dimensional changes within the interferometer optics, and both source output and detector instabilities.

Optimization of Polarization Modulation Spectroscopy

Optical Components

Although the experimental setup for the PMGRS method consists of only a few additional components, the specifics pertaining to these are critical. The components for the modulation experiment are incorporated into a Nicolet 60SXB FTIR spectrometer. A Hinds International series II photoelastic modulator (PEM), fitted with an octagonal ZnSe isotropic crystal, is utilized. It is mounted in the optical train within the existing sample chamber, in front of a Harrick VRA external reflection assembly. The positioning of this modulator unit with respect to the incident infrared radiation is important. The optical window of the ZnSe crystal is only about 1 cm in diameter and losses due to reflection from its front and back surfaces can be detrimental. A Cambridge Physical Sciences wire grid polarizer has been mounted directly onto the leading face of the photoelastic modulator. Its orientation is such that its plane of polarization is in the direction bisecting the two principle axes of the induced birefringence in the ZnSe crystal. This is done to remove the difference in intensity between polarizations that is inherent to the interferometer optics. The VRA reflection assembly, PEM, and the polarizer positions are shown in Figure 45.

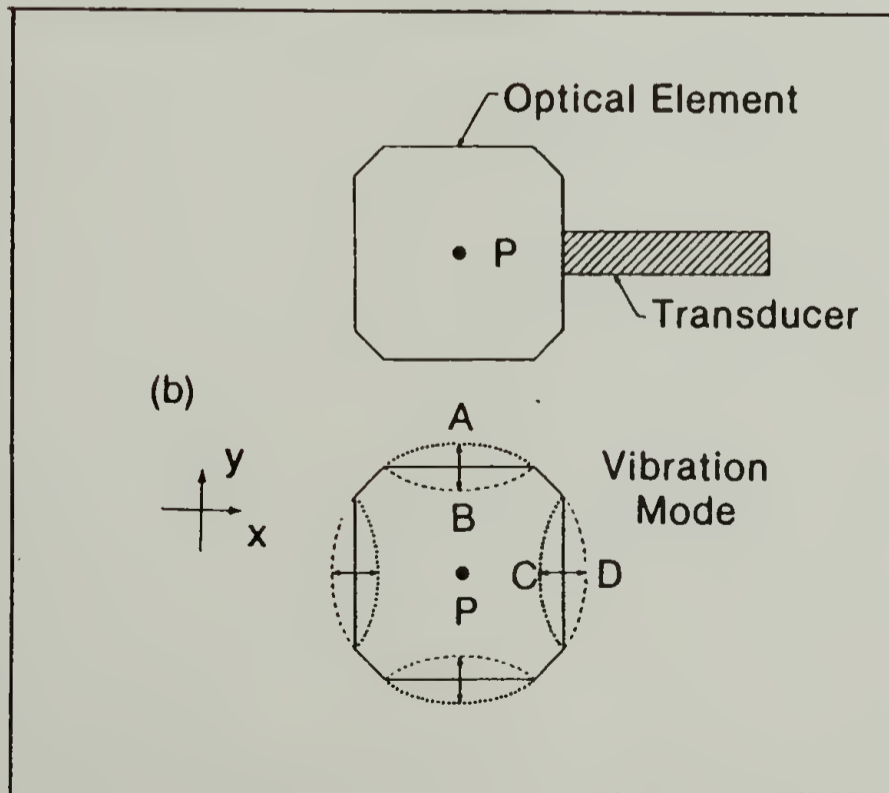
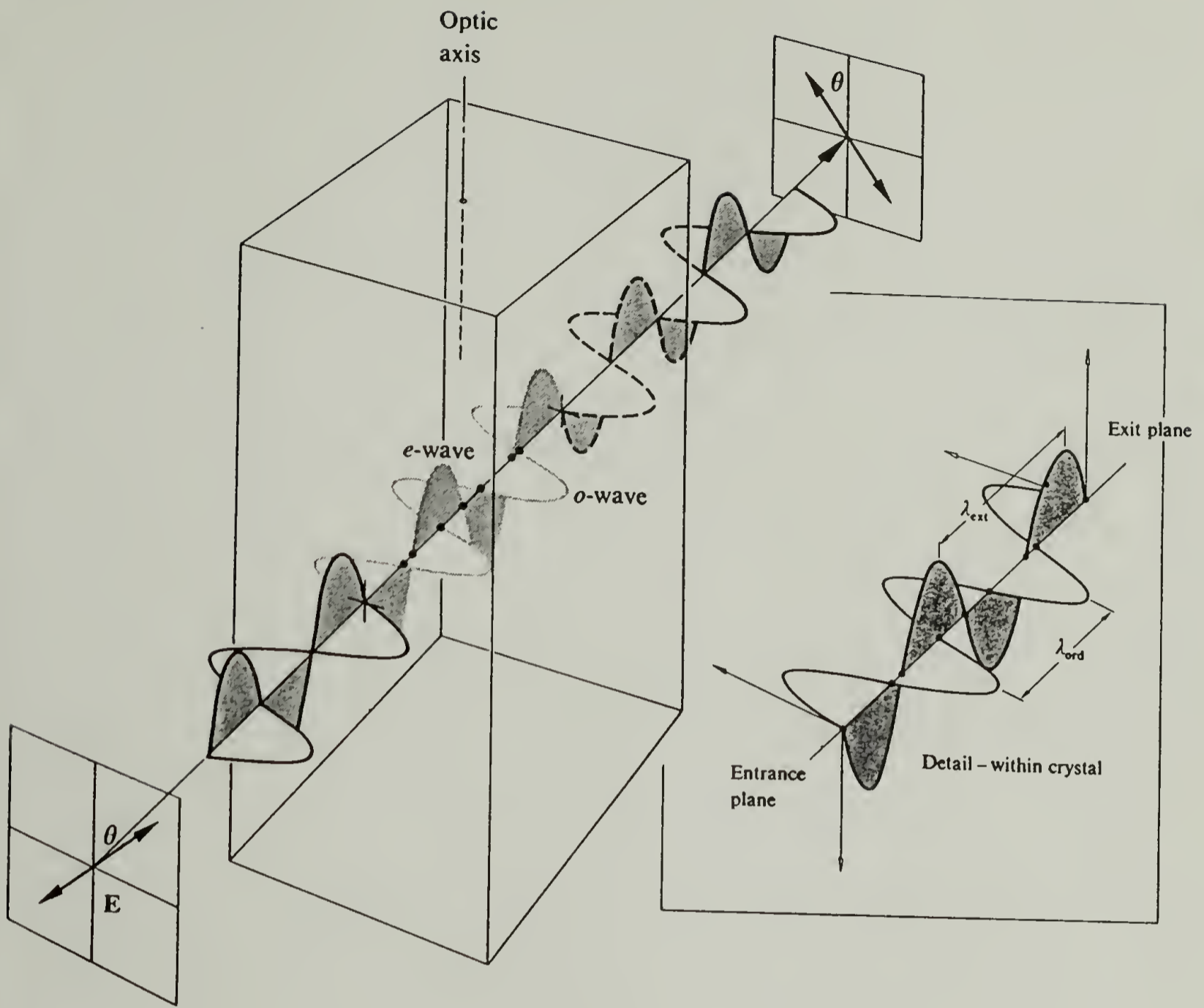
FIG. 45 Schematic for the grazing incidence reflection cell and polarizer components mounted inside the Nicolet 60SX sampling compartment. P is a wire grid polarizer, PEM is the ZnSe photoelastic modulator, M1 is the incident takeoff mirror, S the sample mirror, M2 the reference mirror, M3 the focusing mirror, M4 the detector takeoff mirror, and D is a narrow band MCT detector. The angle between the stress axes of the ZnSe crystal, x and y, and the polarizer direction (parallel) is $\alpha = 45^\circ$. The PEM is mounted in a base tilted 45° from vertical to achieve this.



The optic axes of the ZnSe crystal are determined by the location of the bonded crystal quartz traducers. The axes are parallel to the front and back surfaces of the crystal. One axis is parallel to the sides of the head unit while the other is parallel to the top and bottom. The ZnSe crystal undergoes both extension and compression in a cycle which is π out of phase with the mechanical vibration of the quartz. The oscillating amplitude of the vibration determines the degree of induced birefringence, and thus the retardation and relative phase difference between the outgoing electric field components. A schematic for a half-wave retardation plate and the resulting rotation of the incident electric field plane of polarization is shown in Figure 46.

When the modulator is set to act as a halfwave plate the resultant linear components are equal in amplitude. The output plane of polarization will alternate at twice the frequency of the sinusoidal strain imparted to the ZnSe crystal, or 142 kHz. At the quiescent point of the vibration cycle the output plane of polarization is E_{par} while at the extrema of the extension and compression it is E_{per} . This high frequency of polarization rotation enables a clear separation from the instrument interferogram frequencies. These are a function of the mirror velocity and position. A mirror velocity setting of 45 corresponds to a retardation velocity of 0.235 cm/sec. The modulated interferogram signal is then composed of a band of electrical frequencies in the

FIG. 46 Schematic for a half-wave retardation plate, (top), and the resulting 90° rotation of the incident electric field plane of polarization, as depicted by the electric field vectors at the incident and exit planes of the crystal. The transverse magnetic and electric wave components are represented by the o-wave and e-wave components respectively. [Adapted from Hecht, E.; Zajac, A., 1974 (Ref 21.)] Schematic of the PEM optical element (ZnSe), (bottom), showing the quartz transducer, the vibration mode of the crystal where C and D are the extrema of the compression and extension cycles respectively, the crystal sides as the quiescent point locations, and the crystal optic axes in the x and y directions, rotated 45° from the incident electric field.



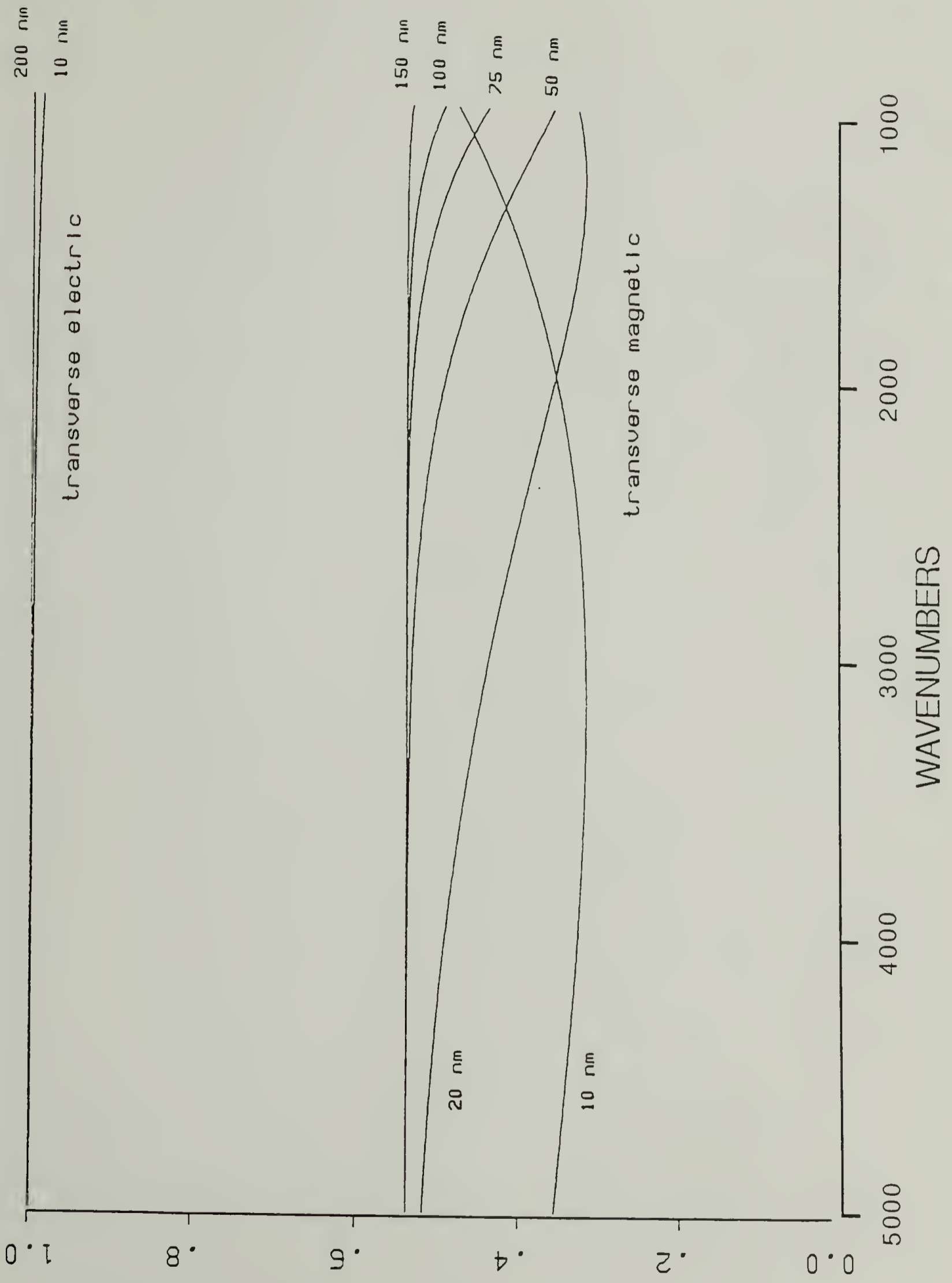
audio region from 2.07 kHz at 700 cm^{-1} to 11.8 kHz at 4000 cm^{-1} . This range can be easily separated from the doubly modulated signal, composed of a band of frequencies of 142 ± 2 to 12 kHz, by lock-in amplification methods. This detection enables the differential polarization signal to be obtained directly. Furthermore, the double modulated signal will not be passed by the existing FTIR bandpass filters when it is necessary to obtain the DC interferogram solely. The DC interferogram is much less sensitive to both variations in incident angle, and to the specific half-wave peak to peak retardation setting of the photoelastic modulator which effects the amplitude of the sinusoidal strain.

The linearly polarized light that exits the Hinds modulator impinges on the Harrick VRA external reflection assembly. The VRA has been carefully leveled by the addition of a supporting base. This traverses diagonally under the unit's existing base at the same height as the stop on its sliding vertical mount. The reflection unit is mounted such that the incident mirror is a flat reflector, from which the IR radiation reflects directly to the sampling mirror. The sampling mirrors are Fisherbrand glass microscope slides. These have been cleansed, followed by vapor deposition of Au from resistively heated tungsten baskets at a base pressure of 2×10^{-6} mm. Vapor deposition is carried out in a modified Balzers MED 010 vapor deposition apparatus.

The evaporated Au film thickness was controlled by monitoring the deposition process with a quartz crystal thickness monitor. The Au substrates were prepared with film thicknesses of at least 1800 Å, in all cases. This minimum Au layer thickness was established from theoretical reflectivity calculations. These have demonstrated that the reflectivity of Au, at the optimum incident angle of 88°, exhibits a thickness dependent frequency dispersion for the difference between parallel and perpendicular reflection over the frequency range of interest. This would unnecessarily complicate the resultant polarization difference spectra. As shown in Figure 47, the difference in reflectivity for the two polarizations does not approach a constant value, independent of frequency, unless the thickness of the Au layer is a minimum of 1800 Å.

After deposition the evacuated chamber was filled with prepurified nitrogen. The Au film substrates were immediately placed in Schlenk tubes and stored under nitrogen or vacuum when not in use in the reflection assembly. It was determined from grazing angle XPS measurements, that the outer 10 angstroms of vapor deposited films, prepared in the above fashion, can actually contain up to 65% carbon as a result of adventitious adsorption. Polarization modulation experiments exhibited C-H stretching bands representative of short chain hydrocarbons. These bands create problems in the subsequent data analysis of absorbed polymeric species on

FIG. 47 Calculated reflectivity as a function of wavenumber for transverse electric and magnetic components reflected from gold layers 10, 20, 50, 75, 100, 150, and 200 nm in thickness, at the optimum incident angle of 88° . Dispersion in the differential reflectivity for the two components is caused by the transverse magnetic component for gold layer thicknesses below 150 nm. This dispersion can easily overwhelm the small differential signal that arises from ultra thin adsorbed polymer films.

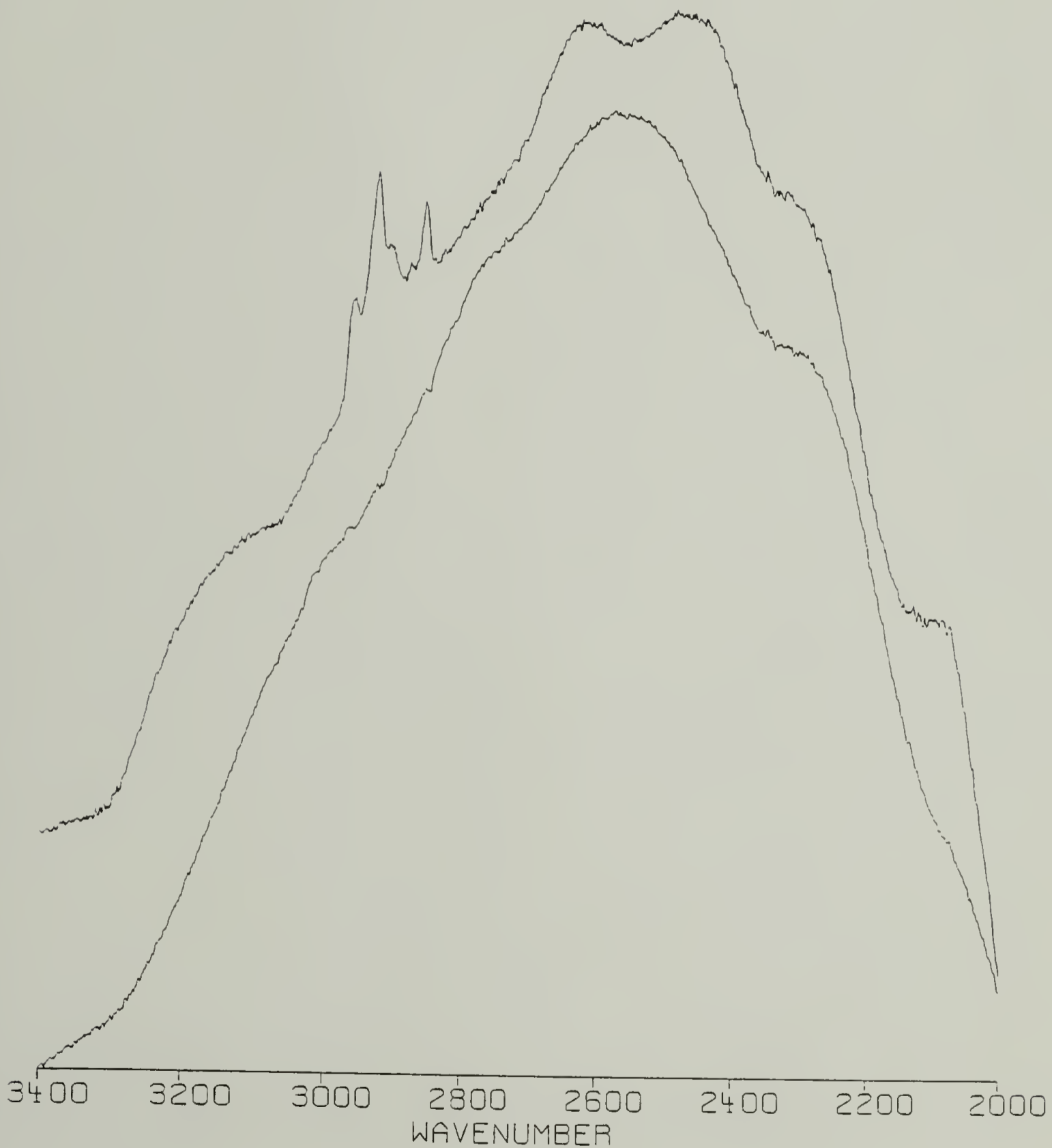


these Au film substrates. A heat treatment process for the sample Au slides was therefore undertaken after the deposition process. The slides were annealed at 350°C for 30 minute intervals until the polarization modulation spectra exhibit minimal evidence of C-H stretching bands. It is these slides which are used for the initial background spectra. They were then subsequently exposed to dilute polymer solutions from which spontaneous adsorption occurs. An example of the relative decrease in intensity for the C-H stretching bands when the Au surface is heated is shown in Figure 48.

Alignment Procedure

The reflection cell contains a reference mirror which is situated at an angle slightly larger than 90° from the above sample mirror. A gold coated glass slide (1/4 inch thick), purchased from Edmund Scientific, is used for this mirror. It is positioned close to normal to the optical train and is thus not critical. The incident mirror and the sample-reference mirror stage rotate independently. This means that a certain angle, as read off the provided scale, is subject to the actual positioning of the incident mirror. A detailed masking off process was therefore undertaken for alignment of the reflection cell, although other research groups in this field do not mention such a process. This is critical because if the incident mirror is positioned such that the concern is with throughput of the reflection assembly, then

FIG. 48 Single beam polarization modulation grazing incidence external reflection infrared spectra for reflectivity from a vapor deposited Au surface, 2000 Å in thickness, immediately after deposition, (top), and for same surface after slide was heated to 350 °C under nitrogen purge for two 30 minute intervals, (bottom). Evidence of adventitious hydrocarbon adsorption is shown in the C-H stretching region before heating cycles are carried out.



at angles near grazing incidence part of the beam could be impinging directly upon the reference mirror. Unwanted signal is then detected as part of the overall signal, which in turn would result in decreased sensitivity and increased dynamic range constraints.

Such an alignment would be detrimental for the desired sensitivity, so the IR beam is masked off at the leading edge of the sample mirror in such a manner that none of the beam can directly reflect from the reference mirror. The sample-reference mirror staging is then rotated toward the glancing condition in small angle intervals, with corresponding alignments done to the remaining reflection cell components until the glancing condition is actually realized. Even though the VRA reflection assembly gives 1:1 imaging, at these high angles of incidence vignetting of the IR beam is necessary in order to reduce the resulting beam spread and unwanted incidence on the reference mirror. For a sample mirror length of 5 cm and a beam diameter of 3 mm, at 88° , only a 58% fraction of the beam spot can interact with the sample mirror without impinging upon the reference mirror. The grazing position of the sample-reference mirror staging is then utilized as the reference point for 90° . Though vignetting will occur at 88° , the fractional beam spot that does interact only with the sample mirror will result in increased sensitivity and decreased dynamic range. A decrease in the overall signal will occur, much like the

decrease that arises from the use of a parallel polarizer before the VRA reflection assembly in a normal ERS measurement. This decrease in signal is unavoidable if the major concern is the achievable signal to noise, since it is these factors that are so critical in determining whether the ERS measurements are tractable.

A further improvement could be implemented by modifying the optics of the external reflection assembly, so that the IR beam is collimated. This could be done within the optical path from where the beam reflects from the incident flat mirror to the sample mirror. Collimation would enable one to specifically set the beam spot diameter to a size that would prevent the vignetting that is otherwise necessary at conditions near grazing incidence where sensitivity is greater. The reason that the above masking procedure is not ordinarily followed is because usually ERS measurements are made at incident angles of between 75° and 80° . At these angles this condition is not nearly so critical. In this angular range, however, the inherent sensitivity due to the obtainable reflectance is much lower than that at 88° .

Removal of DC Offset From s-Polarization

The final part of the reflection cell consists of a 25 mm KBr window centered to the exiting IR beam. It is mounted to a 360° rotation stage, about the y axis, for the z axis being defined as the propagation direction. The reason for

the addition of this component is that a significant part of the infrared intensity exiting the reflection cell arises from s-polarized light. At 88° the reflectivity for this polarization is significantly greater than that of p-polarized light. As mentioned previously, upon reflection from a conducting surface a phase shift of 180° occurs for s-polarized radiation.² The resultant standing wave, for near grazing incidence conditions, is characterized by a node in the electric field ($E=0$) for R_{per} at and near the surface, as shown in Figure 44. Therefore, no interaction with a thin ($< 40 \text{ \AA}$) absorbing film will take place for vibrations with transition dipoles oriented within a few degrees of parallel to the surface.

Any excess contribution of s-polarized light to the overall signal detected is thus wasted signal, resulting in decreased sensitivity and increased dynamic range constraints. By rotation about the y axis the KBr crystal can be utilized as a compensating dielectric reflecting surface. This enables the s-polarized light to be preferentially reflected away relative to the p-polarized light. It is only the p-polarized light that contains the information pertaining to the sample. The resulting compensation of polarization reflectivity is monitored both by the interferogram display, and the zero centered output panel meter of the lock-in. The output represents the RMS value of the differential output signal, or the detected

signal amplitude. When this value is zeroed the inherent difference in reflectivity for the two polarizations is minimized. Although reduction of this DC offset in the AC signal lowers the detected signal amplitude, ideally the final differential signal contains contributions due only to absorbance of the R_{par} component. This enables a maximization in sensitivity, and minimizes the dynamic range requirements necessary to achieve acceptable signal to noise in the resulting differential polarization spectra.

Lock-in Detection

The resulting radiation is detected by a liquid nitrogen cooled narrow band MCT detector, which is housed in protective shielding to reduce external pick up. The signal is removed from the detector amplification circuitry after the first amplifier circuit, and sent via a ground strap shielded B and C cable to a EG&G Princeton Applied Research model 124A lock-in amplifier. Before the signal is passed into the model 116 differential preamplifier, it is first shunted through a shielded one stage high pass RC filter. The RC filter was constructed to have a cut-off frequency of about 10 kHz. This step is critical since the detected signal up to this point contains both the DC and AC signal components, as well as the associated noise. Most of the signal amplitude at the lock-in input is due to the DC component. Since the pre-filter has a -3 dB octave roll off value of 10 kHz, the majority of the DC signal is prevented

from reaching the lock-in. Otherwise it would have to be filtered by the phase sensitive detector (PSD), and the large DC amplitude can easily overload the PSD circuitry. Furthermore, by employing a filter at this stage a reduction in the noise level ahead of the mixer in the phase sensitive detector can be effected. This eliminates a portion of the input noise before it reaches the PSD, thereby reducing spurious DC outputs that arise from high level noise. Such reduction effects an increase in the dynamic reserve of the lock-in, thus allowing signals to be measured which would not be otherwise. The dynamic reserve is the ratio of the peak level of asynchronous signals, that will just cause significant nonlinearity, to the peak level of the full scale synchronous signal. The latter signal is the desired one.

The signal is passed from the pre-RC filter into the model 116 preamplifier. The preamplifier is operated in direct mode, since the amplitude transfer curves for its transformer exhibit large reductions in the output amplitude for the frequency range of interest (142 kHz). This is the case for a source signal with any reasonable impedance. Thus one is not able to take advantage of any noise figure improvements which are typically obtained via transformers. The source thermal noise is usually the dominant factor in determining the input signal to noise ratio. It can be reduced by limiting the equivalent noise bandwidth. This is accomplished by use of the pre RC filter. Other sources of

noise are flicker noise, and non-synchronous signals that may arise from either the experiment or external RF pickup. By operating the Signal Channel selective amp in High Pass mode a reduction in these is realized. High Pass mode also enables rejection of all frequencies below the selected cut off frequency of 110 kHz at a rate of 12 dB octave roll off.

Phase adjustment of the PSD is necessary in order to equate the phase of the reference signal to that of the input signal which it will be rectified with. Otherwise a true difference signal without a large DC offset can not be realized. Phase matching is accomplished by utilizing the 90 degree phase quadrature adjustment. First, for any given angle of the sample slide, the KBr component is rotated to negate the inherent reflectivity difference between R_{per} and R_{par} . This is monitored on the DC RMS output level meter. Then the reference signal at the PSD is adjusted approximately 90 degrees out of phase from the filtered input signal with the quadrature setting. Finally the phase is fine tuned by adjusting and monitoring the result with the interferogram display of the output. When the centerburst of the interferogram is minimized then the 90 degree out of phase position has been located. Adjustment of the phase quadrature another 90 degrees enables the reference and input signals to be rectified correctly.

The rectified output signal is now singly modulated and contains only the differential polarization information along

with a very small DC contribution. This contribution can not be completely eliminated over the entire infrared frequency range. This is due to dispersion effects that arise from (1) the PEM, (2) values of the extinction coefficient (k) for reflection from metal surfaces at the optimum absorption factor angle, and (3) the lock-in circuitry itself. Although it is small it still dominates the overall amplitude of the differential signal. An example of the magnitude of the dispersion effects relative to reflectivity and absorption is shown in the energy spectra in Figure 49, for a gold background and an adsorbed copolymer film.

The output signal is passed through a resistor back to its point of departure on the MCT amplification board. It is then band pass filtered and Fourier processed according to the velocity setting of the interferometer mirror. The single beam result must be ratioed to an ERS result to obtain the final spectrum. The ERS energy spectra corresponding to the gold background and copolymer film of Figure 49 are shown in Figure 50. The low sensitivity relative to the modulation results is noted in the minimal energy losses due to absorption, and the lack of dispersion effects. The resultant absorption intensity is proportional to absorbance due to transition moments with a component that is parallel to the scattering plane, or E_{par} . This component is oriented such that it is perpendicular to the film surface and thus provides the necessary structural information.

FIG. 49 Single beam polarization modulation grazing incidence external reflection infrared spectra for reflectivity from a vapor deposited Au surface, 2000 Å in thickness, immediately after deposition, (bottom), and for same surface after adsorption of copolymer PS₉₅-PPS₅ from dilute solution (1 mg/ml), (top). Evidence of adsorbed layer is exhibited by aliphatic and aromatic C-H stretch modes, C=C stretch, and C-H in plane deformation modes. Above 2000 cm⁻¹ bands are positive going, while below they are negative going due to dispersion effects and phase correction routine.

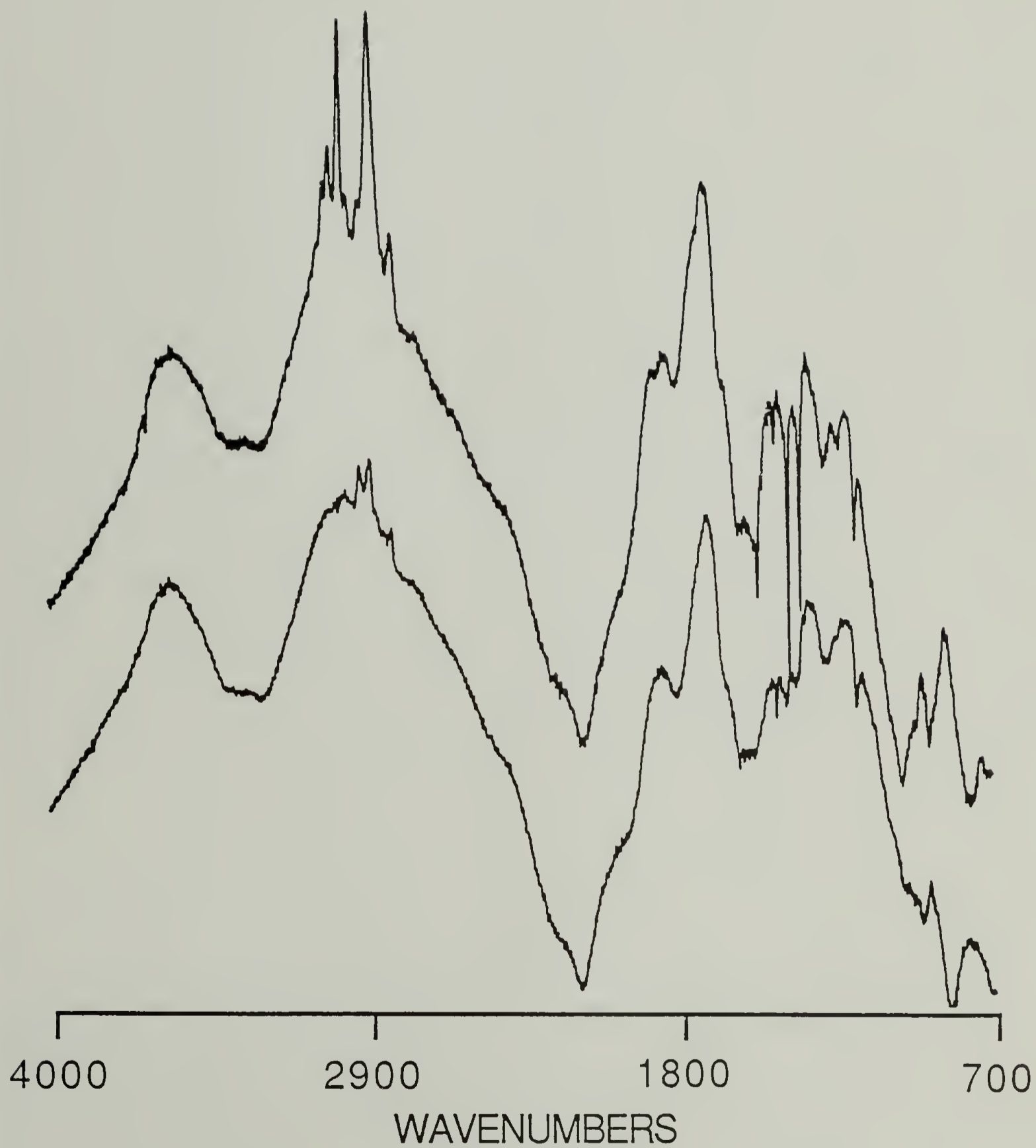
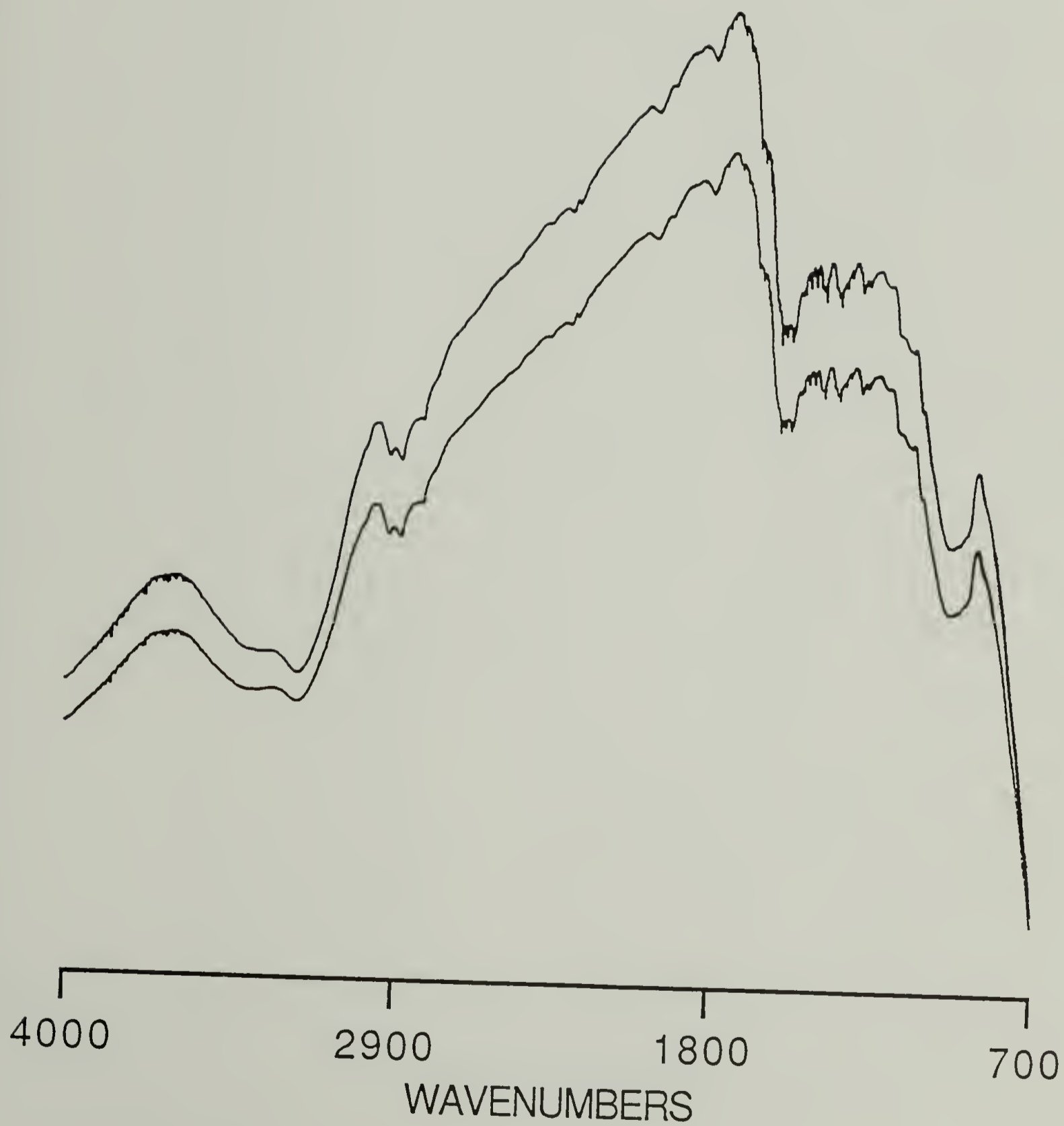


FIG. 50 Single beam grazing incidence external reflection infrared spectra for reflectivity from a vapor deposited Au surface, 2000 Å in thickness, immediately after deposition, (bottom), and for same surface after adsorption of copolymer PS₉₅-PPS₅ from dilute solution(1 mg/ml), (top). The surface for (top) and (bottom) spectra are the same as in Figure 49. Note the lack of evidence for existence of an adsorbed layer, and the insensitivity of this method to dispersion effects.



Mathematical Treatment For Polarization Modulation External
Reflection Infrared Spectroscopy

The following treatment is a composite of that for FTIR spectroscopy from Griffiths and de Haseth,⁹ and those for double modulation spectroscopy developed by Nafie and Overend.^{5,6}

In FTIR external reflection spectroscopy the interferogram may be expressed using a cosine integral, as $V(\delta)$, which represents the detector output in volts as a function of the retardation (δ). Since the retardation changes at twice the velocity of the moving mirror, v , this interferogram can also be considered as a function of time, as $V(t)$. If an additional sinusoidal modulation between two reflection polarization states $I_p(\bar{\nu})$ and $I_s(\bar{\nu})$ occurs at $(2\omega_m)$, then $V(t)$ becomes

$$V(t) = \int_0^{\infty} [B_{dc}(\bar{\nu}) + B_{ac}(\bar{\nu}) \sin(\omega_m t)] \cos [4\pi v \bar{\nu} t - \theta(\bar{\nu})] d\bar{\nu} \quad (30)$$

where $B(\bar{\nu})$, the measured amplitude of the incident infrared radiation, is inclusive of the detector and amplifier wavenumber response functions, and $\theta(\bar{\nu})$ is introduced into the phase angle as a result of filters in the amplifier and dispersion in the beamsplitter. The polarization modulation $2\omega_m$ component is completely removed by bandpass filtering when the interferogram is collected in the normal fashion, so the **dc** interferogram is represented by

$$V_{dc}(t) = \int_{\nu_1}^{\nu_2} B_{dc}(\bar{\nu}) \cos[4\pi\bar{\nu}t - \theta_{dc}(\bar{\nu})] d\bar{\nu} \quad (31)$$

where $\theta_{dc}(\bar{\nu})$ now includes the additional electric phase shifts resulting from the bandpass filters. The **dc** single beam spectrum known as $I_{dc}(\bar{\nu})$ is then obtained via Fourier processing and phase correction of the above **dc** interferogram.

Similarly the **ac** interferogram expressed as

$$V(t) = \int_0^{\infty} B_{ac}(\bar{\nu}) \sin(\omega_m t) \cos[4\pi\bar{\nu}t - \theta(\bar{\nu})] d\bar{\nu} \quad (32)$$

is separated from the **dc** interferogram $V_{dc}(t)$ by (1) pre-filtering with an RC high pass filter, (2) passage into lock-in amplification circuitry in direct mode, and (3) selective amplification in high pass mode. The resultant amplified **ac** signal is then sent to the phase sensitive detector of the lock-in where it is (1) synchronously detected with respect to a phase shifted reference signal of $\sin(2\omega_m t)$, and (2) filtered with a sharp roll off of -12 dB and a time constant, RC, of 500 μ sec. This synchronously demodulated polarization signal is then similarly band pass filtered yielding the **ac** interferogram as

$$V_{ac}(t) = \int_{\nu_1}^{\nu_2} B_{ac}(\bar{\nu}) \cos[4\pi\bar{\nu}t - \theta_{ac}(\bar{\nu})] d\bar{\nu} \quad (33)$$

where $\theta_{ac}(\bar{\nu})$ is now the **ac** phase angle contribution inclusive of phase shifts arising from the phase sensitive detection

and bandpass filters. The **ac** single beam spectrum, or $I_{ac}(\bar{\nu})$, is therefore obtained via Fourier processing and phase correction of the above **ac** interferogram.

Separation of the **ac** and **dc** interferograms can only occur if the difference in frequency, between modulation of the polarization and that effected by the interferometer, is sufficiently high. In this study the interferometer was operated at a mirror velocity of 0.235 cm/sec, resulting in interferometer modulation frequencies ranging from 2.36 kHz at 800 cm^{-1} to 10.34 kHz at 3500 cm^{-1} . These frequencies can be readily separated from the polarization modulation frequencies, generated by the photoelastic modulator at $2\omega_m$ or 140 kHz, via the above mentioned phase sensitive detector.

For this set up linearly polarized light is incident upon the photoelastic modulator such that its plane of polarization bisects the principal axes of the strained crystal. The initial electric field incident upon the fixed polarizer is represented by

$$\mathbf{E} = \mathbf{E}_{\parallel} + \mathbf{E}_{\perp} \quad (34)$$

and its components relative to the crystal axes are

$$\mathbf{E}_{\parallel} = E_{0,\parallel} (\sin \alpha \mathbf{i} + \cos \alpha \mathbf{j}) \quad (35a)$$

$$\mathbf{E}_{\perp} = E_{0,\perp} (\cos \alpha \mathbf{i} - \sin \alpha \mathbf{j}) \quad (35b)$$

where α is the angle between the modulator crystal principal stress axes and the incident electric field directions. The

principal stress axes represent the x and y laboratory coordinate directions \mathbf{i} and \mathbf{j} as shown in Figure 45. Only the component \mathbf{E}_{\parallel} is passed from the polarizer to the modulator, but since $\alpha = 45^\circ$ there will be equal components of the \mathbf{E}_{\parallel} electric field in the x and y principal stress directions of the crystal. Upon exiting the modulator the y component of \mathbf{E}_{\parallel} will be phase shifted by $\delta(\bar{v}, t)$ with respect to the x component resulting in

$$\mathbf{E}_{\parallel, m} = E_{0, \parallel} (\sin \alpha \mathbf{i} + e^{i\delta} \cos \alpha \mathbf{j}) \quad (36)$$

The polarization state of the output therefore varies as the $\cos \delta(t)$, where $\delta(t) = (\delta_0 \sin \omega_m t)$ is the relative phase shift, and $\pm \delta_0$ is the maximum phase shift for a given (\bar{v}) during the period of modulator oscillation. The PEM acts as a half waveplate, $\delta = \pi$ for $\delta_0 = \pi$, when the crystal is at the maximum of its compression and/or expansion cycle. In this case $\omega_m t = \pm \pi/2$, so the plane of the linearly polarized incident light rotates by 90° . The IR radiation output from the PEM thus alternates between \mathbf{I}_{\parallel} and \mathbf{I}_{\perp} depending upon whether the modulator crystal acts as an isotropic crystal or a half waveplate. The IR radiation, incident upon the external reflection assembly, can be represented at $\delta(t) = 0$ by

$$\mathbf{E}_{s,r} = E_{0,s} (\sin \alpha \mathbf{i} + \cos \alpha \mathbf{j}) \quad (37a)$$

and at $\delta(t) = \pi$ by

$$\mathbf{E}_{p,r} = E_{0,s} (\sin \alpha \mathbf{i} - \cos \alpha \mathbf{j}) \quad (37b)$$

where $\mathbf{E}_{s,r}$ and $\mathbf{E}_{p,r}$ are the components perpendicular and parallel to the scattering plane containing the incident and exit radiation. Typical values set for $\delta = \pi$ ranged from 3400 to 4000 nm, corresponding to 2941 and 2500 cm^{-1} respectively.

The total intensity arises from the linearly polarized reflection polarization states which arrive at the detector as a function of time and wavenumber. It contains the sum of the Fourier transforms I_{dc} and I_{ac} defined above, and can be expressed as

$$I_d = I(t, \bar{\nu})_{p,s} = I_{dc}(\bar{\nu}) + I_{ac}(\bar{\nu}) \cos [\delta_0(\bar{\nu}) \sin \omega_{mt}] \quad (38)$$

where $\delta_0(\bar{\nu})$ is due to the achromaticity of the photoelastic modulator. Collection and detection occurred separately for the single beam spectra, corresponding to the average intensity, $I_{dc}(\bar{\nu})$, and a spectrum directly proportional to the difference intensity, $I_{ac}(\bar{\nu})$. These intensities can be expressed in decadic absorbance as

$$I_{dc}(\bar{\nu}) = 0.5 I_0(\bar{\nu}) [10^{-A_{p,r}(\bar{\nu})} + 10^{-A_{s,r}(\bar{\nu})}] \quad (39a)$$

$$I_{ac}(\bar{\nu}) = 0.5 I_0(\bar{\nu}) [10^{-A_{p,r}(\bar{\nu})} - 10^{-A_{s,r}(\bar{\nu})}] \quad (39b)$$

The difference spectrum possesses an additional dependence on $\cos \delta$. When expanded in even-order spherical Bessel functions it yields a modified $B_{ac}(\bar{\nu})$ signal, after separation from $B_{dc}(\bar{\nu})$ but before lock-in demodulation, as

$$\{ B_0(\bar{\nu}) [10^{-A_{p,r}(\bar{\nu})} - 10^{-A_{s,r}(\bar{\nu})}] \sin 2\alpha 2J_2(\delta_0) \cos (2 \omega_{mt})(1 + \cos [4\pi \bar{\nu} t - \theta(\bar{\nu})]) \} \quad (40)$$

Here $A_{p,r}(\bar{\nu})$ and $A_{s,r}(\bar{\nu})$ represent the parallel and perpendicular components of absorption resulting from the adsorbed polymer layer. This represents a double modulation signal with a carrier frequency of ω_m , and components at $\cos \{ (2 \omega_m \pm [4\pi\nu\bar{\nu} - \theta(\bar{\nu})]) t \}$ for $\alpha = 45^\circ$. The doubly demodulated signal therefore results in a single beam spectrum that is dependent on the difference in intensity of the reflection polarization states, and is proportional to

$$\Delta I(\bar{\nu}) = 0.5 I_{ac}(\bar{\nu}) 2J_2 \delta_0(\bar{\nu}) \quad (41)$$

where

$$I_{ac}(\bar{\nu}) = 0.5 (I_{p,r}(\bar{\nu}) - I_{s,r}(\bar{\nu})) \quad (42)$$

for

$$I_{p,r}(\bar{\nu}) = I_{dc}(\bar{\nu}) + I_{ac}(\bar{\nu}) \cos \delta \quad (43a)$$

$$I_{s,r}(\bar{\nu}) = I_{dc}(\bar{\nu}) - I_{ac}(\bar{\nu}) \cos \delta \quad (43b)$$

Since the modulator only receives I_{\parallel} , then at zero retardance ($\delta = 0$), $I_{s,r}(\bar{\nu}) = I_{\parallel}$ and $I_{p,r}(\bar{\nu}) = 0$ at the reflection cell. Therefore at ($\delta = 0$), $I_{dc}(\bar{\nu}) = 0.5 [I_{s,r}(\bar{\nu})]$, and $I_{ac}(\bar{\nu}) = 0.5 [-I_{s,r}(\bar{\nu})]$ and similarly, for ($\delta = \pi$), $I_{p,r}(\bar{\nu}) = I_{\parallel}$ and $I_{s,r}(\bar{\nu}) = 0$, resulting in $I_{dc}(\bar{\nu}) = 0.5 [I_{p,r}(\bar{\nu})]$ and $I_{ac}(\bar{\nu}) = 0.5 [I_{p,r}(\bar{\nu})]$ as expected.

The ratio of the expressions for the single beam intensities $I_{dc}(\bar{\nu})$ and $\Delta I(\bar{\nu})$ can then be expressed as

$$[\Delta I(\bar{\nu}) / I_{dc}(\bar{\nu})] = [I_{ac}(\bar{\nu}) J_2 \delta_0(\bar{\nu})] / I_{dc}(\bar{\nu}) \quad (44)$$

where the ratio of $I_{ac}(\bar{\nu})$ to $I_{dc}(\bar{\nu})$ in decadic absorbance is

$$\frac{I_{AC}}{I_{DC}} = \frac{10^{-A_{p,r}} - 10^{-A_{s,r}}}{10^{-A_{p,r}} + 10^{-A_{s,r}}} \quad (45)$$

Let $A_{p,r} = a$, $A_{s,r} = b$ and $a' = \frac{a}{2}$, $b' = \frac{b}{2}$ then

$$\frac{10^{-a} - 10^{-b}}{10^{-a} + 10^{-b}} = \frac{10^{-2a'} - 10^{-2b'}}{10^{-2a'} + 10^{-2b'}} = \frac{\frac{10^{-2a'} - 10^{-2b'}}{10^{-a'} 10^{-b'}}}{\frac{10^{-2a'} + 10^{-2b'}}{10^{-a'} 10^{-b'}}} = \frac{\frac{10^{-a'}}{10^{-b'}} - \frac{10^{-b'}}{10^{-a'}}}{\frac{10^{-a'}}{10^{-b'}} + \frac{10^{-b'}}{10^{-a'}}} \quad (46)$$

$$= \frac{10^{(-a'+b')} - 10^{(-b'+a')}}{10^{(-a'+b')} + 10^{(-b'+a')}} = \frac{10^{\frac{(b-a)}{2}} - 10^{\frac{(a-b)}{2}}}{10^{\frac{(b-a)}{2}} + 10^{\frac{(a-b)}{2}}} = \frac{10^{\frac{\Delta A}{2}} - 10^{\frac{-\Delta A}{2}}}{10^{\frac{\Delta A}{2}} + 10^{\frac{-\Delta A}{2}}} \quad (47)$$

$$= \tanh\left(\frac{2.303\Delta A}{2}\right) \quad (48)$$

where $\Delta A = A_s - A_p$. Therefore for $I_{ac}(\bar{\nu}) / I_{dc}(\bar{\nu}) \leq 0.1$

$$[\Delta I(\bar{\nu}) / I_{dc}(\bar{\nu})] \cong 1.1515 (A_s(\bar{\nu}) - A_p(\bar{\nu})) J_2 \delta_0(\bar{\nu}) \quad (49)$$

The final form of this equation indicates that the ratio of the single beam spectra obtained via polarization modulation to that without, is directly proportional to the difference in absorptions for the IR beam polarized perpendicular and parallel to the optical scattering plane, $(A_s(\bar{\nu}) - A_p(\bar{\nu}))$. For an adlayer on the order of 10 to 30 Å in thickness, the thickness of the adsorbed polymer films, there exists only a node for $E_{s,r}$. This is true for the entire mid infrared region, since the thickness of the ultra thin

adsorbed polymer film is much less than 1/4 of the infrared wavelengths. This is shown schematically in Figure 44. No contribution to $A_s(\bar{\nu})$ occurs.

The final ratioed spectrum therefore exhibits only an intensity proportional to $[-A_p(\bar{\nu})]$. The phase shift at grazing conditions for $E_{p,r}$ upon reflection at the Au surface is about 90° .^{1,2} Absorption is due to transition dipoles with a component oriented parallel to the scattering plane (normal to the surface). For highly ordered structures the relative band intensities will be directly proportional to $\cos^2\phi_m z$. The transition dipole is m , z is the surface normal, and ϕ is the angle between the transverse magnetic wave orthogonal component normal to the surface and the transition dipole. At grazing incidence the transverse magnetic wave has essentially only a component normal to the film surface or in the z direction. Upon reflection only this component has any amplitude at the surface.

An additional factor must be considered in order to evaluate relative intensities within the $[-A_p(\bar{\nu})]$ spectrum for orientation of specific structural units within the adsorbed polymer layer. The modulator retardation, δ , only equals 0 or π at one wavenumber for a particular peak to peak retardation value. The effect of the polarization modulation efficiency, $J_2 \delta_0(\bar{\nu})$, must be included in order to compare relative intensities within a spectrum. For a peak to peak retardation of $\delta' = 3600 \text{ nm}$, only at one wavenumber, $\bar{\nu} = 2778$

cm⁻¹, will the polarization alternate between I_{s,r}($\bar{\nu}$) and I_{p,r}($\bar{\nu}$) with full efficiency. Since $\delta_0(\bar{\nu}) = \pi \bar{\nu} \delta'$, the maximum amplitude of the retardance can be determined for any other wavenumber, $\bar{\nu}$, for this specific retardation. Below are a few representative values for $\delta' = 3600$ nm.

$\delta_0 = (n/m)\pi$	$\bar{\nu}$	$\Delta(\bar{\nu}) = (\bar{\nu}\delta_0 = \pi - (\bar{\nu}\delta_0 = (n/m)\pi)$
1/2	1389	1389
5/6	2315	463
9/10	2500	278
15/16	2604	174
19/20	2639	138
34/35	2698	78

It is evident that with $\delta' = 3600$ nm, only bands within the CH stretching region have intensities proportional to an absorbance due to alternation between I_{s,r}($\bar{\nu}$) and I_{p,r}($\bar{\nu}$) with close to full efficiency. For polystyrene, the skeletal CH asymmetric stretching vibration at 2925 cm⁻¹ has a value of $\delta_0 = 0.949 \pi$. For the CH symmetric stretching vibration at 2851 cm⁻¹, $\delta_0 = 0.974 \pi$. Similarly, for the highest intensity aromatic CH stretching vibration at 3027 cm⁻¹, $\delta_0 = 0.918 \pi$. In the region of $\delta_0(\bar{\nu}) = \pi$, J₂ $\delta_0(\bar{\nu})$ is a flat function. It changes from 0.481 at $\delta_0 = 0.949 \pi$ to 0.486 at $\delta_0 = 0.918 \pi$. The modulator efficiency will thus only effect the relative intensities within the CH stretch region by about 1 %.

Relative intensity determinations between the CH stretching modes and others such as aromatic inplane CH

bending are necessary for a complete microstructural characterization. This can only be accomplished with differential polarization if the peak to peak retardation is set for each region specifically. In fact, the value of δ' must be set such that δ_0 is close to π where $J_2 \delta_0(\bar{v})$ has a flat dependence. In addition all amplifications of the phase sensitive detection must be constant.

References

1. Greenler, R. G. *J. Chem. Phys.*, **1966**, *44*, 1, 310-315.
2. Greenler, R. G. *J. Chem. Phys.*, **1969**, *50*, 5, 1963-1968.
3. Ohnisi, T.; Ishitani, A.; Ishida, H.; Yamamoto, N.; Tsubomura, H. *J. Phys. Chem.*, **1978**, *82*, 1989.
4. Hipps, K. W.; Crosby, G. A. *J. Phys. Chem.*, **1979**, *83*, 5, 555-562.
5. Nafie, L. A.; Diem, M. *Applied Spectroscopy*, **1979**, *33*, 130.
6. Golden, W. G.; Dunn, D. S.; Overend, J. *J. of Catalysis*, **1981**, *71*, 395-404.
7. Dowrey, A. E.; Marcott, C. *Applied Spectroscopy*, **1982**, *36*, 4, 414-416.
8. Waldman, D. A.; Kolb, B. U.; McCarthy, T. J.; Hsu S. L. *Proc. of A.C.S. Div. of Polym. Mat.*, **1988**, *59*, 326.
9. Griffiths, P. R.; deHaseth, J. A. *Chemical Analysis*, Vol. 83, **1986**, ed. Elving, P. J.; Winefordner, J. D.; Kolthoff, I. M., John Wiley & Sons, N.Y.
10. Ishitani, A.; Ishida, H.; Soeda, F.; Nagasawa, Y. *Anal. Chem.*, **1982**, *54*, 682-687.
11. Allara, D. L.; Swalen, J. D. *J. Phys. Chem.*, **1982**, *86*, 2700-2704.
12. Allara, D. L.; Nuzzo, R. G. *Langmuir*, **1985**, *1*, 45-52.
13. Allara, D. L.; Nuzzo, R. G. *Langmuir*, **1985**, *1*, 52-66.

14. Rabolt, J. F.; Burns, F. C.; Schlotter, N. E.; Swalen, J. D. *J. Chem Phys.*, **1983**, 78 , 2, 946-952.
15. Schlotter, N. E.; Rabolt, J. F. *Applied Spectroscopy*, **1985**, 39, 6, 994-996.
16. Rabolt, J. F.; Jurich M.; Swalen, J. D. *Applied Spectroscopy*, **1985**, 39, 2, 269-272.
17. Naselli, C.; Rabolt, J. F.; Swalen, J. D. *J. Chem. Phys.*, **1985**, 82, 4, 2136-2140.
18. Nuzzo, R. G.; Fusco, F. A.; Allara, D. L. *J. Am. Chem. Soc.*, **1987**, 109, 2358-2368.
19. Porter, M. D.; Bright, T. B.; Allara, D. L.; Chidsey, C. E. D. *J. Am. Chem. Soc.*, **1987**, 109, 3559-3568.
20. Golden, G, W. *Fourier Transform Infrared Spectroscopy*, Vol. 4, **1985**, Academic Press, Inc., Chapter 8.
21. Hecht, E.; Zajac, A. *Optics*, **1974**, Addison Wesley Pub. Co., Inc., Chapter 8.

CHAPTER 7

SPECTROSCOPIC ANALYSIS OF FUNCTIONALIZED POLYSTYRENE ADSORBED ON METAL SURFACES

Introduction

Block copolymers of poly(propylene sulfide) and atactic polystyrenes of various molar block ratios have been synthesized with low polydispersity. The adsorption kinetics and total adsorbance of these polymers onto metallic substrates are significantly affected by incorporation of the sulfur functional groups. Reflectance infrared spectroscopy, incorporating the double modulation technique, has increased the sensitivity limitations of infrared spectroscopy to the level where structural characterization of ultra thin polymer films can finally be realized. Angle resolved x-ray photoelectron spectroscopy provides the depth resolution capability to determine the existence of heterogeneous chemical composition in ultra thin adsorbed polymer films.

Results in this study establish that 1) The chain conformation on the surface differs from the bulk state, provided that the grafting density of polymer chains is sufficiently high, and 2) Heterogeneous chemical composition exists in the adsorbed copolymer films as a function of distance from the substrate surface. The local anisotropy measured for the chains in the adsorbed film has been

compared to the uniaxial orientation functions measured for a coextruded film. Chain orientation within the adsorbed ultra thin polymer films, can be determined relative to the normal of the metal substrate, from the reflection infrared spectroscopic data. The strength of interaction of the polymer subunits with the metal substrate, and the number of strongly interacting subunits, can alter such orientations and effect both the conformation and chemical composition of polymer chains near an impenetrable surface.

Previous spectroscopic studies of adsorbed polymers have been able to address the degree of surface coverage,¹⁻³ but orientation of specific functional groups, and configurational determinations of the adsorbed polymer chains have been hampered by the inherent instrument dynamic range necessitated. This is a consequence of the low degree of packing order as compared to that found in highly ordered polyfunctional organic monolayers prepared by Langmuir-Blodgett and self assembly techniques.⁴⁻¹⁵

In this study the low degree of packing order has been addressed by anionic synthesis of a model polymer system based upon functionalized polystyrene. The molecular weight and the strength of interaction with a metal substrate can thus both be varied in a controlled fashion.^{16,17} These highly monodisperse modified polystyrenes consist of thiol terminated chains of various molecular weights, and diblock copolymers of polystyrene and poly(propylene sulfide) with

compositions of varying molar block ratios but constant overall degree of polymerization (Table 9; Chapter 5). The molecular dimensions over which interactions with the metal surface potentially exist, can therefore be altered because of the sulphur containing structural units.^{14,15,18} This series of modified polystyrenes are readily soluble in common solvents, so they can be readily adsorbed from dilute solution onto metal substrates.

Factors such as polydispersity, molecular weight, quality of solvent, polymer concentration, and the strength of interaction with the substrate, have been shown in the past to affect polymer adsorption. A number of studies have characterized the kinetics and degree of adsorption of an adsorbed polymer layer in solution,^{1-3,19-33} as well as the thickness of the adsorbed layer^{19,24,28-33} from which chain dimensions and expansion factors have been determined. Ellipsometry studies have been particularly useful for such characterizations since adsorbance, adsorption kinetics, and thickness in solution can all be monitored simultaneously.

Generally the adsorption of polymers reaches a equilibrium plateau value which increases with molecular weight to a limiting value that is a function of the solvent power.^{2,19,22,24,26,29,31,32} The adsorbance, and molecular weight level at which it becomes independent of molecular weight, decreases in the order of increasing solvent power, while the thickness of the adsorbed layer increases with

solvent power. The extension of the adsorbed layer measured by ellipsometry is presumed to be an average thickness proportional to that obtained from the concentration profile of the adsorbed layer. Results show that it is linearly proportional to the square root of the molecular weight ($MW^{1/2}$) under θ conditions and to ($MW^{0.4}$) in good solvent, and that the portion of tails of the total segments in the adsorbed layer dominates this thickness.^{2,29,31,32}

The thickness values measured by ellipsometry, however, give no information regarding the specifics of the concentration profile in the adsorbed polymer layer. A recent study has demonstrated that for adsorbed PS chains ($MW > 4 \times 10^5$) the resulting plateau thickness of this adsorbed layer exceeds the diameter of the chain in free solution.³³ This indicates that the PS chains can adsorb onto metal substrates with some distortion from the chain configuration they would possess in free solution, even for the low interaction energy case.

The polymers selected for this study purposely have molecular weights in the range of 60 to 80 K. In this molecular weight regime the overall number of segments are low enough so that the specific S-Au interactions^{14,18} will dominate the energetics of the typical surface/segment binding energy contribution to the overall adsorption energy, ΔG_{ads} . Unfunctionalized polystyrene in this molecular weight range does not adsorb under good solvent conditions (from

THF) while the above polymers do.³⁴ These chemically modified polystyrenes therefore decrease the dependence of adsorbance and thickness on the thermodynamic quality of the solvent. Solvent/solvent, segment/segment, and solvent/segment interactions will not be a significant factor in ΔG_{ads} .

The expected result is that adsorption of these polystyrenes will be affected by their chemical composition, with the endcap case enabling the highest grafting density and the longest propylene sulfide block copolymer the lowest.^{26,27} Recent theories have considered the adsorption of copolymers in which one block is preferentially attracted to the substrate surface.³⁵⁻³⁹ The expectation of segregation in the chemical composition of the adsorbed layer, and thicknesses and bond orientations that depend upon interaction energies and grafting density, is evaluated in this study by adsorption of the polymers listed in Table 9. Furthermore, since the substrate surface is Au, factors that must be considered for adsorption of polystyrene onto metal-oxide surfaces, such as hydration effects^{40,41} on the potential polymer-surface interaction sites and adsorbed polymer structure, can be ignored.

X-ray photoelectron spectroscopy is used both to establish the existence of the adsorbed polymer interface and to measure the chemical composition of the adsorbed films as a function of distance from the substrate. Thickness of the adsorbed ultra thin polymer films are also determined.

Contact angle measurements are sensitive enough to indicate that the polymer monolayers constitute interfaces having low interfacial free energies. Reflection and transmission infrared spectroscopy is used to determine the existence of anisotropy within the film structure as a function of grafting density (PPS block length).

Experimental

Materials

Fisherbrand glass microscope slides (25 x 50 mm) were rinsed with acetone, distilled deionized water, and methanol, washed with H₂SO₄/H₂O₂, and dried with a stream of nitrogen and then vacuum. Gold wire (Alfa-0.5 mm) was 99.998% pure. Evaporated gold film substrates were prepared using a modified Balzers MED 010 vapor deposition apparatus. Gold was evaporated from resistively heated tungsten baskets at a base pressure of 1×10^{-6} mm. Film thickness was controlled to a minimum of 1800 Å (due to dispersion effects found in reflectivity calculations), by monitoring the deposition process with a quartz crystal thickness monitor. After deposition, the chamber was backfilled with prepurified nitrogen and the substrates were immediately placed in Schlenk tubes and transferred to the nitrogen purged external reflection assembly.

Methods

TEM studies indicate that the prepared gold films are polycrystalline with an average grain size on the order of 500 to 1000 Å. The films are homogeneous and uniformly and sharply reflective to the eye. The as prepared gold surfaces are contaminated by adsorbed impurities as evidenced by advancing contact angles, θ_A , of approximately 60° as compared to $\theta_A \sim 0-8^\circ$ reported for clean gold.^{42,43} It is expected that the sulfur of the propylene sulfide segments strongly coordinates to gold and therefore locally displaces the organic contaminants present on the gold surface so that chemisorption occurs. The thickness of the carbonaceous contaminant layer was determined by argon ion sputtering and XPS to be ~ 3 Å.

All solutions were prepared and reactions carried out using standard Schlenk procedures. Transfers were performed using cannula and syringe techniques. Gel permeation chromatography (GPC) was carried out using Polymer Laboratories PL gel columns (10^2 , 10^3 , 10^4 Å), a Rainin Rabbit-HP pump, a Knauer 98 refractive index indicator, an Apple IIe computer with IMI Chromatix GPC software, and toluene, or THF as the mobile phase. Molecular weights are reported relative to a polystyrene calibration. Gas chromatography (GC) was performed with a Hewlett Packard 5790A gas chromatograph, a Hewlett Packard 3390A recorder-integrator and a 1/8" x 6 ft Analabs AN600 column. UV-vis

spectra were recorded by using a Perkin Elmer Lambda 3A spectrophotometer. Dynamic contact angles were measured utilizing a Ramé-Hart telescopic goniometer with water as the probe fluid. Advancing (θ_A) and receding (θ_R) angles were measured as water was added and removed, respectively, by using a Gilmont syringe. The values reported are averages of five measurements made on different positions of the adsorbed film. X-ray photoelectron spectra (XPS) were obtained with a Perkin Elmer-Physical Electronics 5100 with Mg K α excitation (300 W, 15 KeV). Spectra were typically recorded with 4 takeoff angles, with this angle being defined as that between the film surface and the analyzer. Atomic ratios were determined using Physical Electronics software and programmed sensitivity factors, for multiplexed spectra obtained with a pass energy of 35.75eV. Transmission infrared measurements, of extruded films and KBr pellets of adsorbate polymers, were obtained on a Bruker IFS 113v FTIR spectrometer, with a MCT detector, at a resolution of 2 cm $^{-1}$, and 256 scans.

Thiol-Terminated Polystyrene (PS_x-SH)

Preparation and characterization as reported in Chapter 5 of thesis.

Styrene-Propylene Sulfide Block Copolymers (PS_A-PPS_B)

Preparation and characterization as reported in Chapter 5 of thesis.

Adsorption of Polymers

Adsorption studies were carried out to steady state conditions on glass supported Au surfaces, as determined by a previous LSC study on similar polymers.³⁴ Standard Schlenk procedures were used in order to maintain as clean conditions as possible during adsorptions. Typical concentrations ranged from 0.5 to 2 mg/mL, in distilled solvents such as THF and cyclohexane. Solution temperatures for adsorption were ambient for THF, and for cyclohexane either 45 °C or the θ temperature for polystyrene (35 °C). After steady state conditions were achieved the solution was removed via cannulation, and fresh solvent was similarly introduced. The fresh solvent was allowed to bathe the substrate for about 10 minutes, at or above the adsorption temperature. The solvent was then removed and examined with UV spectroscopy for the presence of polystyrene. In this way it could be determined whether any physisorbed polymer was present on the Au substrate. It was expected that the physisorbed species would re-enter the solvent phase, while the polymers chemisorbed via their reactive endgroup or block would remain bonded to the Au substrate.^{14,34} UV-vis results indicated that after two such washing procedures, less than 1% of the polystyrene concentration existed relative to that in the initially removed adsorbate solution. A control was run with unfunctionalized polystyrene, under identical adsorption conditions. The slides were dried under a stream of purified

nitrogen and under vacuum until a base pressure of 25 mTorr was attained.

Coextruded Films

Solid state coextruded films with uniaxial orientation were prepared from cast films. Toluene solutions of 2% concentration were used resulting in 10 μm initial thickness. Sections of these films, 0.6 cm^2 , were coextruded with split high density polyethylene billets at temperatures slightly below the T_g of polystyrene, at a rate of 1 or 2 mm/min.

Polarization Modulation External Reflection

Spectroscopy (PMGRS)⁴⁴

External reflectance infrared spectra were obtained with polarization modulation, by incorporation of the necessary optical and electronic components as reported in Chapter 6 of thesis. The DC reflection signal was collected in the normal fashion. All files were transferred to an IBM 9000 computer, where subsequent analysis was performed with software developed in this laboratory.

Results And Discussion

A necessary condition for adsorption of polymers to a surface, is that the cumulative magnitude of the binding energy (surface-segment interactions) must be sufficient to overcome the resulting enthalpic barriers (due to loss of solvent/surface and polymer/solvent interactions), and the

entropic barriers caused by the decrease in translational and conformational entropy (0.5 and 1.0 kT respectively)⁴⁵ accompanying adsorption of polymer segments. For sulfur functionalized polystyrenes, the magnitude of the specific interactions, between available surface sites and the incorporated functional groups, has been increased substantially over the typical nonbonded and/or weak hydrogen bonding surface/segment interaction energies. Studies on small molecule thiols and sulfides have estimated that the binding energies due to coordination of sulfur to 3 Au atoms is on the order of 15 to 30 kcal/mole,¹⁴ or about 15 to 50 times greater than the above surface/segment energies.

The functionalized anionically synthesized polystyrenes studied here, are either polystyrene endcapped with a thiol, or polystyrenes copolymerized with propylene sulfide such that different length propylene sulfide blocks are incorporated.

Adsorption of these modified polystyrenes has been effected from θ and good solution conditions, for which the concentration was of the order of 1mg/ml, and the solvent/surface interactions were weak. This concentration is in the plateau region reported for polystyrene of similar and higher molecular weights adsorbed onto metal-oxide surfaces.^{2,31-33} It is considerably below the overlap concentration (C^*), where $C^* = M/(4/3)\pi\langle S^2 \rangle^{3/2}N_A = 56$ mg/ml for $M = 80K$, and $\langle S^2 \rangle^{1/2} = 8.26$ nm in cyclohexane at 35°C.

The polymer concentration in this study is, however, sufficiently high so that the adsorbed polymers are expected to contain buoy and anchor features.⁴⁶ These consist of a population of tails and trains respectively, as shown schematically in Figure 51. Such structures will occur as a result of the specific interactions mentioned above, reinforced by the effect of the concentration. This will cause interfacial exchange to occur between sequences of polystyrene segments initially adsorbed in flattened conformations, and functionalized polymer segments still in solution.^{29,31,33,47,48-50} As the propylene-sulfide block is shortened until only the thiol endcap terminally attached case exists, the anchors will increase in number but decrease in length. This results in a greater packing density and eventually the high grafting density brush model.^{37,39,46,51} In such cases the single chain self avoidance is larger than the distance between grafted chains. The chains emerging from the surface are more likely to encounter each other, thereby causing repulsion and extended configurations as depicted in Figure 51.

Characterization With XPS And Contact Angle

Evidence that adsorption of these functionalized polystyrenes occurred was determined by 1) dynamic contact angle measurements at the air/water interface, and 2) the presence of the S_{2p} photoemission, and a $\pi \rightarrow \pi^*$ shake up component in the photoemission from the C_{1s} core level

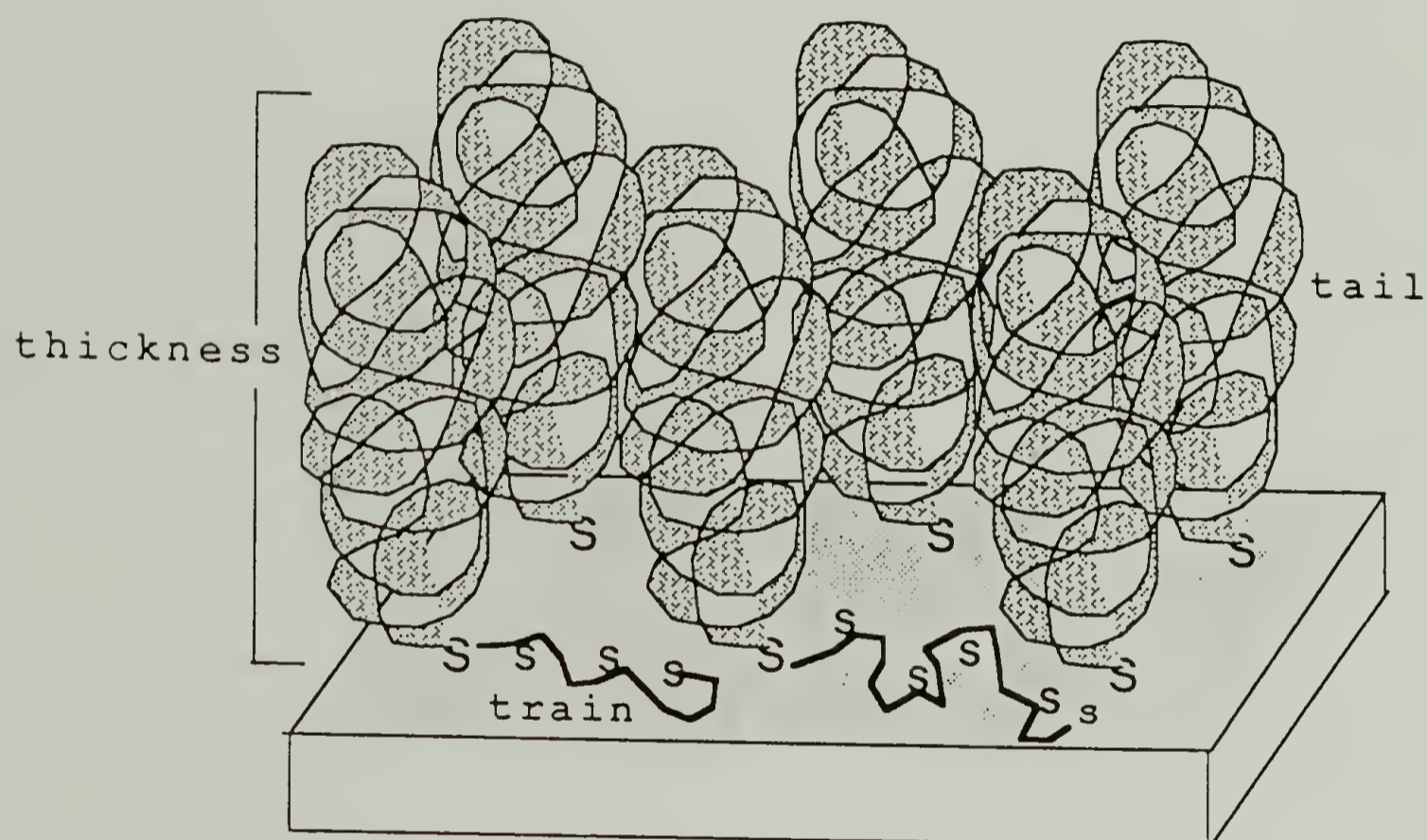
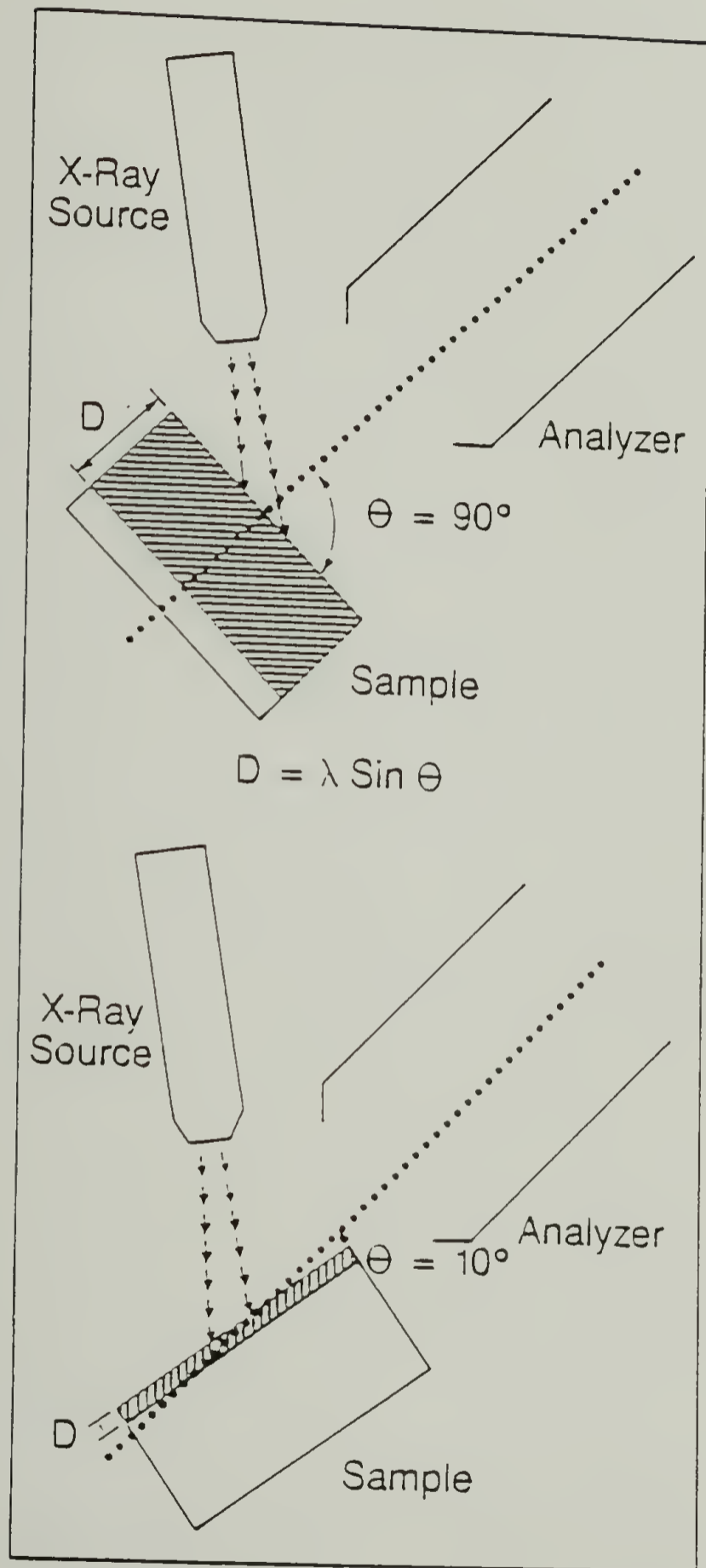


FIG. 51 Schematic for the structure of copolymers with a strongly interacting block, after adsorption to a metal substrate. Adsorbed structure contains buoy and anchor features represented by weakly interacting tails and strongly interacting trains, respectively.

measured by x-ray photoelectron spectroscopy (XPS). Compositional information within the adsorbed film was determined by XPS utilizing angle resolved atomic ratios. A change in the takeoff angle relative to the detector corresponds to sampling ejected electrons from a different effective depth, as shown in Figure 52. Thus the chemical composition can be found as a function of distance from the film surface.

Film thickness was determined by the extent of attenuation of the absolute intensity of the Au_{4f} core level before (I_0) and after (I_s) adsorption. The XPS intensity for photoemission from a particular core level for a bulk Au surface, as determined from the peak area, is directly proportional to $K\lambda\sin\theta$. The constant K includes instrumentation contributions, density of atoms, photoelastic cross section in a given shell, and area of exposed surface, and λ denotes the electron mean free path. The mean free path of ejected electrons is short (on the order of tens of Å). It is strongly dependent upon kinetic energy, so sampling depths for photoemitted electrons from different elements will differ. The value of the mean free path is taken as the distance of travel for ejected electrons through a material such that 0.67 of the bulk intensity is detected. Attenuation of the signal from the substrate core level (Au_{4f}), due to an adsorbed overlayer of a certain thickness d , will be proportional to $e^{-d/\lambda\sin\theta}$ where θ is the takeoff

FIG. 52 Schematic depicting the change in the effective XPS sampling depth, $D = \lambda \sin\theta$, due to rotation of the sample stage so that the takeoff angle, θ , relative to the detector (analyzer) corresponds to 90° (top), and 10° (bottom). In order to sample 95 % of the ejected electrons, the sampling depth is actually $3(\lambda \sin\theta)$ or 66 Å and 11 Å respectively, for photoemission from the Au_{4f} orbital for a gold substrate.



angle. The decreasing exponential relations as a function of takeoff angle and overlayer thickness, for a mean free path value of 22\AA for Au_{4f} photoelectrons of KE 1170 eV ejected through an adsorbed polymer layer,⁵² are shown in Figure 53. A tabulation of the attenuation in intensity as a function of takeoff angle and overlayer thickness is given in Table 10. The experimental Au_{4f} absolute intensities were reproducible within 3 % for each of the different takeoff angles used.

XPS survey spectra, with 75° and 15° takeoff angles respectively, of a freshly deposited 1500\AA Au surface, are shown in Figure 54. Atomic compositions of this surface for Au_{4f} , C_{1s} and O_{1s} core levels, were 56:42:2 and 38:58:4 for 75° and 15° respectively. These C/Au ratios (0.75 at 75° , 1.53 at 15°) represent typical values for vapor deposited Au surfaces, due to the presence of adventitious ambient hydrocarbons which are readily adsorbed to the Au surface. Evidence of the core levels Au 5p, 4f, 5s, 4d, 4p and C_{1s} is exhibited in the above spectra, while the O_{1s} at about 530eV is resolved only in the 15° spectrum. The XPS thickness of this contaminant layer was determined by first ablating the surface via argon ion sputtering to obtain I_0 , and then subsequently exposing it in the anti chamber until the typical C/Au ratio was reached. From the ratio of the new Au_{4f} intensity (I_s) to I_0 for different takeoff angles an average value of 3\AA was determined.

FIG. 53 Plot of substrate intensity attenuation for XPS photoemission signal, I^S , showing calculated decreasing exponential relations as a function of takeoff angle, θ , and overlayer thickness, Z , for a mean free path value, λ_s , of 22 Å for Au_{4f} photoelectrons of KE 1170 eV ejected through an adsorbed polymer layer.

$$I^s = k_s \lambda_s \sin \theta e^{-\frac{z}{\lambda_s \sin \theta}}$$

SUBSTRATE INTENSITY ATTENUATION

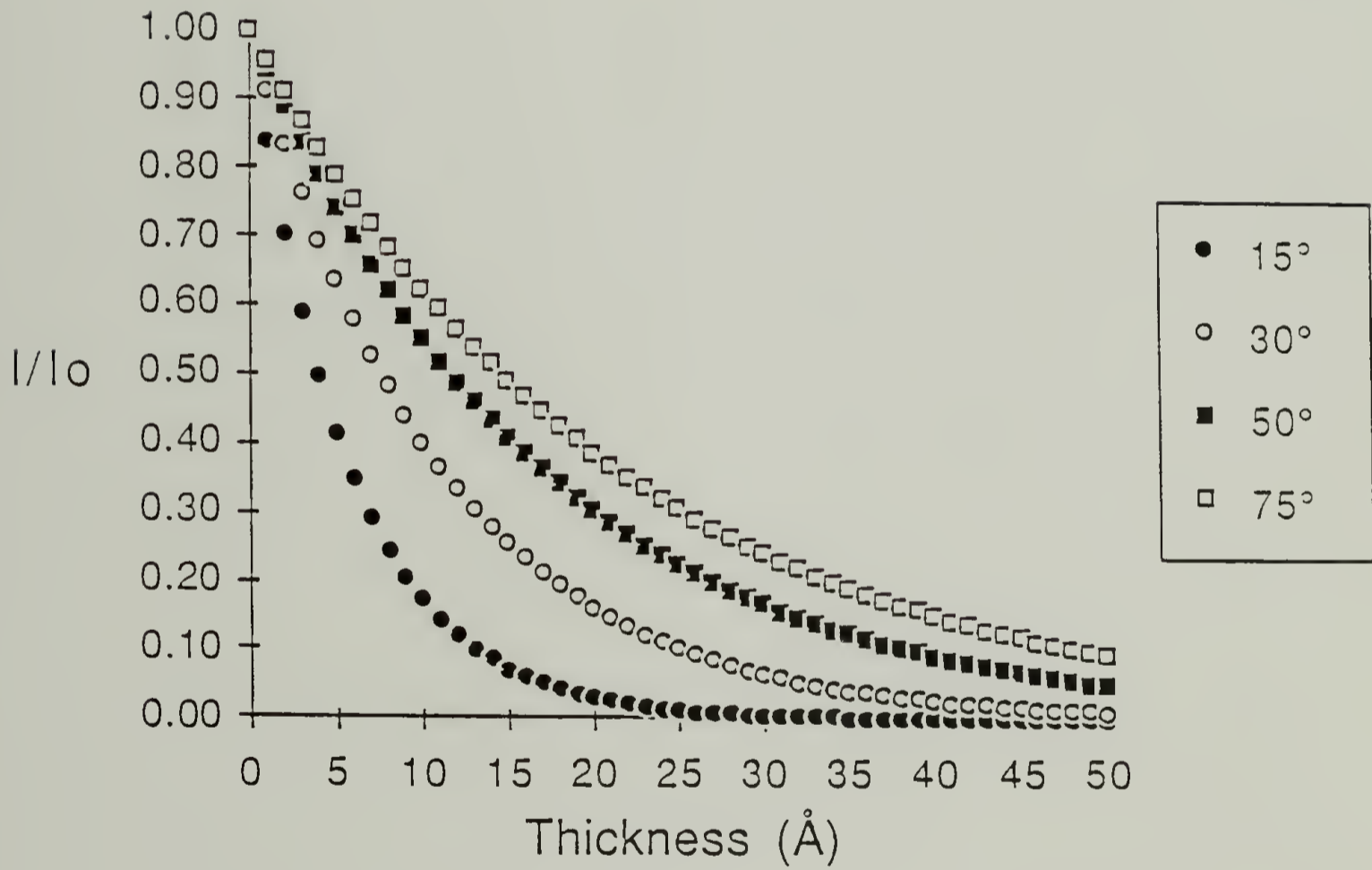


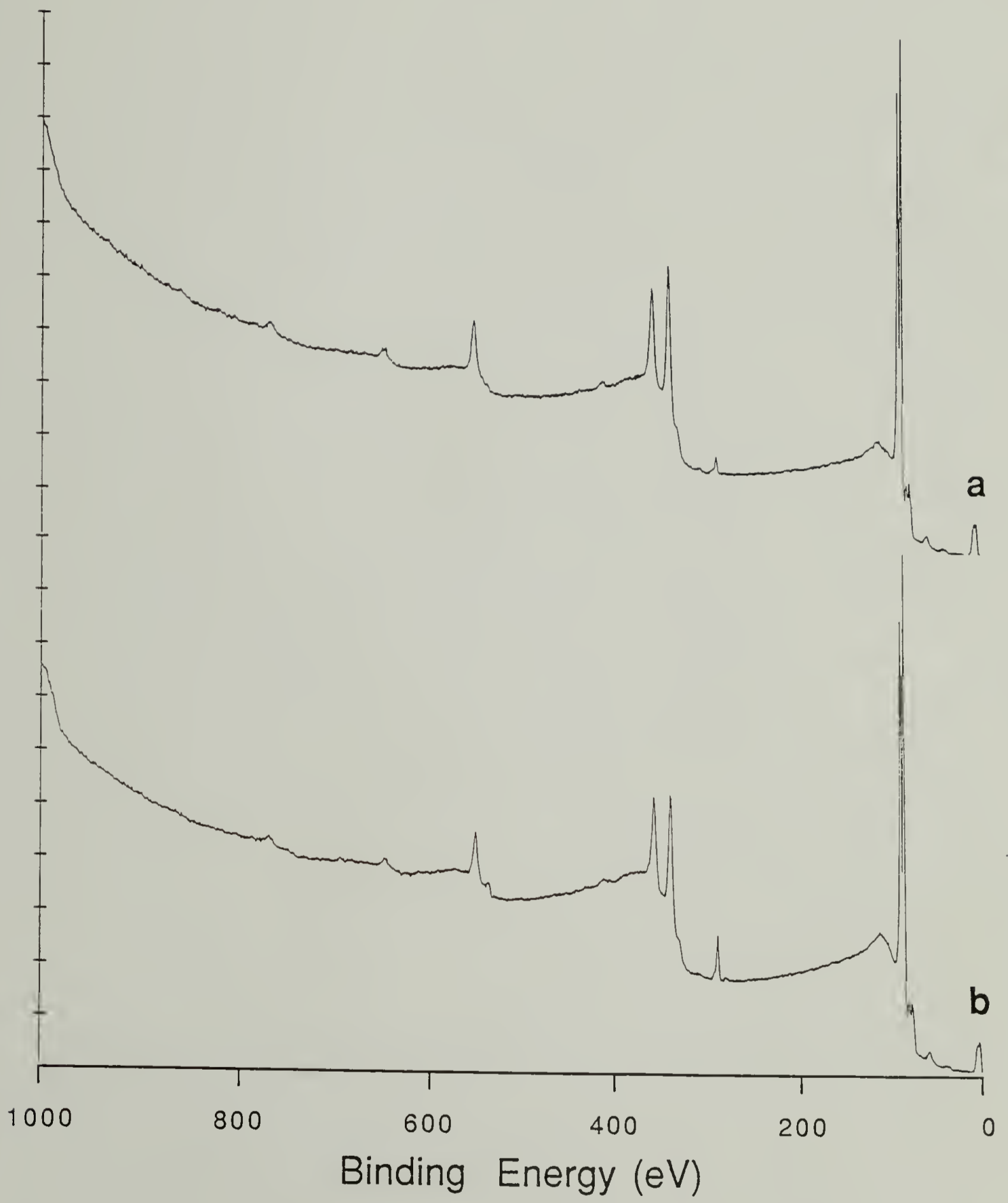
TABLE 10. Table showing calculated attenuation in the XPS photoemission signal, I^S , as a function of takeoff angles, $\theta = 15, 30, 50, \text{ and } 75^\circ$, for overlayer thicknesses of $z = 1.0$ to 50 \AA , for a substrate mean free path, λ_s , of 22 \AA .

TABLE 10

Attenuation of XPS Intensity For Au_{4f} Level as a Function of
Overlayer Thickness

Thickness (Å)	15°	30°	50°	75°
0.0	1.000000	1.000000	1.000000	1.000000
1.0	.838923	.913101	.942386	.954031
2.0	.703793	.833753	.888092	.910175
3.0	.590428	.761300	.836925	.868335
4.0	.495324	.695144	.788707	.828418
5.0	.415539	.634736	.743266	.790337
6.0	.348605	.579578	.700444	.754005
7.0	.292453	.529213	.660089	.719345
8.0	.245346	.483225	.622057	.686277
9.0	.205826	.441233	.586219	.654729
10.0	.172673	.402890	.552445	.624632
11.0	.144859	.367879	.520617	.595918
12.0	.121526	.335911	.490622	.568524
13.0	.101951	.306721	.462355	.542390
14.0	.085529	.280067	.435717	.517457
15.0	.071752	.255729	.410614	.493669
16.0	.060195	.233506	.386957	.470976
17.0	.050499	.213215	.364663	.449326
18.0	.042365	.194687	.343653	.428670
19.0	.035541	.177769	.323854	.408965
20.0	.029816	.162321	.305195	.390165
21.0	.025013	.148215	.287612	.372230
22.0	.020984	.135335	.271042	.355118
23.0	.017604	.123575	.255426	.338794
24.0	.014768	.112836	.240710	.323220
25.0	.012390	.103031	.226842	.308362
26.0	.010394	.094078	.213772	.294187
27.0	.008720	.085902	.201456	.280663
28.0	.007315	.078437	.189849	.267761
29.0	.006137	.071621	.178911	.255453
30.0	.005148	.065397	.168604	.243710
31.0	.004319	.059714	.158890	.232506
32.0	.003623	.054525	.149736	.221818
33.0	.003040	.049787	.141109	.211622
34.0	.002550	.045461	.132979	.201893
35.0	.002139	.041510	.125317	.192613
36.0	.001795	.037903	.118097	.183758
37.0	.001506	.034609	.111293	.175311
38.0	.001263	.031602	.104881	.167252
39.0	.001060	.028856	.098839	.159564
40.0	.000889	.026348	.093144	.152229
41.0	.000746	.024058	.087778	.145231
42.0	.000626	.021968	.082721	.138555
43.0	.000525	.020059	.077955	.132186
44.0	.000440	.018316	.073464	.126109
45.0	.000369	.016724	.069231	.120312
46.0	.000310	.015271	.065242	.114781
47.0	.000260	.013944	.061483	.109505
48.0	.000218	.012732	.057941	.104471
49.0	.000183	.011626	.054603	.099669
50.0	.000154	.010615	.051457	.095087

FIG. 54 XPS survey spectra, at 75° (a) and 15° (b) takeoff angles, of a freshly vapor deposited 1500 \AA Au surface on a glass microscope slide, for Mg $K\alpha$ excitation (300 W, 15 KeV). The C_{1s} core level is due to adventitious adsorption of a 3 \AA hydrocarbon contaminant layer on the Au surface.



XPS survey spectra for PS₇₅-PPS₂₅ adsorbed to Au from 1mg/ml cyclohexane solution at 35.5°, are shown in Figures 55(a) and 55(b) for 75° and 15° respectively. The decrease in Au core level intensities and the increase in C_{1s} intensity as compared to the corresponding spectra in Figure 54, indicates that an adsorbed overlayer exists. Multiplex spectra for the C_{1s} region, at a resolution of 0.5 eV, are plotted in Figure 56(a) and 56(b) for 75° and 15° respectively. The $\pi \rightarrow \pi^*$ component, expected at a binding energy 6.6 eV higher due to the polystyrene block, is evident in the 15° spectrum, while at 75° its intensity is diminished relative to that of the C_{1s} core level. From these results it can be surmised that the propylene sulfide block (DP=181) in the adsorbed copolymer is residing at or near the Au/polymer interface, while the polystyrene domains are excluded to regions nearer the air/film interface. In such a case, the CH, CH₂, and CH₃ groups in the propylene sulfide block would effectively dilute the overall C_{1s} signal at 75°, thereby decreasing the polystyrene contribution and the $\pi \rightarrow \pi^*$ shake up relative intensity, as observed.

This is further supported by both increases in the sulfur composition (Figure 57) and decreasing values for the C/S atomic composition ratios (Figure 58), as takeoff angle is increased which increases the effective escape depth. C/S ratios of 25.1, 19.5, 16.9 and 16.8 were determined from spectra at takeoff angles of 15°, 30°, 50°, and 75°

FIG. 55 XPS survey spectra for PS₇₅-PPS₂₅ adsorbed to Au from 1mg/ml cyclohexane solution at 35.5 °C, for 75°, (a), and 15°, (b), takeoff angles, and for similarly adsorbed PS₉₀-PPS₁₀ for 75°, (c), and 15°, (d), takeoff angles respectively. Surfaces were washed with cyclohexane at 45 °C to remove physisorbed species. Anode is Mg K α excitation (300 W, 15 KeV).

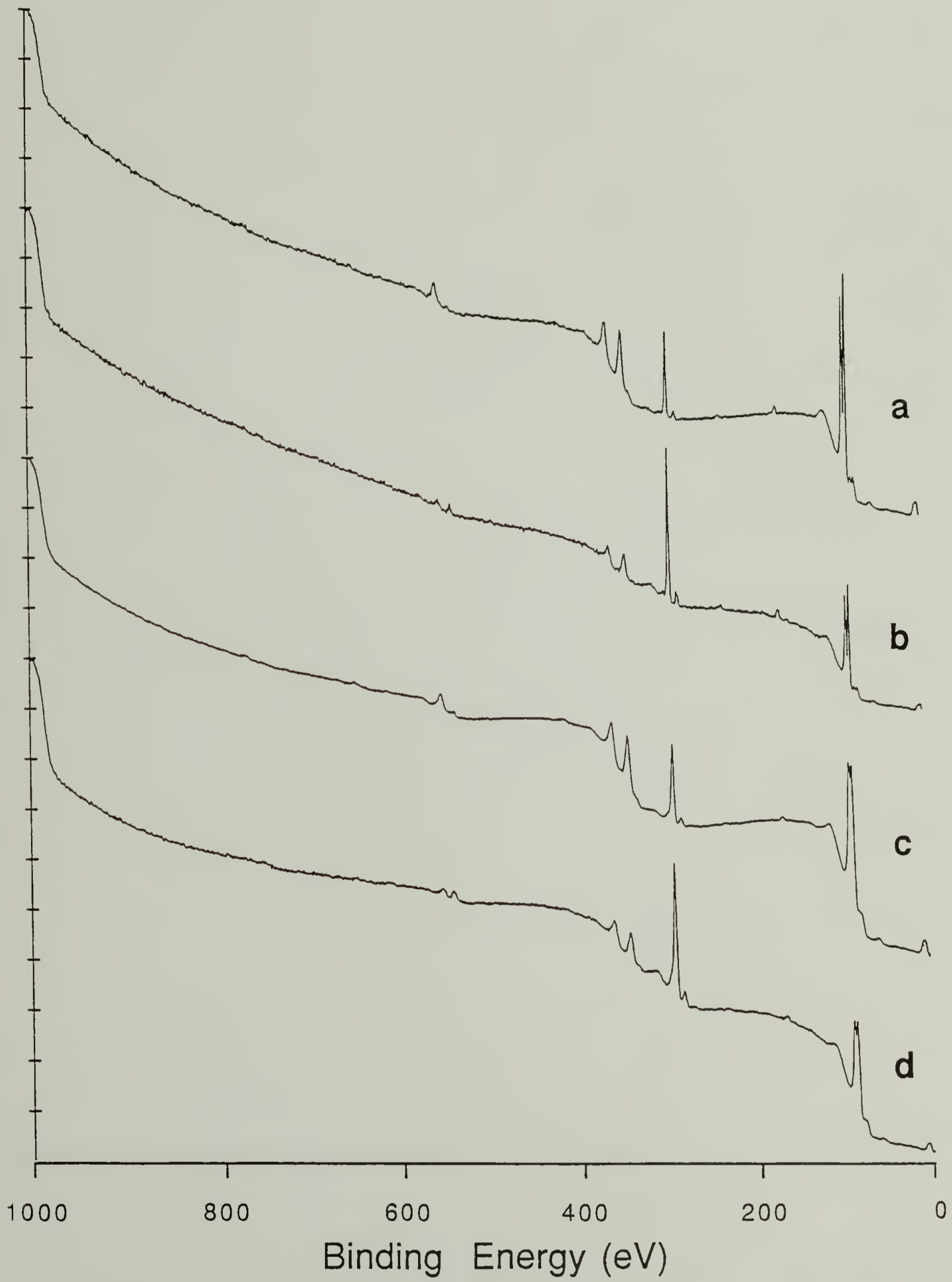


FIG. 56 XPS multiplex spectra for the C_{1s} region, at a resolution of 0.5 eV, for PS₇₅-PPS₂₅ adsorbed to Au from 1mg/ml cyclohexane solution at 35.5 °C, for 75°, (a), and 15°, (b), takeoff angles, and for similarly adsorbed PS₉₀-PPS₁₀ for 75°, (c), and 15°, (d), takeoff angles respectively. Surfaces were washed with cyclohexane at 45 °C to remove physisorbed species. Anode is Mg K α excitation (300 W, 15 KeV).

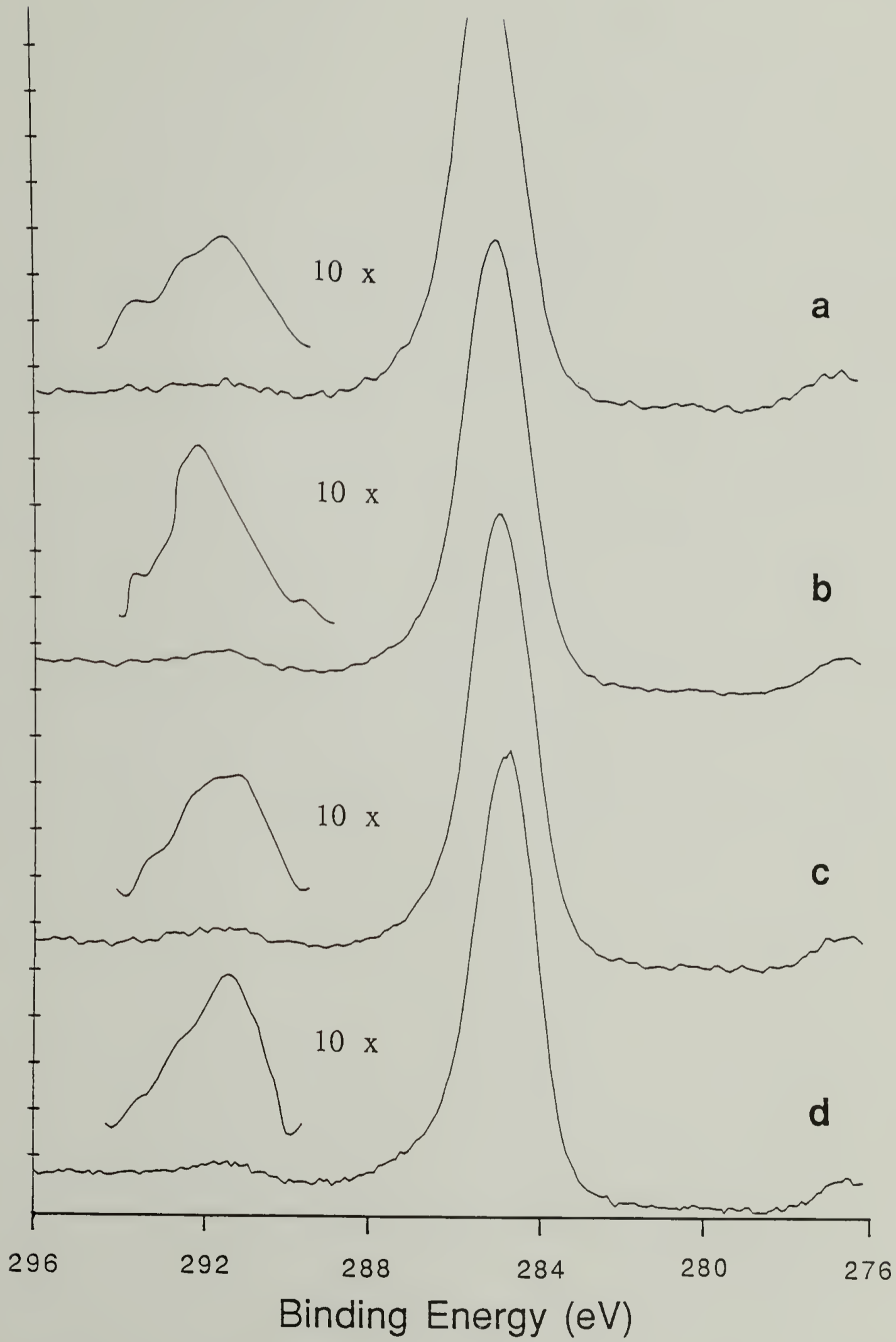
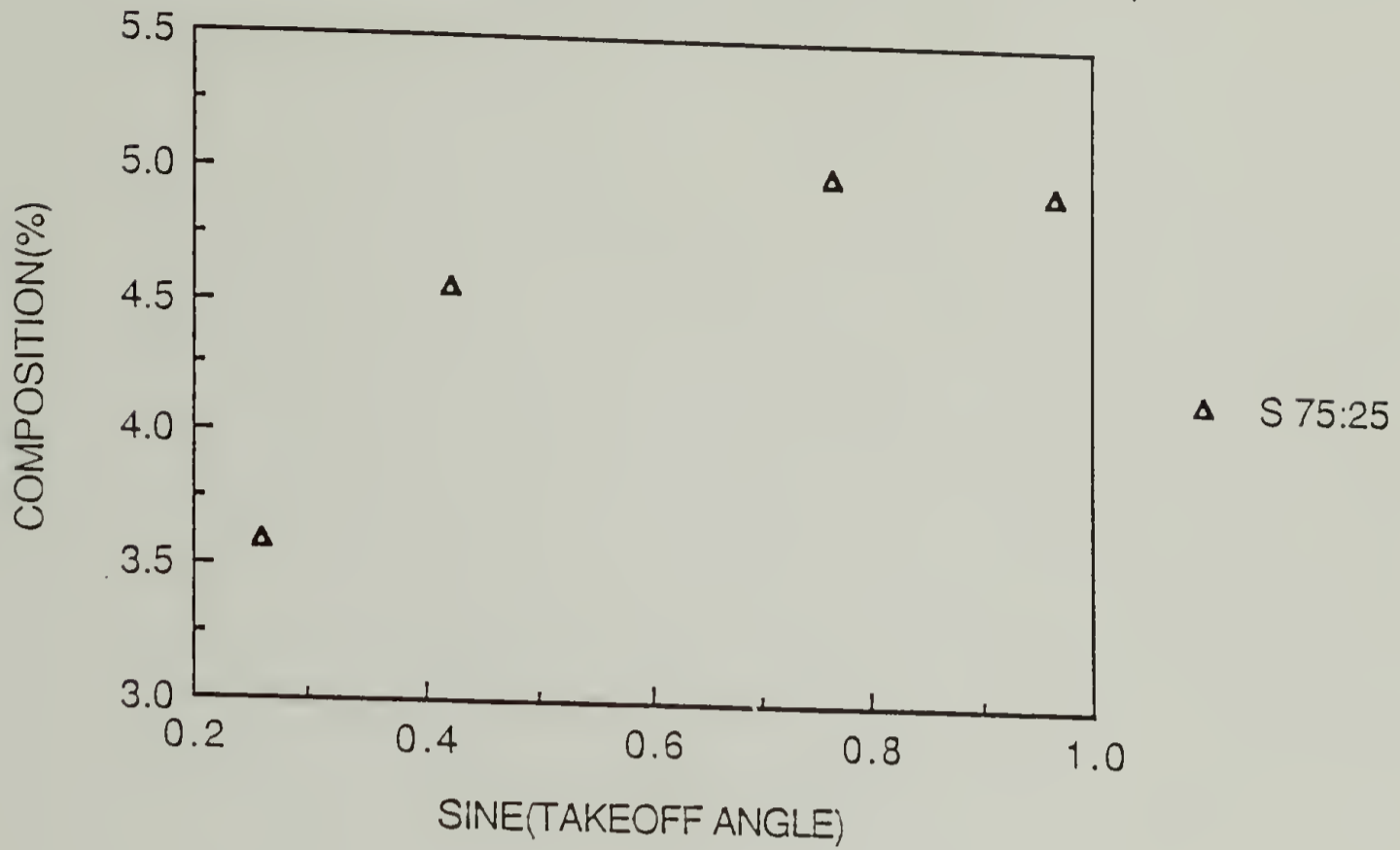


FIG. 57 Sulfur composition as a function of the sine of the takeoff angle, from XPS multiplex spectra for the S_{2p} core level at a resolution of 0.5 eV, for copolymers PS₇₅-PPS₂₅, (top), and PS₉₀-PPS₁₀, (bottom), adsorbed to Au. Anode is Mg K α excitation (300 W, 15 KeV).

SULFUR COMPOSITION IN PS/PPS (75:25)



SULFUR COMPOSITION IN PS/PPS (90:10)

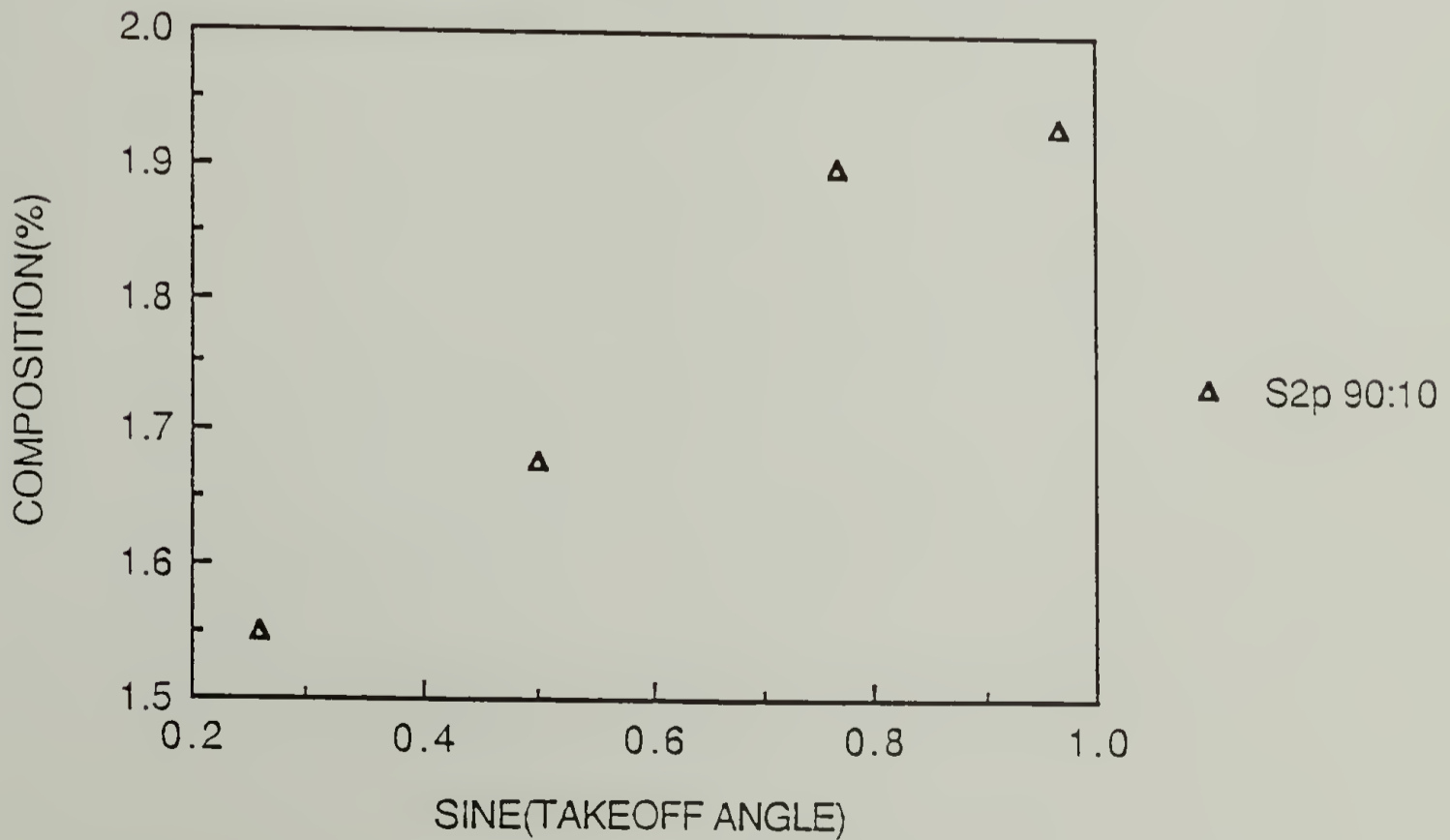
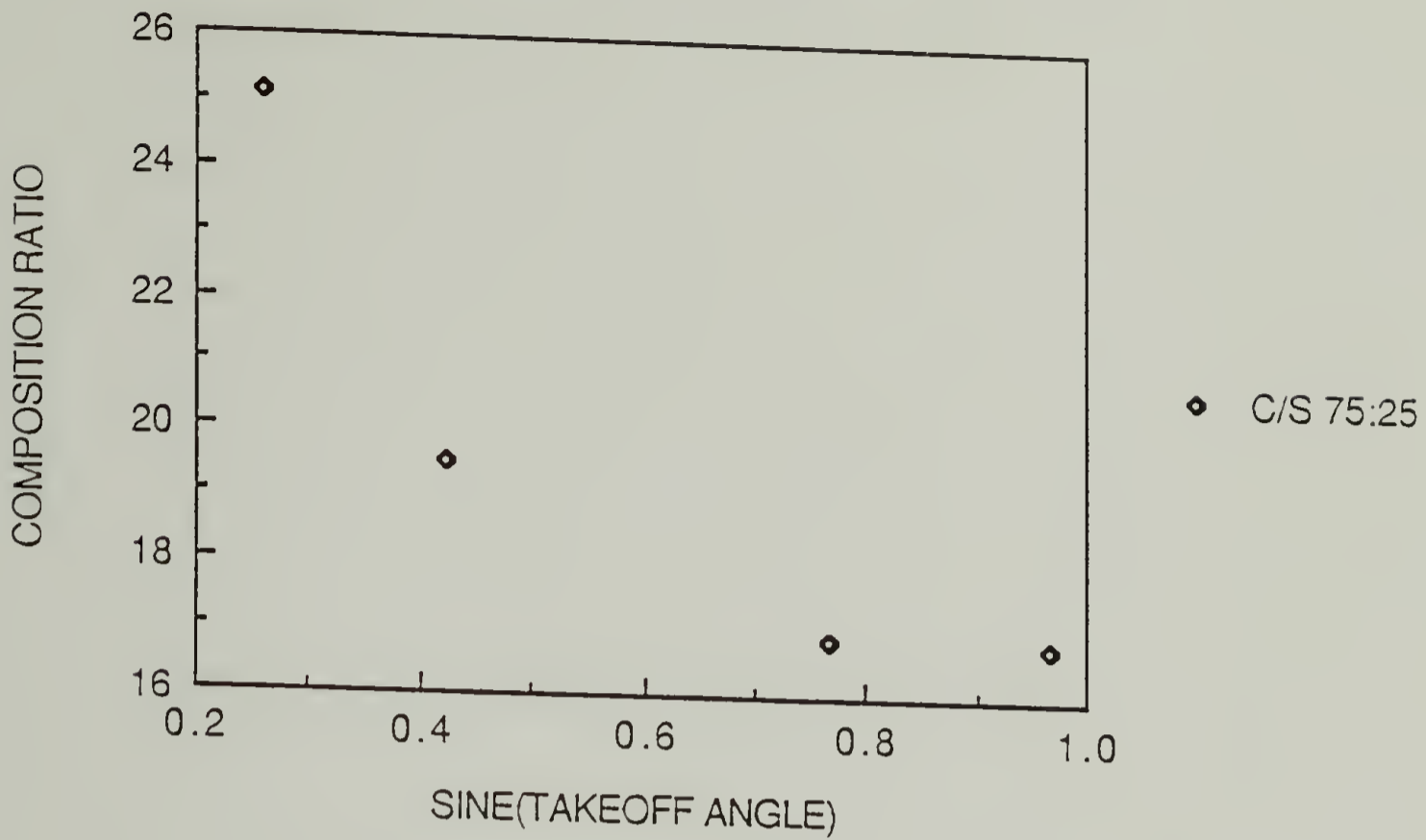
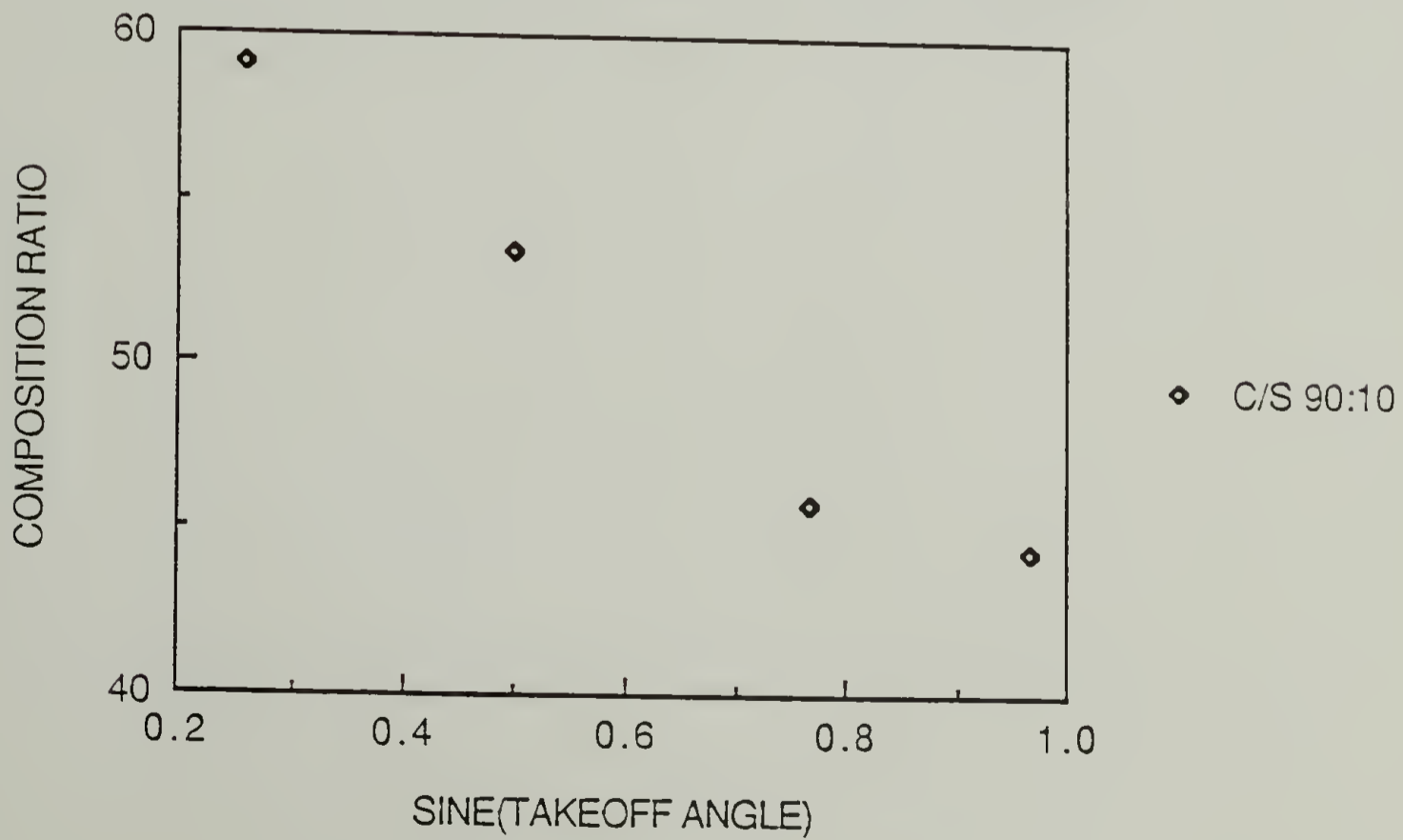


FIG. 58 C/S atomic composition ratios as a function of the sine of the takeoff angle, from XPS multiplex spectra for the C_{1s} , and S_{2p} core levels, at a resolution of 0.5 eV, for copolymers PS₇₅-PPS₂₅, (top), and PS₉₀-PPS₁₀, (bottom), adsorbed to Au. Anode is Mg K α excitation (300 W, 15 KeV).

C/S RATIO IN PS/PPS(75:25) COPOLYMER



C/S RATIO IN PS/PPS(90:10) COPOLYMER

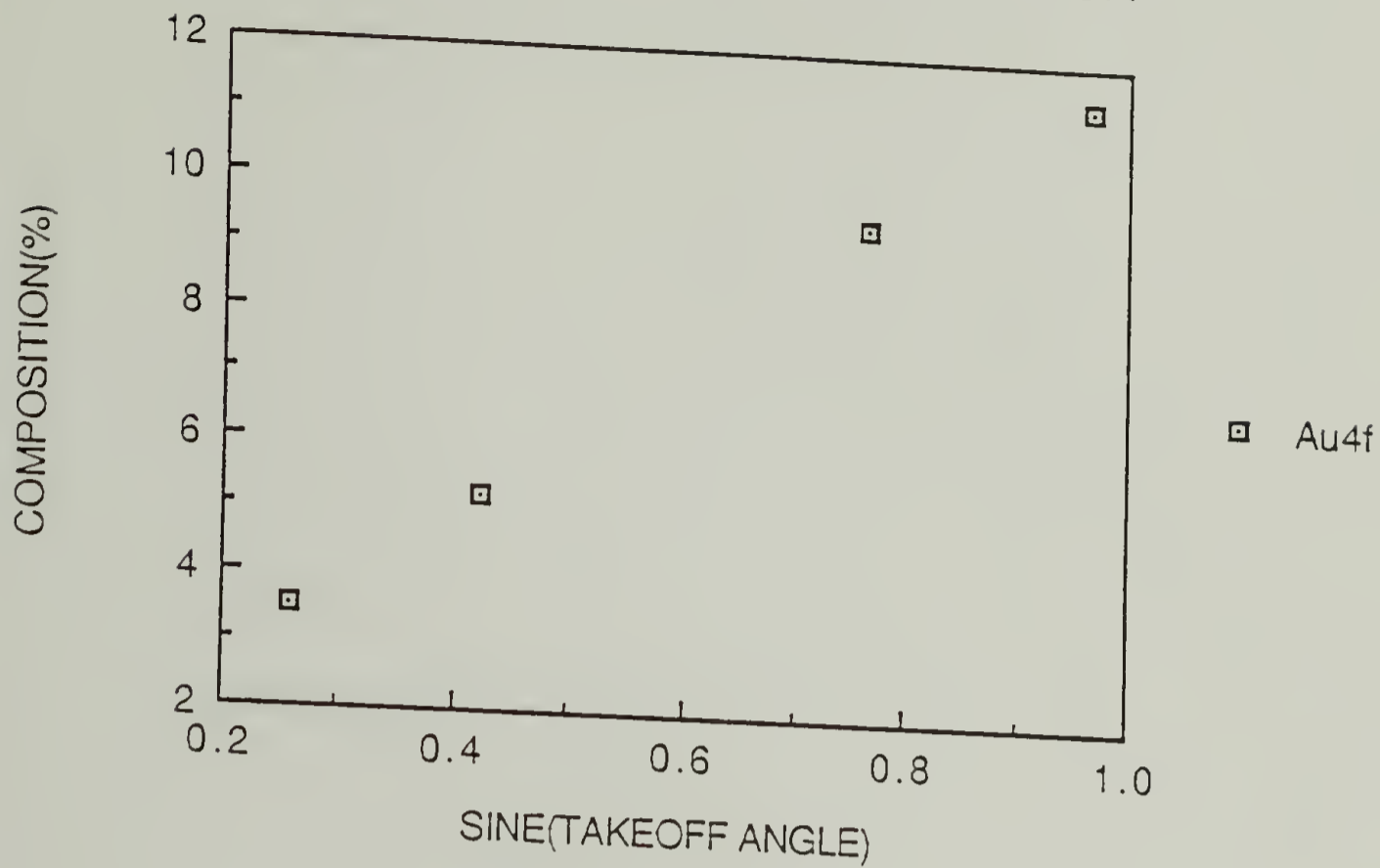


respectively. Depth profiles of the C_{1s} and Au_{4f} compositions (Figure 59) are linear but opposite in behavior, which suggests that the carbon content of the adsorbed film is uniform throughout the film thickness, which itself is uniform. Thus the plateau in the C/S ratio at 50° indicates that the propylene sulfide block must occupy both trains at the Au interface and loops near it. Dynamic contact angle measurements, averaged over multiple readings at 8 locations, changed from $\theta_A/\theta_R = 65^\circ/15^\circ$ for the Au surface to $86^\circ/58^\circ$ for the adsorbed film. This indicates that the polymer surface resembles polystyrene at close proximity to the air/film interface, in agreement with the element compositional results from XPS.

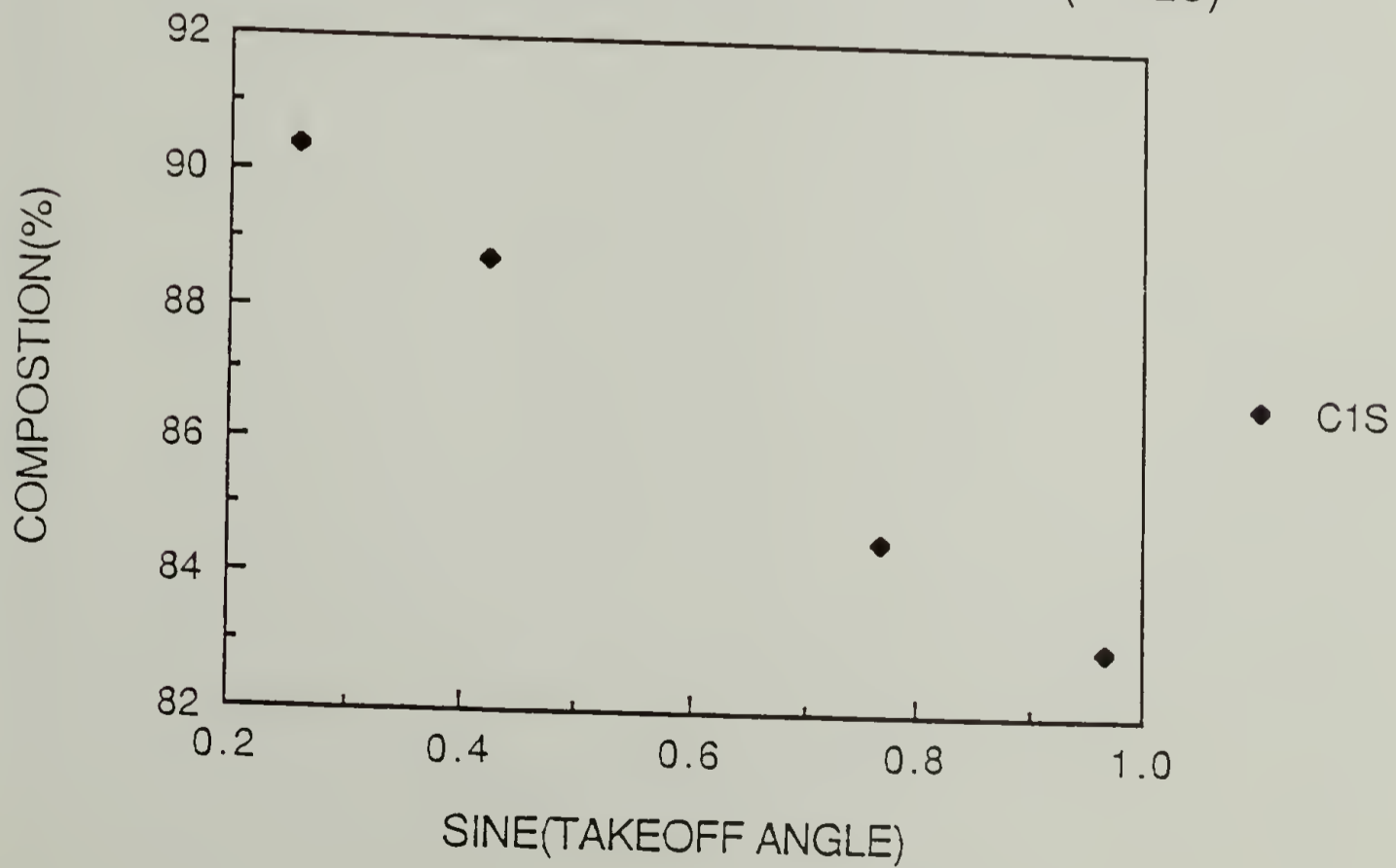
Adsorption of PS_{90} - PPS_{10} was carried out similarly to that above. Dynamic contact angle measurements, averaged over 8 locations on the surface, again demonstrated that adsorption had proceeded, with a value of $\theta_A/\theta_R = 84^\circ/63^\circ$. XPS survey spectra substantiating the existence of the adsorbed overlayer are shown in Figures 55(c) and 55(d) for 75° and 15° takeoff angles. The $\pi \rightarrow \pi^*$ shake up component in the C_{1s} region is plotted in Figure 56(c) and 56(d) for 75° and 15° respectively. The decrease in the relative intensity of the $\pi \rightarrow \pi^*$ shake up component at 75° , and the larger increase in the C/S atomic ratio (Figure 58) from 44.4 at 75° to 59.1 at 15° , indicates that the compositional structure of this adsorbed copolymer is more segregated than for PS_{75} -

FIG. 59 Atomic composition for carbon and gold, as a function of the sine of the takeoff angle, from XPS multiplex spectra for the C_{1s} , and Au_{4f} core levels, at a resolution of 0.5 eV, for copolymers PS₇₅-PPS₂₅, (top), and PS₉₀-PPS₁₀, (bottom), adsorbed to Au. Anode is Mg $K\alpha$ excitation (300 W, 15 KeV).

GOLD FRACTION IN XPS COMPOSITION



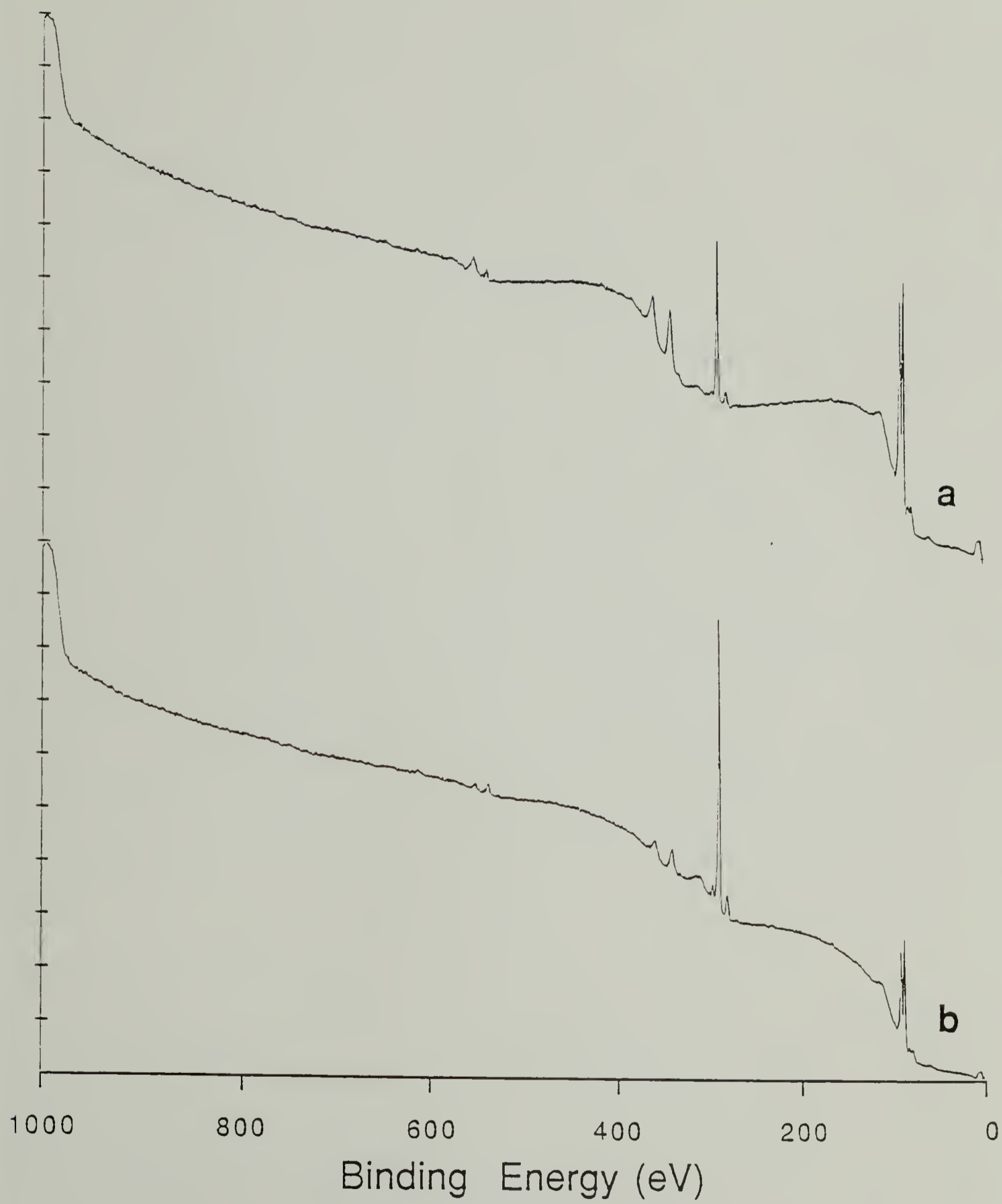
CARBON COMPOSITION IN PS/PPS (75:25)



PPS₂₅. The theoretical value for the ratio of the C/S ratio of PS₉₀-PPS₁₀ to that for PS₇₅-PPS₂₅ is 2.78. This compares favorably with the experimental result of 2.64 at 75°, for which the depth is sampled close to normal ($\sin 75^\circ = 0.97$) to the film surface. The intensity decrease in the $\pi \rightarrow \pi^*$ shake up component is less than for the PS₇₅-PPS₂₅ case, as is expected for a smaller PPS block. Depth profiles of the C_{1s} and Au_{4f} compositions are linear but opposite in behavior, as was shown for PS₇₅-PPS₂₅. From the larger C/S value at 15°, and the monotonic increase of the sulfur composition in a depth profile until 60° (Figure 57), it can be concluded that the PPS block is located at or near the Au/polymer interface, while the polystyrene domains are located between the PPS blocks and the air/polymer interface.

XPS survey spectra, at takeoff angles of 75° and 15°, of PS₉₅-PPS₅ adsorbed to Au as above are shown in Figure 60. The large attenuation of the Au_{4f} level indicates a thicker adsorbed film than for PS₇₅-PPS₂₅ or PS₉₀-PPS₁₀. The C/Au ratios are 33.6/15° and 9.31/75°, 19.0/15° and 7.5/75°, and 25.9/15° and 7.3/75°, for PS₉₅-PPS₅, PS₉₀-PPS₁₀ and PS₇₅-PPS₂₅ respectively. It is expected that the C/Au compositional ratios would increase as a function of film thickness, and that the values at 15° takeoff would be most sensitive. The largest value exhibited by PS₉₅-PPS₅ is reasonable, since the grafting density of this copolymer at the surface should be the highest. The next larger value, however, is for PS₇₅-

FIG. 60 XPS survey spectra, at takeoff angles of 75° , (a), and 15° , (b), of PS_{95} - PPS_5 adsorbed to Au. Surface was washed with cyclohexane at 45°C to remove physisorbed species. Anode is Mg $K\alpha$ excitation (300 W, 15 KeV).

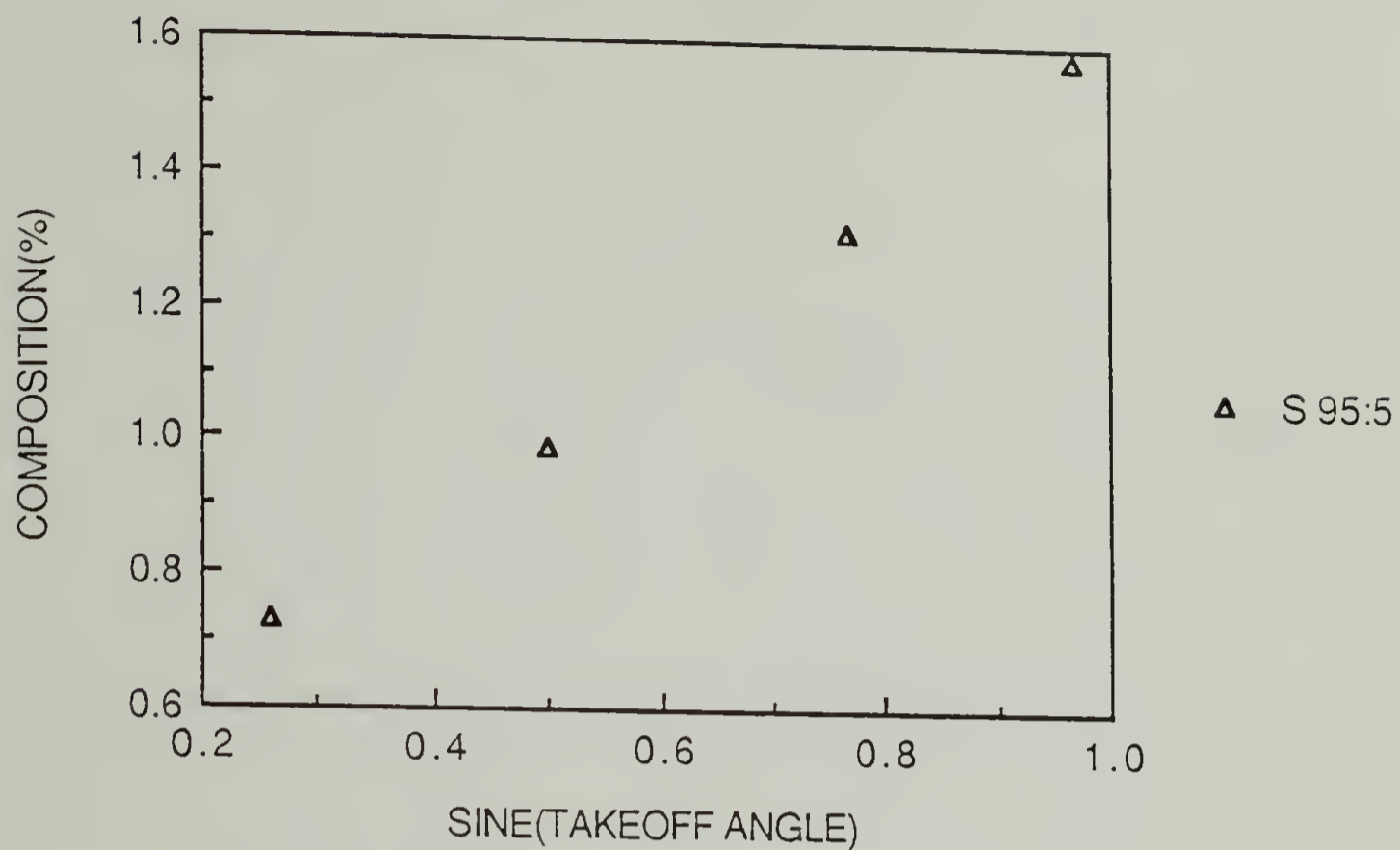


PPS₂₅. This discrepancy is attributed to the larger degree of polymerization for this copolymer relative to PS₉₀-PPS₁₀. The sulfur composition and C/S ratio for PS₉₅-PPS₅ as a function of takeoff angle are shown in Figure 61. Depth profiles for PS₉₅-PPS₅ of the C_{1s} and Au_{4f} compositions are linear but opposite in behavior, which again suggests that the adsorbed film is uniform. Unlike the other copolymers the depth profile of the sulfur composition is linear, although the C/S ratio exhibits some downward curvature at high takeoff angles. This ratio, however, does not plateau as a function of takeoff angle as was the case for the copolymers with longer propylene sulfide blocks. Dynamic contact angle measurements changed from $\theta_A/\theta_R = 65^\circ/15^\circ$ for the Au surface to $86^\circ/58^\circ$ for the adsorbed film.

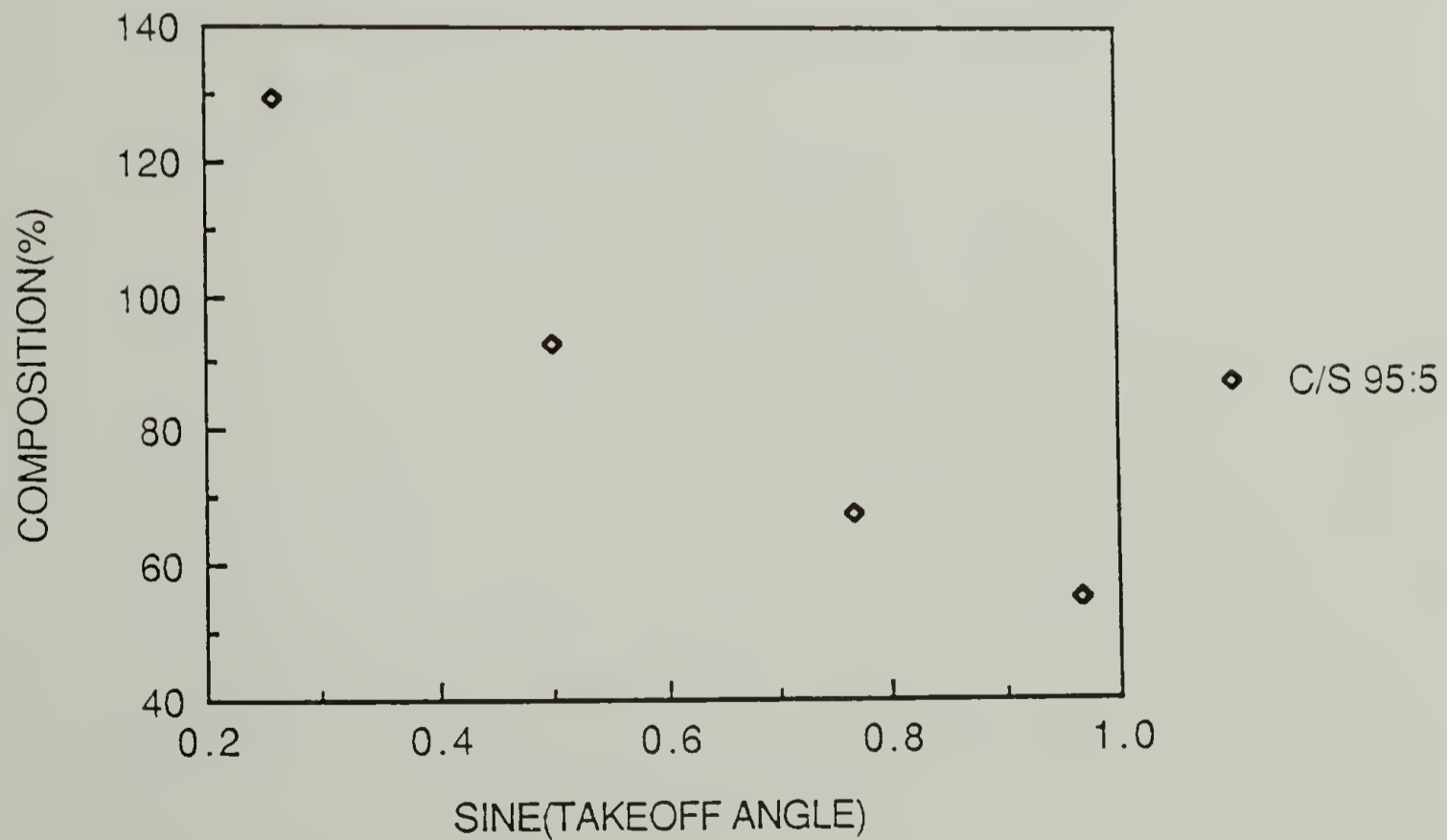
For all three copolymers the C/S ratio at 75° takeoff angle should be close to the true stoichiometric values. It is, however, the 15° XPS values which are close (within about 20 %) while those for 75° are approximately half. The relative magnitude of the programmed sensitivity factors are therefore incorrect (off by a factor), but this will not effect the observed trends. The contact angle measurements indicate that the air/film interface in all three cases resembles that of polystyrene. The differences in the C/S depth profiles suggest that the majority of the propylene sulfide block is located within an increasingly narrow region

FIG. 61 Sulfur composition, (top), and C/S atomic composition ratio, (bottom), as a function of the sine of the takeoff angle, from XPS multiplex spectra for the C_{1s} , and S_{2p} core levels, at a resolution of 0.5 eV, for copolymer PS₉₅-PPS₅ adsorbed to Au. Anode is Mg $K\alpha$ excitation(300 W, 15 KeV).

SULFUR COMPOSITION IN PS/PPS (95:5)



C/S RATIO IN PS/PPS(95:5) COPOLYMER



of depth, at the gold interface, as the molar ratio of the propylene sulfide block decreases from 25 % to 10 % to 5 %.

XPS survey spectra at takeoff angles of 75° and 15° of thiol endcapped polystyrene adsorbed to Au are shown in Figure 62. From the relative attenuation of the Au_{4f} level the thickness was determined to be 34 ± 2Å. This represents an averaged value from measurements taken at 75° and 50° takeoff angles for both the bulk Au surface and the adsorbed polymer surface. In Figure 62(a) there is evidence of the Au 5p, 4f, 4d, 4p and C_{1s} core levels, while in 62(b) there is a large relative attenuation of the Au signal due to the 15° takeoff angle. This attenuation is greater than for the copolymer cases shown in Figures 55 and 60, which indicates that the thickness of the terminally attached adsorbed polymer film is greater. As for the copolymers, the Au and C compositions increased and decreased linearly with increasing sine of the takeoff angle, suggesting film uniformity.

For a 1cm² substrate surface, and a density of 1.05 for polystyrene, the above thickness would correspond to 3.6 X 10⁻⁷ g for the amount adsorbed under θ conditions, or 0.027 adsorbed chains/nm². The C/Au ratio for the thiol endcapped polystyrene adsorbed from cyclohexane at θ conditions is 73.1/15° and 13.5/75°, while when adsorbed from THF it decreased to 38.7/15° and 7.4/75°. This indicates that increased solvent power does lower the grafting density or

FIG. 62 XPS survey spectra for thiol endcapped polystyrene adsorbed to Au from 1mg/ml cyclohexane solution at 35.5 °C, at takeoff angles of 75°, (a), and 15°, (b). Surface was washed with cyclohexane at 45 °C to remove physisorbed species. Anode is Mg K α excitation (300 W, 15 KeV).



adsorbed amount, and therefore the resulting thickness as well be shown below.

Surface Grafting Density

The crossover grafting density occurs when the fraction of surface sites grafted with polystyrene per surface unit (nm^2) is the reciprocal of the square of the Flory radius or $\sigma^* = 1/R_F^2$. The grafting ratio for the thiol endcap case exceeds the critical crossover value of $\sigma^* = N^{-6/5}b^{-2}$ by a factor of 18.7, where σ is the fraction of surface sites grafted with polymer per surface unit (nm^2), b is the length of a segment (4.9 Å), N is the degree of polymerization (769), and $R_F = N^{3/5} b$. The crossover concentration for polystyrene of this molecular weight in a theta solvent is $56.5 \text{ mg/ml} = M/[(4\pi/3) \langle S^2 \rangle^{3/2} N_A]$. The polymer concentration in the bulk solution (1 mg/ml) corresponds to only 2.56×10^{-5} polymer chains per nm^2 , and is in the dilute regime. The concentration, of polymer chains in the adsorbed film, therefore exceeds that of the solution the polymer condensed from by a factor of about 1050. Although the bulk solution concentration is well below the overlap concentration, the adsorbed endcapped chains are no longer isolated, and the resulting surface concentration is well above what would be considered the dilute regime.

In order to achieve an adsorbed polymer film with uniform segment density over the surface, grafting densities

at the surface must always exceed the overlap concentration conditions for a given molecular weight and solvent. This can be concluded from a simple model which only considers the hydrodynamic dimensions of the polymer chain, and the density of an amorphous film.

In good solution, the overlap concentration, C^* , is comparable with the local concentration inside a single polymer coil. The internal monomer concentration, C_{int} , is a function of the degree of polymerization, N , and the dimension occupied for a chain of radius R , according to

$$C_{int} \cong N / R^d \quad (50)$$

The Flory radius obtained from a minimization of energy due to repulsive and entropic considerations, when all correlations between monomers are ignored, can be expressed as⁵³

$$R_F^{d+2} = v a^2 N^3 \quad (51)$$

where a is the monomer length, and v is the excluded volume parameter, or $(1 - 2\chi) a^d$, which has dimensions of a^d . For three dimensions, $d = 3$, R_F can be expressed as

$$R_F \sim N^{3/5} \quad (52)$$

where $R_F \sim N^v$ for $(v = 3/[d + 2])$. Therefore for $d = 3$, the overlap concentration can be written as

$$C^* \cong N / R_F^3 = a^{-3} N^{-4/5} \quad (53)$$

and

$$C^* = M / [(4/3) \pi \langle S^2 \rangle^{3/2} N_A] \quad (54)$$

where $\langle S^2 \rangle$ is the radius of gyration at C^* conditions, and N_A is the Avogadro number.

The density of the polymer chains in solution at C^* can then be written as

$$\rho^* = (MW \text{ g/mole}) (1/N_A) (1/V) = \text{g/cc} \quad (55)$$

for V = chain volume in solution. As an example, for a polystyrene chain of $MW = 1000k$, the hydrodynamic radius is $R_h = 45.6 \text{ nm}$ in toluene, and $\rho^* = 0.0042 \text{ g/cc}$. At C^* the solution can be represented by touching spheres, which are occupied by just one chain which has a radius comparable to the Flory radius. For a 1 cm^2 substrate surface, if the polymer chains adsorb such that C^* is maintained at the surface, then each chain will occupy (πR_h^2) of the surface in solution. The number of adsorbed chains per unit area, N_{ad} , for the above hydrodynamic radius is then $N_{ad} = (1 \text{ cm}^2 / \pi R_h^2) = 1.53 \times 10^{10} \text{ chains adsorbed/cm}^2$. Similarly, the thickness of the adsorbed layer can be written in terms of N_{ad} , the polymer molecular weight (MW), and the density of the condensed layer or collapsed amorphous film, (ρ_a) , as

$$t_{ad} = (N_{ad} / N_A) (MW) (\rho_a)^{-1} (1 \times 10^7 \text{ nm/cm}) \quad (56)$$

Table 11 lists the corresponding number of adsorbed chains and collapsed adsorbed film thicknesses as a function of both the degree of polymerization for polystyrene and the solvent conditions. A few conclusions can be drawn from this table. First only when the MW < 100 K does the assumption of using amorphous density, ρ_a , appear somewhat reasonable for the adsorbed film. Otherwise the film will be a discontinuous patchwork. Second, for MW > 10 K the adsorption conditions would necessitate that $\rho_{soln} > \rho^*$ for a continuous film to exist when the solvent is removed. This is never the case. It can be generally concluded from the thickness values that in order to achieve a continuous uniform film of amorphous density upon removal of the solvent, the adsorption process must achieve a grafting density above the overlap conditions. It is noted that changing the solution from good to theta conditions would decrease R_h and therefore increase ρ^* , N_{ad} , and t_{ad} . This could result in conditions where an otherwise non continuous film becomes continuous upon collapse of the chains during solvent removal.

In Table 12 is listed the number of polymer chains (N_{re}) that would be necessary to exist inside of each sphere at the C^* grafting condition, in order to effect a continuous film of amorphous density and a certain thickness. The number of chains grafted per nm^2 (N_G) for a certain molecular weight and film thickness is also listed. If it is assumed that the minimum film thickness for a continuous film is on the order

TABLE 11. Table showing the calculated number of adsorbed chains, N_{ad} , and collapsed adsorbed film thicknesses, t_{ad} , as a function of both the degree of polymerization for polystyrene and the solvent conditions. Values are based upon the hydrodynamic radius, R_h (nm), and the density of the polymer chains in solution at the overlap concentration, ρ^* (g/ml).

TABLE 11

Thickness of Collapsed Adsorbed Film at C*

MW	R_h (nm)	ρ^* (g/ml)	N_{ad}	Solvent	t_{ad} (Å)
10 K	3.15	0.127	3.20×10^{12}	Toluene	5.0
100 K	11.99	0.023	2.21×10^{11}		3.5
1000 K	45.60	0.0042	1.53×10^{10}		2.4
10,000 K	173.37	0.00076	1.06×10^9		1.7
1000 K	29.20	0.016	3.74×10^{10}	cyclohexane	5.9
10,000 K	92.34	0.0051	3.74×10^9		5.9

TABLE 12. Table showing the calculated number of polymer chains, N_{re} , that would be necessary to exist inside of each sphere at the C^* grafting condition (factor by which C^* must be exceeded), and the number of chains grafted per nm^2 , N_G , in order to effect a continuous film of amorphous density for a certain molecular weight and film thickness.

TABLE 12

Grafting Density Necessary For
Continuous Amorphous Film

MW	R_h (nm)	t_{ad} (Å)	N_{re}	N_G (chains/nm ²)
10 K	3.15	10	$\cong 2$	6.31×10^{-2}
100 K	11.99	10	$\cong 3$	6.31×10^{-3}
1000 K	45.60	10	$\cong 4$	6.31×10^{-4}
10,000 K	173.67	10	$\cong 6$	6.31×10^{-5}
10 K	3.15	20	$\cong 4$	1.26×10^{-1}
100 K	11.99	20	$\cong 6$	1.26×10^{-2}
1000 K	45.60	20	$\cong 8$	1.26×10^{-3}

of 10 Å, then the number of adsorbed chains required per hemisphere can be expressed as

$$N_{re} = [(1.0 \text{ nm}) (1.05 \text{ g/cc}) (1 \times 10^{-21} \text{ cm}^3/\text{nm}^3) \\ (\pi R_h^2) N_A (1/\text{MW})] \quad (57)$$

It is evident that as the molecular weight increases the number of chains necessary inside of each solution sphere, determined by R_h and C^* , must increase in order to achieve a continuous film with amorphous density and of a certain thickness. This is due to the radius of gyration dependence for the unit area to be occupied on the surface. Let C_{sur} be the value required for the local concentration at the surface (relative to C^*) for a uniform amorphous film of thickness t_{ad} . Then it can be expressed by a factor times C^* for a certain molecular weight and film thickness, relative to the molecular weight required to form a continuous 10 Å film, as

$$C_{sur} \cong C^*_{MW} (1.445) [\log (MW/MW_0)] (t_{ad} / 10 \text{ Å}) (1.975) \quad (58)$$

where $MW_0 = 1 \times 10^4$

$C^*_{MW} = C^*$ for the particular MW

$N_{re} = C_{sur} / C^*_{MW} = (1.445) (t_{ad} / 10 \text{ Å})$

Even with this overly simplified model, it is clear that in order to achieve a continuous amorphous film of a certain thickness, the local concentration at the surface must be considerably greater than what exists at the overlap concentration. This implies that structural anisotropy, which necessitates elongated chain conformations, results

directly from a sufficient degree of chain overlap at the surface. The greater the film thickness for a given molecular weight, the greater the required grafting density and resulting chain orientation. Reflection infrared spectroscopy is used in this study to examine the degree of structural anisotropy, as a function of copolymer molar block ratios, resulting when only one block is strongly attracted to the gold surface.

Characterization by Polarization Modulation External Reflection Infrared Spectroscopy

Representative single beam spectra obtained with the (PMGRS) technique are shown in Figures 63 and 64. These spectra were obtained at grazing incidence and 1.5° lower respectively, with 2 cm^{-1} resolution, and had only 512 coadded scans. The top spectrum for both figures is that of an adsorbed layer of 80K thiol endcapped polystyrene, adsorbed from a 0.5 mg/ml cyclohexane solution at θ temperature (34.5°). The bottom spectra in both cases were obtained from the same Au surface before it was exposed to the polymer solution. There is evidence of residual short chain hydrocarbons in the CH stretching regions of the two bottom spectra. XPS analysis of similarly prepared Au surfaces which have been subsequently ion sputtered, followed by short time exposure to ambient atmospheric conditions, supports the existence of such hydrocarbons within the first 3\AA of the surface.

FIG. 63 Polarization modulation external reflection infrared energy spectra, obtained at grazing incidence, for an adsorbed layer of 80K thiol endcapped polystyrene, (top), and for the same Au surface before it was exposed to the polymer solution, (bottom). Resolution = 2 cm^{-1} , and number of scans = 512. Background shape is due to dispersion effects.

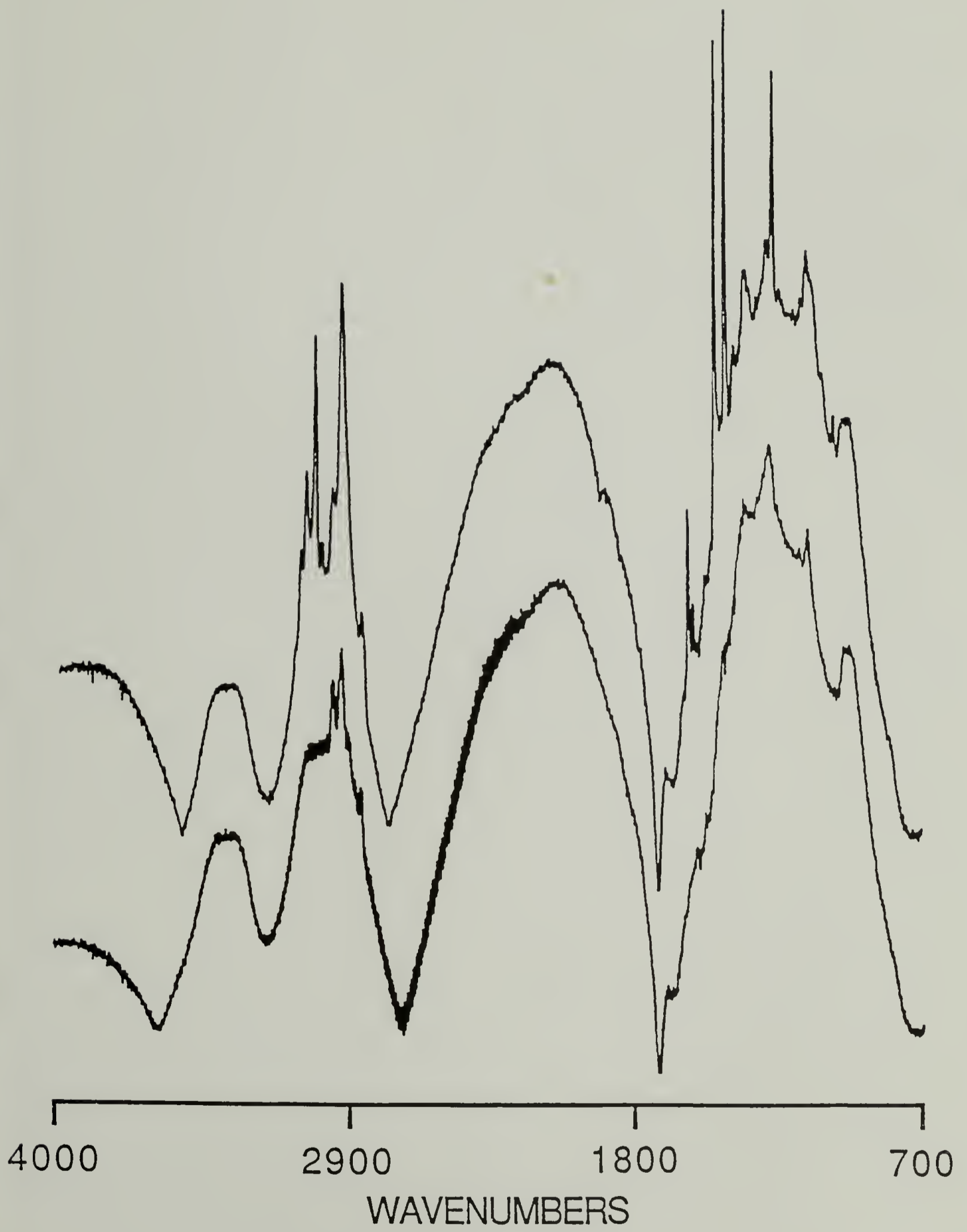
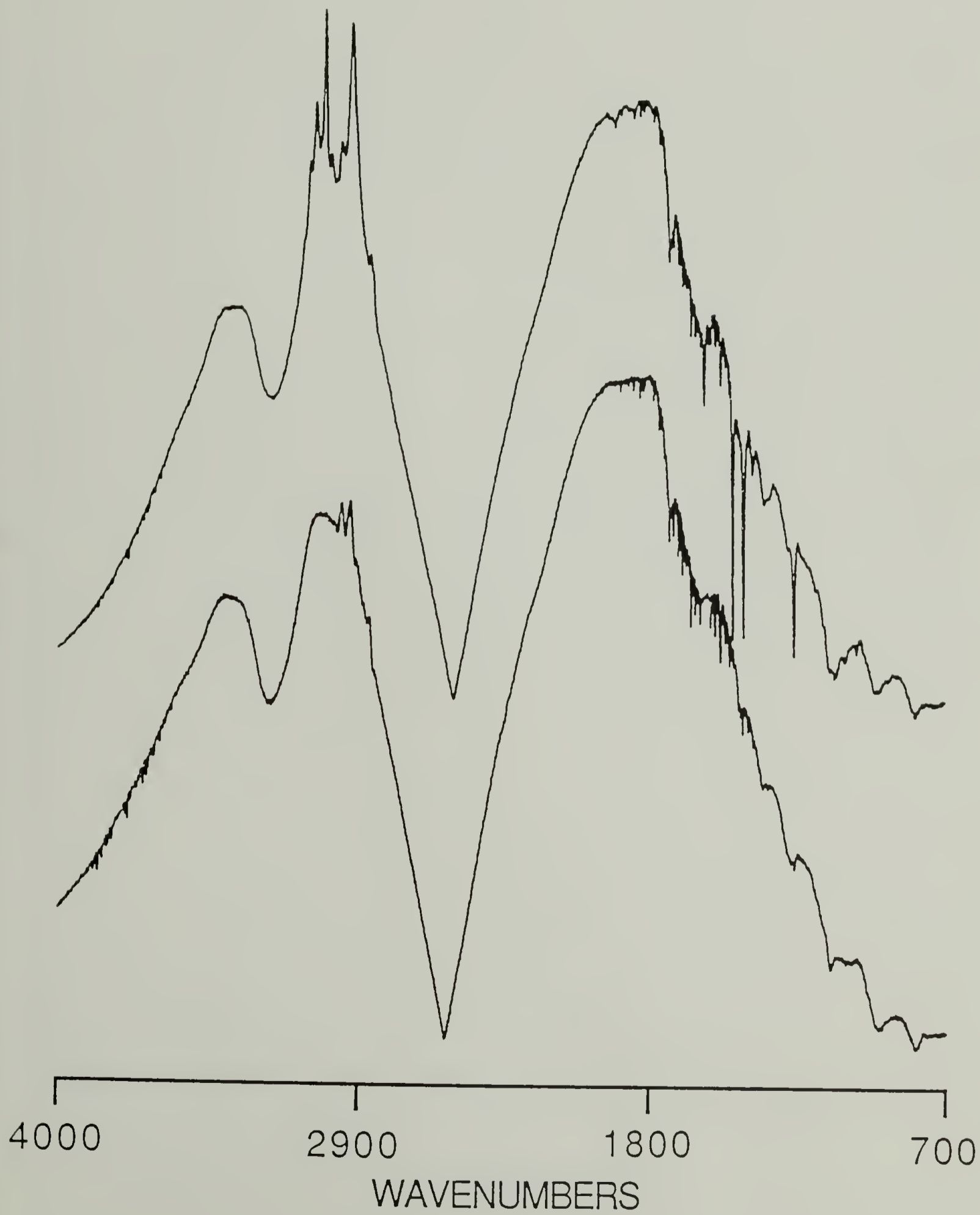


FIG. 64 Polarization modulation external reflection infrared energy spectra, obtained 1.5° below grazing incidence, for an adsorbed layer of 80K thiol endcapped polystyrene, (top), and for the same Au surface before it was exposed to the polymer solution, (bottom). Resolution = 2 cm^{-1} , and scans = 512. Background shape is due to dispersion effects and inversion of peak direction results from phase correction routine.



Each PMGRS spectrum, $\Delta I(\bar{\nu})$, obtained for the adsorbed polymer adlayer, is matched to a similar spectrum obtained for the identical Au surface before it was exposed to the polymer solution, $\Delta I_o(\bar{\nu})$. Subtraction of $\Delta I_o(\bar{\nu})$ from $\Delta I(\bar{\nu})$ is then carried out. This process will eliminate any contributions resulting from the presence of residual short chain hydrocarbons on the initial Au surface. It is not expected that a large number of these would be displaced during the adsorption process as a result of excluded volume interactions between adsorbed polymer chains. This spectrum is subsequently ratioed to the instrument throughput, $I_{dc}(\bar{\nu})$, with the polarizer, modulator, reflection cell, and KBr plate all in place. Appropriate scaling is used to insure the validity of equation 60, so that the final intensities are directly proportional to $[-A_p(\bar{\nu})]$, the absorption resulting from transition dipole components parallel to the scattering plane.

A typical result can than be represented as

$$[\Delta I(\bar{\nu}) - \Delta I_o(\bar{\nu})] / I_{dc}(\bar{\nu}) \cong [\Delta I(\bar{\nu})/I_{dc}(\bar{\nu}) - \Delta I_o(\bar{\nu})/ I_{o,dc}(\bar{\nu})] \quad (59)$$

where

$$[\Delta I(\bar{\nu}) / I_{dc}(\bar{\nu})] \cong 1.1515 (A_s(\bar{\nu}) - A_p(\bar{\nu})) J_2 \delta_o(\bar{\nu}) \quad (60)$$

The final form of this equation indicates that the ratio of the single beam spectrum obtained via polarization modulation, to that without, is directly proportional to the

difference in absorptions for the IR beam polarized perpendicular and parallel to the scattering plane, ($A_s(\bar{\nu}) - A_p(\bar{\nu})$).

The adsorbed films in this study have thickness on the order of 30 Å, so there exists within this layer only a node for $E_{s,r}$, the electric field component polarized perpendicular to the scattering plane. This is true for the entire mid infrared region, since the thickness of the ultra thin adsorbed polymer film is much less than 1/4 of the infrared wavelengths. Thus transition dipoles oriented in this direction will not adsorb the incident radiation. Therefore the final ratioed spectrum will only exhibit an intensity proportional to $[-A_p(\bar{\nu})]$. The instrument throughputs are shown in Figure 65 as the single beam spectra, $I_{dc}(\bar{\nu})$ on top and the reference throughput $I_{odc}(\bar{\nu})$ on bottom, for the same Au surfaces as in Figures 63 and 64. Note that there is absolutely no evidence of adsorbed polystyrene in the single beam spectrum $I_{dc}(\bar{\nu})$, shown on top in Figure 65. The final PMGRS spectra, directly proportional to $[A_p(\bar{\nu})]$, are shown in Figure 66 for the above case. These spectra exhibit exceedingly high signal to noise over the entire spectral range, and for only 512 scans. The high signal to noise ratio is impressive considering that the packing density of the adsorbed polymer is much lower than that of Langmuir-Blodgett or self assembly monolayers.

FIG. 65 Single beam spectra, $I_{dc}(\bar{\nu})$, (top), and the reference throughput, $I_{odc}(\bar{\nu})$, (bottom), representing the instrument throughputs (dc spectra) for the same Au surfaces as Figures 63 and 64. Note there is no evidence of adsorbed polymer.

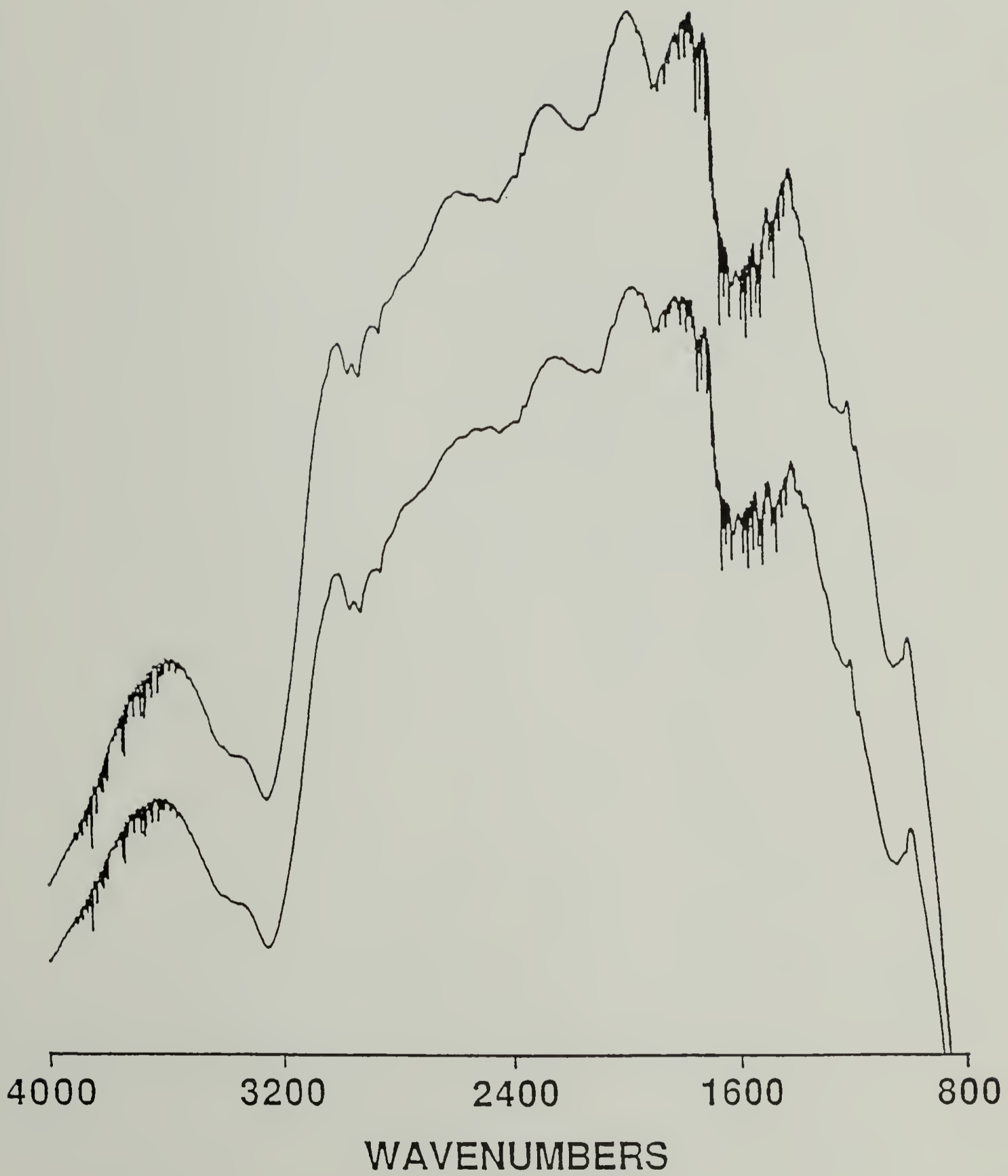
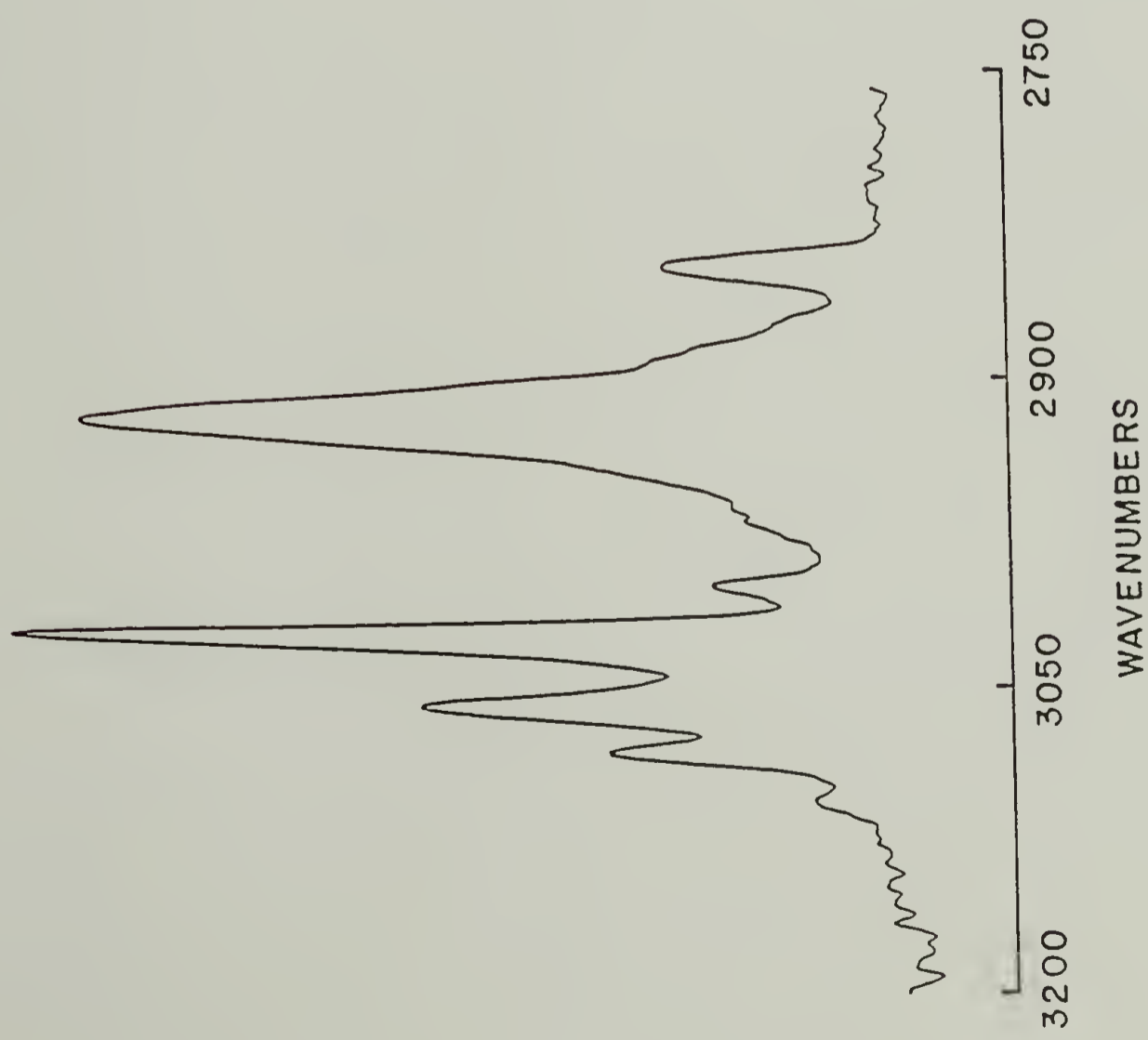
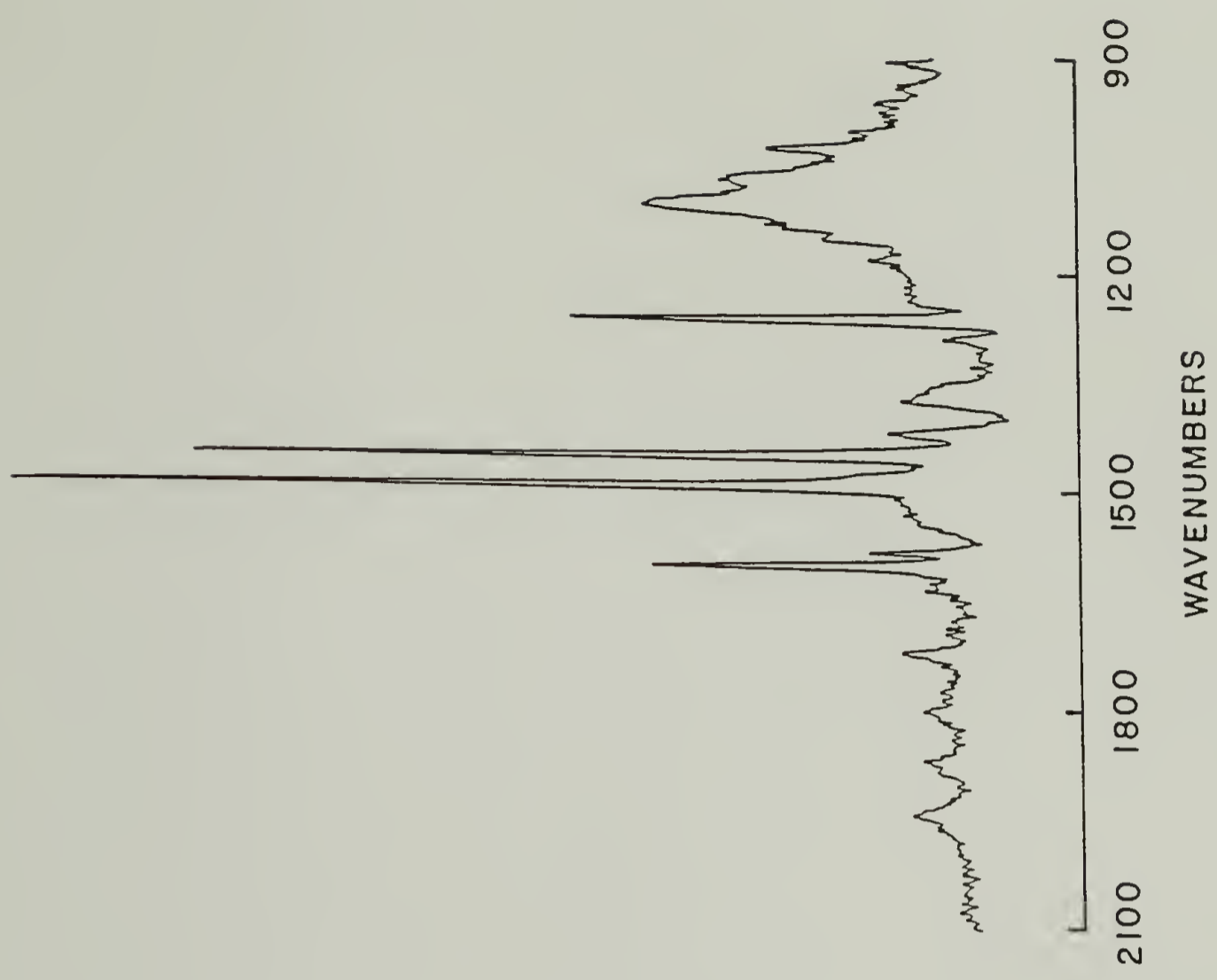


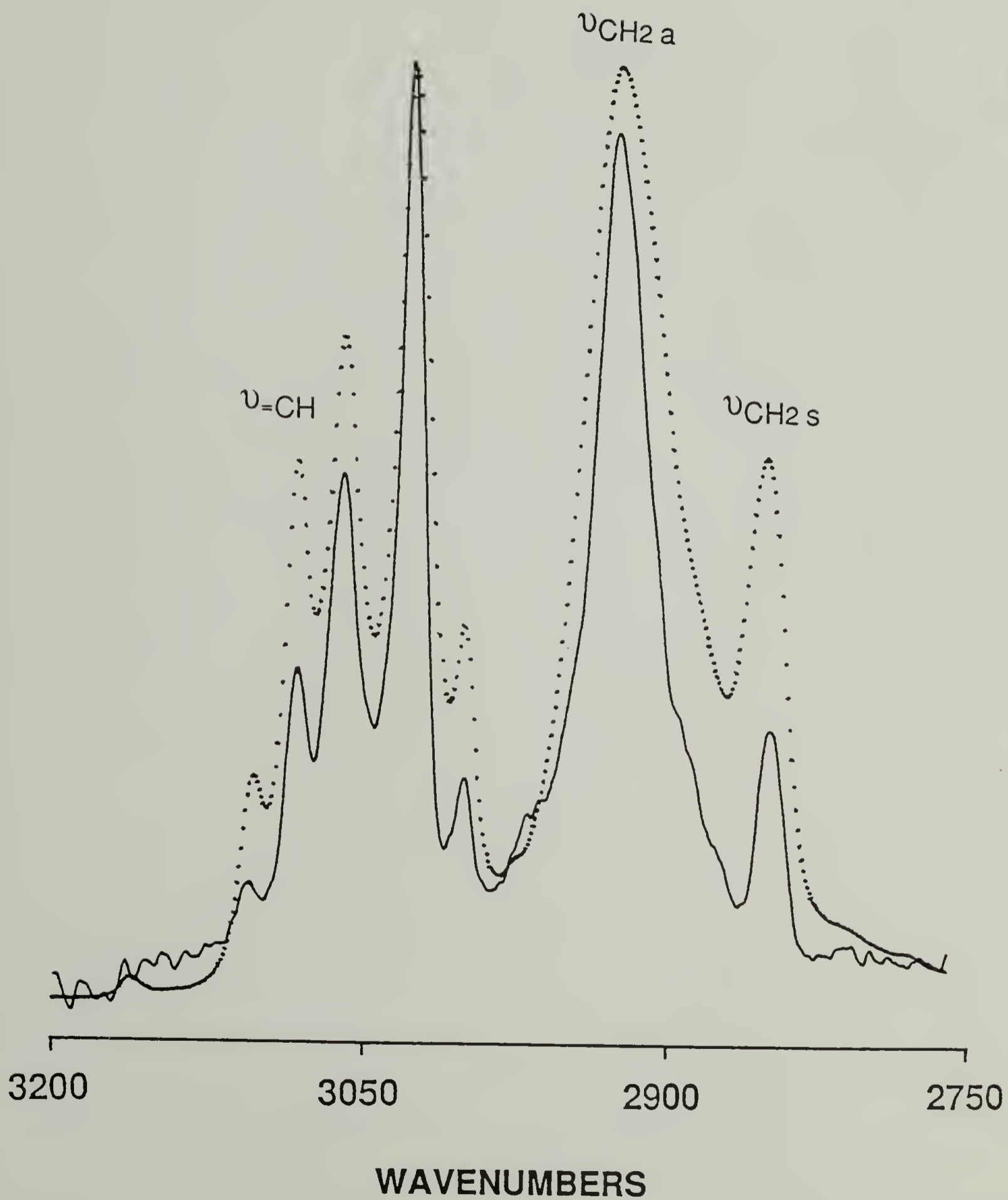
FIG. 66 The differential polarization modulation grazing incidence reflection spectra, directly proportional to $[A_p(\bar{\nu})]$, for an adsorbed layer of 80K thiol endcapped polystyrene. Resolution = 2 cm^{-1} , and number of scans = 512. The sensitivity of these measurements is so high that even the combination bands above 1700 cm^{-1} are clearly resolved.



For these polymers relative orientations of various structural units can be determined from intensities for the C-H in plane bending mode of the aromatic ring at 1028 cm^{-1} , and the C-H stretching modes of the aliphatic backbone. Both of these are conformation insensitive, so comparison to isotropic reference spectra of the adsorbate enables clarification of respective orientations. The wide spectral response exhibited by the PMGRS technique, which is critical for correlation of distinct orientations within the polymer structure, is also impressive. The sensitivity of these measurements is so high that even the combination bands above 1700 cm^{-1} are clearly resolved. The aromatic and aliphatic CH stretch vibrations, the C=C stretch at 1584 and 1602 cm^{-1} and aromatic C-H in plane bending modes at 1454 , 1494 , and 1031 cm^{-1} are all clearly shown in Figure 66. There is also evidence of the 1420 cm^{-1} S-CH₂ bending and the 2965 cm^{-1} methyl stretching. This evidence is unexpected since the 80 K polystyrene would have 769 repeat units, and thus a ratio of at least 385:1 for CH₂ groups due to the polystyrene, versus CH₂ and CH₃ groups due to the terminal propylene sulfide.

In Figure 67 is shown the CH stretching region of the PMGRS spectrum (solid) and transmission spectrum (dotted), for the above adsorbed endcapped polystyrene, and an isotropic dispersion (2% in KBr) respectively. There are significant differences in the relative intensities for the

FIG. 67 The CH stretching region of the PMGRS spectrum, (solid), and transmission spectrum, (dotted), for the adsorbed thiol endcapped polystyrene in Figures 63-66, and an isotropic dispersion of the same polymer(2% in KBr) respectively.



conformationally insensitive 3027 cm^{-1} aromatic CH stretching, 2848 cm^{-1} symmetric and the 2925 cm^{-1} asymmetric CH stretching vibrations. The intensity ratios, based upon peak heights of $\bar{\nu}_{2848}/\bar{\nu}_{3027}$, $\bar{\nu}_{2925}/\bar{\nu}_{3027}$, and $\bar{\nu}_{2848}/\bar{\nu}_{2925}$ are 0.258, 0.902, and 0.286 for the adsorbed film, and 0.609, 1.023 and 0.596 for the isotropic case.

It has been determined that utilization of peak heights is reasonable, since intensity ratios in isotropic spectra of the copolymers, based upon heights for $\bar{\nu}_{2925}/\bar{\nu}_{3027}$, can be used to evaluate for the respective chemical compositions. In addition, peak heights have been used successfully to determine the orientation of uniaxially drawn polystyrene film.⁵⁴ The intensity differences in Figure 67 can be directly related to the anisotropic segmental orientation that exists on the metallic surface. Such orientation was suggested by deGennes' brush model for terminally attached chains with high grafting density. This result represents the first clearcut experimental determination for the existence of orientation in an adsorbed polymer structure.

Orientation Model And Results

The adsorbed polymer film is not expected to be highly ordered relative to the structure found for small molecule cases such as adsorbed alkyl sulfides on Au, or arachidic acid on Ag. Specific orientations of the aliphatic and aromatic groups with respect to the Au substrate surface can, however,

be inferred from intensity ratios in the C-H stretching region. These vibrations are insensitive to conformational changes and their transition dipole directions are well defined with respect to the local backbone and ring molecular axis, for the atactic polymers.^{54,55} Intensity differences between the observed spectra from transmission of an isotropic dispersion and PMGRS of an adsorbed film, can be interpreted as resulting from specific structural features of the adsorbed monolayer. This is a consequence of assuming that the magnitudes of the transition dipole moments for the bulk and adsorbed states do not differ, since the observed peak positions and bandshapes are about the same. In addition these modes are associated with C-H groups which are not expected to be bonded to the Au surface. The integrity of the associated bonds should therefore not change upon adsorption of the modified polystyrene to Au.

Utilization of C-H intensity ratios, enables determination of the average transition moment angles for the aliphatic CH₂ asymmetric and symmetric stretching modes, with respect to the normal to the adsorbed layer surface, which is denoted as the Z direction. From these angles, values for the Hermans orientation function for the CH₂ transition moments are ascertained. These values can then be related to the average angle between the local chain axis and the Z direction, thereby representing the average segmental orientation. This method enables the segmental orientation

function to be determined without dichroic ratio values. Dichroic ratios are not obtainable from modulation results.

If I_i is the intensity of i^{th} mode observed in an infrared reflection spectrum, then it is related to the transition moment of the i^{th} mode (M_i) and the electric field (E) direction according to

$$I_i \propto |M_i \cdot E|^2 \quad (61)$$

where $M_i = \partial u_i / \partial q_i$ for the dipole moment (u) and normal mode (q). The intensity of the i^{th} mode will be dependent upon the angle (θ) between the transition moment and the normal to the surface, since only that electric field component will have amplitude for a thin film geometry. Thus

$$|(M_i \cdot z) / M_i|^2_{\text{surface}} = \cos^2 \theta \quad (62)$$

The average spatial orientation, of a given vibrational mode relative to a specific molecular axis is therefore

$$\cos^2 \theta = 2(R_{\text{obs}}) / 3(A_{\text{iso}}) = R_{\text{obs}} / 3(A_{\text{calc}}) \quad (63)$$

where R_{obs} is absorbance in the reflection spectrum, A_{iso} the absorbance in an isotropic spectrum, and A_{calc} is the calculated absorbance based upon isotropic data. This expression forgoes factors such as twisting of segments within and between chains with respect to each. It is therefore sufficient only for highly ordered systems such as Langmuir-Blodgett layers or self assemblies of small

molecules. For the case of adsorbed polymers, however, the orientation of a given vibrational mode can not related to the molecular axis of a polymer adsorbate or to the spatial orientation of the surface structure easily, because only one specific adsorption can be measured.

The accepted angle between the symmetric (M_S) and asymmetric (M_{As}) transition moments is 90° . Thus for any specific average angle that defines a cone which one transition moment (M_S) sweeps out between itself and a reference axis, which is assigned to be the surface normal (z direction), the other transition moment (M_{As}) exists in a plane normal to M_S . The model for this analysis is shown schematically in Figure 68. An intensity ratio based upon two vibrational modes and one polarization can be expressed as

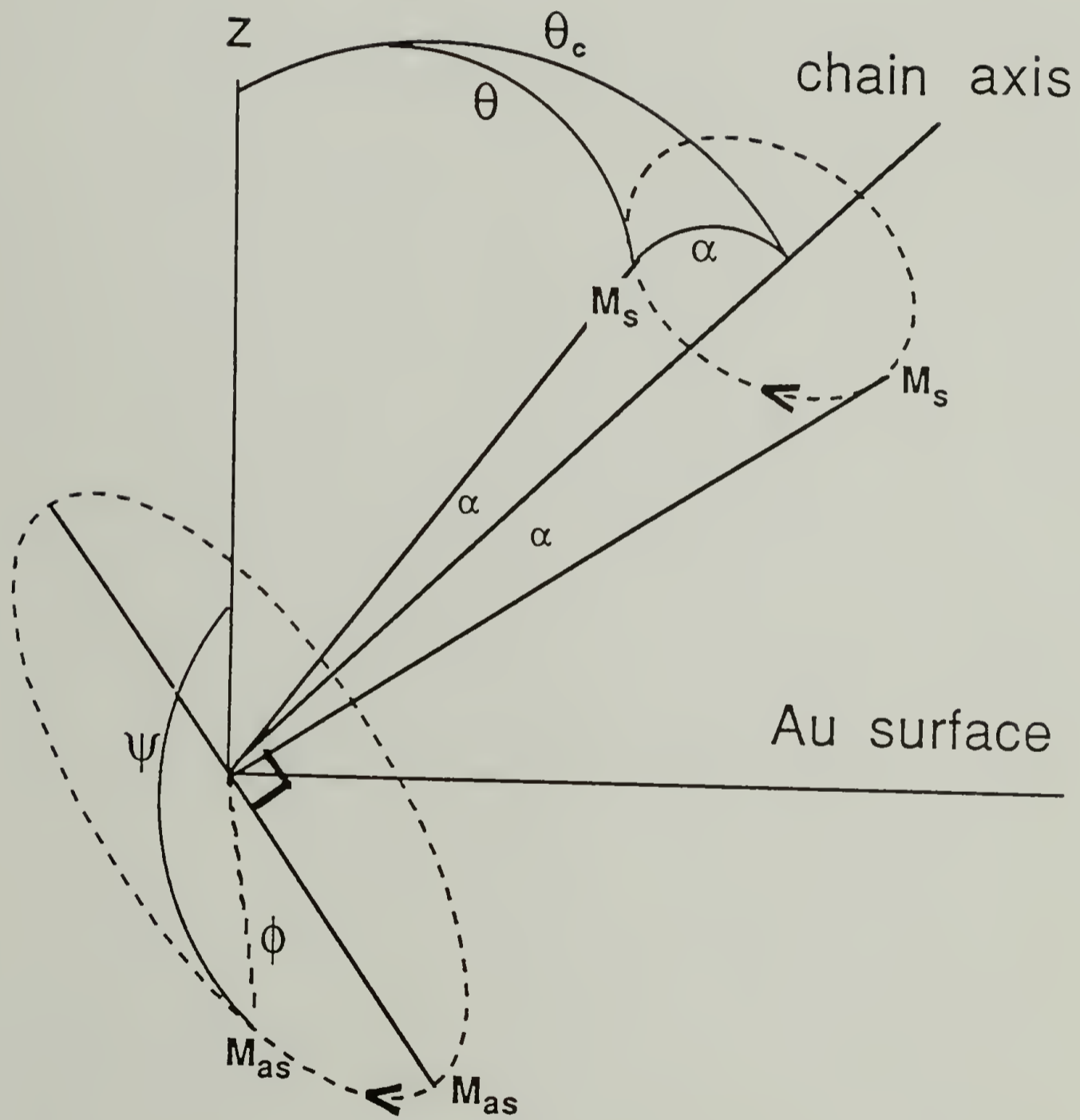
$$\frac{R_{sy}}{R_{as}} = \frac{I_{sy}}{I_{as}} \frac{(\cos^2 \theta)}{\langle (\cos \psi)^2 \rangle} = \frac{C_I (\cos^2 \theta)}{\frac{\int_0^{2\pi} (\cos \phi \sin \theta)^2 p(\phi) d\phi}{\int_0^{2\pi} p(\phi) d\phi}} \quad (64)$$

where

$$\cos \psi = \cos \phi \sin \theta \quad (65)$$

and $C_I = I_{sy}/I_{as}$.

FIG. 68 Schematic for orientation model based solely upon relative intensities for one polarization, where the angle between the symmetric (M_S) and asymmetric (M_{AS}) transition moments is 90° , and for any specific average angle θ that defines a cone which one transition moment (M_S) sweeps out between itself and a reference axis, which is assigned to be the surface normal (Z direction), the other transition moment (M_{AS}) exists in a plane normal to (M_S) with an average angle ψ to z. Once θ and ψ are determined, the average angle between the chain axis and director z, θ_c , can be obtained.



This ratio can be utilized to represent the PMGRS ratio due to the aliphatic CH₂ stretching vibrations, in terms of the inherent transition moment strengths from isotropic data, and any modification of that absorbance arising from orientation of the CH₂ groups. Here θ is the average angle between M_s and the z direction, ψ represents the angle between M_{as} and z, ϕ is the rotational angle between M_{as} and its component in the yz plane, and R and I are the reflection and isotropic absorbances corresponding to a particular vibrational band. If the distribution function is isotropic, both with respect to the surface normal and in the plane normal to M_s , then $p(\phi)$ is a constant and

$$\frac{R_{sy}}{R_{as}} = \frac{C_I(\cos^2\theta)}{\sin^2\theta \int_0^{2\pi} \frac{(1 + \cos 2\phi)}{2} d\phi} \quad (66)$$

$$\frac{R_{sy}}{R_{as}} = \frac{C_I(\cos^2\theta)}{2\pi}$$

Thus $\langle \cos^2\psi \rangle$ reduces to $\sin^2\theta/2$. The modulation external reflection intensity ratio can then be expressed as

$$R_s/R_{as} = I_s/I_{as} (2 \cot^2\theta) \quad (67)$$

and

$$\theta = \cot^{-1} [(R_s/R_{as})/2(I_s/I_{as})]^{0.5} \quad (68)$$

From the experimental intensity ratios given above, pertaining to the aliphatic CH₂ groups, the average angles between the z axis and M_s and M_{as} are 63.9° and 44.4° respectively. These values demonstrate that there is indeed

significant orientation for the adsorbed thiol endcapped polystyrene, since a transition moment vector randomly oriented in space would have an average angle of 54.7° from a given direction.

Since the angle between the transition moment and the chain axis for polystyrene, α , is 70° for M_S , the bisector of the CH_2 group will be located 83.9° from the Z axis. If M_S is situated in the YZ plane, which will then also contain the bisector and Z , then rotation through an angle, δ , about M_S such that M_{as} is 44.4° from Z , is necessary in order to locate the chain axis projection. The implication here is that the average local chain axis will exist in a plane which is tilted 6.1° from the Z axis. This plane also contains M_{as} and the X axis, for the angle between the transition moment and the chain axis is 90° , and the angle between the two transitions moments, M_S and M_{as} , is also 90° . Thus the average angle between the local chain axis, which contains three backbone atoms, and the surface normal, can be represented as

$$\theta_c = \cos^{-1} (\cos \delta)(\cos [\alpha - \theta]) \quad (69)$$

where

$$\delta = \{90 - \cos^{-1} [(\cos \psi)/(\cos [\alpha - \theta])]\} \quad (70)$$

The calculated value for θ_c is 46.3° for the average angle between the local chain axis and the surface normal. An

average chain segment is within a cone of smaller solid angle than for the isotropic case.

The average angle between the local chain axis and the surface normal can also be determined with spherical triangles shown in Figure 69 as

$$\theta_c = \cos^{-1} [(\cos \theta_s)(\cos \alpha_s) + (\sin \theta_s)(\sin \alpha_s)(\cos \alpha)] \quad (71)$$

where $\alpha = \gamma - \beta$ for

$$\gamma = \cos^{-1} \{ [(\cos \theta_{as}) - (\cos \delta)(\cos \theta_s)] / (\sin \delta)(\sin \theta_s) \} \quad (72a)$$

$$\beta = \cos^{-1} \{ [(\cos \alpha_{as}) - (\cos \delta)(\cos \alpha_s)] / (\sin \delta)(\sin \alpha_s) \} \quad (72b)$$

where δ is the angle between M_s and M_{as} , θ_s and θ_{as} are the average angles from z to M_s and M_{as} respectively, α_s and α_{as} are the angles between M_s and M_{as} and the chain axis.

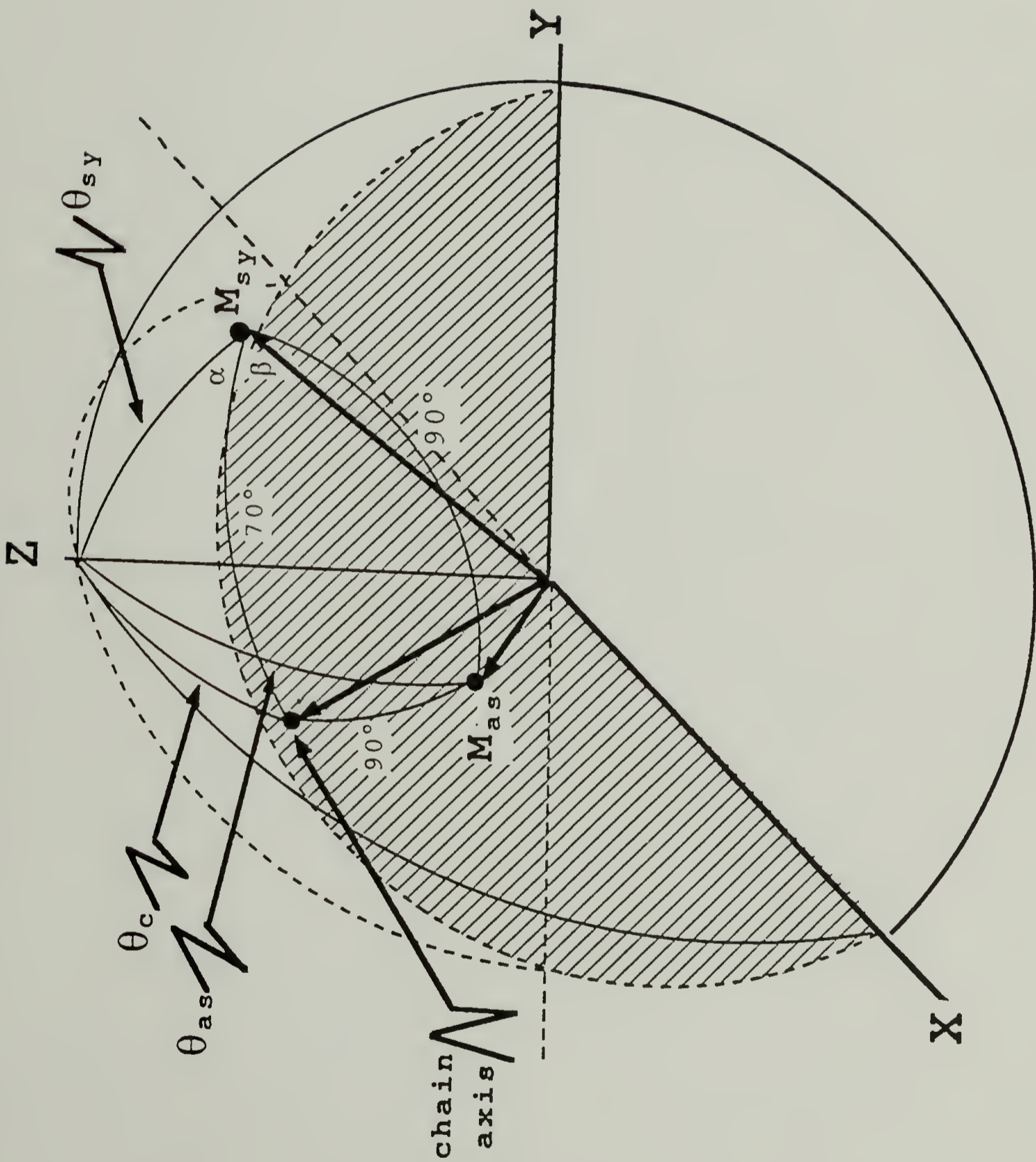
The corresponding values for the orientation function according to the general equation

$$f = (3\langle \cos^2 \theta \rangle - 1) / 2 \quad (73)$$

are -0.21, 0.27 and 0.22 for M_s , M_{as} , and the local chain axis respectively. The orientation value of the terminally functionalized polystyrene adsorbate represents significant structural anisotropy for a glassy polymer.

The degree of orientation can be compared to that found in uniaxially oriented polymers, where the machine direction is the corollary to the surface normal in the adsorbate case.

FIG. 69 Schematic for spherical triangle relationships utilized to determine the average angle between the local chain axis and the surface normal, θ_c , once the average angles from z to M_s and M_{as} , θ_s , and θ_{as} respectively, are obtained. The angle between M_s and M_{as} is δ , and α_s and α_{as} are the respective angles between M_s and M_{as} and the chain axis.



The polarized data for a coextruded film (draw ratio = 3) was obtained for comparison. From the measured dichroic ratios the 300% extruded polystyrene has an orientation function value of just 0.07, which corresponds to $\theta_c = 52.0^\circ$ for the average angle between the local chain axis and the machine direction. This result is in good agreement with an earlier study on uniaxially drawn polystyrene.⁵⁴ Their data indicated that in order to achieve an orientation function value of 0.22, a dichroic ratio for the $\bar{\nu}_{2850}$ band of 0.80 would be required. It can be inferred from their data that polystyrene oriented to this degree would require a draw ratio of about 7.0.

If the machine direction for the stretched films is equated with the direction normal to the Au surface for the adsorbed polystyrene, then these results indicate that the adsorbed chains are oriented such that they extend outward from the Au surface. This is consistent with theoretical predictions^{46,51} and a recent EPR study on PEO adsorbed with different grafting densities onto silica.⁵⁶ For the high grafting ratio case, the solution will be above the crossover regime at or near the substrate surface, so that interchain interactions dominate (repulsion), causing extension out into solution. When the solvent is removed then it is expected that the brush structure present in solution would not be able to collapse completely due to the interchain interactions effected by their close proximity. This is

exactly what is observed in their DSC study,⁵⁶ wherein only the high grafting ratio case exhibited a transition attributed to reorganization of the grafted chains.

The orientation results for the endcapped case support this premise. The collapsed structure within the ultra thin polymer film can be represented by an anisotropic brush structure with chains terminally attached via coordination of the thiol functionality. This suggests that grafting density, which by XPS is high for this case, is important in determining the degree of chain extension in the structure of ultra thin polymer films. High chain extension is a desired property for stabilization of colloidal suspensions. Such a structure acts as a buoy which provides a sterically stabilizing external layer that acts as an elastic medium between particles.

Use of a good solvent (THF) for the adsorption of the endcapped polystyrene, wherein the chains are expected to have greater dimensions in solution, yielded similar results. Previous work has demonstrated that for the thiol endcapped polystyrene, adsorption does occur onto Au surfaces, while for unmodified polystyrene irreversible adsorption does not proceed.³⁴ This result is indicative of the effect of the large binding energy interaction between the incorporated functional groups and the available surface sites. For both the good and θ solvent cases a high density of terminally attached weakly interacting chains is expected within the

adsorbed layer, provided the degree of polymerization is not too high. In the good solvent case the chains will be more extended in solution due to excluded volume interactions.³²

The number of terminally attached thiol endcapped chains should be similar to that at θ conditions, since the number of coordination sites available would remain constant. This is the opposite of what occurs for unfunctionalized polystyrene, where due to competing energetics adsorption decreases with increasing solvent power. Upon removal of solvent it is expected that the endcapped polymer chains will collapse to a similar final state. This is governed principally by repulsive interactions arising from the close proximity of chains in the adsorbed brush structure.⁵¹ A similar orientation of chains relative to the surface normal should result, as was observed. This result is complementary to the high C/Au ratio observed by XPS for endcapped polystyrene adsorbed from THF (38.7/15°) relative to PS₇₅-PPS₂₅ with the same degree of polymerization adsorbed at θ conditions (25.9/15°).

The observed PMGRS spectra, for the ultrathin copolymer films adsorbed from dilute solution, indicate that provided the propylene sulfide block irreversibly adsorbs to the Au surface, large orientational effects will result from different grafting density conditions. These are quite different from the case when polystyrene is merely endcapped with a thiol functionality for similar adsorption conditions.

This is consistent with previous solution studies on competitive and displacement adsorption of polystyrene and poly(ethylene oxide) onto nonporous silica by Takahashi and coworkers.³ Full coverage of the available silanol groups with PEO chains, at such low concentrations, was the result of strong adsorption enthalpy. This was further evinced by the large frequency shift ($\Delta\nu_{\text{OH}} = 375 \text{ cm}^{-1}$) of the silanol groups due to the PEO adsorption

An isotropic spectrum for the copolymer PS₇₅-PPS₂₅, dispersed in KBr, is shown in Figure 70. The methyl asymmetric stretching mode at 2959 cm^{-1} , an increased intensity for the methylene asymmetric stretching mode at 2922 cm^{-1} , and a broadening of the symmetric stretching mode at 2850 cm^{-1} to the high frequency side, is evident in the isotropic spectrum of the copolymer, relative to that of the endcapped polymer. This is expected due to the poly(propylene-sulfide) block which exhibits three strong bands in the CH stretch region at 2962 , 2922 , and 2867 cm^{-1} respectively. An isotropic spectrum for poly(propylene-sulfide) is shown in Figure 71. The isotropic spectrum for PS₇₅-PPS₂₅ also exhibits increased intensity at 1373 and 1452 cm^{-1} , due to contributions from the symmetric and asymmetric methyl bending modes, and a weak band at 1417 cm^{-1} assigned to the CH₂ scissoring for S-CH₂ groups. The former two modes are strong bands in a transmission spectrum for poly(propylene-sulfide), while the latter mode is a medium strong band.

FIG. 70 Isotropic spectrum for the copolymer PS75-PPS25, for a 2% dispersion in KBr. Note the methyl asymmetric stretching mode at 2959 cm^{-1} , an increased intensity for the methylene asymmetric stretching mode at 2922 cm^{-1} , and a broadening of the symmetric stretching mode at 2850 cm^{-1} to the high frequency side, relative to that of the endcapped polymer. Spectrum also exhibits increased intensity at 1373 and 1452 cm^{-1} , due to contributions from the symmetric and asymmetric methyl bending modes, and a weak band at 1417 cm^{-1} assigned to the CH_2 scissoring for S- CH_2 groups.

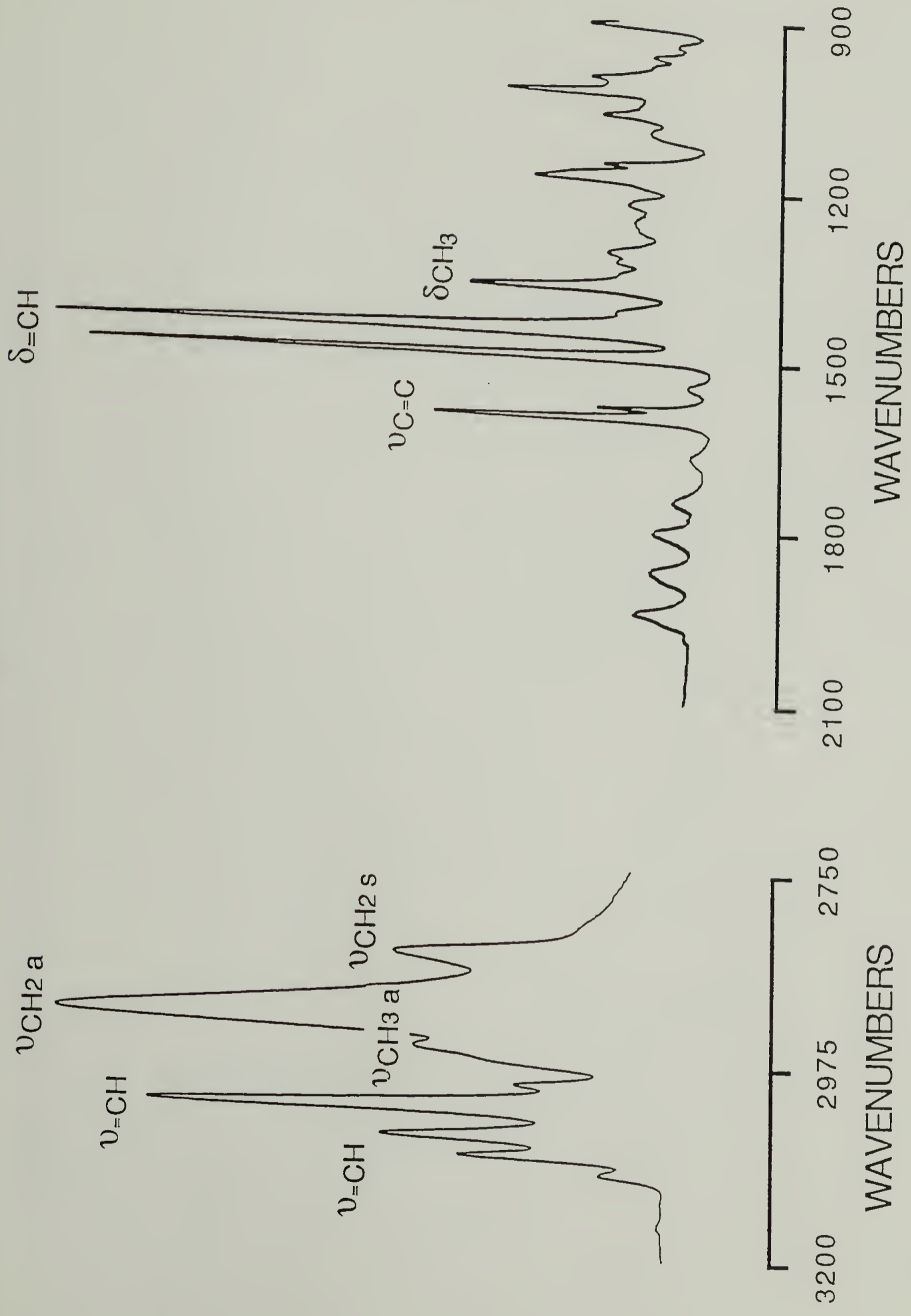
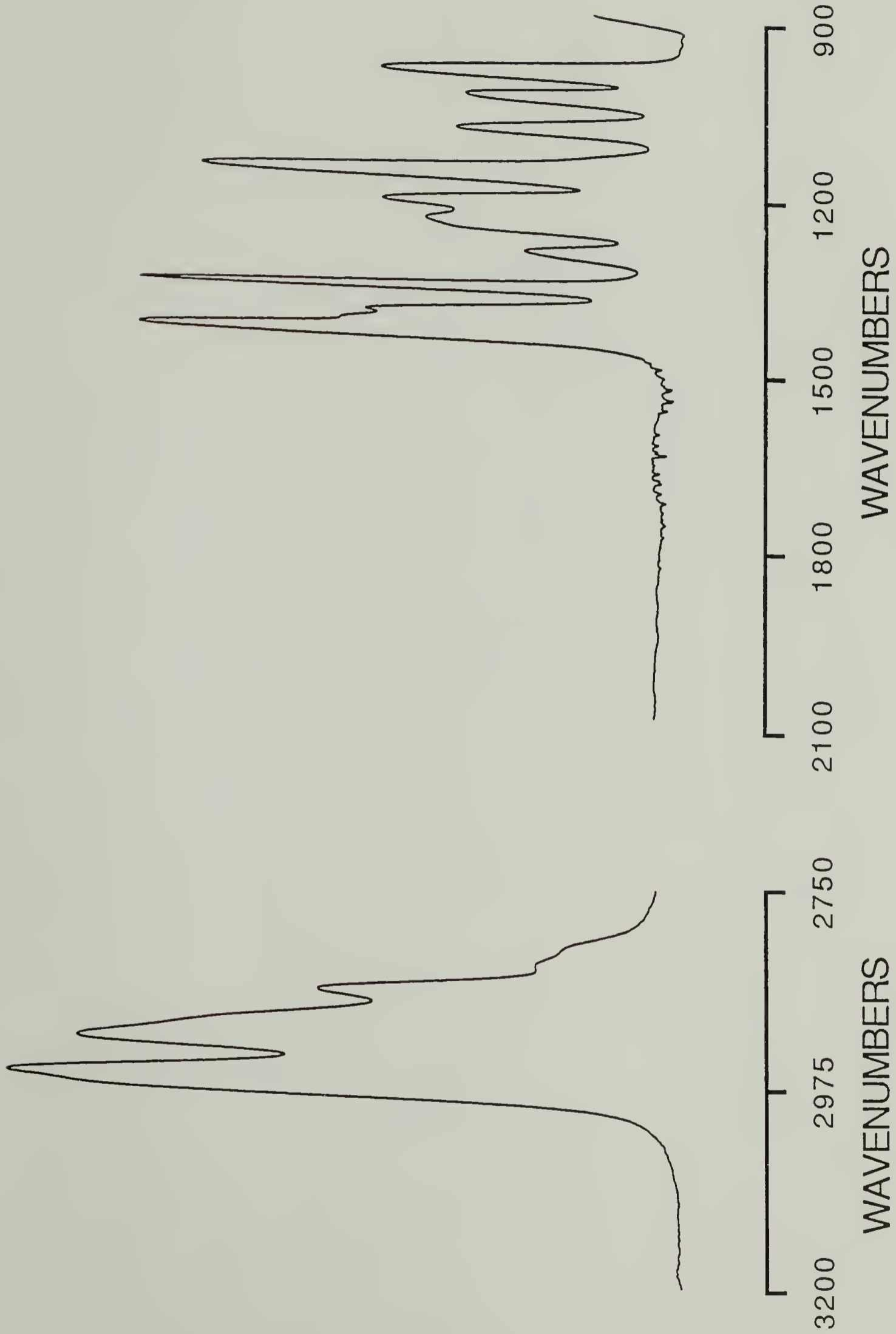


FIG. 71 Isotropic spectrum for poly(propylene-sulfide), for a 2% dispersion in KBr. The three strong bands in the CH stretch region are at 2962, 2922, and 2867 cm^{-1} respectively. The strong bands at 1373 and 1452 cm^{-1} , are due to contributions from the symmetric and asymmetric methyl bending modes, and the strong shoulder at 1417 cm^{-1} is assigned to the CH_2 scissoring for S- CH_2 groups.



In Figure 72 is shown the $[A_p(\tilde{\nu})]$ PMGRS CH stretching region for the above copolymer PS₇₅-PPS₂₅, adsorbed from cyclohexane at 34.5°C, the θ temperature for polystyrene. The CH stretching modes at 2862, 2926, 2964, 3002, 3028, 3062, and 3083 cm^{-1} are resolved for the adsorbed copolymer film. Microanalysis and GPC results indicated that the styrene block consists of 524 units, while the propylene sulfide block has 181 units, and thus 181 sulfurs. Thus each adsorbed chain would potentially tie up many more surface sites, thereby taking up more surface area/chain and blocking other chains from adsorbing. This represents the high adsorption interaction case. The styrene block extending out as tails from the adsorbed block would have greater accessible volume per chain than in the endcapped case. It is expected that upon removal of the solvent the polystyrene tails could collapse into a more relaxed state (mushrooms)⁴⁶ governed by single-chain self avoidance, whereas the propylene sulfide block would remain essentially confined to its adsorbed state conformation.

It is apparent that the aliphatic CH modes dominate in intensity relative to that of the aromatic for the copolymer case. In Figure 73 is shown the $[A_p(\tilde{\nu})]$ PMGRS CH stretching region for copolymer (PS₉₀-PPS₁₀) similarly adsorbed from cyclohexane at 34.5°C, the θ temperature for polystyrene. Although the PMGRS spectra for the two copolymers are quite similar, the asymmetric CH₃ band intensity is diminished while

FIG. 72 The $[A_p(\bar{\nu})]$ PMGRS CH stretching region for the copolymer PS₇₅-PPS₂₅, adsorbed onto a vapor deposited gold substrate from cyclohexane at 34.5°C. Resolution = 2 cm⁻¹, and scans = 1024. Surface was washed with cyclohexane at 45 °C to remove physisorbed species.

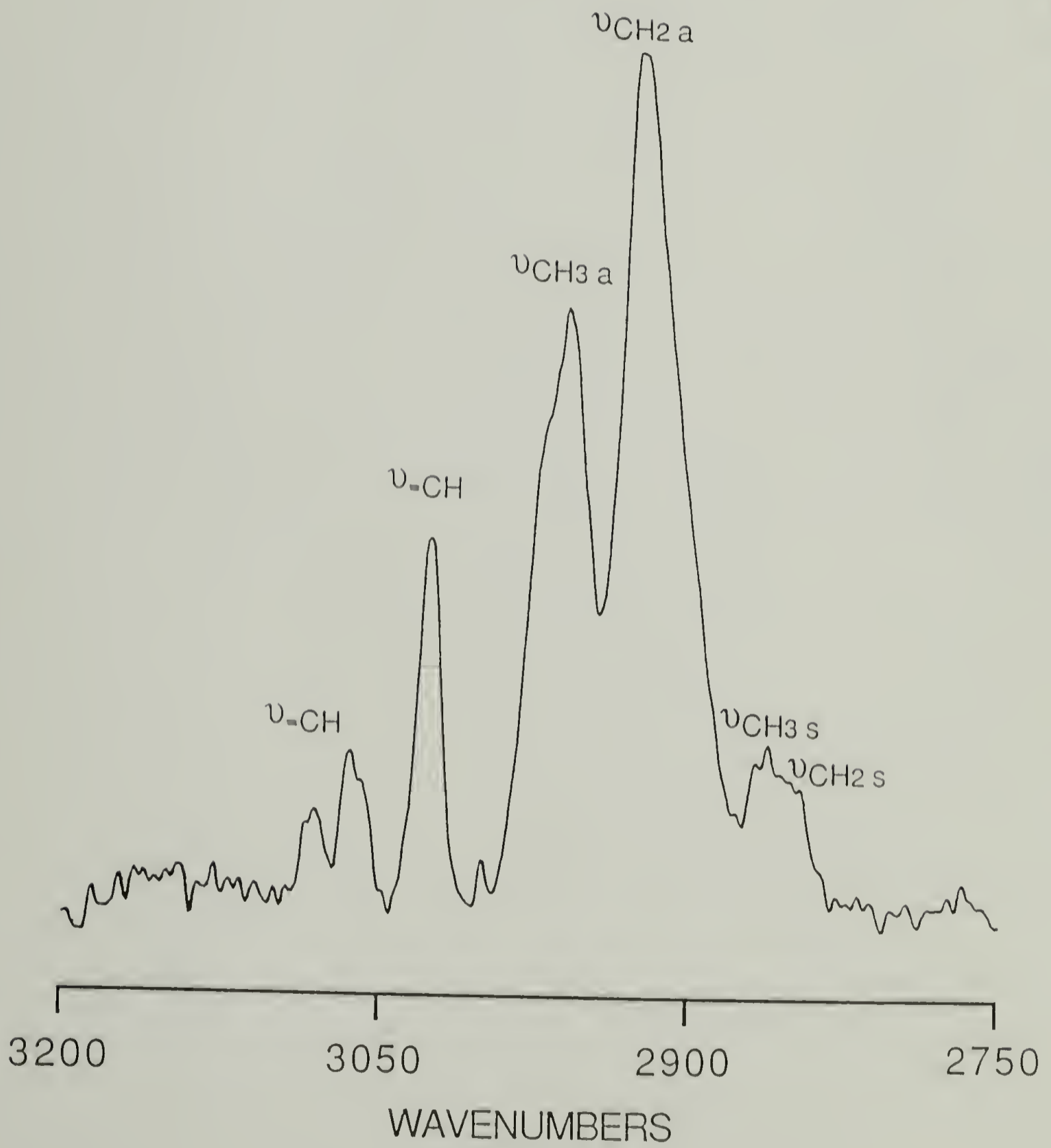
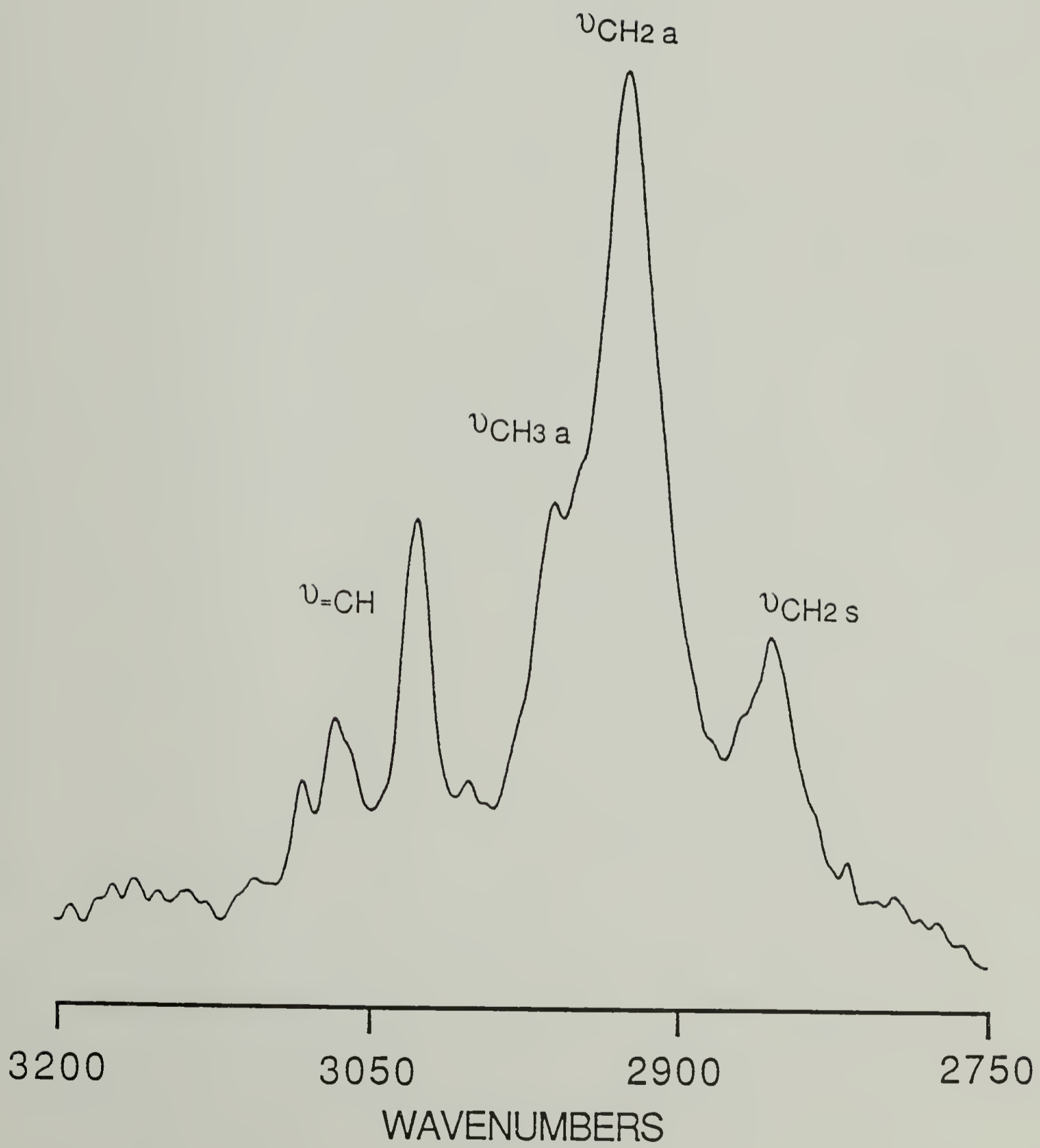


FIG. 73 The $[A_p(\tilde{\nu})]$ PMGRS CH stretching region for the copolymer PS₉₀-PPS₁₀, adsorbed onto a vapor deposited gold substrate from cyclohexane at 34.5°C. Resolution = 2 cm⁻¹, and scans = 1024. Surface was washed with cyclohexane at 45 °C to remove physisorbed species.



the symmetric CH₂ intensity is increased, from that of PS₇₅-PPS₂₅. This would be expected, due to the lower PPS block length and the correspondingly larger PS block, provided that the orientation of the PPS blocks are similar. For both copolymers, the decreased intensity of the aromatic CH stretch modes can be qualitatively attributed to the relaxed state of the polystyrene blocks relative to the surface normal. Only transition moments with components normal to surface would interact with the electric field. It is therefore expected that the aromatic intensities would decrease to a value 1/2 that from the isotropic transmission case. The aliphatic intensities also have contributions from the propylene sulfide block as noted above. Though the relative contributions can be quantitatively separated in the isotropic spectrum using a ratio of the aliphatic asymmetric stretch to the aromatic stretch, this can not be accomplished for the reflection spectrum.

The relative increase in intensities for these modes, however, can only be due to specific ordering of the propylene sulfide block due to it being anchored to the Au surface. The ratio of the asymmetric CH₂ stretch at 2926 cm⁻¹ to the aromatic mode at 3028 cm⁻¹ for the adsorbed PS₇₅-PPS₂₅ copolymer is about 2.1 while for the isotropic case it is 1.26. This represents a 67% increase in this ratio. Similarly the ratio of the asymmetric CH₃ stretch due to the propylene sulfide, to the aromatic stretch is about 1.2 for

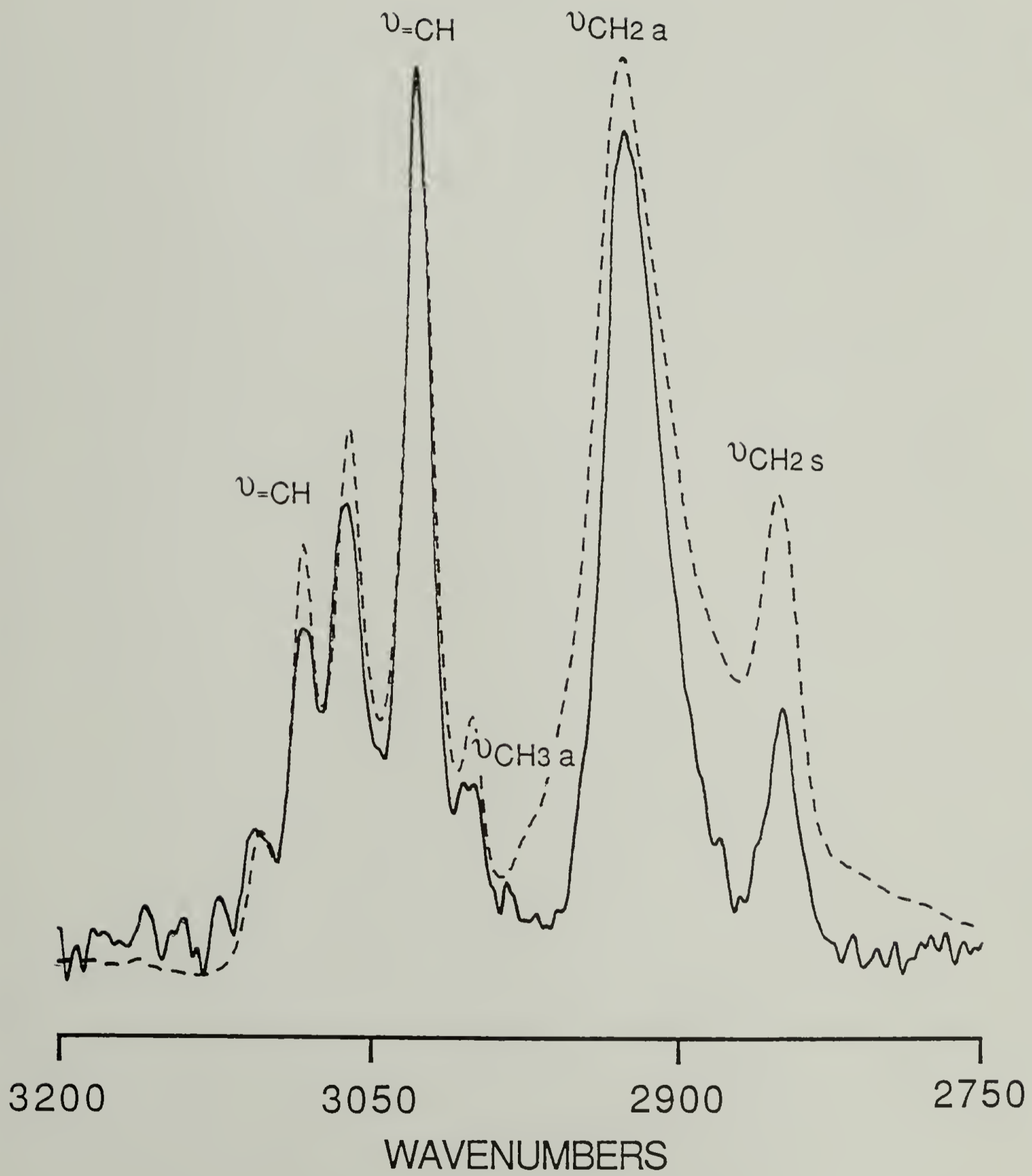
the adsorbed copolymer and 0.50 for the isotropic case. This represents a 140% increase. The propylene sulfide block can not be randomly oriented with respect to the Au normal, and in fact must have a high orientation relative to the surface.

In Figure 74 is shown the $[A_p(\bar{\nu})]$ PMGRS CH stretching region (solid) for the copolymer PS₉₅-PPS₅, also adsorbed from cyclohexane at 34.5°C, the θ temperature for polystyrene. The stoichiometric C/S ratio for PS₉₅-PPS₅ is 155:1 versus 75:1 and 27:1 for PS₇₅-PPS₂₅ and PS₉₀-PPS₁₀ respectively. The grafting density of PS₉₅-PPS₅ should be higher than the other copolymers and similar to the thiol endcapped case. The intensities exhibited in the CH stretching region, relative to the isotropic spectrum (dashed), closely resemble those exhibited by the endcapped polymer in Figure 67. This result is reasonable based upon the XPS C/Au ratio of 33.6/15° for PS₉₅-PPS₅ compared to 19.0/15° for PS₉₀-PPS₁₀ with the same degree of polymerization. The C/Au ratio, thickness and grafting density are related to the degree of orientation in the polystyrene block. Only 5% of this copolymer is not polystyrene, so the chain orientation can be calculated as for the endcapped case without accounting for the propylene sulfide block contribution.

Transition From Anisotropic to Isotropic

The average angles from the symmetric and asymmetric transition moments, and the chain axis, to the surface normal

FIG. 74 The $[A_p(\tilde{\nu})]$ PMGRS CH stretching region for the copolymer PS₉₅-PPS₅, adsorbed onto a vapor deposited gold substrate from cyclohexane at 34.5°C. Resolution = 2 cm⁻¹, and scans = 1024. Surface was washed with cyclohexane at 45 °C to remove physisorbed species.



(Z), are listed in Table 13 for both the endcapped polymer and PS₉₅-PPS₅. The calculated average chain axis orientation relative to the z axis is also compared. The orientation of the polystyrene chain is higher for the PS₉₅-PPS₅ adsorbed film (0.29) than for the endcapped polystyrene (0.22). Referring to the data on uniaxially drawn polystyrene⁵⁴ the orientation function value of 0.29 corresponds to a draw ratio of about 9.0. That this copolymer orientation is higher can be attributed to the slightly longer strongly interacting part of the structure. The length is sufficiently long to enable a high grafting density, but not so long that each individual chain takes up too much surface area, as is the case for the copolymers with longer propylene sulfide blocks.

The polarization modulation infrared reflection results thus indicate that a structural transition occurs in the adsorbed copolymer films between 95:5 and 90:10 molar ratios for a degree of polymerization around 600. The transition from anisotropic to an isotropic polystyrene conformation is related to the XPS film thickness, and thus the grafting density. These films are too thin to consider a microphase separated structure since the interfacial region for block copolymers is of the same thickness. Segregation in the chemical composition, however, does exist as shown by XPS. The degree of segregation is related to the propylene sulfide block length as expected. These results suggest that the

TABLE 13. Table showing the average angles from the symmetric, θ_s , and asymmetric, θ_{as} , transition moments, and the chain axis, θ_c , to the surface normal (Z), and the corresponding average transition moment and segmental orientation for ultra thin films prepared by adsorption of thiol endcapped polystyrene and copolymer PS₉₅-PPS₅.

TABLE 13

Segmental Orientation of Polystyrene

	PS (thiol endcap)	PS ₉₅ -PPS ₅
θ_s	63.9°	60.8°
θ_{as}	44.4°	48.2°
θ_c	46.3°	43.3°
f_s	-0.21	-0.14
f_{as}	-0.27	0.17
f_c	0.22	0.29

important factor in adsorption of copolymers with one strongly interacting block is the length of the block relative to the overall degree of polymerization. If the interaction strength is sufficiently large then a critical block length will exist which will determine whether the buoy structure can form an oriented brush in solution and a collapsed oriented ultra thin film.

References

1. Kawaguchi, M.; Kenji, K.; Takahashi, A. *Polym. J.* **1982**, *14*, 7, 563.
2. Kawaguchi, M.; Maeda, K.; Kato, T.; Takahashi, A. *Macromolecules* **1984**, *17*, 1666-1671.
3. Kawaguchi, M.; Sakai, A.; Takahashi, A. *Macromolecules* **1986**, *19*, 12, 2952-2955.
4. Greenler, R. G. *J. Chem. Phys.* **1969**, *50*, 5, 1963-1968.
5. Ohnisi, T.; Ishitani, A.; Ishida, H.; Yamamoto, N.; Tsubomura, H. *J. Phys. Chem.* **1978**, *82*, 1989.
6. Ishitani, A.; Ishida, H.; Soeda, F.; Nagasawa, Y. *Anal. Chem.* **1982**, *54*, 682-687.
7. Allara, D. L.; Swalen, J. D. *J. Phys. Chem.* **1982**, *86*, 2700-2704.
8. Allara, D. L.; Nuzzo, R. G. *Langmuir* **1985**, *1*, 45-52.
9. Allara, D. L.; Nuzzo, R. G. *Langmuir* **1985**, *1*, 52-66.
10. Rabolt, J. F.; Burns, F. C.; Schlotter, N. E.; Swalen, J. D. *J. Chem Phys.* **1983**, *78*, 2, 946-952.
11. Schlotter, N. E.; Rabolt, J. F. *Applied Spectroscopy* **1985**, *39*, 6, 994-996.
12. Rabolt, J. F.; Jurich M.; Swalen, J. D. *Applied Spectroscopy* **1985**, *39*, 2, 269-272.
13. Naselli, C.; Rabolt, J. F.; Swalen, J. D. *J. Chem. Phys.* **1985**, *82*, 4, 2136-2140.
14. Nuzzo, R. G.; Fusco, F. A.; Allara, D. L. *J. Am. Chem. Soc.* **1987**, *109*, 2358-2368.

15. Porter, M. D.; Bright, T. B.; Allara, D. L.; Chidsey, C. E. D. *J. Am. Chem. Soc.* **1987**, *109*, 3559-3568.
16. Nevin, S. R.; Pearce, E. M. *Polymer Letters* **1965**, *3*, 487-490.
17. Morton M.; Kammereck, R. F.; Fetters, L. J. *Macromolecules* **1971**, *4*, 1, 11-15.
18. Nuzzo, R. G.; Zegarski, B. R.; Dubois, L. H. *J. Am. Chem. Soc.* **1987**, *109*, 733-740.
19. Kolthoff, I. M.; Gutmacher, R. G. *J. Phys. Chem.* **1952**, *56*, 740-745.
20. Frisch, H. L.; Hellman, M. L.; Lundberg, J. L. *J. Polym. Sci.* **1959**, *38*, 441.
21. Felter, R. E.; Moyer, E. S.; Ray Jr., L. N. *J. Polym. Sci.* **1969**, *B7*, 529-533.
22. Felter, R. E.; Ray Jr., L. N. *J. Colloid Interface Sci.* **1970**, *32*, 349.
23. Koopal, L. K.; Lyklema, J. *J. Chem. Soc., Faraday Discuss.* **1975**, *59*, 230.
24. Howard, G.J.; Woods, S.J. *J. Polym. Sci., A-2* **1972**, *10*, 1023-1028.
25. Sadakne G. S.; White, J. L. *J. Appl. Polym. Sci.* **1973**, *17*, 453.
26. Linden, C. V.; Leemput, R. V. *J. Colloid Interface Sci.* **1978**, *67*, 48-62.
27. Linden, C. V.; Leemput, R. V. *J. Colloid Interface Sci.* **1978**, *67*, 63-69.

28. Cohen Stuart, M. A.; Scheutjens, J. M. H. M.; Fleer, G. *J. J. Polym. Sci.: Polym. Phys. Ed.* **1980**, *18*, 559-573.
29. Stromberg, R. R.; Tutas, D. J.; Passaglia, E. J. *Phys. Chem.* **1965**, *69*, 11, 3955-3963.
30. Peyser, P.; Stromberg, R. R. *J. Phys. Chem.* **1967**, *71*, 2066.
31. Takahashi, A.; Kawaguchi, M.; Hirota, H.; Kato, T. *Macromolecules* **1980**, *13*, 4, 884-889.
32. Kawaguchi, M.; Takahashi, A. *J. Polym. Sci.: Polym. Phys. Ed.* **1980**, *18*, 2069-2076.
33. Kawaguchi, M.; Hattori, S.; Takahashi, A. *Macromolecules* **1987**, *20*, 178-180.
34. Stouffer, J. M.; McCarthy, T. J. *Macromolecules* **1988**, *21*, 5, 1204-1208.
35. Marques, C.; Joanny, J. F.; Leibler, L. *Macromolecules* **1988**, *21*, 4, 1051-1059.
36. Rossi, G.; Cates, M. E. *Macromolecules* **1988**, *21*, 5, 1372-1377.
37. Munch, M. R.; Gast, A. P. *Macromolecules* **1988**, *21*, 5, 1366-1372.
38. Theodorou, D. N. *Macromolecules* **1988**, *21*, 5, 1411-1421.
39. Theodorou, D. N. *Macromolecules* **1988**, *21*, 5, 1422-1436.
40. Griot, O.; Kitchener, J. A. *Trans. Faraday Soc.* **1965**, *61*, 1026.
41. Joppien, G. R. *Makromol. Chem.* **1975**, *176*, 1129.
42. Smith, T. J. *J. Colloid Interface Sci.* **1980**, *75*, 51.

43. Schrader, M. E. *J. Colloid Interface Sci.* **1984**, *100*, 372.
44. See chapter 6 for details of experimental setup.
45. Kirshenbaum, I. *J. Polymer Sci.* **1965**, *3A*, 1869-1875.
46. de Gennes, P. G. *Adv. Colloid and Interface Sci.* **1987**, *27*, 189-209.
47. Scheutjens, J. M. H. M.; Fleer, G. J. *J. Phys. Chem.* **1980**, *84*, 178-190.
48. Grant, W. H.; Smith, L. E.; Stromberg R. R. *Discuss. Faraday Soc.* **1975**, *59*, 209-217.
49. Pefferkorn, E.; Carroy, A.; Varoqui, R. *J. Polym. Sci.: Polym. Phys. Ed.* **1985**, *23*, 1997.
50. Pefferkorn, E.; Haouam, A.; Varoqui, R. *Macromolecules.* **1988**, *21*, 2111.
51. Milner, S. T.; Witten, T. A.; Cates, M. E. *Macromolecules* **1988**, *21*, 8, 2610-2619.
52. Clark, D. T. *Advances in Polymer Science* **1977**, *24*, 125.
53. de Gennes, P. G. *Scaling Concepts* **1987**, *27*, 189-209.
54. Jasse, B.; Koenig, J. L. *J. Polym. Sci: Polym. Phys. Ed.* **1979**, *17*, 799.
55. Liang, C. Y.; Krimm, S. *J. Polym. Sci.* **1958**, *27*, 241-254.
56. Ouada, H. B.; Hommel, H.; Legrand, A. P.; Balard, H.; Papirer, E. *J. Colloid Interface Sci.* **1988**, *112*, 2, 441-449.

CHAPTER 8

SUMMARY AND SUGGESTIONS FOR FUTURE STUDY

This chapter summarizes results, and suggests future directions pertaining to the presented two part study of polymer microstructure by vibrational spectroscopy. Specific vibrational modes are utilized to characterize chain conformation and packing in 1) A Spectroscopic Investigation of Crystal Morphology in Semi-crystalline Polymers, and segmental chain orientation with respect to a director axis in 2) A Spectroscopic Investigation of Restricted Geometries in Monolayers of Adsorbed Polymers. Background relating to the specific areas of study, and a brief survey of the content in the respective chapters is contained in Chapter 1.

Chapter 2 provides a background discussion of the longitudinal acoustic mode (LAM) and establishes its usefulness as a morphological tool for the study of long range crystal structure in linear aliphatic polyesters. The basis for choosing linear aliphatic polyesters for such a study is established. These polymers enable the effects on the LAM vibration, of regularly spaced asymmetric mass placements, to be studied.

Chapter 3 contains the details of a Raman spectroscopic study, of the long range crystal structure in dilute solution grown single crystals of linear aliphatic polyesters. The

frequency of the LAM normal mode vibration is inversely related to the crystal stem length. It is thus utilized to directly determine the crystal stem length, the existence and/or incorporation of defects contained within the crystalline core, and the attainable lamellar thickness. The characteristics of the CH₂ bending modes are examined to provide structural details concerning crystalline packing.

The lowest frequency band observed in the Raman spectrum is assigned to the LAM-1 mode for both even-even and odd-odd linear aliphatic polyesters. This conclusion is based upon the frequency, halfwidth, and intensity characteristics of this band, as a function of crystallization and annealing conditions. The intensity of the band is comparable to that of the CH₂ twist and A_g CH₂ bending vibrational modes. The band shifts to lower frequency for crystals grown at higher T_{cryst}, and for crystals annealed at temperatures within 10° C of their melting point. The consequential thickening of lamellae is supported by complementary SAXS results. The band shifts only slightly upward in frequency, when the crystal unit cell is densified by cooling to temperatures below -100 °C, as observed for *n*-alkanes and polyethylene.

The existence of resolvable multiple low frequency components is a distinct characteristic in the Raman spectra of linear aliphatic polyester single crystals. This is particularly the case when such crystals are grown under well defined conditions resulting in a narrowed distribution in

lamellar thickness. The frequency and relative intensity of these components differ as a function of the chemical structure, but multiple bands occur for all conditions studied. These polyesters have one significant structural difference as compared to polyethylene. This arises from the regularly spaced carbonyl groups in the chemical structure. In addition there is an odd-even effect on the placement of the carbonyls with respect to the chain axis.

Chapter 4 contains the results from normal coordinate analysis on model oligomers of linear aliphatic polyesters. These calculations were carried out to investigate the affect of inclusion of off-axis masses (carbonyl groups) on the LAM vibration in transplanar structures. The premise was that an asymmetric mass distribution could cause coupling of longitudinal and transverse vibrations. This could then account for the unusual observations in the low frequency region of the Raman spectra in Chapter 3. The oligomeric structures provided a unique opportunity to determine whether; 1) Regularly spaced off-axis masses can cause such coupling in transplanar backbones and 2) Can this coupling result in a significant redistribution of intensities.

Effects upon LAM-1 due to the overall length of the chain, chain segments of ether or ester linkages, and odd-even versus even-even structures, were investigated. The assumption of single chain structure with the point-mass approximation was used. Since only the skeletal modes are of

interest, the force field was developed in a point-mass approximation specifically to analyze these. Results are based upon calculated intensities and atomic motions for the LAM-1 and other modes of similar frequency.

A LAM-1 characterized by centrosymmetric in-plane longitudinal atomic motions was identified for all oligomers considered. In the case of even-even oligomers, particularly those with overall chain length below 90 Å, additional LAM-1 like modes were calculated at nearby frequencies. These exhibited more complex atomic motions with significant transverse in-plane contributions to the atom displacements. For the odd-even oligomers, however, the existence of a few LAM-like modes over a narrow frequency range, each with reduced intensity from the unperturbed case, is not indicated. The computed results therefore do not agree with the experimentally observed relative intensities for polyester (9-8). Neither an asymmetric band envelope, nor multiple components with significant intensity are predicted. Calculations on longer oligomers should be carried out to determine if there is a length dependence for coupling in the odd-even case that is different from the even-even case.

Intensities of the LAM-like vibrations, for both odd-even and even-even oligomers, are estimated by using the bond polarizability theory. The validity of this intensity calculation depends on an accurate assessment of the polarizability change of each bond and angle. These values

are not well established for any bond or angle internal coordinate that involves oxygen. In this study the ester groups only comprise a small portion of the chain segments. Intensities of LAM-like modes were determined with the polarizabilities of the coordinates of the ester groups set to those of *n*-alkanes. These compared closely with intensities that did not include contributions from internal coordinates involving ester groups.

The geometrical relationship of off-axis masses, relative to the chain length center, affects the resultant contribution of transverse in-plane motions to the vibration identified as LAM-1. The methylene sequence end group structure for (9-8)₄ corresponds to the most symmetric carbonyl arrangement. It had the smallest contribution of transverse in-plane motions to the LAM-1 vibrational mode. Significant contributions of transverse in-plane motions to the LAM-1, occurred long the entire backbone of the (9-8)₄ oligomers for the other possible end group structures. Furthermore, the results indicate that the phase relationship of the calculated transverse motions is not due to specific internal methylene sequence lengths. Instead it is a function of the overall chain length, and is independent of the carbonyl group positions along the backbone.

The cohesive forces in aliphatic polyesters are greater than those in the hydrocarbon chains, while the melting points of these polyesters are much lower. Distances between

atoms in neighboring molecules are characteristic of van der Waals forces. Cross-sectional areas for decamethylene polyesters are $\sim 37 \text{ \AA}^2$, or practically the same as for aliphatic hydrocarbon chains. Since there is no indication of abnormally short interchain spacings, strong forces do not exist between particular atoms of neighboring molecules. The higher cohesive forces, which can be estimated by group contribution methods, are due to the dipoles in the ester groups. Lower melting points result from enhanced molecular flexibility due to the relative ease of rotation about the O-CH₂ bonds. The polymorphism exhibited by both even-even and odd-even linear aliphatic polyesters may arise from such backbone flexibility. This could cause specific disorder to occur in the crystalline phase, such as irregularity in the protrusion of ester groups along the chain.

Crystalline packing changes in single crystal mats, as a function of annealing and supercooling, are supported by band shifts in the low frequency and CH₂ bending regions of the Raman spectra of polyester (9-8). Thermal analysis (DSC), and either electron or x-ray diffraction coupled with a heat stage, could be utilized to verify the above premise. Initial DSC experiments were carried out on polyester (9-8). For the $T_{\text{cry}} = 27 \text{ }^\circ\text{C}$ mat, two narrow endotherms of different ΔH were exhibited at 60.5 and 70.4 $^\circ\text{C}$ respectively. These are due to melting, while the small narrow exotherm separating them can be attributed to recrystallization. A

second and third heating exhibited only one narrow endothermic transition at 69.7 °C. Identical heating conditions for (9-8), $T_{\text{cry}} = 33$ °C, resulted in only one broad endotherm at 70.0 °C, with a small shoulder at 61 °C. Stable crystals can exhibit multiple melting endotherms which are often representative of crystalline lamellae of different discrete thicknesses. This can be interpreted in terms of partial thickening during isothermal growth. The LAM-1 and SAXS data, however, do not support the existence of multiple lamellar thicknesses.

If n times folded polyester single crystals are metastable with respect to $n-1$ times folded ones then chain unfolding (crystal thickening) may occur during heating in the DSC. This would appear either as; 1) Stepwise crystal thickening, or 2) Gradual thickening of folded chain crystals upon heating. In the first case two distinct melting peaks would occur. A decreasing population of the second (high temperature) peak area as compared to the first, is expected when the rate of heating is increased. Absence of an exothermic peak during this thickening process for unstable crystals, would indicate that the chain unfolding does not involve large scale melting followed by recrystallization. Instead, these two processes occur simultaneously, as verified by microscopy. In the second case only one endothermic transition would be observed. The T_m peak value

is expected to increase as the heating rate decreases toward zero. This set of experiments should be carried out.

If neither case is exhibited then the native crystals are either stable until completion of their melting, or undergo changes in crystalline packing. Chains in stable crystals unfold to the lower value of n during crystal growth rather than during heating. Thickening will not be observed by DSC, SAXS, or Raman. The Raman and SAXS results clearly establish that stable crystals do not exist for linear aliphatic polyesters grown under the conditions in this study. This is not surprising since most folded chain polymer crystals are unstable. The large increase in lamellar thickness for polyester (9-8), $T_{\text{cry}} = 27 \text{ }^\circ\text{C}$, as determined from the LAM-1 mode, occurs at the lower endotherm transition. The small increase in thickness ($\sim 6 \text{ \AA}$) between 62 and 66 $^\circ\text{C}$, takes place during the recrystallization process. The concurrent appearance of the 1424 and $\sim 32 \text{ cm}^{-1}$ bands above 62 $^\circ\text{C}$, which are the frequencies exhibited by (9-8), $T_{\text{cry}} = 33 \text{ }^\circ\text{C}$, and the disappearance of the 1418 cm^{-1} band, is not due to thickening lamellae. It can, however, be attributed to an unstable monoclinic crystal which forms a thickened one with stable orthorhombic packing. The low frequency modes not assigned to LAM-1, are expected to be transverse acoustical modes of various phase values from the ν_9^{a} and ν_9^{b} branches. Different crystalline packing affects both the number and frequency of these modes for n -alkanes.

The low frequency spectra for (9-8), grown at 27 and 33 °C, become identical after annealing to the highest temperatures.

Chapter 5 details the procedures utilized for anionic synthesis of functionalized polystyrenes. Thiol endcapped polystyrene, and block copolymers of styrene and propylene sulfide, were synthesized as model polymers for adsorption studies on vapor deposited gold surfaces. Particular care was taken to insure low polydispersity, similar overall degree of polymerization, and stable endcapping to prevent depolymerization of the propylene sulfide block. In addition disulfide linkages were cleaved and stably endcapped to eliminate the fraction of triblock copolymers that form due to oxidative coupling. Size exclusion chromatography results are presented for the polymers used in the spectroscopic part of the study.

The second study (Chapters 6 and 7) investigates the structure of ultra-thin polymer films adsorbed from dilute solution onto external metallic substrates. A necessary condition for adsorption of polymers to a surface, is that the cumulative magnitude of the binding energy (surface-segment interactions) be sufficient to overcome both the resulting enthalpic and entropic barriers. The magnitude of the specific interactions, between available surface sites of a gold substrate and the sulfur functional groups, is increased substantially over the typical nonbonded and/or weak hydrogen bonding surface/ segment interaction energies.

The degree of polymerization of the polymers in this study is low enough, so the specific S-Au interactions dominate the energetics of the typical surface/segment binding energy contribution to the overall ΔG_{ads} . These chemically modified polystyrenes therefore decrease the dependence of adsorption and thickness on the thermodynamic quality of the solvent.

Adsorption of these polystyrenes is influenced by their chemical composition, with the endcap case enabling the highest grafting density and the longest propylene sulfide block copolymer the lowest. The molecular dimensions over which interactions with the metal surface exist, can be altered because of the sulphur containing structural units. To obtain information concerning the molecular packing and orientation of chains in ultra thin polymer films, an approach such as direct differential polarization acquisition is required. This method enables the greatest spectral contrast to be achieved, so that the selectivity and specificity advantages of infrared spectroscopy can be realized. The polarization modulation technique, coupled with grazing incidence external reflection infrared spectroscopy, enables vibrational spectra of adsorbed polymeric surface species to be obtained. The details, and advantages of the differential method optimized in this study, are contained in Chapter 6. The procedure for alignment, removal of the DC offset from the s-polarized reflection component, and the details of the phase sensitive

lock-in detection, are critical in enhancing the sensitivity of this experimental method.

Chapter 7 contains results for evaluation of the ultra-thin adsorbed polymer films from three different but complementary characterization methods. X-ray photoelectron spectroscopy (XPS) is used both to establish the existence of the adsorbed polymer interface and to measure the chemical composition of the adsorbed films as a function of distance from the substrate. Thickness of the adsorbed ultra thin polymer films are also determined. Dynamic contact angle measurements are sensitive enough to indicate that the polymer monolayers constitute interfaces having low interfacial free energies. Reflection and transmission infrared spectroscopy is used to determine the existence of anisotropy within the film structure, as a function of PPS block length dependent grafting density.

Evidence that adsorption of these functionalized polystyrenes occurred was determined by 1) Dynamic contact angle measurements at the air/water interface, and 2) The presence of the S_{2p} photoemission, and a $\pi \rightarrow \pi^*$ shake up component in the photoemission from the C_{1s} core level measured by XPS. Contact angle measurements, averaged over multiple locations on each film, typically changed from $\theta_A/\theta_R = 65^\circ/15^\circ$ for the Au surface to $85^\circ/60^\circ$ for the adsorbed film. This indicates that the polymer surface resembles polystyrene at close proximity to the air/film interface. A

decrease in Au core level intensities relative to the Au substrate, and an increase in the C_{1s} intensity indicates that an adsorbed overlayer exists. The atomic composition ratio for C/Au, must exceed 3.0 at 75° takeoff for an adsorbed 10 Å polymer layer. Values at 75° ranged from 7.3 to 9.3 for the block copolymers studied, and up to 13.5 for the endcapped case, and from 19 to 33.6 and 73.1 respectively at 15°.

In multiplex spectra for the C_{1s} region the $\pi \rightarrow \pi^*$ component, due to the polystyrene block, is evident in the 15° spectrum. At a takeoff angle of 75° the $\pi \rightarrow \pi^*$ intensity is diminished relative to that of the C_{1s} core level, for each of the block copolymers. It can therefore be surmised that the propylene sulfide block resides at or near the Au/polymer interface, in the adsorbed copolymers, while the polystyrene domains are excluded to regions nearer the air/film surface. Depth profiles of the C_{1s} and Au_{4f} compositions are linear but opposite in behavior suggesting film uniformity.

Compositional information for the adsorbed film, was determined by utilizing XPS to obtain angle resolved atomic ratios. This depth resolution capability enabled the existence of heterogeneous chemical composition in the ultra thin adsorbed polymer films to be determined. Increases in sulfur composition, and decreasing values for the C/S atomic ratios, occurred for all the copolymers as a function of increasing takeoff angle. The C/S ratios plateau at increasingly higher angles, 50° and 60° for PS₇₅-PPS₂₅ and

PS₉₀-PPS₁₀ respectively. For PS₉₅-PPS₅ the decreasing ratio did not plateau, but did exhibit some nonlinearity at high takeoff angles. These results indicate that the propylene sulfide block must occupy both trains at the Au interface and loops near it. The differences in the C/S depth profiles suggest that the majority of the propylene sulfide block is located within an increasingly narrow region of depth, at the gold interface, as the molar ratio of the propylene sulfide block decreases from 25 % to 10 % to 5 %. Differences in the thickness of the region containing train structures, can be theoretically modeled by use of XPS intensity relations.

Film thickness was determined by the extent of attenuation of the absolute intensity of the Au_{4f} core level before and after adsorption. This method was shown to have both high precision ($\pm 2 \text{ \AA}$) and sensitivity, contrary to ellipsometry results. All adsorbed films were on the order of 35 \AA or less in thickness. This method could be used to compare film thickness for endcapped and/or block copolymers, as a function of block ratio, overall molecular weight, substrate, and solvent quality. Stability of the chemical and structural anisotropy could be investigated at elevated temperatures using *insitu* XPS. Polystyrene sequences separated by butadiene or isoprene linkages could be synthesized and functionalized for a particular substrate. Novel chain architectures may develop during adsorption, depending upon the length of these sequences, the overall

degree of polymerization, solvent conditions, and tailored functionality. Thickness in solution could be monitored by ellipsometry and compared to the collapsed film state.

The polymer concentration in the bulk solution (1 mg/ml) corresponds to the dilute regime. The concentration of polymer chains in the adsorbed film, however, exceeds that of the solution the polymer condensed from by factors as high as ~ 1000 . In order to achieve a continuous amorphous film of a certain thickness, the local concentration at the surface must be considerably greater than what exists at the overlap concentration. This implies that structural anisotropy, which necessitates elongated chain conformations, results directly from a sufficient degree of chain overlap at the surface. The greater the film thickness for a given molecular weight, the greater the required grafting density and resulting chain orientation. Reflection infrared spectroscopy was used to examine the degree of structural anisotropy, as a function of copolymer molar block ratios, for the case when only one block is strongly attracted to the gold surface.

The ratio of the single beam spectrum obtained via polarization modulation, to that without, is directly proportional to the difference in absorptions for the IR beam polarized perpendicular and parallel to the scattering plane, $(A_s(\tilde{\nu}) - A_p(\tilde{\nu}))$. Since the adsorbed films in this study are on the order of 30 Å thick, there exists within this layer

only a node for $\mathbf{E}_{s,r}$, the electric field component polarized perpendicular to the scattering plane. Transition dipoles oriented in this direction will not adsorb the incident radiation. The final ratioed spectrum will therefore only exhibit an intensity proportional to $[-A_p(\bar{\nu})]$. Absorbance bands in isotropic spectra of the copolymers (dispersions in KBr), have different relative intensities than corresponding ratios in spectra from grazing incidence reflection infrared measurements of the adsorbed films. The intensity ratio of the aliphatic CH_2 stretching vibrations for adsorbed films can be represented in terms of the inherent transition moment strengths from isotropic data, and any modification of that absorbance arising from orientation of the CH_2 groups.

The details of a general orientation model based solely on intensity ratios, is outlined in Chapter 7. This model is utilized to determine the degree of anisotropic segmental orientation in ultra thin films without forgoing factors such as twisting of segments within and between chains. The magnitudes of the conformational insensitive C-H stretch transition dipole moments, for the bulk and adsorbed states, are not expected to differ, since the observed peak positions and bandshapes are similar. The C-H intensity ratios are utilized to determine the average transition moment angles for the aliphatic CH_2 asymmetric and symmetric stretching modes, with respect to the normal to the adsorbed layer surface. From these angles, the Hermans orientation

function values for the aliphatic CH₂ transition moments are obtained. These values can then be related to the average angle between the local chain axis and the surface normal, thereby representing the average segmental orientation.

The average segmental orientation of the polystyrene block in the adsorbed thiol endcapped polystyrene, and PS₉₅-PPS₅, is 0.22 and 0.29 respectively. The adsorbed chains are oriented such that they extend outward from the Au surface. In fact an atactic polystyrene film oriented to this degree would require draw ratios of about 7.0 and 9.0. The higher value for the copolymer orientation can be attributed to the slightly longer strongly interacting part of the structure. The length is sufficient to enable a high grafting density, but not so long that each individual chain takes up too much surface area, as is the case for the copolymers with longer propylene sulfide blocks. When the solvent is removed, the brush structure present in solution due to the high grafting density is not able to collapse completely. This results from the interchain interactions effected by their close proximity. For PS₇₅-PPS₂₅ and PS₉₀-PPS₁₀ the grafting density is lower, resulting in thinner adsorbed films with no preferred orientation in the polystyrene backbone. Specific orientations of the propylene sulfide block and/or the styrene phenyl ring, can be determined if a quarter waveplate is utilized in the polarization modulation reflection setup. This enables further structural analysis of the polymers.

BIBLIOGRAPHY

1. Allara, D. L.; Nuzzo, R. G. *Langmuir*, **1985**, *1*, 45-52.
2. Allara, D. L.; Nuzzo, R. G. *Langmuir*, **1985**, *1*, 52-66.
3. Allara, D. L.; Swalen, J. D. *J. Phys. Chem.*, **1982**, *86*, 2700-2704.
4. Barnes, J. D.; Fanconi, B. M. *J. Chem. Phys.*, **1972**, *56*, 5190.
5. Bates, R. B.; Kroposki, L. M.; Potter, D. E. *J. Org. Chem.*, **1972**, *37*, 560.
6. Blundell, D. J.; Keller, A.; Kovacs, A. J. *J. Polym. Sci.: Part B*, **1966**, *4*, 481.
7. Blundell, D. J.; Keller, A.; *J. Macromol. Sci.*, **1968**, *B2*, 301.
8. Blundell, D. J.; Keller, A.; *J. Macromol. Sci.*, **1968**, *B2*, 337.
9. Boerio, F. J.; Bahl, S. K.; McGraw, G. E. *J. Polym. Sci.: Polym. Phys. Ed.*, **1976**, *14*, 1029.
10. Boileau, S.; Sigwalt, P. *Compt. Rend.*, **1961**, *252*, 882.
11. Campos-Lopez, E.; Leon-Gross, A; Ponce Velez, M. A. *J. Polym. Sci.*, **1973**, *11*, 3021.
12. Chang, C. Ph.D. Thesis, University of Michigan, **1983**.
13. Chang, C.; Krimm, S. *J. Polym. Sci.: Polym. Phys. Ed.*, **1979**, *17*, 2163.
14. Chang, C.; Krimm, S. *J. Appl. Phys.*, **1983**, *54*, 10, 5526.
15. Chang, C.; Krimm, S. *J. Polym. Sci.: Polym. Phys. Ed.*, **1984**, *22*, 1871.
16. Chang, C.; Wang, Y. K.; Waldman, D. A.; Hsu, S. L. *J. Polym. Sci.: Polym. Phys. Ed.*, **1984**, *22*, 2185.
17. Chatani, Y.; Okita, Y.; Tadakoro, H.; Yamashita, Y. *Polym. J.*, **1970**, *1*, 555.
18. Clark, D. T. *Advances in Polymer Science*, **1977**, *24*, 125.
19. Cleland, W. W.; *Biochemistry*, **1964**, *3*, 4, 480.

20. Cohen Stuart, M. A.; Scheutjens, J. M. H. M.; Fleer, G. *J. J. Polym. Sci.: Polym. Phys. Ed.*, **1980**, *18*, 559-573.
21. Conti, G.; Minoni, G.; Zerbi, G. *J. Molec. Struc.*, **1984**, *118*, 237.
22. Cooper, W.; Hale, P. T.; Walker, J. S. *Polymer*, **1974**, *15*, 175.
23. Ditchburn, R. W. *Light 3rd ed.*, **1977**, Academic Press.
24. Dlugosz, J.; Fraser, G. V.; Grubb, D.; Keller, A.; Odell, J. A.; Goggin, P. L. *Polymer*, **1976**, *17*, 471.
25. Dowrey, A. E.; Marcott, C. *Applied Spectroscopy*, **1982**, *36*, *4*, 414-416.
26. Fanconi, B.; Crissman, J. *J. Polym. Sci.: Polym. Lett. Ed.*, **1975**, *13*, 421.
27. Felter, R. E.; Moyer, E. S.; Ray Jr., L. N. *J. Polym. Sci.*, **1969**, *B7*, 529-533.
28. Felter, R. E.; Ray Jr., L. N. *J. Colloid Interface Sci.*, **1970**, *32*, 349.
29. Flory, P. J. *Statistical Mechanics of Chain Molecules*, **1967**, John Wiley & Sons, Inc., N.Y.
30. Folkes, M. J.; Keller, A.; Stejny, J.; Goggin, P. L.; Fraser, G. V.; Hendra, P. J. *Colloid Polym. Sci.*, **1975**, *253*, 354.
31. Fraser, G. V.; *Polymer*, **1978**, *19*, 857.
32. Fraser, G. V. *Ind. Journ. Pure & Appl. Phys.*, **1978**, *16*, 344.
33. Fraser, G. V.; Hendra, P. J.; Cudby, M. E. A.; Willis, H. A. *J. Mater. Sci.*, **1974**, *9*, 1270.
34. Fraser, G. V.; Keller, A.; George, E. J.; Dreyfuss, D. *J. Macromol. Sci. Phys.*, **1979**, *B16*, 295.
35. Fraser, R. D. B. *J. Chem. Phys.*, **1953**, *21*, 1511.
36. Fraser, R. D. B. *J. Chem. Phys.*, **1956**, *24*, 89.
37. Fraser, R. D. B. *J. Chem. Phys.*, **1958**, *28*, 1113.
38. Frisch, H. L.; Hellman, M. L.; Lundberg, J. L. *J. Polym. Sci.*, **1959**, *38*, 441.

39. Fuller, C. S.; Erickson, C. L. *J. Am. Chem. Soc.*, **1937**, *59*, 344.
40. Fuller, C. S.; Frosch, C. J. *J. Am. Chem. Soc.*, **1939**, *61*, 2575.
41. Fuller, C. S.; Frosch, C. J. *J. Phys. Chem.*, **1939**, *43*, 323.
42. Fuller, C. S.; Frosch, C. J.; Pape, N. R. *J. Am. Chem. Soc.*, **1942**, *64*, 154.
43. de Gennes, P. G. *Adv. Colloid and Interface Sci.*, **1987**, *27*, 189-209.
44. de Gennes, P. G. *Scaling Concepts*, **1987**, *27*, 189-209.
45. Girolamo, M.; Keller, A.; Stejny, J. *Die Makromolekulare. Chemie*, **1975**, *176*, 1489.
46. Glotin, M.; Mandelkern, L. *J. Polym. Sci.: Polym. Phys. Ed.*, **1983**, *21*, 29.
47. Golden, G. W. *Fourier Transform Infrared Spectroscopy*, Vol. 4, **1985**, Academic Press, Inc., Chapter 8.
48. Golden, W. G.; Dunn, D. S.; Overend, J. *J. of Catalysis*, **1981**, *71*, 395-404.
49. Gornick, F.; Hoffman, J. D. *Ind. Eng. Chem.*, **1966**, *58*, *2*, 41.
50. Gourdenne, A. *Block Copolymers*, ed. Aggarwal, S., **1970**, Plenum Press, New York.
51. Grant, W. H.; Smith, L. E.; Stromberg, R. R. *Discuss. Faraday Soc.*, **1975**, *59*, 209-217.
52. Greenler, R. G. *J. Chem. Phys.*, **1966**, *44*, *1*, 310-315.
53. Greenler, R. G. *J. Chem. Phys.*, **1969**, *50*, *5*, 1963-1968.
54. Griffiths, P. R.; deHaseth, J. A. *Fourier Transform Infrared Spectroscopy*, Chemical Analysis, Vol. 83, ed. Elving, P. J.; Winefordner, J. D.; Kolthoff, I. M., **1986**, John Wiley & Sons, N.Y.
55. Griot, O.; Kitchener, J. A. *Trans. Faraday Soc.*, **1965**, *61*, 1026.
56. Hale, P. T.; Pope, G. A. *Eur. Polym. J.*, **1975**, *11*, 677.

57. Harley, R. T.; Hayes, W.; Twisleton, J. F. *J. Phys. (C) Solid State*, **1973**, *6*, L167.
58. Hartley, A.; Leung, Y. K.; Booth, C.; Shepherd, I. W. *Polymer*, **1976**, *17*, 354.
59. Hayashi, S.; Umemura, J. *J. Chem. Phys.*, **1975**, *63*, 5, 1732.
60. Hecht, E.; Zajac, A. *Optics*, **1974**, Addison Wesley Pub. Co., Inc.
61. Hendra, P. J.; Majid, H. A. *Polymer*, **1977**, *18*, 573.
62. Herzberg, G. *Infrared and Raman Spectra of Polyatomic Molecules*, **1945**, Van Nostrand, N.Y.
63. Hipps, K. W.; Crosby, G. A. *J. Phys. Chem.*, **1979**, *83*, 5, 555-562.
64. Hoeve, C. A.; DiMarzio, E. A.; Peyser, P. J. *Chem. Phys.*, **1965**, *42*, 7, 2558-2563.
65. Holland-Moritz, K.; Hummel, D. O. *J. Molec. Struc.*, **1973**, *19*, 289.
66. Howard, G. J.; Woods, S. J. *J. Polym. Sci., A-2*, **1972**, *10*, 1023-1028.
67. Hsu, S. L.; Ford, G. W.; Krimm, S. *J. Polym. Sci.: Polym. Phys. Ed.*, **1977**, *15*, 1769.
68. Hsu, S. L.; Krimm, S. *J. Appl. Phys.*, **1976**, *47*, 4265.
69. Hsu, S. L.; Krimm, S. *J. Appl. Phys.*, **1977**, *48*, 4013.
70. Hsu, S. L.; Krimm, S.; Krause, S.; Yeh, G. S. Y. *J. Polym. Sci., Polym. Lett. Ed.*, **1976**, *14*, 195.
71. Ishitani, A.; Ishida, H.; Soeda, F.; Nagasawa, Y. *Anal. Chem.*, **1982**, *54*, 682-687.
72. Jakes, J.; Krimm, S. *Macromolecules*, **1971**, *4*, 605.
73. Jasse, B.; Koenig, J. L. *J. Polym. Sci.: Polym. Phys. Ed.*, **1979**, *17*, 799.
74. Joppien, G. R. *Makromol. Chem.*, **1975**, *176*, 1129.
75. Kanamoto, T. *J. Polym. Sci.: Polym. Phys. Ed.*, **1974**, *12*, 2535.

76. Kanamoto, T.; Tanaka, T.; Nagai, H. *J. Polym. Sci.: Polym. Phys. Ed.*, **1971**, *9*, 2043.
77. Kawaguchi, M.; Hattori, S.; Takahashi, A. *Macromolecules*, **1987**, *20*, 178-180.
78. Kawaguchi, M.; Kenji, K.; Takahashi, A. *Polym. J.*, **1982**, *14*, *7*, 563.
79. Kawaguchi, M.; Maeda, K.; Kato, T.; Takahashi, A. *Macromolecules*, **1984**, *17*, 1666-1671.
80. Kawaguchi, M.; Sakai, A.; Takahashi, A. *Macromolecules*, **1986**, *19*, *12*, 2952-2955.
81. Kawaguchi, M.; Takahashi, A. *J. Polym. Sci.: Polym. Phys. Ed.*, **1980**, *18*, 2069-2076.
82. Khoury, F.; Fanconi, B.; Barnes, J. D.; Bolz, L. H. *J. Chem. Phys.*, **1973**, *59*, 5849.
83. Kirshenbaum, I. *J. Polymer Sci.*, **1965**, *3A*, 1869-1875.
84. Koenig, J. L.; Tabb, D. L. *J. Macromol. Sci. Phys.*, **1974**, *B9*, 141.
85. Kolthoff, I. M.; Gutmacher, R. G. *J. Phys. Chem.*, **1952**, *56*, 740-745.
86. Koopal, L. K.; Lyklema, J. *J. Chem. Soc., Faraday Discuss.*, **1975**, *59*, 230.
87. Leibler, L.; Orland, H.; Wheeler, J. *J. Chem. Phys.* **1983**, *79*, 3550.
88. Liang, C. Y.; Krimm, S. *J. Polym. Sci.*, **1958**, *27*, 241-254.
89. Linden, C. V.; Leemput, R. V. *J. Colloid Interface Sci.*, **1978**, *67*, 48-62.
90. Linden, C. V.; Leemput, R. V. *J. Colloid Interface Sci.*, **1978**, *67*, 63-69.
91. March, J. *Advanced Organic Chemistry 2nd ed.*, **1977**, McGraw-Hill.
92. Marques, C.; Joanny, J. F.; Leibler, L. *Macromolecules*, **1988**, *21*, *4*, 1051-1059.
93. Marrinan, H. *J. Polymer Sci.*, **1959**, *39*, 461.
94. Mazur, J.; Fanconi, B. *J. Chem. Phys.*, **1979**, *71*, 5069.

95. Milner, S. T.; Witten, T. A.; Cates, M. E. *Macromolecules*, **1988**, *21*, 8, 2610-2619.
96. Minoni, G.; Zerbi, G. *J. Chem. Phys.*, **1982**, *86*, 4791.
97. Mizushima, S. I.; Shimanouchi, T. *J. Am. Chem. Soc.*, **1949**, *71*, 1320.
98. Morton, M.; Fetters, L. J. *Rubber Chem. & Tech.*, **1975**, *8*, 3, 359.
99. Morton, M.; Kammereck, R. F. *J. Am. Chem. Soc.*, **1970**, *92*, 10.
100. Morton, M.; Kammereck, R. F.; Fetters, L. J. *Macromolecules*, **1971**, *4*, 11.
101. Morton, M.; Mikesell, S. L. *J. Macromol. Sci.- Chem.*, **1973**, *A7*, 7, 1391.
102. Munch, M. R.; Gast, A. P. *Macromolecules*, **1988**, *21*, 5, 1366-1372.
103. Nafie, L. A.; Diem, M. *Applied Spectroscopy*, **1979**, *33*, 130.
104. Naselli, C.; Rabolt, J. F.; Swalen, J. D. *J. Chem. Phys.*, **1985**, *82*, 4, 2136-2140.
105. Nevin, R. S.; Pearce, E. M. *Polymer Letters*, **1965**, *3*, 487-490.
106. Nuzzo, R. G.; Fusco, F. A.; Allara, D. L. *J. Am. Chem. Soc.*, **1987**, *109*, 2358-2368.
107. Nuzzo, R. G.; Zegarski, B. R.; Dubois, L. H. *J. Am. Chem. Soc.*, **1987**, *109*, 733-740.
108. Ohnisi, T.; Ishitani, A.; Ishida, H.; Yamamoto, N.; Tsubomura, H. *J. Phys. Chem.*, **1978**, *82*, 1989.
109. Ohno, A.; Oae, S. *Organic Chemistry of Sulfur*, ed. Oae, S., **1977**, Plenum Press, New York.
110. Olf, H. G.; Fanconi, B. *J. Chem. Phys.*, **1973**, *59*, 1, 534.
111. Olf, H. G.; Peterlin, A.; Peticolas, W. L. *J. Polym. Sci.: Polym. Phys. Ed.*, **1974**, *12*, 359.
112. Ouada, H. B.; Hommel, H.; Legrand, A. P.; Balard, H.; Papirer, E. *J. Colloid Interface Sci.*, **1988**, *112*, 2, 441-449.

113. Pefferkorn, E.; Carroy, A.; Varoqui, R. *J. Polym. Sci.: Polym. Phys. Ed.*, **1985**, *23*, 1997.
114. Pefferkorn, E.; Haouam, A.; Varoqui, R. *Macromolecules*, **1988**, *21*, 2111.
115. Peterlin, A. *Colloid and Polymer Sci.*, **1975**, *253*, 809.
116. Peticolas, W. L.; Hibler, G. W.; Lippert, J. L.; Peterlin, A.; Olf, H. *Appl. Phys. Lett.*, **1971**, *18*, 87.
117. Peyser, P.; Stromberg, R. R. *J. Phys. Chem.*, **1967**, *71*, 2066.
118. Porter, M. D.; Bright, T. B.; Allara, D. L.; Chidsey, C. E. D. *J. Am. Chem. Soc.*, **1987**, *109*, 3559-3568.
119. Rabolt, J. F.; *J. Polym. Sci.: Polym. Phys. Ed.*, **1979**, *17*, 1457.
120. Rabolt, J. F.; Burns, F. C.; Schlotter, N. E.; Swalen, J. D. *J. Chem Phys.*, **1983**, *78*, *2*, 946-952.
121. Rabolt, J. F.; Fanconi, B. *J. Polym. Sci.: Polym. Lett. Ed.*, **1977**, *15*, 121.
122. Rabolt, J. F.; Jurich, M.; Swalen, J. D. *Applied Spectroscopy*, **1985**, *39*, *2*, 269-272.
123. Reneker, D. H. *J. Polym. Sci.*, **1962**, *59*, S39.
124. Reneker, D. H.; Fanconi, B. *J. Appl. Phys.*, **1975**, *46*, 4144.
125. Roe, R. J.; Krigbaum, W. R. *J. Appl. Phys.*, **1964**, *35*, 2215.
126. Roggero, A.; Zotteri, L.; Proni, A.; Gandini, A.; Mazzei, A. *Eur. Polym. J.*, **1976**, *12*, 837.
127. Rossi, G.; Cates, M. E. *Macromolecules*, **1988**, *21*, *5*, 1372-1377.
128. Sadakne G. S.; White, J. L. *J. Appl. Polym. Sci.*, **1973**, *17*, 453.
129. Schaufele, R. F.; Shimanouchi, T. *J. Chem. Phys.*, **1967**, *47*, 3605.
130. Scherer J. R.; Snyder, R. J. *J. Chem. Phys.*, **1980**, *72*, *11*, 5798.
131. Scheutjens, J. M. H. M.; Fleer, G. J. *J. Phys. Chem.*, **1980**, *84*, 178-190.

132. Schlotter, N. E.; Rabolt, J. F. *Applied Spectroscopy*, **1985**, 39, 6, 994-996.
133. Schrader, M. E. *J. Colloid Interface Sci.*, **1984**, 100, 372.
134. Scott, J. F. *The Spex Speaker*, **1972**, 17, 2, Spex Industries, Metuchen, NJ, 1972.
135. Shimanouchi, T.; Tasumi, M. *Indian J. Pure Appl. Phys.*, **1971**, 9, 958.
136. Shu, P. H.; Burchell, D.J.; Hsu, S. L. *J. Polym. Sci.: Polym. Phys. Ed.*, **1980**, 18, 1421.
137. Sigwalt, P.; Spassky, N. *Ring Opening Polymerization Vol. 2*, ed. Ivin, K. J. and Saegusa, T., **1984**, Elsevier Press, Chapter 10.
138. Simonds, R. P.; Goethals, E. J. *Makromol. Chem.*, **1978**, 179, 1689.
139. Smith, T. J. *J. Colloid Interface Sci.*, **1980**, 75, 51.
140. Snyder, R. G.; Krause, S. J.; Scherer, J. R. *J. Polym. Sci.: Polym. Phys. Ed.*, **1978**, 16, 1593.
141. Snyder, R. G.; Scherer, J. R. *J. Polym. Sci.: Polym. Phys. Ed.*, **1980**, 18, 421.
142. Stein R. S. *J. Polymer Sci.*, **1958**, 28, 83.
143. Stille, J. K.; Empen, J. A. *Polym. Prepr.*, **1965**, 6, 619.
144. Stouffer, J. M.; McCarthy, T. J. *Macromolecules*, **1988**, 21, 5, 1204-1208.
145. Streitwieser, A.; Heathcock, C. *Introduction to Organic Chemistry 2nd ed.*, **1981**, Macmillan Pub.
146. Strobl, G. R.; Eckel, R. *J. Polym. Sci.: Polym. Phys. Ed.*, **1976**, 14, 913.
147. Strobl, G. R.; Eckel, R. *Colloid & Polym. Sci.*, **1980**, 258, 570.
148. Strobl, G. R.; Hagedorn, W. *J. Polym. Sci.: Polym. Phys. Ed.*, **1978**, 16, 1181.
149. Stromberg, R. R.; Tutas, D. J.; Passaglia, E. *J. Phys. Chem.*, **1965**, 69, 11, 3955-3963.

150. Swales, T. G. E.; Teo, H. H.; Domszy, R. C.; Viras, K.; King, T. A.; Booth, C. J. *Polym. Sci.: Polym. Phys. Ed.*, **1983**, 21, 1501.
151. *Raman Spectroscopy Vol. 2*, ed. Szymanski, H. A., 1970, Plenum Press, N.Y.
152. Tadokoro, H. *Structure of Crystalline Polymers*, 1979, John Wiley & Sons, N.Y.
153. Tadokoro, H.; Kobayashi, M.; Yoshidome, H.; Tai, K.; Makino, D. *J. Chem. Phys.*, **1968**, 49, 3359.
154. Takahashi, A.; Kawaguchi, M.; Hirota, H.; Kato, T. *Macromolecules*, **1980**, 13, 4, 884-889.
155. Takeuchi, H.; Shimanouchi, T.; Tasumi, M.; Vergoten, G.; Fleury, G. *Chem. Phys. Lett.*, **1974**, 28, 449.
156. Tasumi, M.; Krimm, S. *J. Chem. Phys.*, **1967**, 46, 755.
157. Tasumi, M.; Shimanouchi, T. *J. Chem. Phys.*, **1965**, 43, 1245.
158. Theodorou, D. N. *Macromolecules*, **1988**, 21, 5, 1411-1421.
159. Theodorou, D. N. *Macromolecules*, **1988**, 21, 5, 1422-1436.
160. Tobin, M. C. *Laser Raman Spectroscopy*, Chemical Analysis, Vol. 35, ed. Elving, P. J. and Kolthoff, I. M., **1971**, John Wiley & Sons, N.Y.
161. Treloar, L. R. G., *The Physics of Rubber Elasticity*, **1949**, Oxford.
162. Turnbull, D.; Fisher, J. C. *J. Chem. Phys.*, **1949**, 17, 71.
163. Waldman, D. A.; Hsu, S. L. *Bull. Am. Phys. Soc.*, **1986**, 31, 3, 405.
164. Waldman, D. A.; Hsu, S. L. *Bull. Am. Phys. Soc.*, **1988**, 33, 3, 760.
165. Waldman, D. A.; Hsu, S. L. *Bull. Am. Phys. Soc.*, **1990**, 35, 3, 652.
166. Waldman, D. A.; Kolb, B. U.; McCarthy, T. J.; Hsu S. L. *Proc. of A.C.S. Div. of Polym. Mat.*, **1988**, 59, 326.
167. Waldman, D. A.; Kolb, B. U.; McCarthy, T. J.; Hsu S. L. *Langmuir*, **1990**, in press.

168. Wang, Y. K.; Shu, P. H. C.; Stein, R. S.; Hsu, S. L. *J. Polym. Sci.: Polym. Phys. Ed.*, **1980**, *18*, 2287.
169. Wang, Y. K.; Waldman, D. A.; Stein, R. S.; Hsu, S. L. *J. Appl. Phys.*, **1982**, *53*, 10, 6591.
170. Wang, Y. K.; Waldman, D. A.; Lasch, J. E.; Stein, R. S.; Hsu, S. L. *Macromolecules*, **1982**, *15*, 1452.
171. Wilson, E. B.; Decius, J. C.; Cross, P. C. *Molecular Vibrations*, **1965**, McGraw-Hill, N.Y.
172. Woodward, L. A.; Long, D. A. *Trans. Faraday Soc.*, **1949**, *45*, 1131.
173. Wu C.; Nicol, M. J. *Chem. Phys.*, **1973**, *58*, 11, 5150.
174. Wunderlich, B. *Macromolecular Physics: Crystals, Structure, Morphology and Defects, Crystal Melting, Vol. 1-3*, **1973**, Academic Press.

